

LASER TREATMENT FOR LIVER METASTASES
Thermal and Photodynamic Therapy

LASER TREATMENT FOR LIVER METASTASES

Thermal and Photodynamic Therapy

LASER BEHANDELING VOOR LEVERMETASTASEN
Thermische en Photodynamische Therapie

PROEFSCHRIFT

ter verkrijging van de graad van doctor
aan de Erasmus Universiteit Rotterdam
op gezag van de rector magnificus
Prof. Dr. P.W.C. Akkermans M.Lit.
en volgens het besluit van het College van Dekanen.
De openbare verdediging zal plaats vinden op
woensdag 13 oktober 1993 om 15.45 uur

door

Richard van Hillegersberg

geboren te Rotterdam

Promotiecommissie

Promotor: Prof. Dr. O.T. Terpstra

Co-promotor: Dr. W.J. Kort

Overige leden: Prof. Dr. Ir. M.J.C. van Gemert
Prof. Dr. J. Jeekel
Prof. J.H.P. Wilson

This publication was made possible thanks to financial contributions of
M.A.O.C. Gravin van Bylandt Stichting
D.L. Westbroek Stichting

This study was supported by
The Netherlands Digestive Disease Foundation (grant WS 89-14)

Cover: Nd:YAG laser coagulated colon carcinoma encapsulated by connective tissue and surrounded by normal hepatic tissue.

CIP-GEGEVENS KONINKLIJKE BIBLIOTHEEK, DEN HAAG

Hillegersberg, Richard van

Laser treatment for liver metastases: thermal and
photodynamic therapy / Richard van Hillegersberg.
- [S.l.: s.n.]. - Ill.

Proefschrift Rotterdam - Met index, lit. opg.

- Met samenvatting in het Nederlands.

ISBN 90-9006313-7

Trefw.: lasers in de geneeskunde / leverziekten.

PASMANS OFFSETDRUKKERIJ BV 's GRAVENHAGE

Aan mijn ouders

Aan Jacqueline

Preface

Medical laser applications are one of the points of interest of the Department of Surgery of the Erasmus University Rotterdam. In 1988, experiments were conducted at the Laboratory for Experimental Surgery to investigate the use of laser in destroying liver metastases. These studies led to the research program "Laser treatment of experimental liver metastases", that was supported by the Netherlands Digestive Disease Foundation from beginning 1990 to the middle of 1992. Within this project, studies were carried out in close collaboration with the Departments of Pathology, Internal Medicine II, and Radiology of the Erasmus University. Joint studies were performed with the groups of the Department of Physics of the Dr. Daniël den Hoed Cancer Center and the Laser Center of the Academic Medical Center Amsterdam.

This thesis describes the results of the studies mentioned above. The General Introduction gives an outline of the problem of hepatic metastases, the aims of the study, and the tumor model applied. The following parts on thermal and photodynamic therapy start with an introduction of the fundamentals of these laser applications. The second last part presents initial studies on the complex matter of laser-tissue interaction. Finally, general considerations are given for possible clinical use.

Rotterdam, 1993

Richard van Hillegersberg

List of Contributing Authors

Ing. M. Aalders, Laser Center, Academic Medical Center, Meibergdreef 9, 1105 AZ Amsterdam.

Dr. J.F. Beek, Laser Center, Academic Medical Center, Meibergdreef 9, 1105 AZ Amsterdam.

Dr. J.W.O. van den Berg, Laboratory for Internal Medicine II, University Hospital Rotterdam "Dijkzigt", Dr. Molewaterplein 40, 3015 GD Rotterdam.

Prof. Dr. F.J.W. ten Kate, Department of Pathology, Erasmus University Rotterdam, Dr. Molewaterplein 50, 3015 GE Rotterdam
At present Department of Pathology, Academic Medical Center, 1105 AZ Amsterdam.

Dr. W.J. Kort, Department of Surgery, Erasmus University Rotterdam, Dr. Molewaterplein 50, 3015 GE Rotterdam.

Dr. Ing. J.P.A. Marijnissen, Department of Clinical Physics, Dr. Daniël den Hoed Cancer Center, Groenehilledijk 301, 3075 EA Rotterdam.

Dr. J.W. Pickering, Laser Center, Academic Medical Center, Meibergdreef 9, 1105 AZ Amsterdam.

Dr. W.M. Star, Department of Clinical Physics, Dr. Daniël den Hoed Cancer Center, Groenehilledijk 301, 3075 EA Rotterdam.

Drs. H.J van Staveren, Department of Clinical Physics, Dr. Daniël den Hoed Cancer Center, Groenehilledijk 301, 3075 EA Rotterdam.

Prof. Dr. O.T. Terpstra, Department of Surgery, University Hospital Rotterdam "Dijkzigt", Dr. Molewaterplein 40, 3015 GD Rotterdam.
At present Department of Surgery, University Hospital Leiden, Rijnsburgerweg 10, 2333 AA Leiden.

LIST OF CONTRIBUTING AUTHORS

M. Vermeij, Department of Pathology, Erasmus University Rotterdam, Dr. Molewaterplein 50, 3015 GE Rotterdam.

Prof. J.H.P. Wilson, Department of Internal Medicine II, University Hospital Rotterdam "Dijkzigt", Dr. Molewaterplein 40, 3015 GD Rotterdam.

Drs. M.T. de Witte, Department of Radiology, University Hospital Rotterdam "Dijkzigt", Dr. Molewaterplein 40, 3015 GD Rotterdam.

Drs. P.E. Zondervan, Department of Pathology, Erasmus University Rotterdam, Dr. Molewaterplein 50, 3015 GE Rotterdam.

Contents

PART I GENERAL INTRODUCTION

1. Hepatic Metastases: Aims of the Study 1
2. Tumor Model and Parameters for Tissue Damage 7

PART II THERMAL THERAPY

3. Fundamentals of Laser Medicine 17
4. Noncontact Nd:YAG Laser Treatment
Adapted from: J Surg Res 1992;53:128-135 31
5. Water-jet-cooled Nd:YAG Laser Coagulation
Adapted from: Lasers Surg Med 1991;11:445-454 39
6. Interstitial Nd:YAG Laser Coagulation
Adapted from: Lasers Surg Med (accepted) 51

PART III PHOTODYNAMIC THERAPY

7. Fundamentals of Photodynamic Therapy
Adapted from: Drugs 1993 (in press) 73
8. Interstitial Photodynamic Therapy
Adapted from: Br J Cancer 1992;66:1005-1014 87
9. 5-Aminolevulinic acid-induced Endogenous Photosensitization
Adapted from: Gastroenterology 1992;103:647-651 103

CONTENTS

PART IV PREDICTING LASER-TISSUE INTERACTION

10. Tissue Optical Properties at 633 nm and 1,064 nm
Adapted from: Lasers Surg Med 1993; 13: 31-39 115
11. Ultrasonography of Nd:YAG Laser Coagulation
Adapted from: Lasers Surg Med 1993; 13: 332-343 125

PART V GENERAL DISCUSSION

12. General Discussion: Considerations for Clinical Application . . 141
- Summary 151
- Samenvatting 157
- References 165
- Subject Index 187
- Dankwoord 193
- Curriculum Vitae 197

PART I

GENERAL INTRODUCTION

1. Hepatic Metastases: Aims of the Study

LIVER METASTASES

Metastatic disease of the liver is a major cause of death in cancer patients, colorectal carcinoma being the most common primary tumor (Foster, 1990). In The Netherlands annually about 7400 new cases of colon and rectum carcinoma are diagnosed (LOK, Netherlands Cancer Registry, 1992). At time of treatment of the primary tumor, liver metastases are already present in 20-25% of these patients and ultimately liver metastases develop in over 50% (Bengmark & Halfstrom, 1969; Welch & Donaldson, 1979; Finlay & McArdle, 1986).

Various studies showed that the occurrence of liver metastases is the primary determinant of survival in patients with colorectal carcinoma (Wagner *et al.*, 1984; Steele & Ravikumar, 1989). Mean survival time in untreated patients with hepatic metastases from colorectal carcinoma is 6 months (Jaffe *et al.*, 1968; Cady, 1983; Wagner *et al.*, 1984). A retrospective study of 404 patients by Wood *et al.* (1976) showed a division into three main groups, according to the volume of tumor within the liver:

1. In patients with widespread metastases (73%) the mean survival time was 3 months.
2. In those with multiple, but unilobar metastases (13%) the mean survival time was 17 months, or 11 months in case of extrahepatic disease.
3. In those with solitary metastases (14%) the mean survival time was 25 months, or 17 months in case of extrahepatic disease.

The patients in the last two groups without extrahepatic disease may be amenable to curative treatment, whereas palliation may be the only option in the other patients.

Current Treatment Modalities

To date most treatment modalities have been found ineffective or associated with major complications owing to systemic or hepatic toxicity and unpredictable tissue damage.

Chemotherapy. Systemic chemotherapy has caused severe toxicity, despite the use of varied schedules of administration and chemotherapeutic agents. Generally, partial response rates were lower than 30% (Sugerbaker & Kemeny, 1989). Therefore, regional approaches were developed, aiming at a high local drug dose and less systemic toxicity. As intrahepatic tumor bloodsupply is thought to be mainly arterial (Breedis & Young, 1954), hepatic artery

infusion with an implantable pump was used to deliver the chemotherapeutic agent to the tumor. The standard chemotherapeutic agent has been floxuridine (FUDR), as it was demonstrated that this agent is extracted by the liver in the first pass (Ensminger, 1989). Randomized trials have shown a significantly higher partial response rate with intrahepatic infusion (37-62%) versus systemic infusion (0-38%) in patients with hepatic metastases of colon cancer (Kemeny, 1992). However, a clear survival advantage has not been demonstrated and despite hepatic artery infusion, side effects have been common, leading to liver damage, gastritis, ulcer disease, diarrhea, and biliary sclerosis.

Radiotherapy. External radiotherapy has also been limited by the problem of its hepatic toxicity (Sherman *et al.*, 1978). The interstitial application may have better results as higher doses can be delivered to the tumor with little effect on the surrounding parenchyma. Nauta *et al.* (1987) treated 12 patients with liver metastases at laparotomy using an interstitial iridium-192 source during 3-7.5 h. No complications were reported. A drop in the raised carcino-embryonic antigen (CEA) levels was found in 6 patients within 2.5 months of treatment. Computed tomography (CT) at 1 week showed a halo of radio-oedema around the treated nodules. Dritschilo *et al.* (1988) showed the feasibility of percutaneous interstitial radiotherapy in 11 patients with hepatic metastases of colorectal carcinoma. They used afterloading catheters to guide the placement of an iridium-192 radiation source delivering a dose of 20 GY in a single procedure. To date, little information exists on the efficacy and safety of this approach.

Alcohol injection. Percutaneous intratumoral injection of 98% ethanol can produce coagulation necrosis as was shown by Shiina *et al.* (1987). However, the amount of damage to tumor and surrounding normal tissue is rather unpredictable owing to uncontrolled perfusion of the alcohol to the tissue (Van Eyken *et al.*, 1991). Complete destruction of intrahepatic metastases was found difficult to achieve, probably as a result of the alcohol bypassing areas of high resistance (e.g., fibrous areas) in the heterogeneous tumor (Livraghi *et al.*, 1991). The effect of treatment can not be monitored by ultrasonography or CT until actual necrosis has occurred at 2 weeks post-treatment.

Cryotherapy. Cryotherapy (cooling to -196°C), uses a 8-12 mm in diameter liquid nitrogen probe that is placed interstitially into the tumor under intraoperative ultrasonography. The technical feasibility of this technique in patients with hepatic metastases from colorectal cancer was demonstrated by Ravikumar *et al.* (1987) and Charnley *et al.* (1989). The time for freezing ranged from 1-36 minutes; frozen normal liver appeared hyperechoic on intraoperative ultrasonography after thawing. No significant complications were reported. At follow-up, CT showed evidence of necrosis and tumor shrinkage, and in 1 patient, resection of the lesion showed coagulative necrosis, 5 months post-treatment. Thus, cryotherapy may induce localized tumor destruction without major complications. However, this procedure has to be performed under laparotomy, with associated morbidity and mortality rates.

Hepatic artery ligation. Temporary hepatic artery ligation is based on the observation, that intrahepatic tumor blood supply is mainly arterial (Breedis & Young, 1954). Portal venous blood constitutes approximately 70% of the total hepatic blood flow, and for that reason, normal liver tissue can survive the effects of total artery occlusion. The liver is dearterialized by an inflatable vascular occluder implanted around the hepatic artery and

connected to a subcutaneous injection chamber. As continuous dearterialization is associated with formation of collaterals, daily interruption of the artery has been performed for 1-2 h for 1-17 months (Persson *et al.*, 1992). However, the technique was found non-selective, and usually associated with high morbidity and complication rates (Bengmark *et al.*, 1988). In 11 patients with hepatic metastases from colorectal carcinoma, this treatment was combined with intraperitoneal infusion of 5-fluorouracil. However, no improvement of survival was found compared with patients given 5-fluorouracil only (Persson *et al.*, 1992).

Hepatic artery embolization. Hepatic artery embolization is based on the same principle (Blumgart & Allison, 1982). The hepatic artery is selectively catheterized and through the catheter embolizing microspheres are brought into the arterial circulation of the liver. Particularly patients with secondary tumor deposits from endocrine tumors, such as carcinoid, have shown good palliation (reduction in 5-hydroxyindole acetic acid) (Allison & Booth, 1990). Complications of embolization include derangement of liver function, local abscess formation, and septicemia. Attempts have been made to achieve selective chemotherapy or radiotherapy by coupling Yttrium-90 or cytotoxic drugs to the microspheres. In 26 patients treated with the Yttrium-90 technique, the CEA dropped 50-70% and in 18 of the 22 evaluable patients a reduction in tumor volume (up to 50%) was observed on CT (Gray *et al.*, 1992). The use of angiotensin II may increase microsphere targeting to the tumor (Anderson *et al.*, 1992). The incorporation of cytotoxic drugs into microspheres reduced systemic toxicity, but still considerable side effects, such as chemical and ischemic hepatitis, severe thrombopenia and icterus occurred relatively frequent (Borner *et al.*, 1992; Hennigan *et al.*, 1992).

Hyperthermia. The concept of hyperthermia is based on a possible increased heat sensitivity of neoplastic tissue (Field, 1987). Therefore, tumors are exposed to temperatures of 41-45°C for about 1 h. Initially whole body hyperthermia was applied, however this resulted in thermal damage of the normal hepatic tissue, leading to decreased liver function (Wills *et al.*, 1976). Later studies investigated regional whole liver hyperthermia using extracorporeal circulatory methods (Quebbeman *et al.*, 1984), regional radiofrequency annular array (Sapozink *et al.*, 1985), or microwave phased array (Petrovich *et al.*, 1988). However, these techniques could not induce a homogeneous temperature throughout the tumor, resulting in unpredictable necrosis and unacceptable high morbidity and mortality rates.

Surgical Resection

Surgical resection is the only potentially curative treatment modality currently available, improving 5-year survival rates to 20-40% in selected patients (Steele & Ravikumar, 1989; Van Ooijen *et al.*, 1992; Ballantyne & Quin, 1993). Most studies show a 5-year disease free survival of 20-25%. Unfortunately, only 10-20% of those considered are amenable for surgery (Foster & Berman, 1977; Wagner *et al.*, 1984; Sugarbaker, 1990). Absolute contraindications include extrahepatic disease (e.g., multiple pulmonary metastases, peritoneal seeding, periportal or retroperitoneal lymph node involvement), systemic conditions (e.g., cardiovascular or respiratory disease), or additional disease in the liver that makes resection technically hazardous or useless.

The factors influencing prognosis after resection of liver metastases from colorectal cancer

are still under investigation and controversial results have been published. The Dukes' classification of the primary colorectal carcinoma was found important, as the 5-year survival rate was longer in patients with Dukes' B (47%) than in patients with Dukes' C (23%) (Hughes *et al.*, 1988). Also the number of the metastases (≥ 4), as well as the presence of metastases surrounded by satellite nodules, has been associated with a poor prognosis after surgical resection (Hughes *et al.*, 1988; Cady *et al.*, 1992; Hodgson *et al.*, 1992). Scheele *et al.* (1990) reported that in patients with satellite nodules, the 5-year survival was 19%, compared to 41% without. Several studies have shown the need of a ≥ 1 cm resection margin to achieve complete intrahepatic tumor removal. The 5-year survival was found 28% in patients with a 1-4 mm resection margin, 34% in patients with a 5-9 mm margin, and 50% in patients with a free margin ≥ 10 mm (Scheele *et al.*, 1990). Cady *et al.* (1992) found the preoperative CEA level (<200 ng/ml), and postoperative weight of hepatic tissue resected (<1000 g), significantly related to 5-year disease free survival. Tumor recurrence, either in the liver alone (42-60% of all recurrences), or as part of disseminated disease, was found more common when the pathologic margins of the hepatic resection were positive and in the presence of bilobular disease (Franco, 1991; Van Ooijen, *et al.*, 1992; Lind *et al.*, 1992).

Although mortality rates in specialized centers are now between 5-10% (overall ranging from 4-25%), major hepatic resection imposes considerable physiological stress (Suc *et al.*, 1992) and the operative morbidity rates are still relatively high (16-46%) (De Jong *et al.*, 1989; Van Ooijen *et al.*, 1992; Ballantyne & Quin, 1993). An average post-operative intensive care unit stay of 3.2 days (range 1-12), and hospital stay 15 days (range 6-45) has been reported (Cole & Ferguson, 1992). The post-operative stay averages 10-16 days (Steele & Ravikumar, 1989; Lind *et al.*, 1992).

Bleeding is one of the most feared complications in liver surgery. However, since better surgical techniques, such as the ultrasonic surgical dissector (CUSA) and segmental approach to liver anatomy, have been exploited, intraoperative hemorrhage has not been reported a major complication anymore (Sugarbaker, 1990; Hodgson *et al.*, 1992). The most common postoperative complications are (De Jong *et al.*, 1989; Petrelli *et al.*, 1991; Lind *et al.*, 1992):

1. Hepatic failure.
2. Biloma/abscess formation.
3. Pleural effusion.
4. Intra-abdominal sepsis.

These complications are most directly related to the extent of resection required and the amount of devitalized tissue at the resection plane (Cole & Ferguson, 1992). The hepatic resection may also represent an important cause of tumor recurrence. There is increasing evidence of release of hepatic growth factors following partial hepatectomy, that may stimulate liver as well as tumor regeneration or hematogenous metastasis (Asaga *et al.*, 1991; Loizidu *et al.*, 1991). Furthermore, the surgical manipulation may cause recurrence, as was demonstrated in animal experiments (Nishizaki *et al.*, 1990; Mitzutani, 1992).

AIMS OF THE STUDY

The substantial improvement of survival rates after resection of hepatic metastases, demonstrates the rational for treating these tumors in selected patients. However, as described above, the current treatment modalities are limited, mainly by associated normal tissue damage. Therefore, better results would be expected from a treatment that would selectively destroy the malignant tissue, combined with minimal hepatic damage.

Laser in Oncology

Two promising laser applications in oncology are photodynamic therapy (PDT) and thermal Neodymium:Yttrium-Aluminum-Garnet (Nd:YAG) laser coagulation. The laser has several unique qualities, that enable delivery of high amounts of energy to a narrowly defined location (Polanyi, 1985; Absten, 1991).

In photodynamic therapy, a photosensitizer is administered systemically to accumulate in the tumor (Dougherty & Marcus, 1992). Subsequent illumination with light of an appropriate wavelength creates a reactive species that generates a photochemical reaction, which results in tumor destruction. Mostly the tunable argon-dye laser is used, as this system can deliver light of any particular wavelength between 350 and 700 nm. Photofrin[®] (Lederle Laboratories, Pearl River, NY, U.S.A.), a mixture of oligomer porphyrin molecules, is the most commonly used photosensitizer, having an absorption peak of 625 nm.

In thermal laser therapy the highly concentrated monochromatic laser light is transformed into thermal energy upon absorption by a tissue chromophore. Here, the Nd:YAG laser is used, as its wavelength of 1,064 nm penetrates up to 10 mm into tissue (Jacques, 1992). At temperatures of 60-140°C the tissue is coagulated, while at temperatures of 300-1000°C tissue ablation, vaporization and carbonization occurs (Thomsen, 1991).

The laser light may be delivered noncontactly by aiming the laser beam on the tissue surface, or interstitially by implanting the light delivery fibers directly into the tissue (Murray *et al.*, 1992; Masters & Bown, 1992). Deep seated intrahepatic lesions may only be treated interstitially, whereas an advantage of the noncontact technique could be a reduced chance of tumor spread owing to minimal tissue manipulation (Nishizaki *et al.*, 1990; Hashimoto *et al.*, 1985).

Laser Treatment for Liver Metastases

The studies described in this thesis are aimed at assessing the effects of laser treatment upon solid tumor and surrounding normal hepatic tissue, to determine whether laser therapy could be an alternative to surgical resection. A rat tumor model for hepatic metastasis of colon cancer was chosen for the experiments, to allow investigation under standardized *in vivo* conditions. The effects of various forms of light delivery or drug administration were determined at different time intervals using histological, biochemical, and physical parameters.

Thermal Laser Therapy. As noncontact laser ablation of intrahepatic tumors had caused extensive bleeding of the hepatic tissue (Nims & McCaughan, 1983), our thermal studies were all aimed at the selective coagulation of tumor. In Part II, we investigated three

different ways of light delivery, using various methods to avoid tissue carbonization:

1. The noncontact Nd:YAG laser with a focussing handpiece in a pulsed temporal mode, to allow cooling of the tissue between laser pulses (Chapter 4).
2. The noncontact Nd:YAG laser transmitted by a water-jet, pumped through the fiber system, to cool the tissue surface (Chapter 5).
3. The interstitial Nd:YAG laser with a cylindrical diffusing fiber-tip, to provide for homogeneous heat distribution by uniform light delivery (Chapter 6).

Photodynamic Therapy. PDT of liver tumors had been restricted due to effective accumulation of photosensitizers in hepatic tissue, causing substantial liver necrosis after superficial tumor illumination (Bellnier *et al.*, 1989; Pimstone *et al.*, 1982). In Part III, our PDT research was therefore directed towards either:

1. Interstitial tumor illumination as a means of selective PDT after photosensitization with Photofrin (Chapter 8).
2. Selective photosensitizer accumulation by endogenous production of protoporphyrin during 5-aminolevulinic acid administration (Chapter 9).

Predicting Laser-tissue Interaction. The tissue effects of both PDT and thermal laser therapy may extend deeply into the tissue, whereas the only visible effect is superficial. In Part IV, we used two different approaches to predict the quantitative and spatial extent of a lesion:

1. Determining the optical properties of the tissues, for modelling the light transport; estimating temperature rise or photosensitizer activation (Chapter 10).
2. Comparing the effects of Nd:YAG laser coagulation on ultrasonography and histology, to assess the value of ultrasonography in imaging laser-induced tissue damage (Chapter 11).

2. Tumor Model and Parameters for Tissue Damage

INTRODUCTION

A rat tumor model for hepatic metastasis of colon cancer was chosen for the experiments. This tumor model allowed investigation under standardized *in vivo* conditions, i.e., the various forms of light delivery or drug administration could be assessed on solid malignant tumor, surrounded by normal well perfused hepatic tissue. This would not have been possible in *in vitro* models, such as tissue phantoms or cell cultures.

The effects of a certain treatment were determined at different time intervals, by histological, biochemical and physical parameters.

This chapter describes the tumor model as well as the parameters for tissue damage.

MATERIALS AND METHODS

Animals

Male inbred Wag/Rij rats (Harlan CPB, Austerlitz, The Netherlands), weighing 180-250 g were used for the experiments. The animals had free access to rat chow and tap water. All animal handling was carried out by experienced biotechnicians acquired with the latest developments in husbandry, nutrition and animal housing.

Tumor Model

Colon adenocarcinoma CC531, a dimethylhydrazine-induced moderately differentiated and syngeneic tumor (Figure 2.1) transplantable to Wag/Rij rats, was maintained subcutaneously (Marquet *et al.*, 1984). On the day of inoculation the tumor was excised from the donor rat, cut into pieces of approximately 2 mm³ and kept in Hank's balanced salt solution. Under ether anaesthesia a midline laparotomy was performed, and the liver was spread over a gauze soaked in saline, to avoid spill of tumor cells in the abdominal cavity. Following that, a small incision with microsurgical scissors was made in the left lateral lobe of the liver and a piece

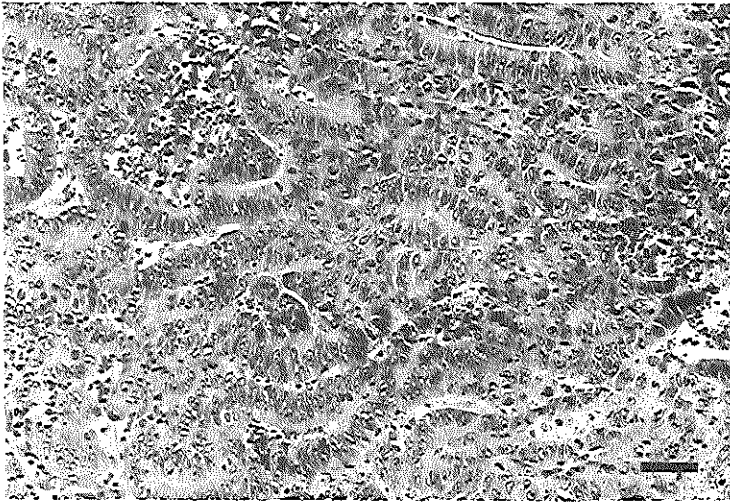


Figure 2.1. Histological section of untreated tumor, 20 days after intrahepatic implantation. Rat colon carcinoma CC531 is a moderately differentiated adenocarcinoma, showing acinous formation. Bar: 25 μ m (hematoxylin, azophloxin & saffron stain).

of tumor was implanted. The implant was covered with Lyostypt® (B. Braun Melsungen AG, Melsungen, Germany) for the purpose of both hemostasis and tumor shielding. In the first study (Chapter 4), 3 tumors were implanted in the liver of each animal; in all other studies 1 tumor was implanted per animal.

In pilot studies, intraportal or intrahepatic injection of suspended tumor cells induced less standardized tumor deposits (i.e., a larger variation in tumor size, number, and localization). These observations were recently confirmed by Yang *et al.* (1992).

Intrahepatic Tumor Growth

Intrahepatic tumor growth was determined in 25 animals at various periods after implantation. The animals were sacrificed in groups of 5, at 7, 14, 21, 28 and 35 days after intrahepatic tumor implantation. The tumor was dissected and measured in three dimensions with sliding calipers. The largest diameter was used for the analysis. An exponential growth curve was found with doubling time of 2 weeks (Figure 2.2).

The measurements on the dissected tumor corresponded well to measurements on the diameter of the intrahepatic tumor (in situ). This last value was used as an indication for tumor size in the experiments.

Treatment was usually performed on day 20 after implantation, when the tumor was approximately 6 mm in diameter (Figure 2.3). At this stage the tumor showed little central necrosis and was surrounded by normal hepatic tissue, which was slightly compressed immediately adjacent to the tumor (Figure 2.4a).

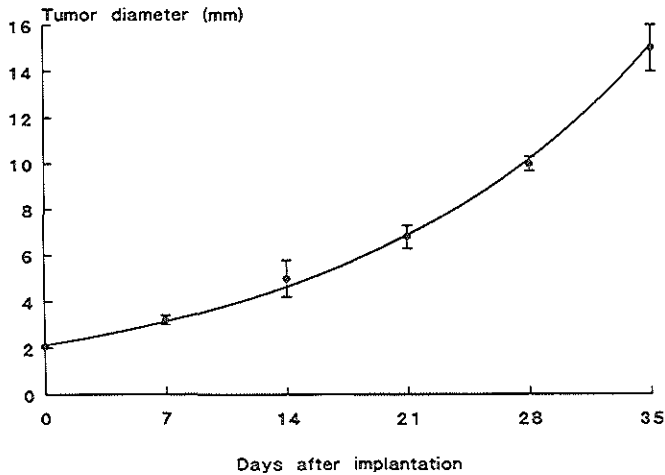


Figure 2.2. Largest tumor diameter vs. days after intrahepatic implantation. Each point represents the mean \pm SEM of 5 experimental results.

Determination of Liver and Tumor Damage

To avoid observer bias, all determinations were made without knowledge of the treatment parameters.

Histopathology. After fixation in a 3.6% buffered formalin solution for 5 days, the livers were sliced through the plane of the largest tumor diameter, embedded in paraffin and sectioned at 5 μ m. Sections were mounted on glass slides and stained with hematoxylin, azophloxin and saffron, for light microscopical examination. Measurements on histology were made by computer-assistance (IBAS 2000, Kontron Bildanalyse GmbH, München, Germany): with a video camera the histological slide was visualized on a monitor, so that with a mouse the different areas could be either outlined (determining the surface area by integration of the circumference) or indicated by two points (measuring the depth or width).

Long-term Tumor Remission. Tumor remission was assessed on the basis of specimens taken from animals sacrificed 36 days post-treatment (56 days after tumor implantation). At that stage the tumor in sham treated animals showed massive outgrowth with infiltration to the adjacent tissues (Figure 2.4b). The interval of 36 days was chosen, as shortly after this period, all sham treated animals in pilot studies had died from disseminated disease. Moreover, in treated animals, outgrowth of uncontrolled tumor implants obscured interpretation of the results after longer intervals post-treatment. These uncontrolled tumor implants are probably caused by spill of tumor cells at time of implantation or metastatic growth of the original implant. The interval of 36 days allowed proper histological assessment of the lesion in all animals at the same period post-treatment.

Complete tumor remission was considered when no tumor outgrowth (i.e., no vital tumor

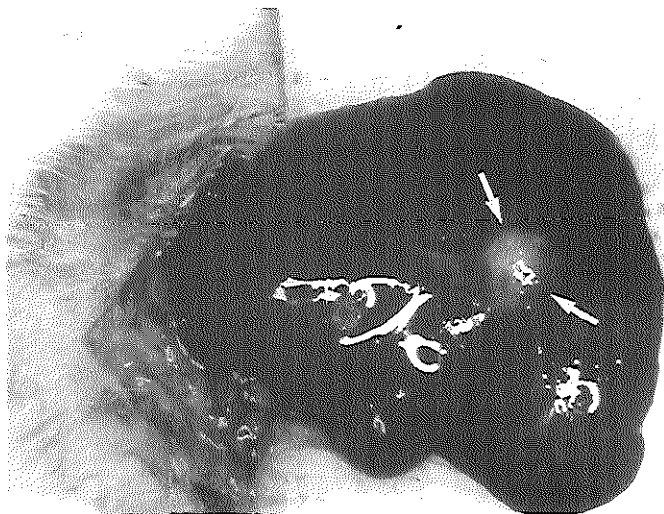


Figure 2.3. Normal macroscopic appearance of tumor CC531 (indicated by arrows) in the left lateral lobe of the rat liver, 20 days after implantation. Tumor, 6.9 mm.

tissue) could be observed by light microscopy. To give an indication of tumor growth retardation the vital tumor areas were measured in Chapters 6 and 8 by computer-assisted integration of the circumference.

Serum ASAT/ALAT. Aminotransferases are widely used to evaluate liver damage, which leads to an increased activity in the serum. The most common view is that leakage of these enzymes to the plasma occurs after hepatocyte death or damage (Zimmermann, 1978). Therefore, the intracellular enzyme localization mainly determines the appearance in the serum. In case of minor damage to the plasmamembrane, mainly alanine aminotransferase (ALAT) is found, which is localized only in the cytoplasm (Sherman, 1991). In case of necrosis, however, the serum level of aspartate aminotransferase (ASAT), which is localized in cytoplasm and mitochondria, is higher owing to the overall higher cellular level (Panteghini, 1990).

The levels of ASAT and ALAT were determined in 0.5 ml blood, taken by orbital-puncture with an intact hematocrit capillary (Van Herck *et al.*, 1991, 1992), using standard laboratory equipment and techniques at 30°C (Automated analysis, Boehringer Mannheim GmbH, Mannheim, Germany).

To establish the value of the serum ASAT and ALAT levels as a measure of liver damage in our model, the activities were measured in tumor CC531 and the liver of 13 rats. Two months after subcutaneous tumor implantation, the tumor without central necrosis, and the left lateral lobe of the liver were isolated. The analysis was carried out on tissue samples homogenized in water (1:10, wt/wt) and suspended in saline (1:10 vol/vol). Tissue protein was measured using the method of Lowry *et al.* (1951).

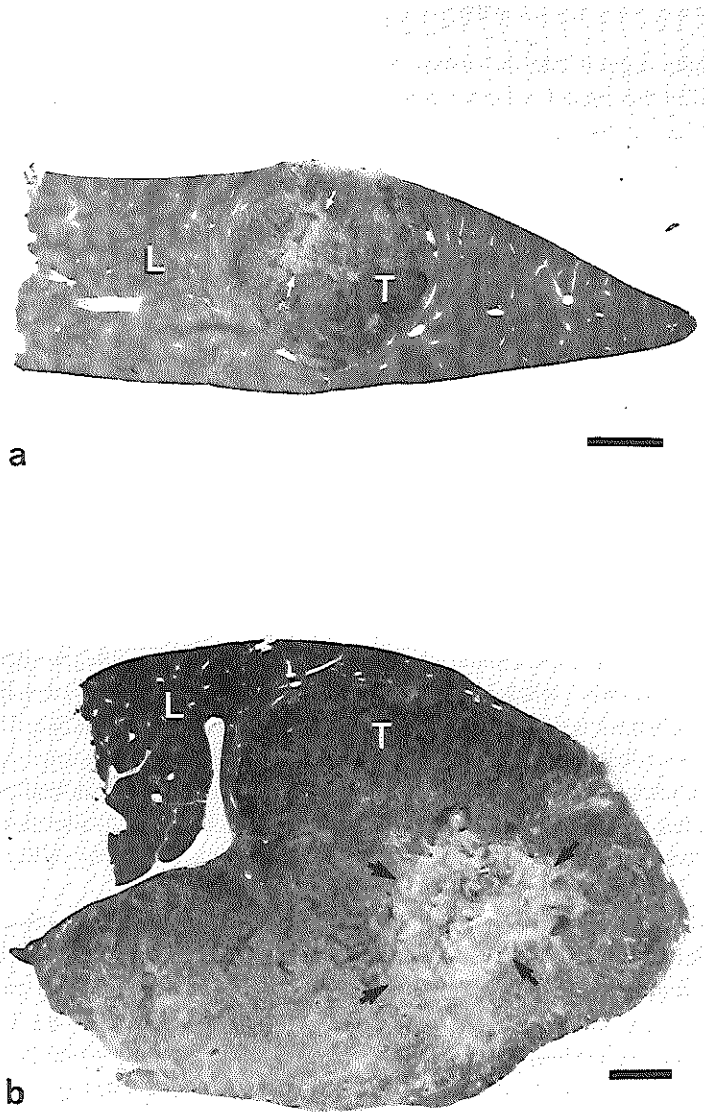


Figure 2.4. Histological sections of tumor CC531 in the liver. (a) 20 days after intrahepatic implantation of a 2 mm³ piece of tumor. (b) Massive outgrowth in a sham treated tumor on day 56 after implantation. The lighter areas in the tumor represent necrosis; central necrosis is indicated by arrows. Bar: 2 mm. T, Tumor; L, Liver (hematoxylin, azophloxin & saffron stain).

The mean \pm SEM ASAT level was found 560 \pm 56 iU/mg protein for liver and 245 \pm 10 iU/mg protein for tumor, resulting in a ratio liver to tumor of 2:1 (Table 2.1). The ALAT level was 313 \pm 46 iU/mg protein for liver and 8.2 \pm 0.3 iU/mg protein for tumor, yielding a ratio of 40:1 (Table 2.1).

These results suggest that the serum ALAT level is the most appropriate parameter for liver damage in this model, whereas serum ASAT may also have a substantial contribution from leakage out of the damaged tumor. However, it has to be noted that the serum level is influenced by unknown factors, such as the degree to which the enzymes are released from either tumor or liver, as well as enzyme inactivation and plasma clearance.

Table 2.1. Mean \pm SEM values of ASAT/ALAT in liver and tumor (in iU/mg protein).*

Enzyme	Liver	Tumor	Ratio
ASAT	560 \pm 56	245 \pm 10	2:1
ALAT	313 \pm 46	8.2 \pm 0.3	40:1

*n=13 for liver and n=11 for tumor.

Antipyrine Clearance Test. Antipyrine (phenazone) clearance has been found a useful method of assessing the functional hepatic parenchymal mass in humans (Luoma & Sotaniemi, 1981; St Peter & Awni, 1991). The major site of antipyrine metabolism is assumed to be the liver. Furthermore, the use antipyrine, is based on the low protein binding and low extraction ratio, which would result in a total body clearance relatively unaffected by binding or changes in hepatic blood flow (Vessell *et al.*, 1975; Blaschke, 1977).

Antipyrine in a dose of 100 mg/kg body weight was administered by penile vein injection, and blood samples of 0.5 ml were collected under ether anesthesia by orbital puncture 1, 2 and 4 hours after administration. The plasma elimination half-life ($T_{1/2}$) was then determined from antipyrine levels measured by high-pressure liquid chromatography (HPLC) according to Shargel *et al.* (1979).

To analyze the value of this test in our model, antipyrine clearance was determined in 15 rats on the first and second day after either 30% or 60% partial hepatic resection. For that purpose the relation between body weight and liver weight (subdivided into the three main rat liver lobes) was previously determined in a separate group of 10 rats. In this group mean \pm SEM body weight was 229 \pm 4 g. The liver (9.1 \pm 0.2 g) took up 4.0 \pm 0.1% of the body weight, divided equally over the three main lobes (right lateral, 3.0 \pm 0.1 g; median 3.1 \pm 0.2 g; left lateral 2.9 \pm 0.1 g).

The 15 animals were randomly assigned to 3 groups of 5 animals each. Before resection, the body weight was determined in all animals (229 \pm 7 g). Resection was carried out following a modified procedure described by Higgins & Anderson (1931). In 2 experimental groups either the median lobe was resected or both the median and right lateral lobe were resected. The wet weight of the resected liver was determined to define the portion of the total liver (4% of the individual body weight). On average 30% and 60% of the hepatic mass

Table 2.2. Mean \pm SEM antipyrine plasma elimination half-life ($T_{1/2}$) levels on the first and second day after partial hepatic resection.

Resection lobe(s)	No. of animals	Portion of liver (%)	$T_{1/2}$ (h)	
			Day 1	Day 2
Control*	5	0	1.3 \pm 0.0	1.2 \pm 0.0
Median	5	28.8 \pm 1.3	3.4 \pm 0.4	2.6 \pm 0.5
Median + Right lateral	5	61.2 \pm 2.9	5.8 \pm 0.9	4.7 \pm 1.1

*Controls underwent a sham treatment (laparotomy and liver manipulation) without any liver resection.

were resected in each respective experimental group (Table 2.2). The animals in the third group served as controls and underwent a sham treatment (laparotomy and liver manipulation) without any liver resection. Regression analysis showed a good correlation between the percentage of hepatic resection and the antipyrine plasma elimination $T_{1/2}$ levels on day 1 ($r=0.85$, $P<0.001$) and day 2 ($r=0.71$, $P=0.03$) post-resection.

In conclusion, antipyrine plasma elimination $T_{1/2}$ levels increased according to the reduction in hepatic mass. These results suggest that antipyrine clearance, measured on the first or second day post-treatment, may be a good parameter to detect loss of liver function, supporting previous observations by Poulsen (1985). Minor changes in liver function, however, may not be detected with this test. It has to be noted that intrahepatic tumor growth has been found to reduce antipyrine clearance (Homeida *et al.*, 1979; Noda *et al.* 1989). This may explain the higher antipyrine $T_{1/2}$ values in the control animals with intrahepatic tumor implants (following chapters), compared with the values found in this chapter. Recent clinical studies, however, show similar antipyrine metabolism in patients with metastatic liver disease and controls (Robertz-Vaupel *et al.*, 1992; Grieco *et al.*, 1992). The differences in control antipyrine $T_{1/2}$ values between the various chapters may be explained by monthly variations in the antipyrine clearance, which has been reported up to a factor of 3 (Bélanger *et al.*, 1984).

PART II

THERMAL THERAPY

3. Fundamentals of Laser Medicine

INTRODUCTION

Normal light sources (e.g., light bulb or sun) produce white light of many different wavelengths, propagating in many different directions. Laser light has three unique qualities:

1. All waves are of the same wavelength (monochromatic).
2. The waves are in phase with each other (coherent).
3. The waves are exactly parallel to each other (collimated).

These properties enable reliable and direct transmission of high amounts of energy over long distances (Absten, 1991; Lipow, 1986).

The word "laser" is an acronym that stands for *light amplification by stimulated emission of radiation*. The possibility of laser action was first suggested by Albert Einstein (1917). In 1954, Charles Townes and colleagues at Columbia University New York built the forerunner of the laser, a *microwave amplifier*, the so called "maser" (Gordon *et al.*, 1954, 1955). At about the same time Basov & Prokhorov (1955) at the Lebedev Institute Moscow independently produced a maser. A few years later, Schawlow & Townes (1958) laid the theoretical foundation for the laser, then referred to as an "optical maser". The first working laser was the ruby laser created by Theodore Maiman (1960). This laser consisted of an active medium of chromium ions contained in a ruby crystal, emitting light of 694 nm. In rapid succession, a variety of other laser media were reported and accordingly many wavelengths became available (Kastler, 1985) (Figure 3.1).

Medical applications of these lasers were investigated extensively during the sixties and resulted in increasing clinical use in the seventies. Cutaneous procedures were pioneered by Goldman *et al.* (1964), who treated a variety of skin tumors, such as melanoma and basal cell epithelioma. Ophthalmologists were among the first to use the selective absorption of Argon laser light in treating ablatio retinae (Zweng & Flocks, 1967). At the same time Yahr & Strully (1966) discovered the cutting abilities of the CO₂ laser. The early CO₂ lasers were quite large, required water cooling and were not easy to handle. Polanyi *et al.* (1970) developed the micromanipulator coupled to an operating microscope. This device allowed delivery of the laser beam to previously inaccessible areas and initiated the use in laryngeal surgery (Jako, 1972; Strong *et al.*, 1973). Short thereafter, CO₂ laser procedures were adapted in the other medical specialties. In gynecology, Bellina (1974) treated condylomata and vaginal adenosis and Baggish (1980a) used the CO₂ laser for vaporization of early cervical

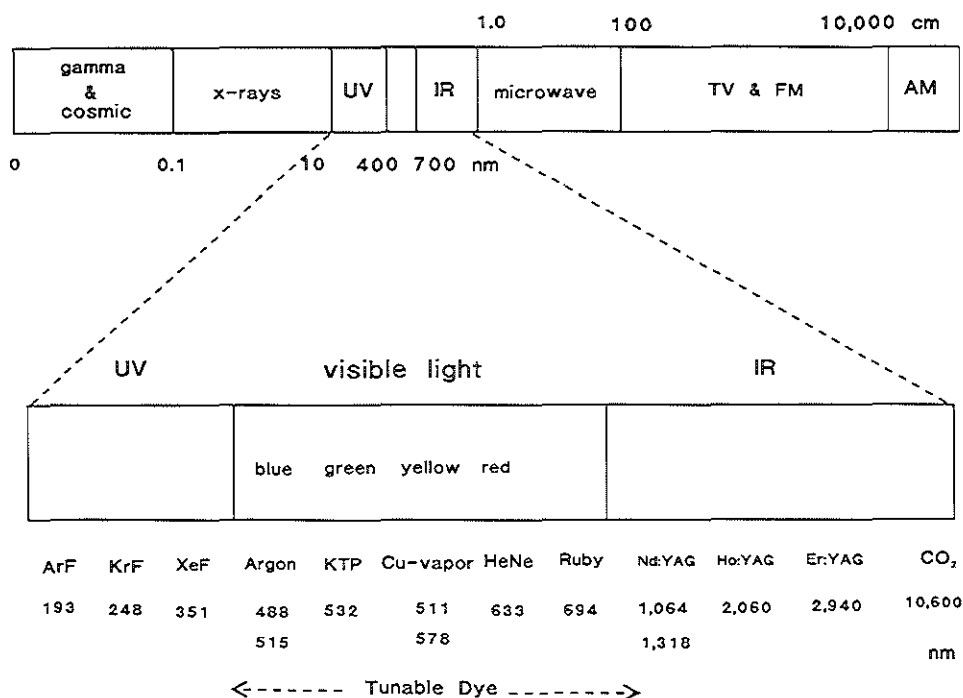


Figure 3.1. Electromagnetic spectrum and wavelengths of the most important medical lasers. UV, ultra violet; IR, infra red. (Adapted from: Polanyi, 1985; Chemaly jr., 1989).

neoplasia. The major advantages of the laser techniques were a high precision of tissue removal, which resulted in sparing of normal tissue and rapid healing with minimal scar formation (Baggish, 1980b). In neurosurgery, the high precision of the CO₂ was exploited by Heppner & Ascher (1977) for excision of brain tumors. Nath (1972), constructed a flexible quartz fiber cladded with teflon for transmittance of Nd:YAG and Argon laser light. The advantages of flexible fiber optics were further explored by Kiefhaber (1977), who was the first to use the Nd:YAG laser for endoscopic tissue coagulation.

Currently lasers are used in almost any medical specialty and several applications have become the standard therapy. Research has shifted towards a more fundamental understanding of the interactions with biological tissue in order to allow treatment planning, optimize laser procedures and invent new techniques. This chapter describes the fundamentals of laser light generation as well as the interaction with living tissue and the principles of thermal therapy. The fundamentals of Photodynamic therapy (PDT) will be described in detail in Chapter 7.

LASER PHYSICS

Molecular basis

In an atom, electrons encircle the nucleus at a distance (orbit) determined by their energy state. The further this orbit from the nucleus, the higher the energy state. When an electron collides with a photon of an energy equalling the required energy for a next orbit, it absorbs the photon and moves to that orbit (Figure 3.2a). This situation, however, is unstable and the electron will return to its ground state under release of a photon, a process called spontaneous emission (Figure 3.2b). The energy quantum of the emitted photon is determined by the energy difference between the two orbits ($E_1 - E_0$):

$$E_1 - E_0 = h \nu$$

where h is Planck's constant (6.6262×10^{-34} J s) and ν the frequency of the radiation. The possible energy states are characteristic for each matter and accordingly the wavelength (λ) of the emitted light is determined by the type of atom excited:

$$\lambda = c / \nu$$

where c is the velocity of light (3×10^8 m/s).

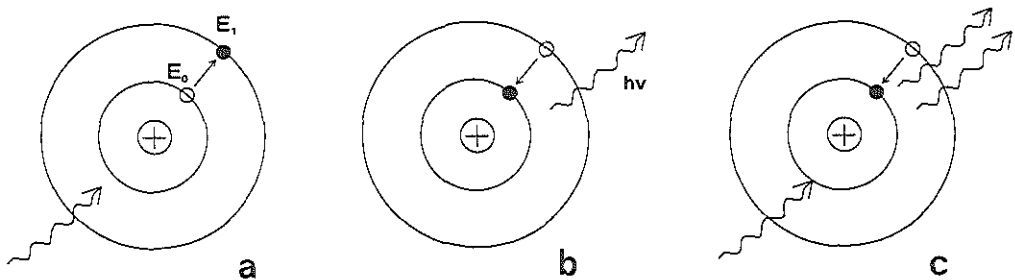


Figure 3.2. In an atom, electrons encircle the nucleus at an orbit determined by their energy state ($E_0 < E_1$). (a) An electron absorbs a photon and moves to the next orbit. (b) This situation is unstable and the electron will return to its ground state under release of a photon (Spontaneous Emission). (c) In Stimulated Emission a photon stimulates an excited electron to undergo orbital decay under emittance of an identical photon. The photons have equal wavelengths and leave the atom in phase.

Stimulated emission

Spontaneous emission is uncoordinated and therefore the released photons are out of phase relative to each other. In stimulated emission an external power source creates a situation called "population inversion", where more of the atoms in a medium are excited than in the ground state. This situation is unstable as well and at a certain moment some atoms may release their photons. Such a photon can stimulate an electron in an excited orbit to undergo a stimulated decay to the ground state under emittance of an identical photon (Figure 3.2c). The original photon and emitted photon have equal wavelengths and leave the atom in phase. In a lasing medium, this process initiates a cascading wave of reactions in which the photons are released at the same moment.

Laser medium

Laser media are mostly prepared to emit light of a single predominant wavelength. The lasing medium may be either gas, solid or liquid. Most often, electrical current is used to pump gas lasers, while incoherent optical flash lamps are used for solid state lasers. Tunable dye lasers contain organic liquid media and are usually pumped by a coherent optical source (e.g., Argon-pumped dye laser). CO₂ and Argon are the most commonly used gas media. An example of a solid state medium is the Neodymium:Yttrium-Aluminum-Garnet (Nd:YAG) crystal.

If a medium consists of a single element suspended in a solid crystal (e.g., Neodymium in YAG) or within a mixture of gasses, the laser light is generated as described above. When the medium consist of several atoms joined by chemical bonds (e.g., CO₂) the energy absorption and photon release may be mediated by other structures such as the atom bond.

The light produced by stimulated emission is already coherent and monochromatic. To create a collimated beam, the produced light is reflected in a resonator chamber between two mirrors, one of which is partially reflective to allow exit of the parallel waves (Figure 3.3). Other waves are lost to the surrounding laser cavity.

LASER TISSUE INTERACTION

Tissue optical properties

When a laser beam is aimed at a tissue layer, four interactions may occur (Polanyi, 1985) (Figure 3.4):

1. A certain fraction of the incident power is reflected from the tissue surface.
2. Some of the penetrating radiation is transmitted through the tissue.
3. Inside the tissue the remaining rays are repeatedly scattered.
4. Finally these remaining rays are absorbed by a tissue chromophore.

Light scattering originates from the inhomogeneous structure of the tissue and is determined by the variations in particle size and index of refraction between different parts of the cell itself and between cells and surrounding media (Fisher, 1985). Laser effects are caused by those rays that are absorbed.

Because of the events described above, the fluence ($\phi = W/cm^2$) parallel to the axis of the

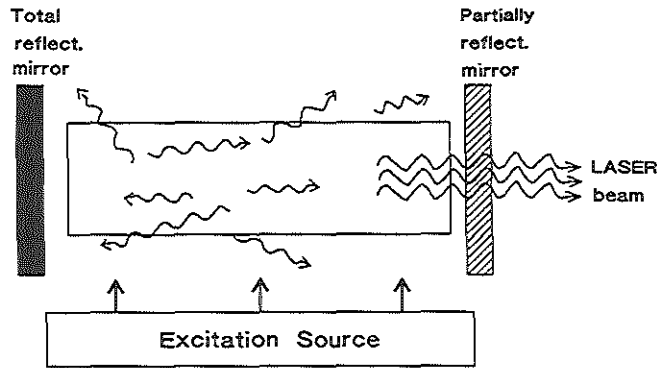


Figure 3.3. To create a collimated beam, the photons are reflected in the resonator chamber between two mirrors one of which is partially reflective. Only the parallel waves leave the chamber as the laser beam.

incident laser beam can have a maximum value just on the tissue surface or, depending on the scattering properties of the tissue and the spot size of the laser beam, below the tissue surface (Marijnissen & Star, 1987; Jacques, 1992). The fluence of the collimated transmitted light at a certain point in the tissue is given by Beer's law:

$$\phi = (I_i - I_r) e^{-Az}$$

where I_i is the irradiance on the beam axis just outside the tissue; I_r is the irradiance reflected from the surface on the beam axis, e is the base of the natural logarithm; z is the distance below the tissue surface measured along the beam axis (cm), and A is the attenuation coefficient, which consists of the tissue absorption coefficient μ_a (cm^{-1}) and scattering coefficient μ_s (cm^{-1}):

$$A = \mu_a + \mu_s$$

The penetration depth is usually defined as the depth at which the light intensity is reduced by a factor of e^{-1} ($\pm 37\%$):

$$z = 1 / (\mu_a + \mu_s)$$

Beer's law model yields good results in cases where absorption strongly dominates

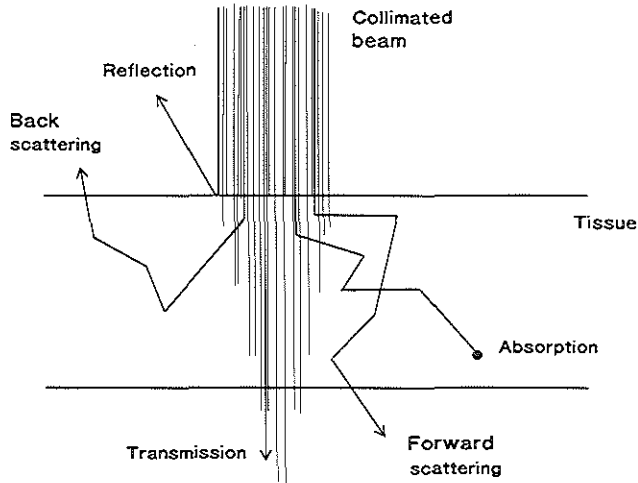


Figure 3.4. A collimated beam that is aimed at a tissue layer has a maximum intensity just outside the tissue surface. Immediately below the surface this value is lower because of reflection and further into the tissue as a result of scattering and absorption. A small fraction is transmitted through the tissue.

scattering. However, in case of significant scattering (for visible and near infra red [IR] wavelengths) the description is much more complicated and requires inclusion of the scattering component (Welch *et al.*, 1989). Thus, the approximation should also assume:

1. Multiple scattering of photons.
2. Anisotropy in the scattering behavior (Jacques *et al.*, 1988; Flock *et al.*, 1987).

The anisotropy factor, g , is the average cosine of the scattering phase function. As g approaches 1.0, more light is scattered forward into the propagating path. *In vitro* measurements have shown an anisotropy factor of 0.80-0.95 for most biological tissues (Cheong *et al.*, 1990). This highly forward scattering suggests that a considerable amount of scattered light is in the same direction as the collimated beam. Often the reduced scattering coefficient (μ_s') is used, defined as:

$$\mu_s' = \mu_s (1 - g)$$

In conclusion, the scattering coefficient, absorption coefficient and the anisotropy factor are important determinants for light distribution in the tissue (Chapter 11).

Laser parameters

Wavelength. The absorption of optical radiation is strongly wavelength dependent (Figure 3.5). Therefore, the effects of laser light upon tissue are largely determined by the laser type

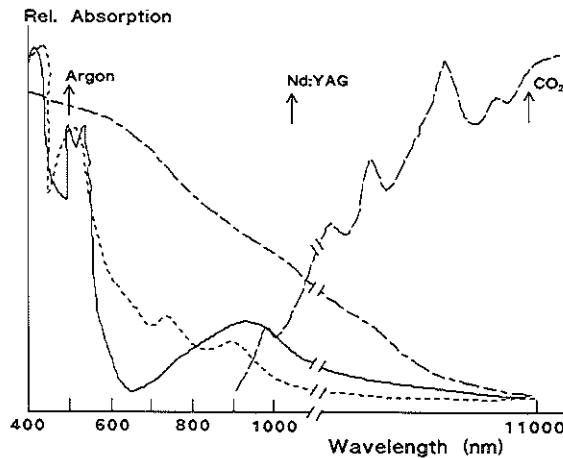


Figure 3.5. Relative absorption (log scale) as a function of laser wavelength. Hemoglobin (---); Oxyhemoglobin (—); Melanin (— · —); Water (— — —). The main Argon laser wavelengths (488 and 514.5 nm) are near the absorption peaks of oxyhemoglobin at 410, 542 and 577 nm. The Nd:YAG laser wavelength of 1,064 nm is between the major absorption peaks, whereas the CO₂ wavelength (10,600 nm) is strongly absorbed by water. (Drawn after: Gijsbers *et al.*, 1984; Fisher, 1985; Haina & Landthaler, 1988).

applied. In the IR region, the CO₂ laser with a wavelength of 10,600 nm is highly absorbed by water, which means that in most tissues the effect is very superficial and localized. In this case absorption completely dominates scattering.

In the near IR, the Nd:YAG laser with a wavelength of 1,064 nm is minimally absorbed by water. Instead, it is absorbed by tissue chromophores. The Nd:YAG laser penetrates tissue up to 10 mm and is highly scattered, so that its light is distributed over a large tissue area.

In the visible spectrum, the Argon laser wavelengths (514.5 nm, 488 nm) are close to the major absorption peaks of hemoglobin (410, 542 and 577 nm).

The tunable liquid dye laser may use one of the different organic dyes, each emitting wavelengths in a spectral band of about 100 nm in width. The emission must be either filtered or tuned to isolate a monochromatic wavelength. In this way all wavelengths of the visible spectrum can be covered (Figure 3.1). The dye laser is mainly used in PDT at a wavelength of 600-700 nm, corresponding to the specific absorption peak of the photosensitizer applied (Part III).

Light Delivery. The CO₂ laser has a wavelength that is absorbed by the optical fibers currently available. Therefore, transmission still requires a rigid system of articulating arms with mirrors. This hinders endoscopic application, but has the advantage that the light emerges collimated and can be focused with higher precision than the diverging beam. The

CO₂ laser is mostly used in conjunction with a focusing lens or micromanipulator coupled to a microscope.

The Nd:YAG, Argon and tunable dye wavelengths can be transmitted through a quartz fiber. The advantage of fiber optic transmission is the flexibility, which allows easy access to the treatment site. An optical fiber transmits light through series of multiple internal reflections along the inner wall, and the light leaves the fiber with a divergence of 10° to 12° (Absten, 1991). This diverging beam may be used for superficial illumination of larger tissue areas. If a small spot is required for high precision application, a focusing lens can be placed in front of the fiber tip. In such case, the spot size over which the power is divided, is an additional important parameter (Figure 3.6). The effects are maximal in *focus*, and decrease with distance from the target in *defocus*. In *prefocus*, the maximal effect is at a deeper level below the tissue surface. In the noncontact application, an important parameter is the irradiance:

$$\text{Irradiance (W/cm}^2\text{)} = \frac{\text{Power (W)}}{\text{Spot Size (cm}^2\text{)}}$$

For deep tissue treatment, the bare fiber may also be implanted directly into the tissue (interstitial therapy). In interstitial therapy, a more homogeneous light delivery can be obtained by using a diffusing fiber end (Chapter 6, 8). In case of a cylindrical diffuser, the power is expressed per length of the emitting fiber end (W/cm).

For contact cutting or vascular recanalization, a contact probe may be used in combination with a Nd:YAG laser. These probes are made of synthetic sapphire or ceramic and were initially thought to focus the beam to the place of tissue contact. In this way, laser effects would be more localized due to reduced scattering and light penetration. However, it has become clear that the laser rather serves as the energy source to heat the crystal and the effects are predominantly from direct heat. In fact, new crystals do not produce the desired tissue effect until blackened (Absten, 1990; Verdaasdonk *et al.*, 1991). Thus, the probe works like a hot knife and allows precise tissue destruction with minimal lateral damage. However, the procedure is relatively slow, hemostasis is compromised and the advantages of no-touch surgery are lost.

Laser Energy. The laser energy (Joules) can be controlled by adjusting either power output (Watts) or exposure time (seconds):

$$\text{Energy (J)} = \text{Power (W)} \times \text{Time (s)}$$

Laser light can be delivered in a continuous wave or in pulsed or superpulsed mode. In the pulsed mode, the light is released for a limited period of time and the tissue is allowed to cool down during the interval between the pulses. The faster the energy is delivered, the more precise the thermal effects will be, with less chance for thermal spread to adjacent tissue.

Tissue Cooling. In the noncontact application the maximum temperature rise will occur at the tissue surface. Tissue cooling (e.g., with a water-jet, Chapter 5) will shift the location

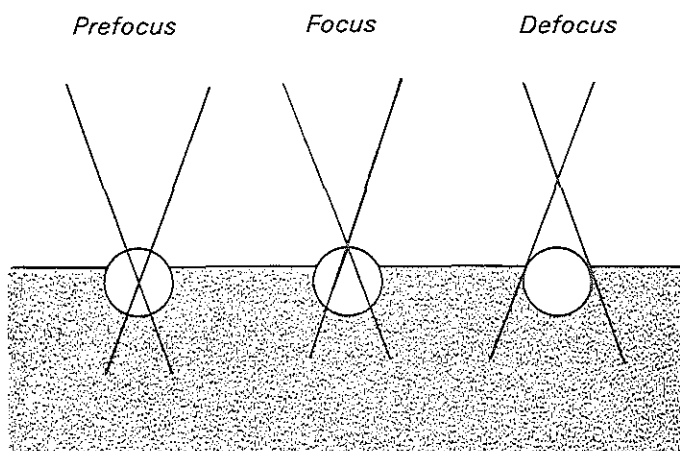


Figure 3.6. Schematic representation of the various focus modes on a spherical tumor in the liver. In *prefocus* the focal point lies behind the tissue surface; In *focus* the laser beam is focussed on the tissue surface and in *defocus* the focal point lies in front of the tissue.

of the maximum temperature to a point located within the tissue (Svaasand *et al.*, 1985). As Nd:YAG light is transmitted through water, no-touch bare fiber coagulation can be performed under saline, providing the necessary heat dissipation. This exciting application has already been used in laparoscopic, cystoscopic and hysteroscopic procedures.

POSSIBLE TISSUE EFFECTS

Upon absorption by a tissue chromophore, laser energy can cause different effects (Jacques, 1992) (Figure 3.7):

1. At very low powers it may trigger specific photochemical (e.g., PDT, Chapter 7) and metabolic reactions.
2. At higher powers, heat production becomes important, causing thermal tissue destruction (e.g., coagulation or vaporization).
3. At extremely high peak powers in the tissue may explode the material even before heating occurs (ablation).

Light distribution is determined by the laser parameters and optical properties of the tissue. As heat is generated upon light absorption, this step depends on the absorption coefficient. Heat transfer, determined by the thermal properties, plays a significant role at longer exposure times (Figure 3.7).

Low-power Helium Neon (HeNe) lasers (632.8 nm) have received much attention for their

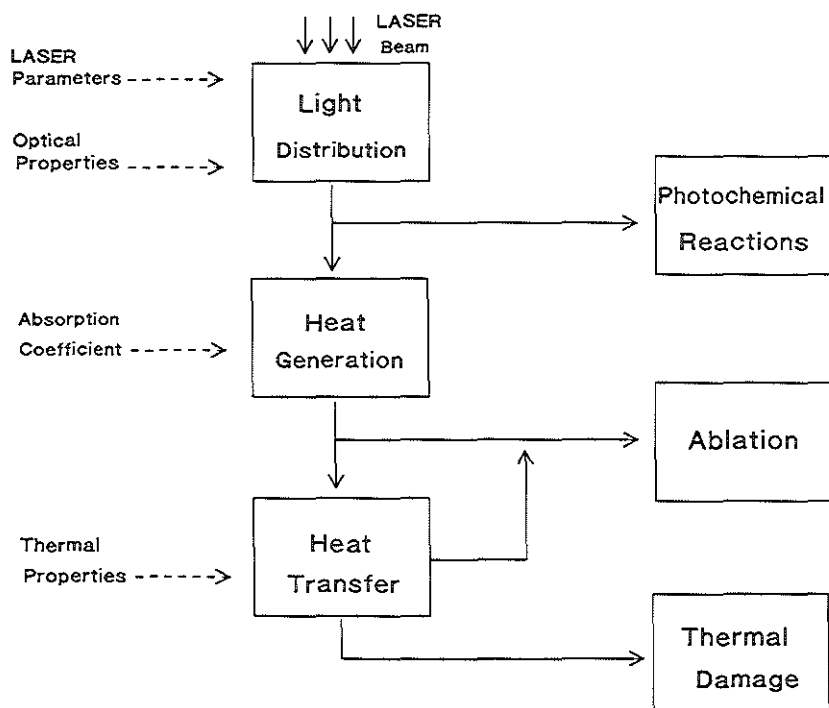


Figure 3.7. Block diagram of the possible effects of laser-tissue interaction. Laser energy can cause photochemical, photomechanical or thermal reactions. Light distribution is determined by the laser parameters and optical properties of the tissue. Heat generation depends on the absorption coefficient. Heat transfer, determined by the thermal properties, plays a significant role at longer exposure times. (Drawn after: Welch *et al.*, 1989; Mordon *et al.*, 1987).

ability to stimulate wound healing and collagen production in a wide variety of conditions, such as decubitus ulcers (Mester *et al.*, 1985). Different effects may be induced by other wavelengths, for example inhibition of DNA synthesis with Nd:YAG light of 1,064 nm (Castro *et al.*, 1983). The low-power application, however, remains controversial and the mechanism of action is still unclear (Basford, 1989).

Photomechanical responses occur during application of extremely high fluence rates (greater than 10^8 W/cm²), which produce shockwaves and plasmas (i.e., free electrons and ionized particles, released from the irradiated tissue; Boulnois, 1986). Shockwaves generated with exposure durations of 1.0 μ s and less, give rise to the photomechanical reaction that may fragment biliary or kidney stones (Thomas *et al.*, 1988).

Lasers with high photon energies that operate in the UV, such as the excimer (excited

dimer) at 193-351 nm, may be used to disrupt tissue by chemical bond breakage (Lipow, 1986). There has been considerable interest in the ArF excimer laser (193 nm) for corneal reshaping (Cotliar *et al.* 1985) and the XeCl (308 nm) excimer laser for angioplasty (Frazier *et al.*, 1992). The 0.5-1.0 μm penetration depth at 193 nm produces a sharp and extraordinary fine cut with less than 1 μm of thermal damage (Marshall *et al.*, 1985). Although excimer photoablation is not termed a thermal process, temperatures of several thousand degrees may occur (Srinivasan, 1986; Gijsbers *et al.*, 1991). The heat is carried away by the ablated material before the residual tissue is heated (Figure 3.7).

THERMAL THERAPY

Thermal Tissue Properties

The thermal properties of living tissue are basically determined by three different mechanisms (Svaasand *et al.*, 1985):

1. Heat transport by thermal conduction
2. Heat storage
3. Heat transfer through the vascular system

The thermal conduction of energy is initiated by the spatial temperature variations; heat will flow from the hotter to the colder regions. The lowest conductivity is found for adipose tissue and the highest for tissue with high water content (Welch, 1984). Thermal energy may also be transported out of the irradiated region by blood perfusion, depending on the perfusion rate of the tissue. The importance of this factor increases with increasing exposure time.

The majority of the current medical procedures involve thermal reactions and the desired end points are either coagulation or tissue ablation/vaporization. The next section will shortly discuss the principles of thermal laser therapy.

Thermal Tissue Destruction

Thermal tissue destruction depends on temperature rise and irradiation time. During heating, many thermal changes occur simultaneously in the tissue. Although, a global division can be made according to the temperature reached (Table 3.1). At temperatures of 40-45°C, deactivation of cellular enzymes may cause reversible damage, that becomes irreversible after exposure from 25 min to several hours. At temperatures of 60-140°C, vaporization of tissue water, cell shrinkage, hyperchromasia (increased intensity of staining), membrane rupture, protein denaturation and hyalinization of collagen have been reported. The tissue is coagulated which can be observed macroscopically by blanching. Explosive vaporization of extracellular steam vacuoles ("popcorn" effect) may occur at further heating. Finally, at temperatures of 300-1000°C, tissue ablation and carbonization occur, causing increased light absorption and smoke generation (Thomsen, 1991; Welch *et al.*, 1991).

Thermal Ablation/Vaporization

The mechanism of thermal ablation relies on rapid energy transfer from the laser beam to the cell. The CO₂ laser with its high absorption in water is mostly used for this purpose. The

Table 3.1. Tissue temperature and histopathologic effect.*

Temperature (°C)	Physical effect	Optical effect	Biological effect
40-45	Heating	None	Enzyme deactivation
60-140	Protein denaturation	Blanching Increased scattering	Cell shrinkage, hyperchromasia, membrane rupture, pyknosis, hyalinization of collagen
100-300	Water vaporization	"Popcorn" effect	Extracellular steam vacuole, cell shrinkage
300-1000	Carbonization Ablation	Charring, smoke Increased absorption	Ablation, vaporization, carbonization

*From: Thomsen, 1991; Hunter & Dixon, 1985; Mathus-Vliegen, 1988; Welch *et al.*, 1991.

cellular water is assumed to be superheated, which causes complete destruction of cellular proteins and an immense pressure build-up within the cell (Fischer, 1985). This results in instantaneous flash boil and vaporization; the cell explodes which can be observed by steam and debris rising from the impact site as the laser plume. Thus, the CO₂ laser can be used to remove a cell layers with great precision. However, coagulation and accordingly hemostasis is relatively poor, due to the shallow tissue penetration. The CO₂ laser has been used especially in laryngeal surgery, neurosurgery, gynecology and dermatology where precise cutting or ablation is required.

The Nd:YAG laser may be used for vaporizing larger tissue areas, combined with better hemostasis. As soon as the tissue is carbonized, vaporization occurs due to efficient Nd:YAG light absorption by the charred material, with rapid increase in local tissue temperature. In oncology, thermal laser vaporization may be used to remove cells at various sites of either superficial or exophytic lesions, such as protruding tumors in the lumen of oesophagus, bronchus or colon (Murray *et al.*, 1992).

Coagulation

Coagulation mainly destroys cells by denaturing the protein, which may be compared with the process of heating egg white. In the visible spectrum, the Argon laser wavelengths are close to the major absorption peaks of hemoglobin (Figure 3.5). Therefore, the Argon has been used for selective coagulation of vascular lesions such as portwine stains and hemangiomas (Noe *et al.*, 1980; Van Gemert *et al.*, 1982; Mordon *et al.*, 1993). In ophthalmology a major application has been the coagulation of proliferative vessels in diabetic retinopathy; the Argon wavelengths are not absorbed by water, and pass through the cornea and the vitreous humor to be absorbed at the retina (Frank, 1975).

Of importance in oncology is the possibility of coagulating solid lesions combined with sealing of blood and lymphatic vessels. For that purpose, the Nd:YAG is the laser of choice as its light is scattered over a large tissue area, producing a well defined zone of tissue necrosis with a sharp boundary. This enables local tissue destruction in delicate areas with

preservation of the structural integrity of the organ involved. The coagulation necrosis produced by laser is identical on the cellular level to that produced by electrocoagulation. However, the laser provides a more predictable heat distribution within the tissue, since it does not follow the paths of least electrical resistance (Keiditsch, 1981; McKenzie, 1990).

The studies described in this part are all aimed at the selective coagulation of solid tumors within the liver.

4. Noncontact Nd:YAG Laser Treatment

*Adapted from: R. VAN HILLEGGERSBERG, W.J. KORT, M. VERMEIJ & O.T. TERPSTRA.
Treatment of Experimental Liver Metastases with a Noncontact Neodymium:YAG Laser.
J Surg Res 1992; 53: 128-135*

INTRODUCTION

In selected patients with hepatic metastases of colon cancer, surgical resection can substantially improve the survival rate. However, owing to damage to the normal hepatic tissue, this treatment is associated with complications such as bleeding, intra-abdominal sepsis and liver failure (Chapter 1).

These complications may be avoided using the laser, a device that produces highly concentrated monochromatic light, which is transformed into thermal energy upon absorption in tissue (Chapter 3). The Neodymium:Yttrium-Aluminum-Garnet (Nd:YAG) laser with a wavelength that penetrates deeply into tissue has proved to be successful in the treatment and palliation of malignant tumors at various sites (Stern *et al.*, 1988; Joffe & Schröder, 1987; Fleischer, 1989; Dixon, 1988; Schmeller & Hofstetter, 1989). Treatment with the Nd:YAG laser can lead to localized contact-free tumor coagulation coupled with sealing of the blood and lymphatic vessels (Keiditsch, 1986; Hofstetter *et al.*, 1984; Zimmermann *et al.*, 1984; Beisland & Kvernebo, 1986). These features may as such diminish surrounding tissue necrosis, inhibit the spread of tumor cells during operation, and prevent bleeding. Moreover, the possibility to pass the light beam down a flexible optical fiber enables treatment through a laparoscope.

The aim of this study was to assess the effects of the Nd:YAG laser upon tumor tissue in the liver, using a noncontact modality with a focussing handpiece. The relationship between total energy delivered and the extent of tissue damage was investigated as well as the healing of the lesions after laser treatment.

MATERIALS AND METHODS

Experimental Design

Fifteen animals were used for the experiments. Twenty-two days after intrahepatic implantation of 3 pieces of tumor in each rat (Chapter 2), a relaparotomy was made and the visible diameter of the tumor was measured using sliding calipers. The tumors were then treated with previously fixed laser energy and power setting. Immediately after laser treatment and 1, 2, 4, and 8 days later 3 animals were sacrificed and the livers isolated for light microscopical evaluation. An ocular scale was used to measure maximal depth and width of the tumor and the tissue damage.

Laser Application

A Nd:YAG laser (Medilas 40N, MBB-Medizintechnik GmbH, München, Germany), producing light with a wavelength of 1,064, nm was used. The laser beam was transmitted through a 0.6 mm glass fiber and a handpiece with a focal distance of 50 mm. A noncontact technique was used. The beam was focused on the center of the tumor sphere, using a stand on which the handpiece was fixed at a right angle to the tumor surface.

The three tumors in each animal were treated at a power output of 20 W and energies (Joule = Watts x seconds of exposure) of either 60, 120 or 180 J, respectively. A repeated pulsed mode, 0.5 s exposure with a pause of 0.3 s, was used to allow tissue cooling during the time pauses. The surrounding tissue was protected from dehydration with a gauze soaked in saline solution.

Statistical Analysis

Values are expressed as mean \pm standard error of the mean (SEM). Multiple linear regression methods were used to analyze the relation of the amount of Joules delivered to the depth and width of damage and ablation. Mean values of days 1 and 2 post-treatment were used. A significant relation was considered at *P* values of <0.05 .

RESULTS

On the day of laser treatment, 22 days after tumor implantation, the mean \pm SEM visible tumor diameter was 5.4 \pm 0.2 mm. Two tumor implants in different animals did not take and another two could not be treated due to adherence to the diaphragm. During treatment the laser effect was macroscopically visible by blanching of the tissue in the case of coagulation and black coloring with smoke development in the case of carbonization with tissue ablation at longer exposure times.

All animals survived the procedure and no bleeding occurred.

Histopathology

In general, light-microscopic examination on different days after laser treatment showed several zones of tissue destruction (Figure 4.1):

1. A superficial crater of ablated tissue.
2. A small zone of black coloring carbonized tissue, covering the superficial crater.
3. A thin layer of cavities separated by structureless coagulated tissue, intensely staining with azophloxin.
4. A zone of heat coagulation, consisting of elongated, distorted cells with densely coagulated cytoplasm and pyknotic nuclei.
5. From days 1 to 8 post-treatment, a broad surrounding zone of thermally damaged cells with acidophilic cytoplasm and pyknotic nuclei.

If vital tumor tissue had remained it was located at the tumor margins and was sharply demarcated from zone 5.

In sections taken from animals sacrificed immediately after laser treatment, zones 1 to 3 were clearly visible. However, it was difficult to identify zone 4, and zone 5 could not be distinguished. By day 1, zone 5 had become apparent around the coagulated tumor cells and a polymorphonuclear inflammatory infiltrate had developed around the entire necrotic area. On day 2, findings of the first four zones were approximately equal to those on day 1. Zone 5, however, had begun to disintegrate as a result of cytolysis, characterized by cells with nuclear fragmentation and an infiltration of polymorphonuclear leukocytes and macrophages. By day 4 the necrotic lesion had become swollen due to the development of edema. The zone of thermally damaged cells (zone 5) was massively infiltrated by inflammatory cells, whereas

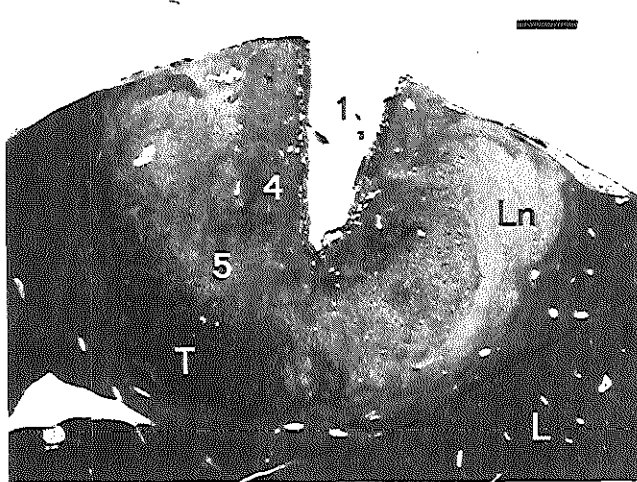


Figure 4.1. Histological section of a tumor 1 day post-laser treatment with 180 J at 20 W, repeated pulsed mode: 0.5 exposure, 0.3 s pause between exposures. The numbering corresponds to the numbering used in the text: 1, Superficial crater, covered with carbonized tissue underlain by the cavitation layer; 4, Heat coagulation necrosis; 5, Zone of thermally damaged cells; T, Vital tumor tissue; Ln, Liver necrosis; L, Normal liver tissue. Bar: 1 mm (hematoxylin, azophloxin & saffron stain).

the zone of heat coagulation necrosis (zone 4) had remained relatively intact. The superficial crater was transformed and filled with cellular debris and fibrin deposits. Early signs of granulation tissue were apparent around the edge of the lesion. On day 8, a layer of connective tissue encapsulated the necrotic area. There was a fibrotic ingrowth of zone 5 and part of zone 4 with fibroblasts, lymphocytes, macrophages and capillary formation.

Dosimetry

The results of the measurements on the tumor, the crater of ablated tissue and the necrotic tissue, consisting of zones 2 to 5 and eventually a zone of liver necrosis, are shown in Table 4.1. On days 4 and 8 after laser treatment, accurate judgement of the laser effect was hampered by swelling and disintegration of the necrotic area, the formation of cellular debris in the transformed crater, and the development of inflammatory infiltrate and granulation tissue. Immediately post-treatment zone 5 was not visible. For these reasons crater measurements from animals sacrificed on days 4 and 8 are not shown in the table and data from days 1 and 2 were used for the dosimetric study.

The relationship between the depth of tissue necrosis and ablation vs. total energy delivered

Table 4.1. Mean \pm SEM depth and width of the tumor, and ablation and tissue necrosis at increasing periods after laser treatment.

Day (J)	Energy	No. of tumors	Ablation		Necrosis		Tumor	
			Depth	Width	Depth	Width	Depth	Width
0	60	3	0.7 \pm 0.4	1.1 \pm 0.5	2.4 \pm 0.7	4.8 \pm 0.7	5.9 \pm 0.2	5.9 \pm 0.3
	120	3	1.5 \pm 0.8	1.1 \pm 0.6	3.4 \pm 0.5	4.4 \pm 1.0	7.0 \pm 1.1	6.3 \pm 0.4
	180	3	2.0 \pm 2.0	0.6 \pm 0.6	4.6 \pm 1.2	4.9 \pm 1.6	5.6 \pm 0.2	5.8 \pm 0.4
1	60	3	0.5 \pm 0.5	0.7 \pm 0.8	3.2 \pm 0.1	6.3 \pm 0.4	6.4 \pm 0.4	6.5 \pm 0.1
	120	3	1.5 \pm 0.9	1.4 \pm 0.7	4.7 \pm 0.8	5.8 \pm 0.6	5.9 \pm 0.2	5.7 \pm 0.1
	180	3	4.9 \pm 0.9	1.1 \pm 0.2	5.1 \pm 0.6	7.1 \pm 0.4	6.1 \pm 0.2	5.3 \pm 0.3
2	60	3	1.2 \pm 0.9	0.8 \pm 0.5	3.5 \pm 0.5	4.7 \pm 0.5	4.8 \pm 1.5	5.0 \pm 1.0
	120	3	0.9 \pm 0.5	1.2 \pm 0.6	3.8 \pm 0.0	5.0 \pm 1.3	5.2 \pm 1.2	4.7 \pm 1.2
	180	1	3.2 \pm 0.0	1.6 \pm 0.0	5.0 \pm 0.0	6.9 \pm 0.0	3.8 \pm 0.0	2.5 \pm 0.0
4	60	3	Not to be measured		3.7 \pm 0.5	4.5 \pm 1.1	6.9 \pm 1.3	6.8 \pm 0.5
	120	3			3.4 \pm 0.2	5.6 \pm 0.0	6.2 \pm 0.8	5.6 \pm 1.1
	180	3			4.4 \pm 0.3	6.0 \pm 0.9	6.3 \pm 2.0	5.0 \pm 1.2
8	60	2	Not to be measured		2.8 \pm 0.0	3.0 \pm 0.1	6.1 \pm 0.8	6.0 \pm 0.4
	120	3			5.0 \pm 1.0	5.6 \pm 1.1	9.5 \pm 2.8	6.9 \pm 0.9
	180	2			4.1 \pm 1.6	4.1 \pm 1.6	5.8 \pm 0.1	6.3 \pm 0.6

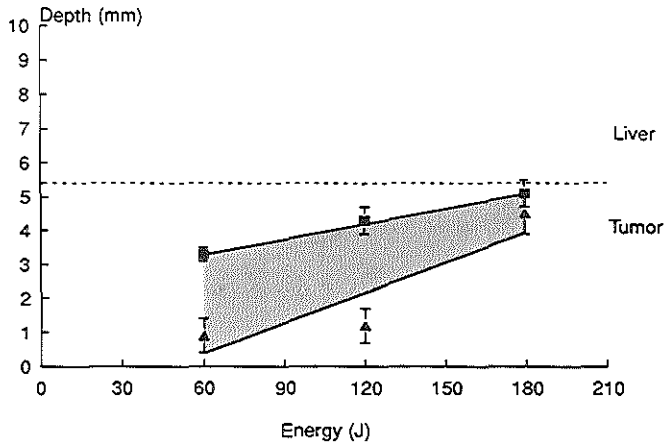


Figure 4.2. Maximal depth of tissue necrosis (■) and ablation (▲) vs. total energy delivered. Each point represents the mean±SEM of the experimental results of days 1 and 2 together. The lines were drawn after calculating the best fitting straight line according to the method of the least squares. The mean depth of the tumor is represented by the striated line. The shaded area represents the necrotic region corresponding to zones 2-5 as mentioned in the text.

for days 1 and 2 post-treatment is shown in Figure 4.2. The mean depth of the tumor is represented by the striated line. The shaded area describes the necrotic region. A linear relationship between laser energy and depth of ablation ($r=0.706$) or depth of tissue damage ($r=0.676$) was found ($P<0.01$). Tumor necrosis and tumor ablation increased with energy delivered. The increase in tumor ablation was stronger than the increase in tissue necrosis, so that at 180 J there was a deep crater of ablated tissue, underlain by a small zone of necrotic tissue. Minimal depth of damage was found at 60 J, with 0.9 ± 0.5 mm ablation and 3.3 ± 0.2 mm necrosis. Treatment at an energy of 120 J showed depth of ablation of 1.2 ± 0.5 mm and necrosis of 4.3 ± 0.4 mm. Maximal depth of tumor ablation and necrosis was found at 180 J, 4.5 ± 0.6 mm and 5.1 ± 0.4 mm, respectively. In three cases, concerning relatively small tumors, a complete in-depth tumor destruction occurred. The average values in Figure 4.2, however, show that total in-depth tumor destruction did not occur in most of the cases as the lines did not reach the striated line.

A non significant relation was found between the width of ablation and the energy delivered ($r=0.239$, $P>0.1$) (Figure 4.3). Width of tissue necrosis showed a significant relationship to laser energy ($r=0.428$, $P<0.05$). The maximal width of necrosis was 7.1 ± 0.2 , found at 180 J. At 60 J and 120 J, values were 5.5 ± 0.4 and 5.4 ± 0.7 , respectively. The width of tumor ablation ranged from 0.8 ± 0.4 mm at 60 J, to 1.3 ± 0.2 mm at 180 J. Complete superficial tumor destruction was found in most of the cases. Damage to the adjacent liver

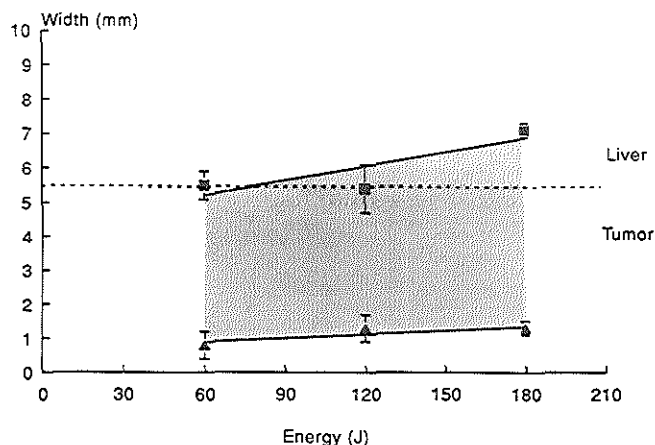


Figure 4.3. Maximal width of tissue necrosis (\blacksquare) and ablation (\blacktriangle) vs. total energy delivered. Each point represents the mean \pm SEM of the experimental results of days 1 and 2 together. The lines were drawn after calculating the best fitting straight line according to the method of the least squares. The mean width of the tumor is represented by the striated line. The shaded area represents the necrotic region corresponding to zones 2-5 as mentioned in the text.

tissue occurred especially at higher energies. This last effect is visible in Figure 4.3, as the line of tissue necrosis appears above the striated line, representing the mean tumor width.

DISCUSSION

The results of this study show the possibility of the noncontact Nd:YAG laser to produce tumor coagulation necrosis with minimal liver damage. No death or bleeding occurred as a result of treatment. A linear relationship between laser energy and depth of tumor damage was found with highest values at 20 W and 180 J. Complete superficial tumor destruction was found. However, total in depth tumor destruction was not accomplished at the given laser parameters.

The appearance of different zones of tumor destruction, as found in this study, is in agreement with other histological studies of Nd:YAG laser effect upon normal tissue (Stern *et al.*, 1988; Brackett *et al.*, 1986). These zones represent the decreasing levels of energy absorbed by the tissue at an increasing radius from the point of maximal laser energy. At temperatures of around 45°C, the cells may be thermally damaged as found in zone 5. When the tissue temperature reaches 60°C, protein denaturation and coagulation occur, resulting in cellular necrosis as found in zone 4. Increase in temperature to 100°C, results in vaporization

of tissue water content, which creates tissue cavities filled with steam (zone 3) and further elevation of temperature leads to tissue carbonization and tissue ablation (zone 1 and 2).

Immediately post-treatment the zone of thermally damaged cells (zone 5) was not visible, and on days 4 and 8 post-treatment histological changes hampered the accurate judgement of the laser effects upon the tissue. From this we conclude that the best histological determination of laser effects can be made on the first or second day post-treatment.

In this study we used a single series of laser exposures with a fixed fiber position to determine the laser effects as standardized as possible. We therefore chose a tumor model in the rat where the mean diameter of the tumor at the time of treatment was 5.5 mm, so that the effects on the tumor and on the adjacent liver tissue could be determined. Larger tumors could only have been treated by moving the fiber along the tissue surface.

The effect of the laser upon tissue depends on many parameters. From the wide range of available types of lasers (wavelengths), the Nd:YAG laser (1,064 nm) has the best coagulating properties and deepest tissue penetration (Chapter 3).

Others have used the contact application or interstitial placement of the bare fiber into tissue to produce necrotic lesions in normal liver tissue (Matthewson *et al.*, 1987; Godlewski *et al.*, 1988). This approach seems very promising in the treatment of deep-seated liver metastases (Chapter 6). For the treatment of superficial tumors, however, the noncontact technique is preferable, avoiding spread of tumor cells and bleeding as a result of tissue manipulation (Nishizaki *et al.*, 1990).

Using the noncontact technique, an important parameter is the focus mode. The maximal penetration of the Nd:YAG laser is 6-10 mm (Stein, 1986; Stern *et al.*, 1988), therefore the beam was focused on the center of the tumor sphere to achieve maximal heat conduction from this point to the tumor margins.

Most studies concern the ablation of tissue at a power output of up to 100 W (Benderov *et al.*, 1987; Nims & McCaughan, 1983; Chevinski & Minton, 1990). As laser ablation of larger areas in highly vascularized tissues often leads to bleeding, in this study a lower output of 20 W was used in order to coagulate the tumor tissue in a controlled and selective manner without ablation or carbonization. For the same reason a pulsed temporal mode was used to allow cooling of the tissue between laser pulses. In most tumors, however, tissue ablation and carbonization occurred, probably resulting in absorption of laser light at these black colored superficial areas. This hindered light transfer into deeper tumor regions. At higher energies this effect was apparent, as the high increase in depth of tumor ablation at these energies was not accompanied by equally high amounts of tissue necrosis (Figure 4.2).

Future studies should therefore use other laser modalities, for example lower power settings with longer exposure durations, in order to avoid charring at the tissue surface to attain a pure coagulative effect. In view of recent work, longer pauses between the laser pulses should probably be applied to allow proper cooling of the tissue (Meijering *et al.*, 1993).

5. Water-jet-cooled Nd:YAG Laser Coagulation

Adapted from: R. VAN HILLEGERSBERG, W.J. KORT, F.J.W. TEN KATE & O.T. TERPSTRA. Water-jet-cooled Nd:YAG Laser Coagulation: Selective Destruction of Rat Liver Metastases. Lasers Surg Med 1991; 11: 445-454

INTRODUCTION

In the previous chapter we investigated the use of the noncontact Nd:YAG laser in destructing colonic tumor deposits in the liver. As laser vaporization of larger areas in highly vascularized tissues often leads to bleeding (Nims & McCaughan, 1983; Schröder *et al.*, 1987; Chevinski & Minton, 1990), we aimed at coagulating the tumor. Indeed at lower laser energies tissue coagulation occurred, however, the effect was only superficial. At higher energy levels vaporization and carbonization of the tissue was inevitable, resulting in a local crater of ablated tissue.

In the present study, we investigated the possibility of cooling the tissue surface during laser treatment to avoid carbonization and to attain an absolute coagulative effect.

MATERIALS AND METHODS

Experimental Design

Sixty-eight animals were used for the experiments. Twenty days after intrahepatic tumor inoculation a relaparotomy was made and the visible diameter of the tumor was measured with sliding calipers. Animals with a tumor diameter <3 mm or >7 mm were excluded from the study. The remaining animals were randomly allocated to two experiments: I, to assess the extent of liver damage and to study short-term laser effects (n=30) and II, to biochemically assess liver damage and function, and to determine long-term effects especially in relation to tumor remission (n=29).

In experiment I, the animals were randomly assigned to 10 groups of 3 animals each. In

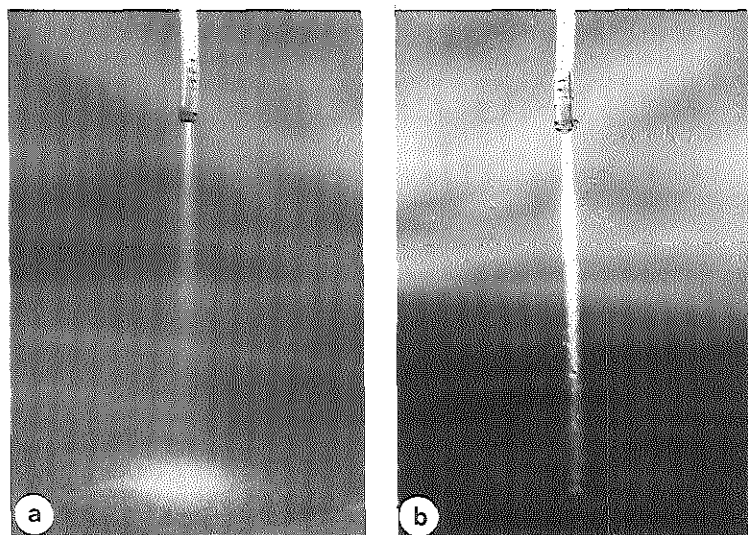


Figure 5.1. The apical tip of the light-transmission system. (a) The Helium Neon pilot laser leaves the fiber with a divergence of 10° . (b) When water is pumped through the system the laser light is guided by the water-jet resulting in an extended transmission with a spot size of 1 mm.

each group laser therapy was performed with a previously fixed energy and power setting. One dose of laser energy (Joule = Watts x seconds of exposure) was applied in each respective treatment group, either 600, 850, 1,200, 1,700 or 2,400 J, at a power setting of either 10 or 20 W in continuous temporal mode. On the first day after laser treatment the animals were sacrificed and the liver was removed for histological determination of short-term laser effects and the measurement of liver damage.

In experiment II, the animals were randomly assigned to 6 groups of 4 animals each and a control group of 5 animals. Here the intermediate steps of 850 and 1700 J were left out so that either 600, 1200 or 2400 J was applied, at a power setting of either 10 or 20 W. The animals in the control group underwent a sham treatment (laparotomy and liver manipulation) without any laser irradiation. To measure the amount of liver destruction, the levels of serum aspartate aminotransferase (ASAT) and alanine aminotransferase (ALAT) were determined on the first and second day post-treatment. Liver function was determined by antipyrine clearance on the second day post-treatment. All animals were sacrificed on day 36 post-treatment for histological determination of long-term effects.

Laser and Delivery System

A continuous wave Nd:YAG laser (Medilas 60N, MBB-Medizintechnik, München, Germany) with a wavelength of 1,064 nm was used. The light-transmission system consisted of a silicone cladded flexible quartz fiber with a diameter of 600 μm enclosed within a teflon hose with a diameter of 2 mm which was clenched to the fiber by an apical metal tip (Sander

et al., 1988). Through the aperture between the fiber and hose a saline solution (22°C) was pumped using a roller pump (HR Flow Inducer, Watson Marlow Lim., Marlow, GB) at a flow rate of 40 ml/min, resulting in a water-jet which transmitted the laser beam beyond the fiber tip with a spot size of 1 mm (Figure 5.1). The water-jet was pointed perpendicularly to the middle of the tumor using a stand on which the fiber system was fixed at a distance of approximately 5 mm to the tissue. The power output was monitored with a separate power meter (Ophir Optics LTD, Jerusalem, Israel).

Determination of Short-term Tissue Damage

On histological slides taken from animals sacrificed on the first day post-treatment, the areas of the tumor and the hepatic necrosis were calculated by computer-assisted integration of the circumference (IBAS 2000, Kontron Bildanalyse GmbH, München, Germany). To estimate the depth and width of the total lesion at each energy, the diameter ($2r$) of the sum of these two areas was then calculated from:

$$r = \sqrt{(A/\pi)}$$

where r is the radius and A is the area of the necrotic region.

Statistical Analysis

The values are expressed as mean \pm standard error of the mean (SEM). A multiple regression model was used to analyze the relation of the diameter of tissue damage and the ASAT, ALAT levels on the power or energy applied. The influences of energy or power on tumor remission were tested by respectively an Exact-trend test or an Exact test for association (adjusted for energy). Comparisons between antipyrine elimination half-life values were made using the Student's t -test. A difference was considered to be significant at P values of <0.05 .

RESULTS

Nine out of 68 rats were excluded from the study as the tumor diameter was smaller than 3 mm or larger than 7 mm. No bleeding appeared as a result of laser treatment. In one animal tissue damage occurred as a result of explosive vaporization ("pop-corn" effect) during laser treatment at 20 W and 600 J. This animal was excluded from the study. Another animal died during anesthesia. Two control animals died with generalized tumor spread before sacrifice on day 36. These animals were attached to the group "tumor outgrowth on day 36".

Histopathology

The general pattern of laser induced tissue damage was unaffected by the variations in power setting or energy applied.

On the first day post-treatment, the tumor tissue did not appear to be damaged as the histological and cytological structures had remained intact. The tumor cells, however, had acidophilic

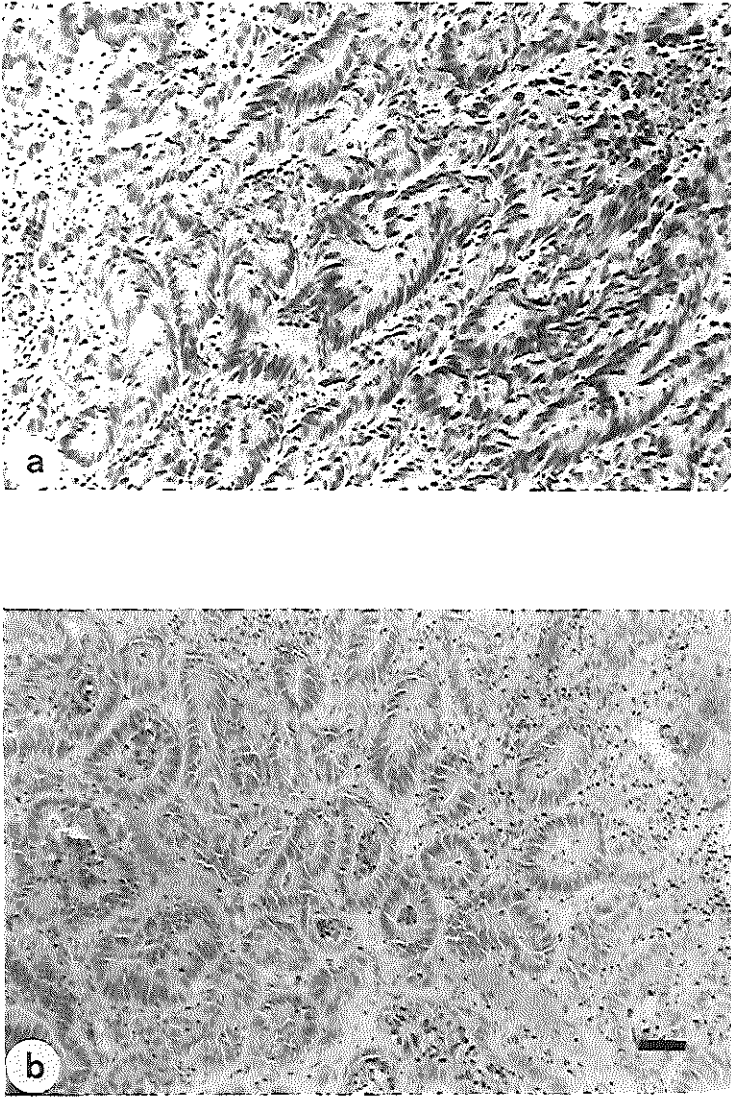


Figure 5.2. Histological sections of tumor tissue in the liver. (a) On the first day post-laser treatment the cells appear characteristically with dark elongated nuclei and acidophilic cytoplasm. (b) Thirty-six days post-laser degenerative changes are visible. Bar: 50 μm (hematoxylin, azophloxin & saffron stain).

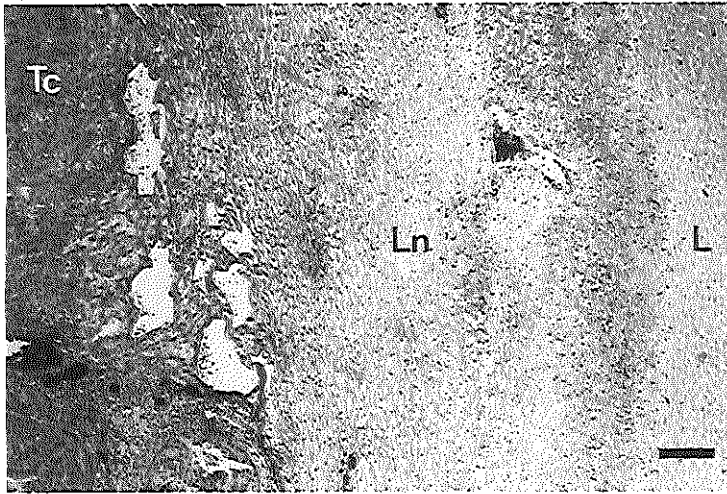


Figure 5.3. Histological section on the first day post-treatment. On the border between tumor and liver tissue large cavities are visible. Tc, Tumor coagulation; Ln, Liver necrosis; L, Normal liver tissue. Bar: 150 μm (hematoxylin, azophloxin & saffron stain).

cytoplasm with dark elongated nuclei (Figure 5.2a; for normal tumor histology see Figure 2.1). Large cavities surrounded by densely coagulated cells with pyknotic nuclei were often observed, especially on the border to liver tissue (Figure 5.3). These cavities are caused by boiled tissue water that creates bubbles of steam within the tissue. Around the tumor, a sharply demarcated concentric rim of necrotic liver tissue was visible (Figure 5.4a; for pre-treatment histology see Figure 2.4a), which could be divided into two zones:

1. Hepatocytes with vacuolated acidophilic cytoplasm and normal or slightly swollen faintly staining nuclei. The sinusoids in the periphery of this layer were dilated.
2. A zone of acidophilic necrosis containing deliquesced cells without nuclei. The sinusoids in this zone were often hyperemic. A mild inflammatory response was noted in this layer (Figure 5.5).

On day 36 post-treatment the major tissue structures could still be identified (Figure 5.2b, 5.4b). Around a core of tumor tissue with degenerative changes, a rim of completely necrotic liver parenchyma was visible. This necrotic area was separated from the vital liver parenchyma by a band of connective tissue, in which a histiocytic reaction with multinucleated giant cells was present (Figure 5.6).

Short-term Laser Effects

Liver damage. The total diameter of the tumor plus the rim of hepatic necrosis vs. energy

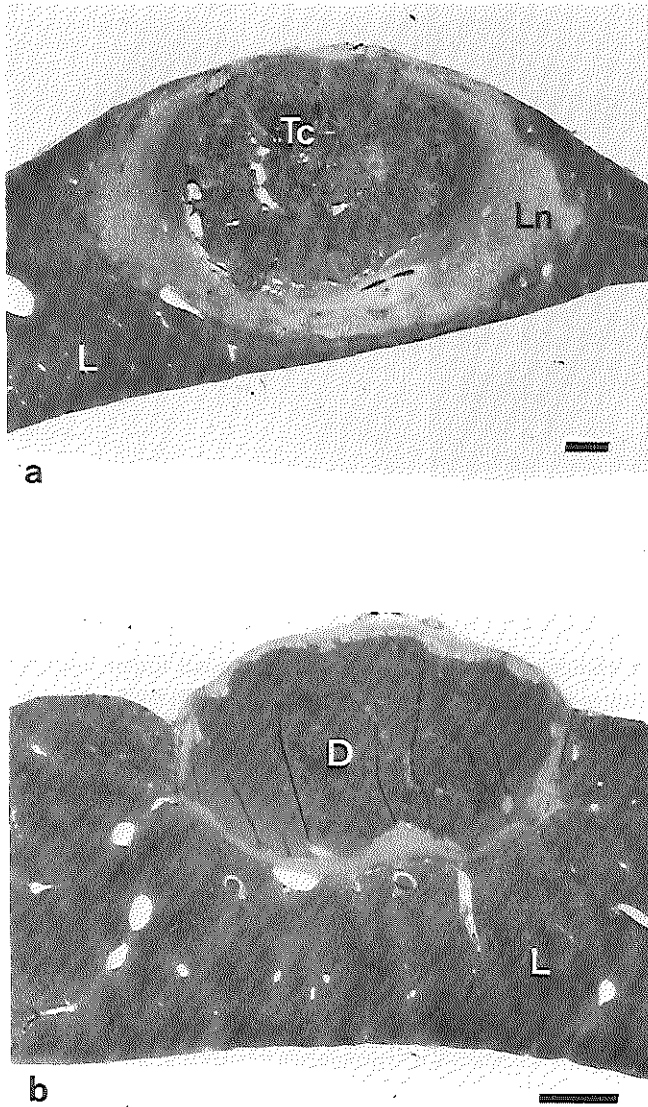


Figure 5.4. Histological sections of tumor tissue in the liver post-laser treatment. (a) On day 1 post-treatment, the tumor is surrounded by a concentric rim of necrotic liver. (b) Complete tumor remission on day 36, the necrotic area is encapsulated by a band of connective tissue. Bar: 1 mm. Tc, Tumor coagulation; Ln, Liver necrosis; L, Normal liver; D, degenerative core (hematoxylin, azophloxin & saffron stain).

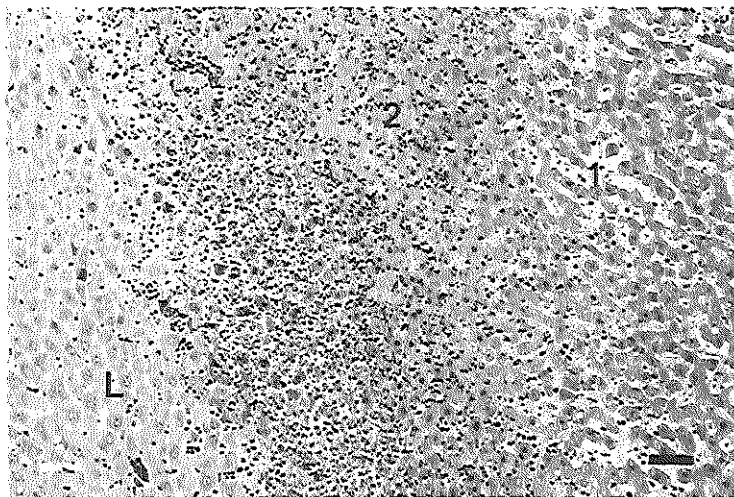


Figure 5.5. Histological section of the periphery of the rim of necrotic liver on day 1 post-laser. Numbering corresponds to the text. Zone 1: hepatocytes with vacuolated cytoplasm. Zone 2: deliquesced hepatocytes, infiltrated by inflammatory cells. L, Normal liver. Bar: 50 μ m (hematoxylin, azophloxin & saffron stain).

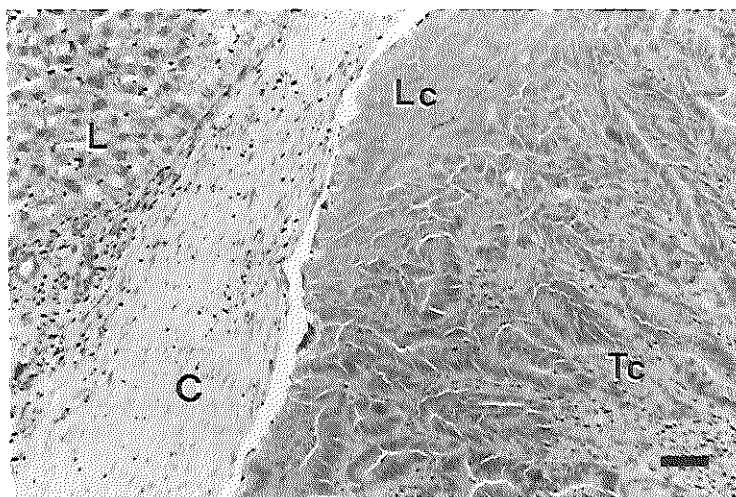


Figure 5.6. Histological section on day 36 post-laser. The core of coagulated tumor and liver is encapsulated by connective tissue. Tc, Tumor coagulation; Lc, Liver coagulation; L, Normal liver tissue; C, Connective tissue. Bar: 50 μ m (hematoxylin, azophloxin & saffron stain).

delivered on the first day post-treatment is shown in Figure 5.7. The total diameter estimates at each energy the mean depth and width of laser induced tissue damage. The tumor, a spheroid with a mean diameter of 5.0 ± 0.1 mm, is represented by the dotted line. As the mean tumor diameter is a constant factor, the curves above the dotted line describe the 1.4-5 mm rim of hepatic necrosis that surrounded the tumor after laser treatment. The diameter of liver damage was directly related to the laser energy applied and was fitted by a logarithmic curve ($P=0.01$, $R^2=0.50$). The curves of 10 and 20 W paralleled during the entire energy range. At 10 W the diameter ranged from 6.4 ± 0.3 mm at 850 J to 8.0 ± 0.8 mm at 2400 J. At 20 W the damaged area was significantly larger (22%) than at 10 W ($P<0.001$), ranging from 7.7 ± 0.2 mm at 600 J to 10.0 ± 0.1 mm at 1700 J.

Serum ASAT/ALAT. The enzyme levels were increased on the first day post-treatment (Figure 5.8). The ALAT and ASAT values, regressed upon power, energy and their interaction, showed a significant, respectively borderline significant relation ($P=0.04$ and $P=0.06$, respectively). The curves of 10 and 20 W, however, diverged at higher energies, indicating a larger increase in liver damage at 20 W. The ALAT level rose from 32.2 ± 8.6 iU/l at 600 J, 10 W to 59.1 ± 12.8 iU/l at 2400 J, 10 W and from 52.8 ± 11.9 iU/l at 600 J, 20 W to 130.0 ± 19.4 at 2400 J, 20 W compared to controls of 17.9 ± 1.2 iU/l. For ASAT, these values were 74.0 ± 13.4 iU/l to 111.9 ± 17.1 iU/l and 117.3 ± 19.8 iU/l to 213.3 ± 16.0 iU/l, respectively compared to control values of 49.4 ± 5.3 iU/l. On the second day post-treatment the values of both enzymes were normalized again.

Antipyrine Clearance Test. Liver function was not affected by laser treatment as measured with an antipyrine clearance test. No differences were found in antipyrine plasma

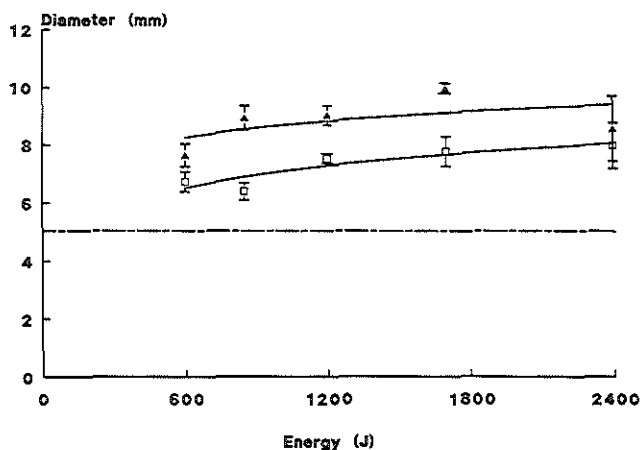


Figure 5.7. Diameter of the tumor plus hepatic necrosis vs. energy delivered at 10 W (\square) or 20 W (\blacktriangle) on the first day post-laser treatment. Each point represents the mean \pm SEM of 3 experimental results. The dashed line describes the mean tumor size.

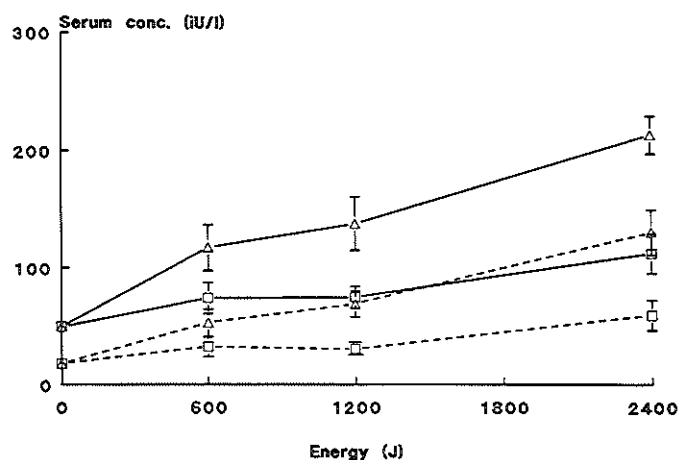


Figure 5.8. Serum ASAT (—) and ALAT (---) levels vs. energy delivered at 10 W (□) or 20 W (△) on the first day after laser treatment. Each point represents the mean \pm SEM of 4 experimental results.

elimination half-life levels ($T_{1/2}$) on the second day after laser application compared to controls (mean $T_{1/2}=2.8\pm0.2$ hours) (Table 5.1).

Long-term Effect on Tumor Remission

The long-term effects on tumor remission is listed in Table 5.2. All tumors in control animals showed massive outgrowth with infiltration to adjacent tissue. In treated animals tumor outgrowth depended on the amount of energy applied. A significant relation was found between the amount of energy delivered and the number of tumors in remission ($P<0.001$). Thirty-six days after 2400 J treatment no malignant cells could be demonstrated by light microscopy, whereas after 600 J outgrowth was observed in 3/4 of the cases at 10 W, and 1/4 of the cases at 20 W. The difference between treatment at 10 or 20 W was nonsignificant ($P=0.07$).

DISCUSSION

In this study the ability of the water-jet cooled Nd:YAG laser to effectively coagulate tumor tissue within the liver was demonstrated. Cooling of the tissue surface allowed irradiation with energies of 2400 J at either 10 or 20 W, without carbonization or tissue ablation. This finding is in agreement with a previous study by Sander *et al.* (1989), where the water-jet guided Nd:YAG laser was found to be superior over the noncontact modality

Table 5.1. Mean \pm SEM antipyrine plasma elimination half-life ($T_{1/2}$) on the second day post-laser.

Energy (J)	No. of animals	$T_{1/2}$ (h)	
		10 W	20 W
Control*	5	2.8 \pm 0.2	2.8 \pm 0.2
600	8	3.4 \pm 0.2	3.4 \pm 0.6
1200	8	2.4 \pm 0.3	2.6 \pm 0.2
2400	8	2.6 \pm 0.4	2.4 \pm 0.1

*Control animals underwent a sham treatment of laparotomy and liver manipulation.

Table 5.2. Tumor remission on day 36 post-treatment.*

Energy (J)	No. of animals	Tumor remission†	
		10 W	20 W
Control‡	5	0/5 (0)	0/5 (0)
600	8	1/4 (25)	3/4 (75)
1200	7	1/4 (25)	3/3 (100)
2400	7	4/4 (100)	3/3 (100)

*Laser treatment was performed 20 days after tumor inoculation.

†No. of tumors in remission/No. of tumors treated, (percentage).

‡Control animals underwent a sham treatment.

in the treatment of gastrointestinal ulcers. The water-jet enabled precise targeting on the tumor surface resulting in complete tumor remission at 2400 J, combined with a minimum of liver damage and preservation of liver function.

On the first day after laser treatment the tumor tissue showed characteristic changes with acidophilic cytoplasm and dark elongated nuclei, similar to the zone underneath the carbonization layer that was found in other studies without water-cooling (Van Hillegersberg *et al.* 1992, Stern *et al.* 1988, Brackett *et al.* 1986, Rosenberg *et al.* 1990). Although these histological structures had remained intact up to 36 days post-treatment, tumor outgrowth could not be observed in all animals treated with 2400 J. Most probably only the tissue frame had remained, consisting of denatured tissue proteins. This feature of heat-fixation has previously been described by Stern *et al.* (1988). The nonvital heat-fixed tissue is hardly

infiltrated by inflammatory cells and is therefore cleared up very slowly. Although it is likely that complete remission was achieved, the potential of these heat-fixed tumor cells to survive has to be established at longer periods after laser treatment.

On the first day post-treatment at all energies a concentric rim of liver necrosis was visible around the tumor. As the laser was aimed at the superficial tumor and was closer to the tumor than to the surrounding liver tissue, one would have expected complete tumor destruction at all energies. However, at 600 or 1200 J at 10 W in 3/4 of the cases vital tumor cells had remained, which resulted in tumor outgrowth 36 days post-treatment. This apparent higher vulnerability of the hepatic tissue could be the result of the darker color of the liver, compared to the whitish tumor, which effectively absorbed the Nd:YAG laser light (Chapter 3). Another explanation could be the lesser heat drainage from the deeper tissue regions that were furthest removed from the water-cooled surface (Svaasand *et al.*, 1985).

A power setting of 20 W resulted in 22% more liver damage than at 10 W. This indicates that at 20 W higher temperatures occurred, so that larger areas reached a fatal temperature level. This temperature level is very critical, as the necrotic liver tissue consisted of two distinct zones, sharply demarcated from the normal parenchyma. Notably, the most peripheral zone showed more degenerative changes than the zone adjacent to the tumor tissue. This could be explained by a decline in temperature over the two zones resulting in heat-fixation in the zone adjacent to the tumor and thermal damage in the peripheral zone. The tissue temperature was not measured, as in a pilot study very slight changes in the thermoprobe position caused large variations in temperature measurements.

The experimental results of tissue damage versus laser energy applied, which were fitted to a logarithmic relation, indicate that higher energies could easily be applied without much more liver damage. At the same time this implies that there is a relative maximum in depth of tissue damage. The depth of the laser effect depends upon light penetration and heat diffusion (Chapter 3). In this study, the maximal depth of tissue damage was 10 mm, measured at 1700 J and 20 W. It has to be established to what extent higher power settings can enlarge this value. Most probably depth of necrosis will increase with increasing power, but a plateau will occur above a certain power level. The maximal power setting at which water-cooling can still avoid carbonization, will be related to the laser energy applied. In this study a water temperature of 22°C was used. Lower temperatures will to a certain extent improve the cooling capacity of the water-jet.

A significant relationship was found between the amount of energy delivered and the number of tumors in complete remission, irrespective of the power setting applied. This may imply that within the power range used in this study, the degree of tumor coagulation is primarily determined by the laser energy applied. On the other hand, the total diameter of tissue damage was significantly larger at a power setting of 20 W than at 10 W. Thus, the diameter of tissue damage is mainly determined by the power setting applied (Figure 5.7). Tumors of various size could as such be treated by adjusting power (diameter of tissue damage) and energy (degree of tumor coagulation). Tumors with a size as used in this experiment (i.e., a mean diameter of 5 mm) can be treated most effectively at an energy level of 2400 J (Table 5.2). To minimize adjacent liver damage, a power setting of 10 W would be preferable to 20 W, as the diameter of tissue damage is related to the laser power applied.

In this study we used a single laser exposure with a fixed fiber position to determine the laser effects as standardized as possible. In the clinical setting, however, repeated exposures and/or step-like movements of the fiber along the tissue surface may be needed to treat larger tumors. As the whole fiber system can be passed down the instrument channel of a laparoscope, laparoscopic treatment of several superficial tumors at different liver lobes would be possible. This local treatment of tumor can substantially reduce the surgical trauma and may diminish complications bleeding, tumor spread and liver failure.

6. Interstitial Nd:YAG Laser Coagulation

Adapted from: R. VAN HILLEGERSBERG, H.J. VAN STAVEREN, W.J. KORT, P.E. ZONDERVAN & O.T. TERPSTRA. Interstitial Nd:YAG Laser Coagulation with a Cylindrical Diffusing Fiber-tip in Experimental Liver Metastases. Lasers Surg Med (accepted)

INTRODUCTION

Thermal laser therapy has proved to be successful in treating or palliating solid malignant tumors at various sites (Dixon, 1988; Krasner, 1991; Murray *et al.*, 1992). In the previous studies we found that noncontact Neodymium:Yttrium-Aluminum-Garnet (Nd:YAG) laser treatment can produce selective destruction of experimental liver metastases (Chapters 4, 5). Deep seated tumors, however, are not accessible in the noncontact mode owing to limited light penetration. For that purpose, the light may be delivered interstitially by implanting the laser fiber directly into the malignant tissue (Bown, 1983; Masters & Bown, 1990; Masters *et al.*, 1991; Steger, 1991). This type of therapy has been applied experimentally and clinically with varying degrees of success to brain, skin, pancreatic and hepatic tumors (Table 6.1). Three different methods of thermal destruction can be distinguished, depending mainly on the exposure time to an increased tissue temperature (determined by laser parameters and tissue optical and thermal properties; Chapter 3):

1. Hyperthermia at temperatures of 42-45°C, causing reversible damage to cellular enzymes, that may become irreversible after longer exposure times (25 minutes to several hours).
2. Coagulation and vaporization at temperatures of 60-140°C, causing protein denaturation, hyalinization of collagen and cell shrinkage, which can be observed macroscopically by tissue blanching.
3. Carbonization and ablation at temperatures of 300-1000°C, causing charring with increased light absorption and smoke generation.

Until now, thermal interstitial laser destruction has been achieved by either hyperthermia or tissue carbonization/ablation combined with coagulation.

Table 6.1. Review of interstitial Nd:YAG laser treatment in various tissues *in vivo*.

Power (W)	Energy (J)	Time (s)	Fiber	Tissue (<i>in vivo</i>)	Lesion (mm)	Histopathologic effect	Reference
<i>Combined ablation and coagulation</i>							
0.5-2	100-1200	50-2400*	400 μ m bare fiber	liver rat	16	well defined lesion, charring at 2 W, transmission reduced to 30%	Matthewson <i>et al.</i> (1987)
80	800	10	600 μ m water cooled	liver pig	12-20	spheroidal lesion, central charring, no fiber burning, echogenic on US	Godlewski <i>et al.</i> (1988)
15-60	75-300	5	600 μ m bare fiber	prostate canine	15/9	well defined lesion, echogenic on US, size independent of laser power	Littrup <i>et al.</i> (1988)
1 2		100-400* 100*	400 μ m bare fiber	colon ca., i.s. rat	(4-20) tumor size	sharply defined necrosis: 100% in tumors <8 mm at 1 W and 300 s, higher risk of perforation at >300 s	Matthewson <i>et al.</i> (1988)
1.5	750-1005	500-670	200-400 μ m bare fiber	tumors† patients		depends on tumor type, number, and sites of treatment	Steger <i>et al.</i> (1989a)
1.2 2	720; 1440 1200	600*; 1200* 600*	400 μ m bare fiber	fibro sa., s.c. rat	(10-15) tumor size	well defined necrosis, best results at 2 W and 600 s: remission: 5/10, cure: 2/10	Matthewson <i>et al.</i> (1989)
5	500	100	600 μ m water cooled	mamma ca., i.s. rat	5-8	main necrosis, surrounded by islands of necrosis	Dowlatshahi <i>et al.</i> (1990)
1.3-4	468-1440	360	600 μ m bare fiber	liver pig	10	cylindrical lesion, central charring, echogenic on US	Dachman <i>et al.</i> (1990)

Table 6.1 (Continued). Review of interstitial Nd:YAG laser treatment in various tissues *in vivo*.

Power (W)	Energy (J)	Time (s)	Fiber	Tissue (<i>in vivo</i>)	Lesion (mm)	Histopathologic effect	Reference
1	500	500	400 μ m bare fiber	liver dog	10	spherical lesion, central charring	Van Eyken <i>et al.</i> (1991)
1.5	900	600	600 μ m bare fiber	liver pig	10-15	spherical-ellipsoid lesion, central charring, echogenic on US	Bosman <i>et al.</i> (1991)
2-4		30-120	1200 μ m circ. diffusing	brain rat	3-5	coagulation necrosis	Bettag <i>et al.</i> (1991)
1	300	300	frosted sapphire	pancreatic ca. hamster, i.s.	2.1	well defined necrosis with damage to capillaries on microangiography	Nuutinen <i>et al.</i> (1992)
2 3	120-600 540-900	60-300 180-300	600 μ m bare fiber	liver rabbit	9/7-17/13 21/13-27/15	ellipsoid lesion, central charring	Matsumoto <i>et al.</i> (1992)
5	300	60	600 μ m bare fiber	brain muscle liver rabbit	13/9 12/5 8/5	ellipsoid lesion; central cavity, size measured by MRI; smaller size in liver due to effective vascular heat diffusion (?)	Higuchi <i>et al.</i> (1999)
1.5	1500	1000	400 μ m bare fiber	brain cat	11	central cavity surrounded by charring and coagulation	Tracz <i>et al.</i> (1993)
3 2-6	1500	500 30	1100 μ m circ. diffusing	brain rat	12 2-10	ellipsoid coagulation necrosis	Schober <i>et al.</i> (1993)

Table 6.1 (Continued). Review of interstitial Nd:YAG laser treatment in various tissues *in vivo*.

Power (W)	Energy (J)	Time (s)	Fiber	Tissue (<i>in vivo</i>)	Lesion (mm)	Histopathologic effect	Reference
<i>Hyperthermia, 42-45°C, controlled by thermoprobe feedback</i>							
3	3600	1200	frosted sapphire computer contr.	pancreatic ca. nude mouse	10-20	tumor necrosis 70-80%	Daikuzono <i>et al.</i> (1988)
6	8000	600	frosted sapphire water cooled	tumors‡ patients	15-20	hypodensic necrosis (CT), 4 wks. post-treatment	Hahl <i>et al.</i> (1990))
3-4		1800	frosted sapphire computer contr.	muscle dog	10/20	cylindrical lesion, height: 10 mm; diameter: 20 mm	Panjehpour <i>et al.</i> (1990)
2-3	3600-5400	1800 1800-2400	frosted sapphire computer contr.	brain cat brain tumors§ patients	-	coagulation necrosis, surrounded by edema, no charring follow up by CT§	Sugiyama <i>et al.</i> (1990)
2-3		600	diffusing probe	liver rabbit	20	coagulation necrosis	Huang <i>et al.</i> (1991)
4	2400	600	400 µm bare fiber; frosted sapphire water cooled	liver pig	5 4	clearly demarcated necrosis 7 days post-treatment	Castrén <i>et al.</i> (1992)

The concept of hyperthermia is based on a possible higher susceptibility of the malignant tissue to slight temperature increase (Field, 1987; Robins *et al.*, 1989). The tissue temperature can be kept at the indicated level of about 43°C, using temperature feedback systems and frosted or water-cooled fiber ends (Table 6.1). Disadvantages of hyperthermia, however, are the long exposure times and unpredictable sensitivity of the malignant tissue (Dunlop & Howard, 1989; Anderson & Kapp, 1990).

Tissue ablation combined with coagulation has been applied most commonly with a bare tipped fiber (Table 6.1). This is a normal flexible quartz fiber of which the distal cladding has been stripped for 3–4 mm. The heat generated by this fiber, however, is very localized and intense, as the emission of the laser light is concentrated at the fiber tip. Several studies have reported the development of a blackish clot at the insertion site, which absorbed the laser light efficiently and suppressed the transmission into the tissue by several orders (Elias *et al.*, 1987; Matthewson *et al.*, 1987; Panjehpour *et al.*, 1990). Thus, a charred fiber acts as a hot-tip, which may limit precision and extent of the induced necrosis by depending on heat diffusion rather than light penetration and subsequent heat diffusion (Svaasand *et al.*, 1985).

Charring may be avoided using an cylindrical diffusing fiber-tip with uniform light delivery, producing homogeneous heat distribution (Arnfield *et al.*, 1986, 1989). Cylindrical diffusing tips have been applied in photodynamic therapy for illumination of photosensitized solid tumors (Dougherty *et al.*, 1981; Gatenby *et al.*, 1987; Van Hillegersberg *et al.*, 1992a). However, these diffusers are only applicable at lower power output levels of <1 W. We therefore developed a more heat resistant cylindrical diffuser for thermal laser coagulation.

The aim of this study was to assess whether the use of this fiber-tip could lead to selective coagulation of malignant tumor within the liver.

Legend to Table 6.1

*Pulse duration 100 μ s, 40 pulses /s

†Liver metastasis 35 mm; repeated fiber insertion (4x, distance < 1.5 cm); treatments 0, 6, 10 months: no increase in tumor size. Pancreatic head tumor 20 mm; repeated fiber insertion (3x); No success. Breast tumor; repeated fiber insertion (3x); good response, no complete remission.

Skin metastases 12x5 mm, 8x5 mm; fiber insertion (2x, 1x); reduction, complete remission (?).

Liver metastasis 50x50 mm; 4 simultaneous fibers; CT 2 months: necrosis 50 mm, but another tumor deposit.

‡Superficial liver tumors; 1 primary, 6 metastatic.

§Glioma 10x20x15 mm; complete remission, 31 months. Glioma 24x30x25 mm; complete remission, 9 months. Metastatic lung ca. 50x34x35 mm; complete remission, 29 months. Glioma 10x8x12 mm; recurrence, 23 months. Metastatic lung ca. 26x24x28 mm; died of primary tumor, 11 months.

Abbreviations: ca., carcinoma; circ., circumferential; contr., controlled; CT, Computed tomography; i.s., in situ; MRI, magnetic resonance imaging; sa., sarcoma; s.c., subcutaneous; US, ultrasonography.

MATERIALS AND METHODS

Experimental Design

Laser treatment was performed 20 days after intrahepatic tumor implantation in 42 animals. A relaparotomy was made and the visible diameter of the tumor was measured with sliding calipers. The animals were randomly allocated to two experiments: I. to assess short-term laser effects and the biochemistry of liver damage ($n=18$) and II, to assess liver function and long-term effects, especially in relation to tumor remission ($n=24$).

In experiment I, the animals were randomly assigned to 5 experimental groups and 1 control group of 3 animals each. In the experimental groups interstitial laser therapy was performed with a previously fixed energy and power setting. The animals in the control group underwent a sham treatment with diffuser insertion only. To determine liver damage, blood was collected for serum aspartate aminotransferase (ASAT) and alanine aminotransferase (ALAT) on the first and second day after laser treatment. The animals were sacrificed on the second day post-treatment, and the liver was removed for histological determination of short-term effects.

In experiment II, the animals were randomly assigned to 5 experimental groups and 1 control group of 4 animals each. The animals underwent the same laser treatment as in experiment I. To determine liver function, an antipyrine clearance test was performed on the second day post-treatment. The animals were sacrificed on day 36 after laser treatment for histological assessment of long-term effects. The proliferative activity of the tumor cells was

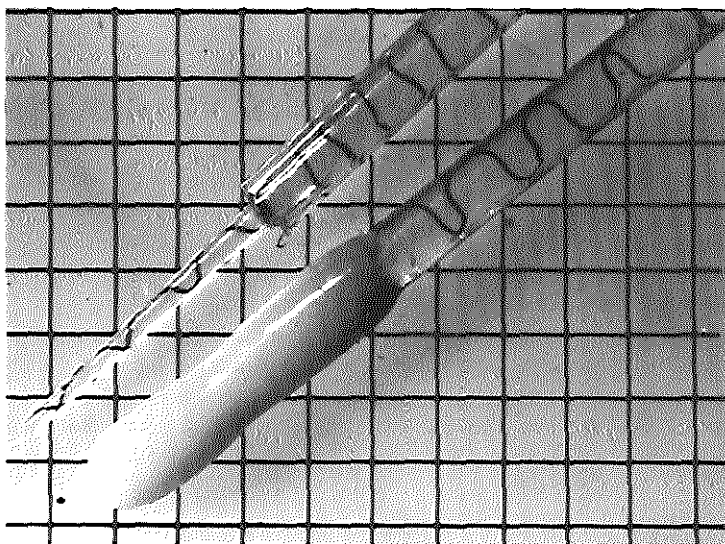


Figure 6.1. (Up) The 600 μm silicone cladded quartz fiber, stripped for the distal 0.5 cm and formed into a stepwise conical end by immersing into hydrofluoric acid solution. (Down) A cylindrical diffuser is created by coating the taper with a strongly scattering layer of Helioseal®, cured by illumination with blue light of 488 nm.

determined by bromodeoxyuridine (BrdU) incorporation during 2 h before sacrifice.

Cylindrical Diffuser

To create a cylindrical diffuser (Figure 6.1), the coating and cladding of a 600 μm silicone cladded flexible quartz fiber were stripped for the distal 0.5 cm. The fiber core was formed into a stepwise conical end by immersing it into hydrofluoric acid (HF solution 48-50%, Janssen Chimica, Geel, Belgium) in 4 steps of 1 mm each. At each step a different time for chemical etching was chosen (core radius decrease 1.45 $\mu\text{m}/\text{min}$). In this way 5 rings (seen from the fiber top) were made with equal surface areas ($5.65 \times 10^3 \mu\text{m}^2$) emitting the light evenly over the taper length (Figure 6.1). Following that, the fiber was coupled to an argon-ion laser (Model 5450AWC, Ion Laser Technology, Salt Lake City, UT, U.S.A.) and the taper immersed into Helioseal[®] (Vivadent, Schaan, Liechtenstein). This strongly scattering substance consists of titanium dioxide particles suspended in a polymer containing a photoinitiator that cures under illumination with blue light (peak absorption at 467 nm, temperature stability 150°C) (Lekka *et al.*, 1989; Henderson, 1990). Initially a soft layer was applied by illumination with blue light of 488 nm at 15 μW during 3 min. The soft Helioseal diffuser was then completely cured in paraffin, at 20 mW during 10 min. This procedure resulted in a cylindrical diffuser with typical dimensions of 0.5 cm length and a maximum diameter of 1.3 mm (Figure 6.1). As the amount of Helioseal curing depended upon the light energy distribution along the taper end, the emitted light was scattered to a higher degree on places of higher energy, approaching isotropic light distribution from the diffuser.

Laser Application and Dosimetry

A continuous wave Nd:YAG laser (Model 4060N, MBB-Medizintechnik, München, Germany) with a wavelength of 1,064 nm was used at a power setting of 2 W (i.e., 4 W/cm diffuser length). In pilot studies with 4 W (8 W/cm) diffuser charring occurred after repeated application or at energies $\geq 1,200 \text{ J/cm}$. This could be detected immediately by a strong decrease in the energy fluence rate, followed by smoke development and carbonization of the tissue.

The output power of the cylindrical diffuser was measured before and after each laser treatment using an integrating sphere (Model 2550, United Detector Technology, Hawthorne, CA, U.S.A.) with a radiometer (Optometer, Model 181, United Detector Technology). The intra-experimental variation in diffuser output power was always less than 5%. As different diffusers were used during the experiments, the inter-experimental diffuser output power varied between 1.9-2.3 W. A 19 gauge needle was used to create an entry into the center of the tumor. To prevent adherence to the tissue, some silicone-grease was put on the diffuser. Following that, the needle was withdrawn and the diffuser inserted using a stand on which the fiber system was fixed (for a schematic representation of the experimental set-up see Figure 8.1). One dose of laser energy was applied in each respective treatment group, either 600, 1,200, 2,400, 3,400 or 4,800 J/cm. To indicate the actual light dose delivered and to detect the occurrence of tissue carbonization or diffuser breakdown, the energy fluence rate (mW/cm^2) at the tumor boundary was measured with a spherical isotropic detector (Henderson *et al.*, 1990; Marijnissen & Star, 1987). To determine the inner tumor

temperature, a needle thermocouple connected to a read out instrument (Thermodig N800, AIS, France) was positioned opposite to the light detector. Both fluence rate and temperature were recorded every 30 seconds.

Determination of Tissue Damage

On slides taken from animals sacrificed on the second day after laser treatment the tumor area and maximal width and depth of the laser induced lesion were determined by computer-assisted measurements (IBAS 2000, Kontron Bildanalyse GmbH, München, Germany). To give an indication of tumor growth retardation, the long-term vital tumor area was measured by IBAS (Chapter 2).

Bromodeoxyuridine Incorporation

This method of determining the proliferative activity, is based upon the incorporation of BrdU, a thymidine analogue, into reduplicating DNA. Two hours before sacrifice the animals were injected intraperitoneally with BrdU 50 mg/kg body weight. A 5 μ m paraffin section from the same site as used for light microscopy was taken and treated according to Schutte *et al.* (1987), for immunocytochemical detection with antibody against BrdU.

Statistical Analysis

The values are expressed as means \pm standard error of the mean (SEM). A multiple regression model was used to analyze the relation between fluence rate increase, short-term lesion size or ASAT, ALAT levels on the energy applied. The relation between long-term tumor area or antipyrine serum half-life ($T_{1/2}$) to laser energy was tested by Spearman's rank order correlation. A random coefficient model for repeated measures was used to test the relation between temperature against exposure time. The influence of energy on tumor remission was determined by an Exact-trend test. Other comparisons were made using the Student's t-test. A difference was considered to be significant at P values of <0.05 .

RESULTS

One animal died during anaesthesia; all remaining animals survived the procedure. On the day of laser treatment the mean \pm SEM visible tumor diameter was 5.3 ± 0.1 mm ($n=41$).

Laser Application, Temperature and Fluence Rate

The Helioseal coating technique described here, allowed easy production of a cylindrical diffusing fiber end. Diffuser damage did not occur at given laser parameters.

The mean \pm SEM core temperature at the tumor boundary was $27.3\pm0.3^{\circ}\text{C}$ ($n=34$), varying from 22.8 to 31.2°C . Temperature increased logarithmically with energy delivered ($P<0.0001$) (Figure 6.2). At 250 s of exposure (600 J/cm), the mean value was $59.0\pm1.5^{\circ}\text{C}$ ($n=34$), ranging from 46.0 to 77.3°C . After 1,200 s (4800 J/cm) the mean value was $69.7\pm2.1^{\circ}\text{C}$

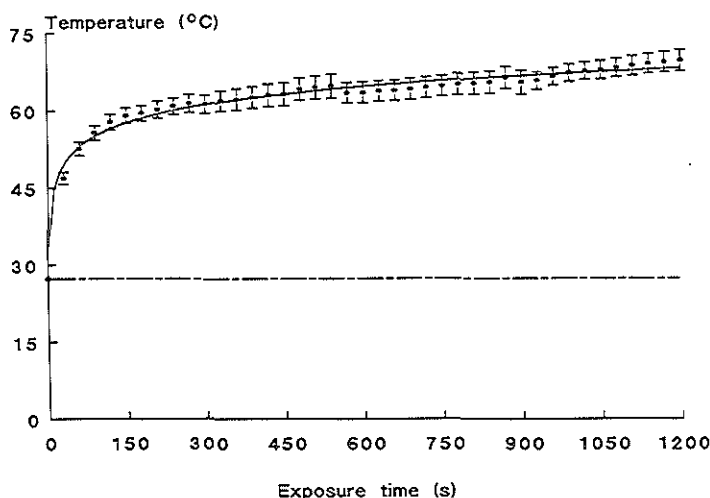


Figure 6.2. Temperature measured at the tumor boundary vs. exposure time to interstitial laser therapy with 4 W/cm from a 0.5 cm cylindrical diffuser (laser output power 2 W). Each point represents the mean \pm SEM in all groups ($n=34$ at 150 s, 600 J/cm, to $n=7$ at 1,200 s, 4,800 J/cm). The dashed line describes the mean temperature at the start of treatment ($27.3\pm0.3^{\circ}\text{C}$, $n=34$).

($n=7$), ranging from 60.3 to 75.2°C.

The mean \pm SEM fluence rate at the beginning of laser treatment (30 s of exposure) was 3.1 ± 0.2 W/cm 2 ($n=34$). Considerable differences were found in the individual starting values, 1.7-5.3 W/cm 2 , probably caused by inaccuracy in the positioning of the detector probe relative to the cylindrical diffuser. Fluence rate changes were therefore expressed as percentage of the individual starting value (Table 6.2). These values were significantly related to laser energy applied ($P=0.012$, $r=0.428$), increasing from $101\pm2\%$ ($n=6$; range 92-107%) after 600 J/cm, to $122\pm11\%$ ($n=7$; range 87-170%) after 4,800 J/cm.

Histopathology

Sections on the second day after laser treatment showed sharply demarcated lesions around the place of laser application (Figure 6.3a; for pre-treatment histology see Figure 2.4a). The border between normal and necrotic tissue consisted of a practically straight line, irrespective of the margin between tumor and hepatic tissue. The necrotic area always extended the dorsal border of the liver. As sections were taken through the tumor center, the place of diffuser insertion could be observed in most of the cases (Figure 6.3a); non of the samples showed tissue carbonization.

In general, laser induced tissue necrosis showed a mixed pattern of coagulated and deliquesced areas, often infiltrated by inflammatory cells. At energies of $\geq 1,200$ J/cm, heat coagulation was predominant in tumor tissue showing characteristic changes as described

Table 6.2. Mean \pm SEM fluence rate change after laser energy applied, expressed as percentage of the individual starting value.*

Energy (J/cm)	No. of animals	Fluence rate change (% of starting value)
600	6	101 \pm 2
1200	7	107 \pm 2
2400	7	113 \pm 5
3400	7	114 \pm 4
4800	7	122 \pm 10

*Laser energy was delivered interstitially with a 0.5 cm cylindrical diffuser, output power 4 W/cm. Mean starting value 3.1 \pm 0.2 mW/cm².

previously (Chapters 4, 5); histological and cytological structures had remained intact and tumor cells appeared with acidophilic cytoplasm and pyknotic elongated nuclei. At laser energies up to 1,200 J/cm, heat coagulation could only be observed at the site of diffuser insertion. Mainly deliquesced tumor cells were visible with acidophilic cytoplasm, without or with faintly staining nuclei. This necrotic tumor tissue could hardly be distinguished from the surrounding liver necrosis.

The pattern of hepatic necrosis was also related to the amount of energy delivered. In case of higher laser energies, heat coagulation had extended the surrounding hepatic tissue, so that the hepatic necrosis could be divided into two zones (Figure 6.3b):

1. An inner zone containing hepatocytes with normal nuclei and dilated sinusoids.
2. An adjacent zone of liver necrosis containing deliquesced cells without or with faintly staining nuclei and rough vacuolated acidophilic cytoplasm. The peripheral sinusoids in this zone were often hyperemic. An inflammatory response was noted in this layer.

When lower laser energies had been applied, only the second zone of liver necrosis was visible.

Thirty-six days after laser treatment two different situations could be observed:

1. Complete tumor destruction.
2. Tumor outgrowth.

In case of complete destruction the area of necrosis had been replaced by a degenerative core in which the major tissue structures could often be identified (Figure 6.4a,b). These structures did not label with BrdU, whereas a strong labelling was found in the cellular nuclei of outgrown tumor (Figure 6.5a,b). The degenerative area was surrounded by a rim of polymorphonuclear and mononuclear inflammatory infiltrate, separated from the vital liver parenchyma by a band of connective tissue in which a histiocytic reaction with multinucleated giant cells was present (Figure 6.4b).

Short-term Laser Effects

Lesion size. The maximal width of the lesion was directly related to the laser energy applied and well fitted by a logarithmic curve ($P<0.0001$, $R^2=0.984$) (Figure 6.6).

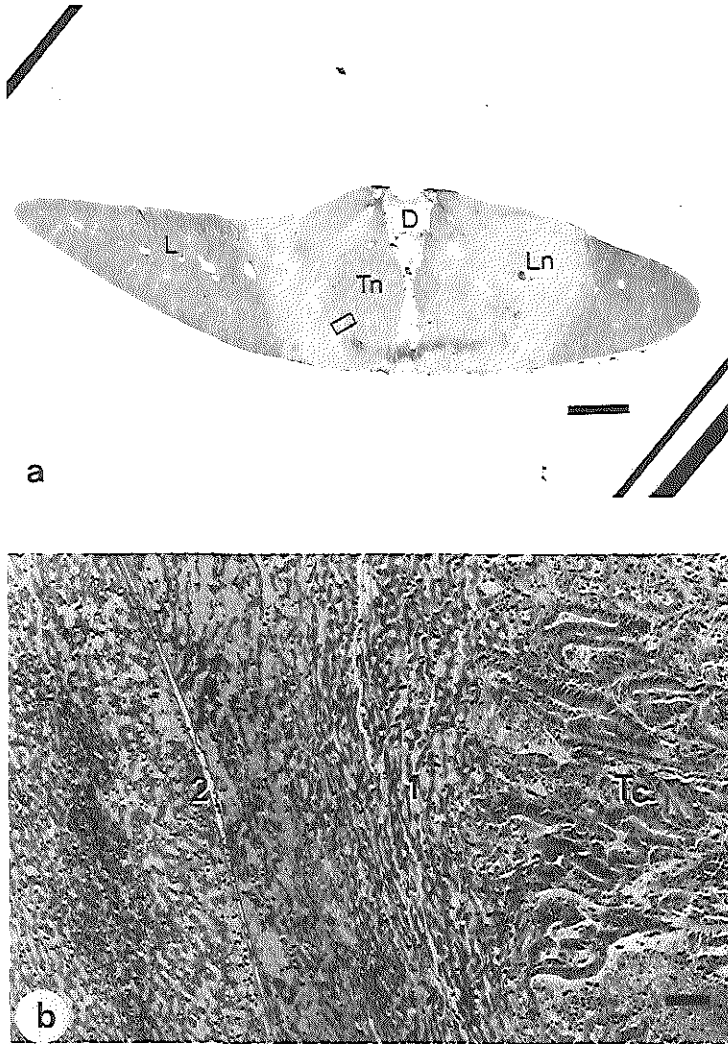


Figure 6.3. Histological section of a lesion on the second day post-treatment with 2,400 J/cm. (a) The tumor is completely involved and the place of diffuser insertion is clearly visible; no carbonization occurred. Bar: 2 mm. (b) Magnification of the area indicated by the square. The tumor is surrounded by hepatic necrosis that can be divided into two zones (numbering corresponds to the text): 1) an inner zone containing hepatocytes with normal nuclei and dilated sinusoids; and 2) an adjacent zone of liver necrosis containing deliquesced acidophilic cells without or with faintly staining nuclei and rough vacuolated acidophilic cytoplasm. Bar: 50 μ m. Tn, Tumor necrosis; D, Diffuser insertion site; Ln, Liver necrosis; L, Liver; 1, 2, zones of hepatic necrosis (hematoxylin, azophloxin & saffron stain).

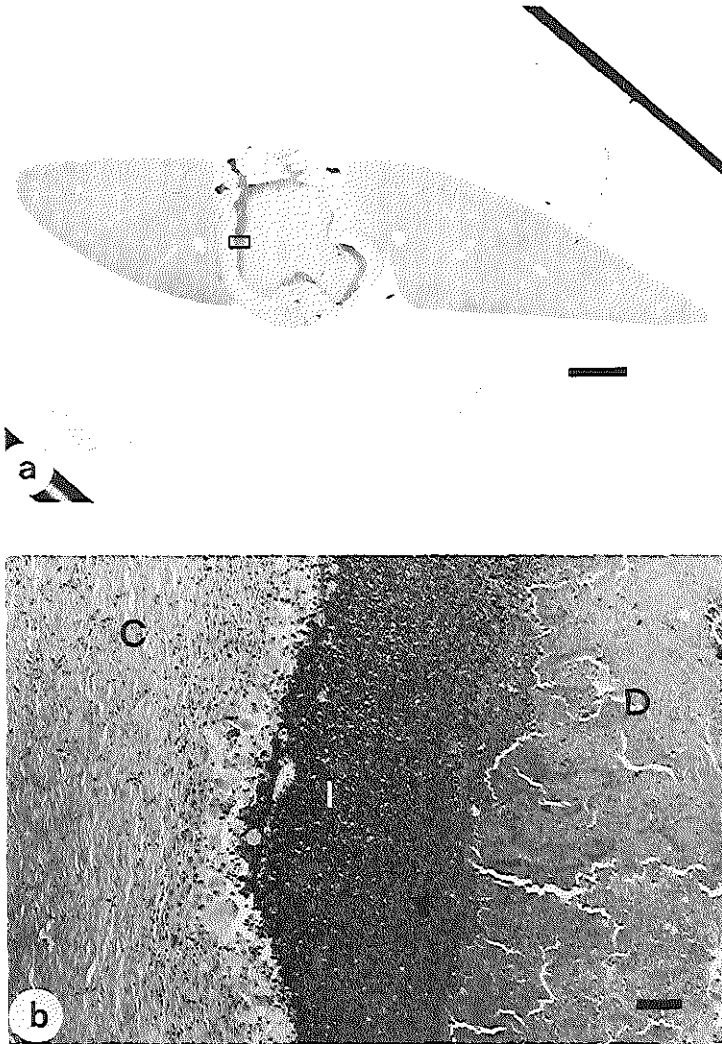


Figure 6.4. Histological section of a completely destroyed tumor, 36 days after laser treatment. (a) The necrotic area is replaced by a degenerative core surrounded by inflammatory infiltrate, and a band of connective tissue. Bar: 2 mm. (b) Magnification of the area indicated by the square. The core contains coagulated tumor and liver of which the histological structures can still be identified. The margins are infiltrated by inflammatory cells and encapsulated by connective tissue in which a histiocytic reaction with multinucleated giant cells is present. Bar: 50 μm . D, degenerative core; I, inflammatory infiltrate; C, connective tissue (hematoxylin, azophloxin & saffron stain).

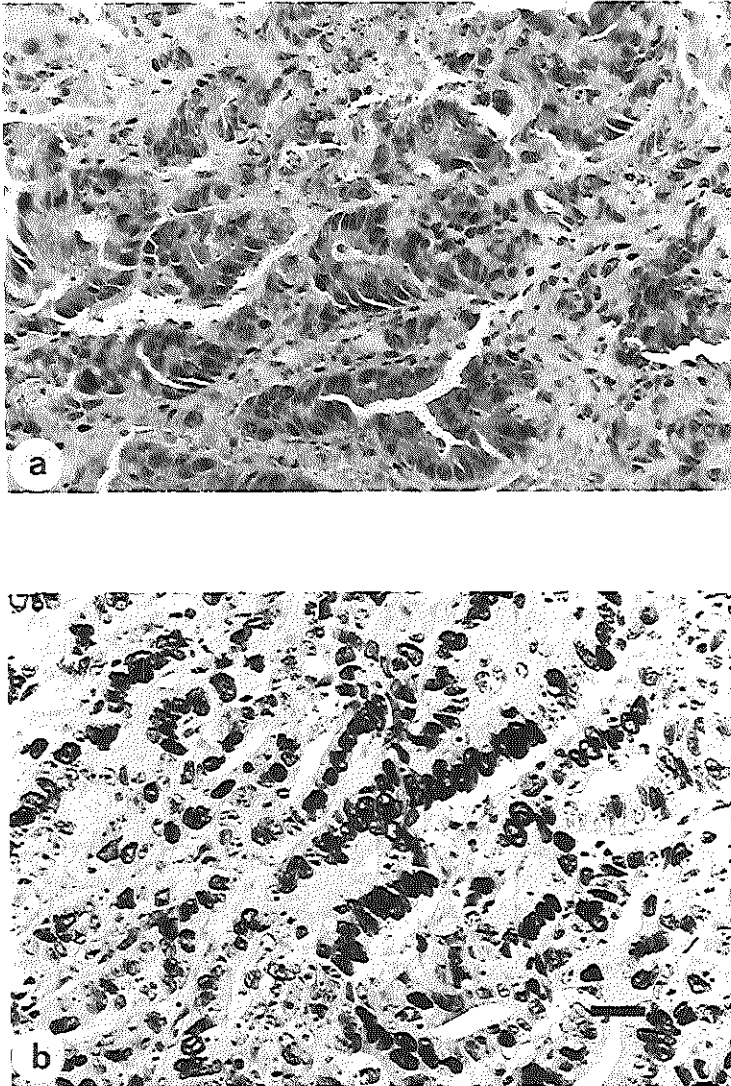


Figure 6.5. BrdU histochemistry on histological sections 36 days post-treatment. (a) The nuclei of the coagulated tumor in the degenerative core do not label with BrdU. (b) Strong labelling in the cellular nuclei of outgrown tumor. Bar: 15 μm (hematoxylin, azophloxin & saffron stain).

Table 6.3. Mean \pm SEM antipyrine plasma elimination half-life ($T_{1/2}$) on the second day after post-treatment.*

Energy (J/cm)	No. of animals	$T_{1/2}$ (h)
Control†	4	3.8 \pm 0.4
600	3	4.7 \pm 0.4
1200	4	4.1 \pm 0.3
2400	4	3.4 \pm 0.4
3400	4	3.6 \pm 0.5
4800	4	3.4 \pm 0.2

*Laser energy was delivered interstitially with a 0.5 cm cylindrical diffuser (output power 4 W/cm), 20 days after tumor implantation.

†Control animals underwent a sham treatment with diffuser insertion only.

Mean values varied from 7.4 \pm 0.7 mm after 600 J/cm treatment to 11.2 \pm 0.3 after 4,800 J/cm. The mean \pm SEM tumor diameter, derived from measurements of the tumor area on the cut histological samples was 5.5 \pm 0.2 mm ($n=18$). This value is represented in Figure 6.6 by a dashed line, showing that liver damage occurred at all laser energies applied.

As at all energies liver necrosis reached the dorsal liver border (Figure 6.3a), the lesion depth did not depend on energy delivered. Mean \pm SEM lesion depth was 7.0 \pm 0.2 mm ($n=15$).

Serum ASAT/ALAT. The measurements on lesion size were in agreement with the increased serum ASAT and ALAT values on the first day post-treatment; both enzyme levels were logarithmically related to energy applied ($P=0.007$, $R^2=0.339$ for ASAT; $P=0.003$, $R^2=0.411$ for ALAT) (Figure 6.7). In control animals mean values of 127.2 \pm 2.9 iU/l for ASAT and 45.4 \pm 1.9 for ALAT were found. On the second day post-treatment, ASAT levels in control animals were lower than on the first day, 85.0 \pm 9.4 iU/l ($P=0.013$), whereas no significant difference was found for ALAT ($P=0.133$). The increased serum ASAT level on the first day post-treatment in control animals may be due to release of ASAT from the tumor as a result of diffuser insertion. In preliminary studies we found that the tumor ASAT content is relatively high compared to liver (ratio 40:1), whereas the tumor ALAT content is lower than liver (ratio 1:2) (Chapter 2). In the experimental groups, the values on day 2 were still slightly increased, with maximum values of 128.4 \pm 9.2 iU/l for ASAT (1,200 J/cm) and 76.6 \pm 7.9 iU/l for ASAT (2,400 J/cm).

Antipyrine clearance test. The antipyrine plasma elimination $T_{1/2}$ levels on the second day after laser application were not significantly related to laser energy applied ($P=0.071$), indicating that major deterioration in liver function did not occur, which is in agreement with the small liver volume damaged by this procedure. Mean \pm SEM values varied between 3.4 \pm 0.2 h ($n=4$) after 4800 J/cm, and 4.7 \pm 0.4 h ($n=3$) after 600 J/cm, compared to controls of 3.8 \pm 0.4 h ($n=4$) (Table 6.3).

Table 6.4. Tumor remission and vital tumor area on the 36th day post-treatment.*

Energy (J/cm)	No. of tumors in remission†	Vital Tumor area (mm ²)‡				
		Individual value				Mean±SEM
Control§	0/4	139	204	228	235	201±22
600	1/3	0	84	-	268	117±79
1200	2/4	0	0	148	187	84±49
2400	1/4	0	92	153	158	101±37
3400	1/4	0	49	68	202	80±43
4800	3/4	0	0	0	12	3±3

*Laser energy was delivered interstitially with a 0.5 cm cylindrical diffuser (output power 4 W/cm), 20 days after tumor implantation.

†No. of tumors in complete remission / no. of animals.

‡Measured by computer assisted integration of the circumference.

§Control animals received diffuser insertion without any laser treatment.

Long-term Effect on Tumor Remission

All tumors in control animals showed massive outgrowth with infiltration to adjacent tissue. In the experimental groups, however, several animals showed complete remission (Table 6.4). Best results were obtained at 4800 J/cm with complete remission in 3 out of 4 animals. No significant relation was found between number of tumors in remission and energy delivered ($P=0.135$). The size of the vital tumor area, however, decreased with laser energy ($P=0.016$) (Table 6.4). There was no correlation between the vital tumor area and the original tumor size.

DISCUSSION

The advantage of laser compared with other modes of energy delivery is the high precision of the laser induced necrosis (Keiditsch *et al.*, 1981; Steger, 1991; Masters *et al.*, 1991). However, preservation of light penetration during laser treatment is conditional for controlled and predictable tissue heating. In previous studies several attempts have been made to avoid carbonization, which strongly suppresses light transmission. Constant liquid cooling of the fiber tip has been used by Godlewski *et al.* (1988) and Dowlatsahi *et al.* (1990). However, the fluid pool created by this method increases interstitial pressure, which may induce tumor spread and is not accepted in neurosurgical applications. Others have investigated the use of a frosted sapphire tip to give a wider angle of illumination (Table 6.1). However, Van Eden *et al.* (1988) showed that without cooling or temperature feedback, this probe was acting much more as a point heat source, owing to heating the metal connector and sapphire assembly. In addition, the width of the sapphire tip and the metal collar required to connect it to the fiber, limits percutaneous application. The use of gas-cooling with coaxial air flow

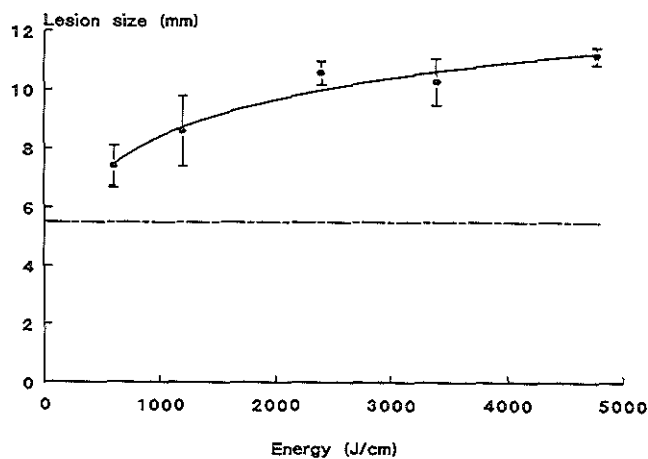


Figure 6.6. Short-term lesion size vs. laser energy delivered. Each point represents the mean \pm SEM of 3 experimental results. The dashed line describes the mean tumor size (5.5 ± 0.2 mm).

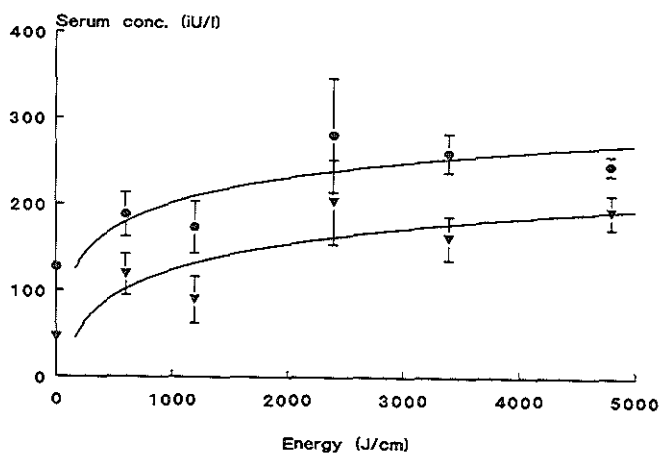


Figure 6.7. Serum ALAT (▼) and ASAT (●) levels vs. laser energy delivered. Measurements on the first day after laser treatment. Each point represents the mean \pm SEM of 3 experimental results.

has initially been used for cooling the sapphire tip, but is now obsolete as air embolism can occur which may be fatal (Schröder *et al.*, 1989). Nolsøe *et al.* (1992) found that light delivery through a conical taper end without a scattering coating, can not avoid charring of hepatic tissue *in vitro*. In our study, the use of a cylindrical diffusing fiber-end with homogeneous light delivery, resulted in tissue coagulation without any charring. The light transmission, measured at the tumor boundary, did not decrease during laser treatment as was previously described in case of carbonization (Elias *et al.*, 1987; Matthewson *et al.*, 1987; Panjehpour *et al.*, 1990). On the contrary, an increase in fluence rate was found during laser treatment (up to 170%), probably as a result of changing the optical properties of coagulating tissue. Such changes were previously observed in Nd:YAG laser coagulated myocardium and thought to be caused by increased scattering owing to protein denaturation (Halldorsson *et al.*, 1981; Derbyshire *et al.*, 1990; Splinter *et al.*, 1991). However, the measured changes may have been enhanced by shrinkage of the coagulating tissue, bringing the isotropic detector nearer to the diffuser.

The maximal lesion size found in this study was 11 mm after 4 W/cm and 4800 J/cm (power output 2 W; energy 2400 J; diffuser length of 0.5 cm). This value is comparable to the lesion size found in previous studies using combined ablation and coagulation (accompanied by charring), indicating that the use of a cylindrical diffuser would not significantly increase the treatment range (Table 6.1). However, most investigations have been with normal hepatic tissue or subcutaneously implanted tumors, whereas in this study the effects were determined on tumor as well as on surrounding hepatic tissue. As the various tissues have distinct optical properties, the effect of a certain laser treatment will be related to the relevant tissue type (Patterson *et al.*, 1991; Van Hillegersberg *et al.*, 1993). Therefore, a proper comparison between the lesion size created with a cylindrical diffuser or a bare fiber-tip would require a standardized experimental set-up in a single tumor model. Recently, Wyman *et al.* (1992) compared *in vitro* the extent of lesions produced by a bare tipped fiber (point optical source, distributed heat source) and a fiber with a small steel sphere (point heat source). They found that at the same Nd:YAG laser output power and exposure duration (1.6 W for 300 s), the point heat source produced larger lesions (with charring) than the point optical source (without charring). Charring of a bare tipped fiber, which transforms it from a distributed heat source into a point heat source, will therefore increase the extent of a lesion. However, for both types of heat sources the maximum coagulation volume is reached at a temperature of 300-1000°C at the fiber tip, above which undesirable tissue ablation occurs, limiting further heat transfer into the tissue (Thomsen, 1991). As the temperature gradient from the fiber tip towards the tissue periphery of a point heat source is much higher than that of a distributed heat source (Wyman *et al.*, 1992), the coagulation volume of the distributed heat source will be larger. The crux is, that it requires a higher output power for the fiber tip of a distributed heat source to reach the ablation temperature than for the tip of a point heat source. So, although at the same (lower) power output a point heat source will give a larger lesion than a distributed heat source, with the latter one can potentially apply a much higher output power to the tissue and accordingly reach a larger coagulation volume.

In this study, lesion size was found to increase logarithmically with energy applied, which could be confirmed by the serum ASAT and ALAT levels on the first day post-treatment.

Matthewson *et al.* (1987) have determined a dose response relationship in normal rat liver using a bare tipped fiber at 0.5-2.0 W and 100-1200 J (Table 6.1). Necrosis increased with increasing power with a plateau above 1 W, and for a given power setting, increased with increasing total energy with a plateau between 600 and 1000 J. The plateau above 1 W was probably caused by carbonization which reduced light transmission to 30% of the original value at 2 W. However, the plateau at increasing energies is comparable with the results of this study (Figure 6.6). This plateau is determined by the maximal penetration depth of the laser light, indicating that higher laser energies could be applied without much more liver damage. However, at the same time this implies that the production of larger lesions would require much higher energies (i.e., longer exposure times).

A logarithmic relation was found between tissue temperature and laser energy applied. After a strong initial temperature increase up to 600 J/cm (150 s exposure), mean values remained between 60-70°C, which allowed gentle tissue heating within the coagulation range (Figure 6.2). There has been some dispute about the terminology in thermal interstitial laser therapy (Dachman *et al.*, 1990; Sweetland *et al.*, 1989; Steger *et al.*, 1989b). In this chapter we used the indication "thermal therapy" instead of "hyperthermia" to prevent confusion with the application between 42 and 45°C. We are aware of the fact that in our study temperatures in the order of 43°C also occurred at a certain distance from the diffuser. However, these temperatures only played a minor role in tissue necrosis, as even at 600 J/cm measurements at the tumor boundary ranged from 46 to 77°C. Moreover, maximal exposure time in this study was 20 min, whereas exposure times of at least an hour are usually required for irreversible damage from hyperthermia (Reinhold & Overgaard, 1990; Pigliucci *et al.*, 1990). In the opposite manner, temperatures of 50-100°C have been measured at the fiber insertion site during interstitial laser hyperthermia (Daikuzono *et al.*, 1988; Sugiyama *et al.*, 1990).

Short-term histology showed a mixed pattern of deliquesced and coagulated cells, probably representing the temperature distribution in the tissue. In areas of higher temperature, i.e., around the diffuser and post-treatment with higher laser energies, tumor cells appeared elongated and spindle formed with acidophilic cytoplasm. These characteristic changes of heat coagulation have previously been found after superficial laser coagulation in this model (Chapters 4, 5). Thomsen (1991) described similar changes in thermally damaged epithelial cells, which were thought to be secondary to the collapse of the cytoskeleton. The appearance of 2 zones of adjacent hepatic necrosis can be explained by a decline in temperature towards the periphery of the lesion, resulting in coagulation in the inner zone and degenerative changes in the outer zone.

Tumor remission was determined on the basis of tumor outgrowth 36 days post-treatment. The aspect of the long-term coagulated area was comparable to that found in our previous studies on superficial Nd:YAG laser coagulation; the coagulated area healed gradually with preservation of the structural integrity. Incorporation of BrdU was used as an additional test on viability of the coagulated material. Labelling was always negative, indicating that proliferation did not occur (Figure 6.5). In case of tumor outgrowth, the vital tumor area was significantly reduced at higher laser energies applied. Complete tumor remission occurred at all energies, but was predominant after 4800 J/cm with complete tumor remission in 3 out of 4 cases (Table 6.4). This may indicate that with 4 W/cm, energies over 4800 J/cm should

be applied.

The scattering properties of the diffuser coating used in this study are determined by the size of the suspended particles in the Helioseal polymer (diameter 15 μ m) (Henderson, 1990). Theoretically, a larger particle size would produce more scattering of the Nd:YAG laser light (Van Staveren *et al.*, 1991), indicating that the diffusing capacity of the cylindrical fiber end may to a certain extent be improved by adjusting the polymer composition. A diffusing length of 0.5 cm was chosen for this particular application, i.e., to treat tumors with a mean diameter of 5.5 mm. Larger lesions may be produced by using a longer diffuser length and higher laser power. In pilot experiments, however, at a power output of 8 W/cm and 1200 J/cm diffuser breakdown occurred probably due to temperatures at the cylindrical diffuser exceeding the temperature stability of the Helioseal cap (150°C). Under such circumstances ceramic (Al₂O₃) seems to be a promising alternative to Helioseal, as this material can withstand temperatures of up to 1800°C (in air). However, even at higher power outputs there will be a maximum lesion size owing to limited light penetration and heat diffusion into the tissue. At that stage, multiple diffuser may be applied using simultaneous light delivery from one laser source with a beam splitting device (Davis *et al.*, 1988; Steger *et al.*, 1992). In the clinical setting ultrasound scanning can be used to position the fiber correctly within the tumor and monitor the development of thermal necrosis in real time and through the subsequent period of healing (Dachman *et al.*, 1990; Bosman *et al.*, 1991; Steger *et al.*, 1989a, 1992). This method is potentially applicable to solid tumors in many parts of the body and may be performed percutaneously.

PART III

PHOTODYNAMIC THERAPY

7. Fundamentals of Photodynamic Therapy

Adapted from: R. VAN HILLEGEERSBERG, W.J. KORT & J.H.P. WILSON. Current Status of Photodynamic Therapy in Oncology. Drugs 1993 (in press)

INTRODUCTION

Photodynamic therapy (PDT) shows considerable promise as a new treatment modality for localized superficial or solid malignant tumors. This type of therapy is based on the accumulation of a photosensitizer in malignant tissues after systemic administration. Subsequent illumination with light of an appropriate wavelength creates a photochemical reaction that results in tissue destruction (Figure 7.1).

The first observation of chemical sensitization of tissue for light was reported by Raab (1900). The basic concept of PDT dates from 1903, when Von Tappeiner & Jesionek (1903) used topically applied eosin and sunlight to treat skin cancer patients. Ten years later, Meyer-Betz (1913) self-administered hematoporphyrin to determine its biological effects. This early work, however, did not initiate the clinical application of PDT, but the biological processes involved in photodynamic cell killing were studied intensively. In the 1940s, Auler & Banzer (1942) reported the affinity of hematoporphyrin for neoplastic tissues, which was confirmed by Figge *et al.* (1948), using the fluorescence of the accumulated porphyrins under ultra violet (UV) light. Schwartz *et al.* (1955) proposed that the selective fluorescence of malignant tissues after systemic administration might be due to an impurity in the crude preparation rather than to hematoporphyrin itself. Lipson *et al.* (1961), improved tissue localization of hematoporphyrin by first acetylating and then reducing the crude substance. The mixture produced by this procedure was termed hematoporphyrin derivative (HpD).

The discovery of HpD as an effective tumor-localizing photosensitizer, and subsequently the development of suitable lasers and optical light delivery systems, led to a renewed interest in the 1970s. Initially, the use of HpD was in the area of tumor detection and localization by fluorescence at exposure to short wavelength visible light or UV. Diamond *et al.* (1972) reevaluated the therapeutic effects in mouse glioma, and Dougherty *et al.* (1975) started the

first major studies directed at photodynamic therapy in animal tumors. The first full clinical report of PDT concerned a patient treated for bladder cancer using Hpd and trans-urethral irradiation (Kelly & Snell, 1976). Since that time, there has been an increasing interest worldwide that has led to a large number of experimental and clinical studies in a variety of tumor types and sites. This chapter describes the fundamentals of photodynamic action as well as the various factors that may influence the biological response to PDT.

PORPHYRINS AS PHOTOSENSITIZERS

The Hpd developed by Lipson *et al.* (1961) has been used in many basic and clinical studies during the 1970s and early 1980s. This substance is a complex mixture of various porphyrin species, many of which are less efficient *in vivo* tumor photosensitizers (Dougherty, 1984). Using gel filtration, an enriched fraction was isolated that is mainly responsible for the photosensitizing properties of the Hpd (Dougherty *et al.*, 1984). This active fraction is known commercially as Photofrin® (Lederle Laboratories, Pearl River, NY, U.S.A.), and thought to be an aggregated mixture of non-metallic oligomer porphyrin molecules linked mainly through ether bonds (Dougherty, 1987a; Kessel *et al.*, 1987). The oligomers range in size from 2-8 porphyrin units, although the major portion appears to be di and trimeric (Figure 7.2). A small amount (5-10%) of Hpd and its dehydration products are present as well, but probably do not contribute to photosensitization (Dougherty & Marcus, 1992). Currently, Photofrin is the most commonly used agent for clinical photodynamic therapy.

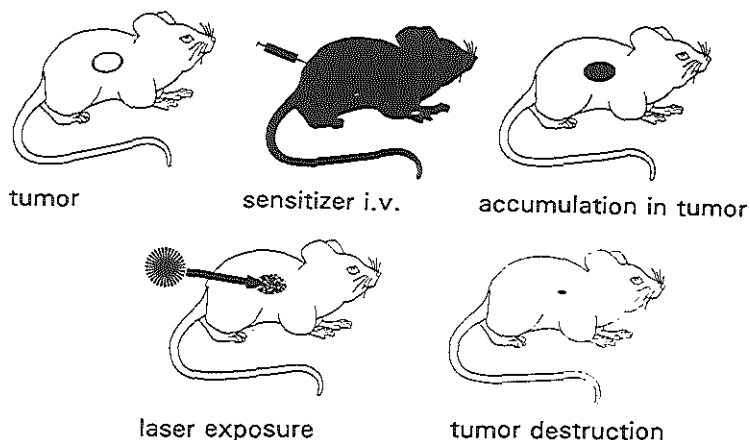


Figure 7.1. Basic principle of Photodynamic Therapy. After systemic administration, the photosensitizer accumulates in the tumor. Subsequent exposure to light of the appropriate wavelength creates a reactive species that generates a photochemical reaction, resulting in tumor destruction.

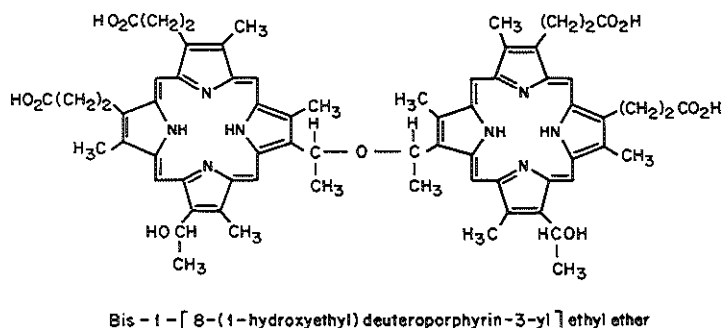


Figure 7.2. Chemical structure of a porphyrin ether dimer, one of the active components of Photofrin. (From: Dougherty *et al.*, 1984)

Toxicology

A photosensitizer should have a low systemic toxicity. For Photofrin, the 50% lethal doses (LD50) at 24 h in mice without light exposure was found about 140 mg/kg (Dougherty *et al.*, 1989). Death in all cases was attributed to liver and kidney necrosis. The porphyrins were considerably more toxic when animals were exposed to whole body illumination for 5 h to full spectrum xenon light (6 mW/cm²) resulting in a LD50 of 4 mg/kg, 24 h after administration (Dougherty, 1986). Under these circumstances death was attributed to a shock-like syndrome.

As Photofrin efficiently accumulates in skin, a generalized skin photosensitivity is induced by systemic administration, which can cause a severe sunburn-type reaction. This means that patients after receiving Photofrin must avoid bright light, including sunlight for 2-8 weeks (Razum *et al.*, 1987; Dougherty *et al.*, 1990). Therefore, the upper limit of the clinical dose of Photofrin (2-5 mg/kg) has been set by skin photosensitivity. The time interval between Photofrin administration and illumination is normally 24-48 h, depending on the porphyrin concentration ratio between tumor and surrounding tissue.

Pharmacokinetics

The plasma clearance of Photofrin after intraperitoneal (i.p) and intravenous (i.v.) injection has been studied by Bellnier *et al.* (1989) using ¹⁴C Photofrin in mice. After absorption from the intraperitoneal cavity (T_{1/2}=1 h), plasma clearance was best fit by a triexponential equation with elimination half lives of 4 h, 9 days and 36 days. Intravenous administration showed different kinetics only in the more rapid initial clearance rate. More than 65% of the

administered ^{14}C Photofrin was excreted over 192 h and 91% of the recovered material was found in the faeces.

It has been reported that after systemic administration, the porphyrins initially (7-8 h) bind to albumin and lipoproteins (equally to low density (LDL) and high density (HDL) lipoproteins) and at longer periods (8 days) almost exclusively to HDL (Jori, 1987; Dougherty, 1987b). The distribution of porphyrins among serum proteins is dependent on their chemical structure. Hydrophilic compounds, such as hematoporphyrin and other monomeric components, preferentially form pseudomicellar structures or non-covalent complexes with albumin and globulins; LDL are the natural carriers of hydrophobic photosensitizers, such as porphyrin oligomers and esters.

Photofrin uptake may be mediated in part via an active transport mechanism, as several studies have shown that the distribution of the circulating porphyrins determines their localization in the tissue (Jori, 1989; Korbelik & Hung, 1991). Thus, three different pools of circulating porphyrins can be divided (Jori *et al.* 1984, Kessel 1986a, Jori 1987):

1. Unbound aggregated components (e.g., micelle-like structures from porphyrin oligomers) are easily available for uptake in macrophages and endothelial or neoplastic cells.
2. Monomeric components, such as hematoporphyrin, form low affinity bonds with albumin and globulins. In malignant tissues, these sensitizers are mainly released to the extracellular matrix.
3. The lipoprotein bound oligomers and porphyrin esters are endocytosed by a receptor mediated process in the neoplastic cells, released in the cytoplasm and bound to apolar endocellular matrices.

Finally, the HDL binding probably accounts for the prolonged presence of 5-8% of the injected photosensitizers in serum.

Pharmacokinetic analysis of ^{14}C - and ^3H - labeled porphyrins demonstrated accumulation in experimental tumor tissue to a higher degree than in skin, muscle, brain and lungs but to a lower degree than in organs of the reticuloendothelial system, e.g., liver, kidney and spleen (Gomer & Dougherty, 1979; Bugelski *et al.*, 1981; Wilson & Van Lier, 1989). Remarkably, Bellnier *et al.* (1989) found lower concentrations in skin located contralaterally to subcutaneously implanted mice tumors, whereas skin overlying the tumors showed concentrations not significantly different. The reason for the preferential concentration in malignant tissue is still unclear, but may be related in part to a porphyrin/lipoprotein affinity, leakiness of tumor vasculature, decreased lymphatic drainage, high LDL receptor activity (Spikes & Jori, 1987) or a decreased conversion to heme owing to low ferrochelatase activity (Wilson JHP *et al.*, 1991).

Photochemistry

Porphyrins have an intense absorption in the blue region around 400 nm (termed the Soret band) and four additional absorption bands (with decreasing intensity) between 500 nm to 650 nm (Figure 7.3). As the penetration of light in tissue increases at higher wavelengths (Van Gemert *et al.*, 1985; Wilson *et al.*, 1985; Wilson, 1989), the weakest absorption band at about 630 nm is normally used for illumination of Photofrin sensitized tissue (Gomer *et al.*, 1984). Although 630 nm has been applied most commonly, Star *et al.* (1990) have recently

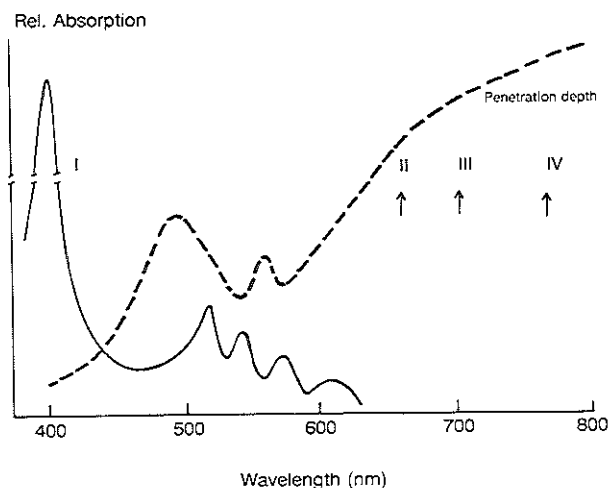


Figure 7.3. Typical absorption spectrum for porphyrins such as Photofrin and Protoporphyrin IX (PROTO) (—) and relative penetration depth in tissue (---) (log scales) vs. wavelength. The arrows indicate the various absorption peaks of second generation photosensitizers: II, Phthalocyanines and Chlorins; III, Phthalocyanines, Purpurins, Verdins and Benzoporphyrin derivative; IV, Bacteriochlorin-a. The actual penetration depth depends on the type of tissue involved, ranging from 1-5 mm in lightly pigmented tissue (e.g., brain) to 0.1-1 mm in highly pigmented tissue (e.g., liver) (Wilson, 1989). (Drawn after: Bonnet & Berenbaum, 1989; Wilson, 1989).

shown that light of 625 nm wavelength has a higher biological activity.

The tissue damage induced by PDT is believed to occur primarily as a result of singlet oxygen ($^1\text{O}_2$) formation out of the available tissue oxygen ($^3\text{O}_2$) (Weishaupt *et al.*, 1976). Several studies have documented the requirement of oxygen for photosensitizing action: Gomer & Razum (1984) reported complete resistancy of hypoxic tumor tissue to PDT, which has been confirmed by several other studies *in vivo* and *in vitro* (Mitchell *et al.*, 1985; Moan & Summer, 1985; Henderson & Fingar, 1989; Chapman *et al.*, 1991) and singlet oxygen scavengers were found to suppress the photocytotoxic effect (Valenzo, 1987).

The singlet oxygen is generated via the so called Type II mechanism of photosensitized oxidation (Foote, 1991) (Figure 7.4): Upon absorption of a photon, the porphyrin molecule is brought to an excited singlet state which has an extremely short half-life. From this singlet state the photosensitizer can decay back to the ground state and emit light in the form of fluorescence. For the photodynamic effect, however, the photosensitizers should undergo intersystem crossing to the excited triplet state of the molecule. This triplet species is more stable with a longer lifetime (millisecond range) than the singlet species (less than 1 μs) (Gomer, 1989). Therefore, the excited triplet state has a high probability of interacting with ground state oxygen). The transfer of energy from the triplet photosensitizer generates the

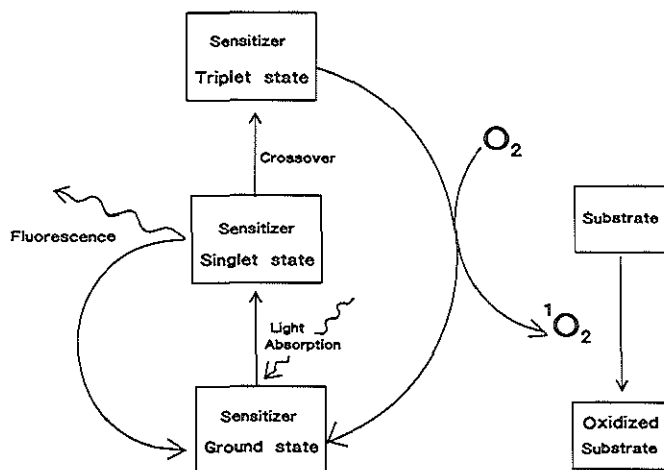


Figure 7.4. Schematic representation of the Type II photochemical reaction, which is thought to be the most important mechanism of PDT cytotoxicity. O_2 , oxygen; 1O_2 , singlet oxygen.

highly reactive singlet oxygen. The electrophilic nature of singlet oxygen makes it very efficient at producing oxidized forms of biomolecules. After transfer of electronic energy to oxygen, the sensitizer returns to its ground state (Figure 7.4). The excitation efficiency of a photosensitizer is defined as the triplet state quantum yield, i.e., the probability of triplet state formation per photon absorbed. The alternative Type I pathway involves the direct interaction of an excited triplet photosensitizer with a biomolecule by electron or hydrogen transfer. This interaction produces radical forms of the substrate or photosensitizer. The radicals can react directly with molecular oxygen to produce active species such as hydroxyl radicals, hydrogen peroxide and superoxide anion (Buettner & Need, 1985; Van Steveninck *et al.*, 1986; Athar *et al.*, 1989). The minor role of Type I interactions in PDT is due to the competition between substrates and oxygen for triplet photosensitizers. The porphyrins in Photofrin undergo slow photodestruction (photobleaching) during *in vivo* light exposure, which can proceed by:

1. Ground state porphyrin reaction with singlet oxygen.
2. The excited triplet state reaction with tissue components.

The products of the processes do not contribute to further photodynamic activity (Mang *et al.*, 1987), but the remaining undamaged portion has been found adequate in destructing tumors under curative light doses (Potter *et al.*, 1987). As lower drug concentrations occur in skin, photobleaching has even been used to diminish cutaneous photosensitivity (Boyle & Potter, 1987).

Targets for Photodamage

The initial target of PDT damage is still uncertain due to the efficient interaction of toxic substrates with many cellular sites, including biomolecules and subcellular organelles such as microsomes, mitochondria and nucleus (Zhou, 1989; Moan *et al.*, 1989; Jori, 1990).

There is evidence that the cellular membranes are a significant target for damage (Girotti, 1990; Chapman *et al.*, 1991; Okunaka *et al.*, 1992). Unsaturated fatty acids can be photo-oxidized and lipid peroxidation, as well as membrane protein cross-linking have been found following PDT. This damage can lead to an increased permeability and inhibited transport of amino acids, nucleosides and sugars (Kessel, 1986b). As mitochondria are a major site for porphyrin localization, these organelles are thought to be an important target for PDT (Gomer *et al.*, 1988a; Salet & Moreno, 1990). Porphyrin photosensitization can also induce single-strand breaks, alkali labile lesions or sister chromatid exchange in DNA (Jori & Spikes, 1984; Evensen *et al.*, 1988). However, nuclear damage is probably not a main target in photodynamic destruction, as PDT has been shown to induce comparable levels of cytotoxicity in normal human fibroblasts and in DNA repair-deficient fibroblasts (Gomer *et al.*, 1988b). Moreover, porphyrin mediated PDT is negative for mutation and transformation induction (Gomer *et al.*, 1989).

Although *in vitro* studies have shown direct tumor cell death, it has been suggested that tumor vasculature is a primary target for in photodynamic therapy (Star *et al.*, 1986; Gomer *et al.*, 1988a). Several observations point towards an important role of vascular injury:

1. Clonogenicity of tumor cells is not decreased if harvested immediately following PDT that causes significant toxicity in the host animal (Henderson *et al.*, 1985).
2. Blood flow and oxygen tension strongly decreases during PDT (Selman *et al.*, 1984).
3. Hpd concentration is higher in vascular stroma than in tumor cells (Bugelski *et al.*, 1981; Bellnier *et al.*, 1989).

Thus, the initial sites of PDT-injury would involve the subendothelial collagen matrix and endothelial cells of the microvasculature (Nelson *et al.*, 1987a). It is, however, most likely that both vascular and cellular PDT damage are required to achieve complete tumor destruction.

LIGHT SOURCES AND DELIVERY SYSTEMS

Light Source

Initially conventional lamps have been used for surface illumination, particularly on the skin (Figure 7.5a). Filtering of the light spectrum emitted by such a lamp is required to select the relevant photoactivating wavelength and to eliminate the infrared components which otherwise cause significant heating of the tissue. Disadvantages of these conventional gas discharge lamps are limited methods of light delivery, precision, control, intensities (typically about 50 mW/cm²), and heat production (Wilson & Patterson, 1986; Matiello *et al.*, 1987).

The introduction of lasers combined with single-strand optical fibers has increased the applicability of PDT, as light of a narrowly defined wavelength and power output can be delivered to practically every site in the human body, either interstitially or endoscopically.

Although the simple and reliable Helium Neon (HeNe) laser with a wavelength of 632.8 nm would appear to be a suitable laser for Photofrin-sensitized tissue, its low power output limits the application in PDT. Therefore, the tunable argon-dye laser is mostly used with the additional advantage of delivering light of any particular wavelength between 350 and 700 nm. The 5-25 W continuous wave argon laser at 514.5/488 nm serves as the energy source that optically pumps the dye laser containing a dye fluid which fluoresces in the 630 nm region, such as Rhodamine B or Kiton-red. In this way, effective power levels of up to 3 or 4 W can be obtained, of which 80-90% can be coupled into optical fibers of 200-600 μm core diameter. Unfortunately argon-dye lasers are rather expensive and clinically not easy to handle. The gold vapor laser is less complex and cheaper, but has the limitation of operating at a single fixed wavelength of 628 nm, unsuitable for other photosensitizers than Photofrin.

Light Delivery

For superficial tumors, e.g., tumors of the skin or oral cavity, a simple lens and aperture optics may be used to produce a uniform illumination (Figure 7.5b). For solid or deep seated tumors the fiber optic may be placed directly into the tumor tissue (interstitially) through a biopsy needle and eventually under ultrasound guidance (Figure 7.5c,d). For intraluminal or intracavitary illumination of tumors such as in bronchus, oesophagus or bladder, the flexible quartz fiber can be placed within the instrument channel of a standard endoscope (Figure 7.5e,f). By modifying the fiber end (Marijnissen *et al.* 1985) or placing the fiber in a light

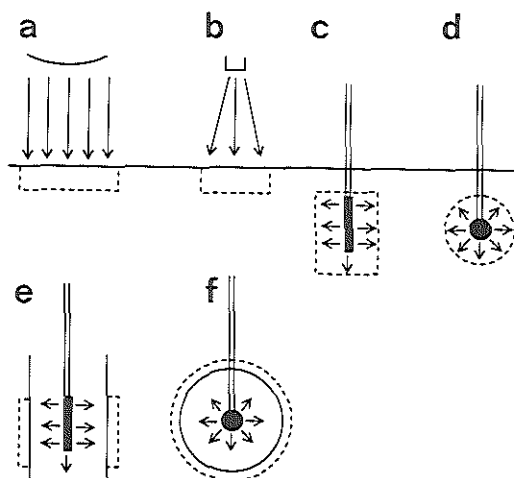


Figure 7.5. Various forms of light delivery in PDT. Superficial illumination with (a) a conventional lamp and (b) laser light guided through a quartz fiber optic. Interstitial illumination with (c) a cylindrical diffuser and (d) a spherical diffuser. Intraluminal and intracavitary illumination with (e) a cylindrical diffuser and (f) a spherical isotropic diffuser. The dashed line represents the light distribution in highly scattering tissue.

diffusing medium (Muller & Wilson, 1987), the spatial distribution of the light to the target tissue can be controlled. The output from the fiber can be made isotropic by building onto the tip a small spheroidal volume of highly scattering material. Similarly, a cylindrically symmetric line source can be produced by coating the fiber along its end with a diffusing material (Arnfield *et al.*, 1986) (Figure 6.1). Multiple fibers can be placed interstitially to treat a larger tissue volume (Marijnissen *et al.*, 1992). With simultaneous placement, a beam splitter is required to divide the optical power between the fibers.

Light Dosimetry

At present, light exposure regimens are largely empirical and have usually been expressed in terms of the incident areal power density in W/m^2 or areal energy density in J/cm^2 (Joules = Watts x seconds of exposure). Predicting, reproducing and comparing photodynamic effects, would require knowledge about the spatial distribution of absorbed light energy in tissue.

Activation of a photosensitizer at a certain point in the tissue is proportional to the energy fluence rate, multiplied by the absorption coefficient of the photosensitizer (Star *et al.*, 1992). The energy fluence rate is defined as the radiant energy incident per second on a small sphere, divided by the cross sectional area of that sphere (W/m^2). Multiplication with the irradiation time yields the energy fluence (J/m^2). Light distribution can be assessed by:

1. Determining the optical absorption and scattering properties of the tissue and calculating the fluence distribution using a radiation transport model (Patterson *et al.*, 1991a, 1991b).
2. Direct measurements of the local fluence rate using optical fiber light detectors (Marijnissen & Star, 1987).

In vivo measurements provide direct information of the actual light distribution. Marijnissen *et al.* (1989) have developed a modified cystoscope, emitting isotropic light, for monitoring and controlling light delivery during bladder PDT in patients. By using this device, they have shown the importance of adequate light dosimetry, as it appeared that the real fluence at the bladder wall was 5-6 times larger than the incident unscattered light dose. This difference is caused by the fact that the back-scattered light reenters the bladder wall elsewhere. The clinical application of this device for PDT of multifocal bladder carcinoma, has demonstrated considerable variation in the ratio between total and nonscattered light dose between different patients. However, by measuring the actual light dose on the bladder wall and adjusting the output power accordingly, a similar light dose could be applied to all patients (D'Hallewin *et al.*, 1992). Light dosimetry may also be useful in controlling interstitial PDT. In that case, the isotropic detectors are placed at critical points in the target area (e.g., tumor boundary) (Chapter 8).

FUTURE DIRECTIONS

The goal of each cancer treatment is to destroy the tumor selectively, with minimal damage to the surrounding normal tissue. As, especially in an organ as liver, selectivity in photosensitizer accumulation has not been achieved, the following two chapters of this part are directed towards either:

1. Selective light delivery after photosensitization with Photofrin (Chapter 8).
2. Selective photosensitizer accumulation (Chapter 9).

In this section we will shortly review the current directions in experimental PDT research.

Second-generation Photosensitizers

Although Photofrin has proved to be an effective photosensitizer and tumor localizer, there are limitations which might be overcome by alternative, so called second generation photosensitizers (Kreimer-Birnbaum, 1989) such as phthalocyanines, chlorins, purpurins, bacteriochlorins, verdins or protoporphyrin IX (PROTO) endogenously produced from 5-aminolevulinic acid (ALA). The ideal properties of a photosensitizer are (Bonnet & Berenbaum, 1989; Gomer *et al.*, 1989):

1. Chemical purity.
2. Minimal dark toxicity.
3. Significant absorption at wavelengths above 650 nm.
4. High quantum yields for the generation of Type I or Type II photochemical reactions.
5. Preferential tumor localization.
6. Rapid clearance from normal tissue.

A photosensitizer that has a strong photoactivation at longer wavelengths than Photofrin could provide for a greater effective light penetration into tissue (Figure 7.3). At 630 nm the effective tumoricidal depth is 3-15 mm, depending on tissue type and way of illumination. A greater differential uptake by tumor tissue could improve the therapeutic ratio as well as fluorescence detection and localization.

As LDL mediated endocytosis is thought to be an important factor in photosensitizer uptake, liposome bound photosensitizers have been used for selective tumor targeting (Jori, 1989). However, Kongshaug *et al.* (1989) did not find any correlation between tumor localizing ability of various porphyrins and their affinity for LDL.

Phthalocyanines (PC) are structurally similar to porphyrins, but show a strong absorption in the 650-700 nm range (Rosenthal, 1991). Certain non-metallo as well as metallo derivatives have been studied. Chloroaluminum PC has been shown an effective photosensitizer *in vitro* (Ben-Hur *et al.*, 1987). Brasseur *et al.* (1987) found effective photodynamic action of cerium and aluminum PC complexes, however normal tissue toxicity occurred with cerium PC. Metal-free PC display little PDT effect. Roberts *et al.* (1991) have found good response in spontaneous tumors in pet animals photosensitized with chloro-aluminum sulfonated PC.

The aspartate esters of Chlorin e6 (NPe₆) produce cell death *in vitro* and tumor control *in vivo* (Nelson *et al.*, 1987b; Roberts *et al.*, 1988). This sensitizer has an absorption maximum at 664 nm. Recently, Pandey *et al.* (1991) have shown that the long carbon chain ether

derivatives are better photosensitizers than their ester analogues. The initial clinical results of intraoperative PDT with meso-tetra-(hydroxyphenyl)-chlorin (mTHPC) after surgery for malignant mesothelioma showed selective tumor uptake and tumor necrosis up to 10 mm in depth (Ris *et al.*, 1991).

Purpurins have a reduced pyrrole group and as such are similar to the chlorins. The advantage of these compounds is their much stronger and red-shifted absorption band with a peak near 700 nm. A considerable PDT effect was found after systemic injection in an experimental animal tumor (Morgan *et al.*, 1987a; Selman *et al.*, 1987).

Bacteriochlorin-a has an absorption band at 765 nm and has proved effective in destruction of murine leukemia cells *in vitro* (Beems *et al.*, 1987). Schuitmaker *et al.* (1990) have shown preferential retention of this substance in rabbit eye melanoma.

A Verdin containing a cyclohexanone ring fused to one of the pyrroles of a porphyrin nucleus presents a visible absorption peak at 695 nm. (Morgan *et al.*, 1987b). PDT showed an extensive necrosis in animal tumors *in vivo* (Morgan *et al.*, 1987b; Hayden *et al.*, 1990).

A Benzo-porphyrin derivative of PROTO was prepared by Pangka *et al.* (1986). This compound is known as Benzoporphyrin derivative (BPD) and has an absorption peak at 690 nm. BPD was found a better photosensitizer than Hpd *in vitro* (Richter *et al.*, 1987). Photosensitivity disappears 72 hours after administration to human volunteers. Phase I clinical studies have been started to evaluate its effects on basal cell carcinoma and skin metastases of breast cancer (D. Dolphin, Quadra Logic Technologies Inc., Vancouver, BC, Canada. *Personal communication*, 1992).

Finally, 5-aminolevulinic acid (ALA) induced photosensitization may be a promising approach. This method of photosensitization is based on the following observations:

1. In every cell porphyrins are being produced as precursor of heme.
2. Ferrochelatase, which converts PROTO to heme, has been found decreased in various malignant and regenerating tissues (Rubino & Rasetti, 1966; Schoenfeld *et al.*, 1988; Leibovici *et al.*, 1988).

We therefore proposed that bypassing the rate limiting step in the synthesis of heme, by the oral administration of ALA would result in the selective accumulation of porphyrins in the malignant tissue. Studies in the rat liver metastasis model showed that indeed PROTO accumulated progressively in colon carcinoma with increasing duration of ALA administration, whereas no increase was found in normal liver. A porphyrin concentration ratio of 4:1 (tumor to liver) was found in animals treated with ALA for 11 days. In contrast, the ratio in animals treated with 5 mg/kg i.v. Photofrin was 1:3 (tumor to liver) (Chapter 9). The absorption maximum for PROTO is at 630 nm (Pottier *et al.*, 1986).

From several second-generation photosensitizers, such as aluminum sulfonated phthalocyanines, chlorins and ALA induced PROTO, a reduced skin photosensitivity compared to Photofrin has been reported (Roberts *et al.* 1989, Tralau *et al.* 1989, Ris *et al.* 1991, Bedwell *et al.* 1992). Further research should establish whether one of these or future substances can meet the requirements of the ideal photosensitizer.

Light Delivery

When light is delivered interstitially, the damage is confined to the target volume by the light distribution especially in most solid organs. Therefore, Photofrin concentration in surrounding tissue may not be critical under those circumstances. In our study on interstitial PDT of experimental rat liver metastases, we showed that selective light delivery can prevent major normal tissue damage even in an organ that efficiently retains Photofrin (Chapter 8).

Gibson *et al.* (1990) have studied the effects of various photoradiation regimens on tumor growth delay. They found a significant delay in growth of Photofrin sensitized rat mammary carcinomas treated with periodic illumination using 1 h dark interval, compared to tumors receiving continuous illumination. Remarkably, a growth delay was also found in animals treated continuously, with light of 50 mW/cm² for 2 h (total fluence 360 J/cm²) compared to animals exposed to the same total fluence but with light of 100 or 200 mW/cm² and exposure times of 1 or 0.5 h respectively. These results suggest that modifications in the light delivery regimes can substantially improve PDT efficacy.

Light Source

The currently available argon-dye laser systems are expensive and clinically not easy to handle. Recently, a new PDT laser system has been introduced which uses the easy transportable pulsed 532 nm potassium titanium phosphate (KTP) laser as a pump (Ferrario *et al.*, 1991). However, this system is still relatively complex and large. A better solution would be a diode laser that emits light of 630 nm. Advantages of diode lasers are the low capital cost, negligible running cost, high reliability, and small size and portability (Wilson, 1989). Currently, diode lasers can generate a power of 1 W at 750-800 nm. This wavelength range would already be suitable to treat second-generation photosensitizers such as Bacteriochlorin-a. Until now, however, the intensities of red light emitting diode systems are too low for PDT with Photofrin. Another approach could be the injection of a chemiluminescent activator into the photoactivated tumor (Phillip *et al.*, 1984) or the systemic administration of the activator coupled to a monoclonal antibody directed against the tumor. This last strategy has already been investigated to selectively target a photosensitizer to the malignant tissue (Oseroff *et al.*, 1987; Rakestraw *et al.*, 1990).

Monitoring PDT

Several investigators have studied the possibility of assessing the efficacy of a PDT treatment. Keene *et al.* (1986) have used *in vivo* measurements of the singlet oxygen production during illumination and Tromberg *et al.* (1990) have determined transcutaneous oxygen tension after a PDT treatment. Magnetic resonance imaging (MRI) has been shown useful in monitoring the effects of PDT (Dodd *et al.*, 1989; Moore *et al.*, 1989). Nuclear magnetic resonance (NMR) spectroscopy (Gibson *et al.*, 1989; Mattiello *et al.*, 1990) and ⁹⁹Technetium methylpropylene-amine oxime scintigraphy (Moore *et al.*, 1992) have also been used to examine tumor metabolism and blood flow. To date these PDT feedback methods have only been studied experimentally.

Combination Therapy

In many of the earlier studies, the PDT illumination itself caused significant temperature rise as a result of light absorption by the target tissue. Therefore, rough upper limits have been established for applied power densities to avoid heating effects. Conversely, hyperthermia could be applied deliberately with PDT, either using the PDT-light itself or by an independent laser, microwave or ultrasonic irradiation. PDT has been shown to be synergistic with sub-lethal hyperthermia (Waldow & Dougherty, 1984). A synergistic response was observed when the hyperthermia (generally 45.5°C for 30 min) was delivered either simultaneously or within 30 min of PDT illumination (Matsumoto *et al.*, 1990; Glassberg *et al.*, 1991). Potentiation decreased with increasing time between PDT and heat delivery (Waldow, 1985, 1987). For heat generation, a Neodymium:Yttrium-Aluminum-Garnet (Nd:YAG) laser is very useful, as the light used to activate the photosensitizer (630 nm) and the light used to produce hyperthermia (1,064 nm) can be guided through the same quartz fiber (Mang, 1990). Other combinations of PDT with chemotherapy, radiotherapy and surgery have also been proposed or examined in the laboratory.

The possibility of taking advantage of the hypoxic environment induced by PDT has initiated studies that evaluate the combination with hypoxic cytotoxins, such as misonidazole (Gonzalez *et al.*, 1986). Changes in cellular pH can have a significant influence on porphyrin biodistribution (Pottier & Kennedy, 1990). Thomas & Girotti (1989) showed a transient decrease in cellular pH after multiple glucose injections combined with an increased retention of Hpd. Recently, Nelson *et al.* (1992) demonstrated enhanced cytotoxicity of PDT in combination glucose administration.

As vascular injury is thought to play a major role in PDT damage, combination with vasoactive drugs have been studied. Verapamil was found to enhance PDT induced tumor destruction associated with increased porphyrin uptake (Cowled & Forbes, 1989).

Finally, PDT may be used as an adjunct to other treatments. Thus, previously untreatable tumors may become resectable after PDT reduction or PDT may be used in tumors pretreated with other modalities.

8. Interstitial Photodynamic Therapy

Adapted from: R. VAN HILLEGERSBERG, J.P.A. MARIJNISSEN, W.J. KORT, P.E. ZONDERVAN, O.T. TERPSTRA & W.M. STAR. Interstitial Photodynamic Therapy in a Rat Liver Metastasis Model Br J Cancer 1992; 66: 1005-1014

INTRODUCTION

Photodynamic therapy (PDT) is a relatively new local treatment modality, which has been used successfully in the treatment of various malignant tumors, including cancer of the bladder, skin, upper respiratory tract and gastro-intestinal tract (Dougherty, 1987a, 1989; Manyak *et al.*, 1988; Gomer, 1989; Wilson *et al.*, 1991). This type of therapy is based on the accumulation of a photosensitizer in malignant tissues and the subsequent illumination with light of an appropriate wavelength, which creates a reactive species that upon decay to its ground state transforms available oxygen into singlet oxygen (Chapter 7). It is this very reactive singlet oxygen which is thought to be the most important cytotoxic agent in PDT (Weishaupt *et al.*, 1976), causing direct damage to many cellular sites as well as to the microvasculature (Henderson & Bellnier, 1989). For clinical application, the most commonly used photosensitizers have been hematoporphyrin derivative (Hpd), a mixture of various porphyrins and Photofrin®, a substance derived from Hpd and enriched in the photodynamically active fraction (Lipson *et al.*, 1961; Dougherty *et al.*, 1984; Bonnet & Berenbaum, 1989).

Until now, PDT of tumors in the liver has been restricted as liver tissue accumulates Photofrin more efficiently than the malignant tissue (Gomer & Dougherty, 1979; Bugelski *et al.*, 1981; Cozzani *et al.*, 1984; Bellnier *et al.*, 1989). Therefore, superficial tumor illumination causes substantial liver necrosis (Pimstone *et al.*, 1982). Moreover, the limited light penetration during superficial illumination makes it impossible to treat deep seated or larger solid tumors (Doiron *et al.*, 1983). These limitations could be overcome by implanting the light delivery fibers with diffusing cylinder tips directly into the tumor (interstitial therapy), thus applying the light selectively and with greater accessibility (Dougherty *et al.*,

1981; Holt *et al.*, 1985; Arnfield *et al.*, 1986, 1989; Gatenby *et al.*, 1987; Marijnissen *et al.*, 1992).

In the present study we therefore investigated the effects of photodynamic therapy on tumor and surrounding normal hepatic tissue using interstitial illumination in a rat liver metastasis model.

MATERIALS AND METHODS

Experimental Design

Laser illumination was performed 20 ± 1 days after intrahepatic tumor inoculation in 108 animals. A relaparotomy was made under anesthesia with Hypnorm® (Janssen Pharmaceutica B.V., Tilburg, The Netherlands), 1 mg/kg body weight i.m., and the visible diameter of the tumor was measured with sliding calipers.

The animals were randomly allocated to two experiments: I, to assess short-term photodynamic effects and the biochemistry of liver damage and II, to assess liver function and long-term effects, especially in relation to tumor remission.

In experiment I, the animals were randomly assigned to 4 groups: The experimental group (Photofrin and light, $n=6$ per light dose), a control group (laser light only, $n=6$ per light dose), a control group (Photofrin only, $n=6$) and a control group (diffuser insertion only, $n=6$). Two days before laser illumination Photofrin was administered. To measure the amount of liver damage, blood was collected for serum aspartate aminotransferase (ASAT) and alanine aminotransferase (ALAT) determination on the first and second day after laser treatment. On the second day after laser, the animals were sacrificed and the liver was removed for light microscopical determination of short-term effects.

In experiment II, the animals were randomly assigned to 2 groups. The experimental group ($n=6$ per light dose) underwent the same treatment as in experiment I. The animals in the control group ($n=6$) received Photofrin without any laser illumination. To determine liver function, an antipyrine clearance test was performed on the first day after laser treatment. All animals were sacrificed on day 36 after laser treatment for histological determination of long-term effects.

Photosensitizer

Photofrin® (Lederle Laboratories, Pearl River, NY, U.S.A.) was administered in a dose of 5 mg/kg body weight by penile vein injection. After Photofrin administration the animals were kept in subdued light, with preservation of night-day rhythm, to avoid light induced skin damage as a result of Photofrin accumulation.

Light Source

A Rhodamine B dye laser (Model 375B, Spectra Physics Lasers, Mountain View, U.S.A.) pumped by an argon-ion laser (Model 171, Spectra Physics Lasers) was used to generate red light of 625 ± 2 nm. This wavelength was chosen because light of 625 nm wavelength appears to have a higher biological effectivity than the conventionally used 630 nm (Star *et al.*,

(1990). The dye-laser was tuned by a two-plate birefringent filter using a monochromator. Light intensities were monitored with a calibrated Optometer (Model 81, United Detector Technology, Hawthorne, CA, U.S.A.), which served as the reference.

Light Delivery and Dosimetry

The light was transmitted through a 200 μm silicone cladded flexible quartz fiber (Quartz and Silice, QSF-200) with a custom built cylindrical diffusing end of 0.5 cm length (Marijnissen *et al.* 1985). The overall diameter of both the light diffusing length and fiber itself was 600 μm . The power emitted by the diffuser was determined using an integrating sphere (Model 2550, United Detector Technology) with a radiometer (Optometer, model 181, United Detector Technology). A 19 gauge needle was used to create an entry into the center of the tumor. To prevent adherence to the tissue, some Vaseline was put on the diffuser. Following this, the needle was withdrawn and the diffuser inserted using a stand on which the fiber system was fixed (Figure 8.1). Laser illumination was then performed with energies ($\text{Joule/cm} = \text{Watts/cm} \times \text{seconds of exposure}$) of either 100, 200, 400, 800 or 1600 J/cm (per cm length of cylindrical diffuser) at a power setting of 200 mW/cm. During illumination the liver was covered with a black gauze soaked in saline solution to protect the tissue from dehydration and to avoid influences from ambient light and laser light reflection. During treatment the animals were kept on a heating plate to avoid cooling down and rectal temperature was measured with a thermocouple (Type C-RR2, Exacon). To give an indication of the actual light dose delivered to the tissue, in a number of experiments the light energy

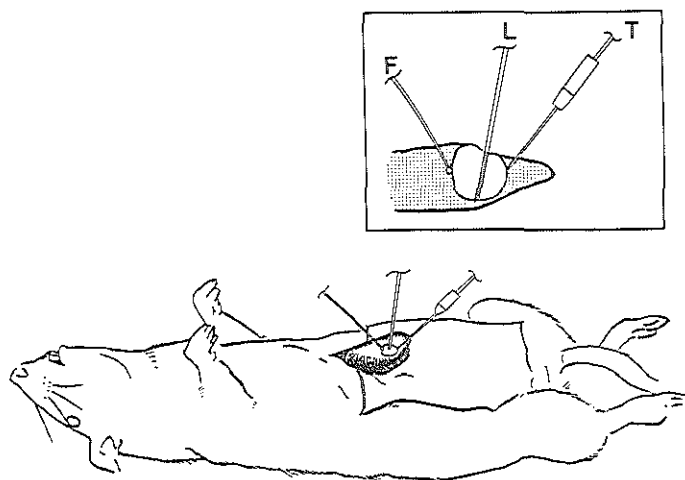


Figure 8.1. Schematic representation of the experimental set-up. The cylindrical diffuser of the laser fiber (dashed end) is inserted into the tumor (L). The radiant energy fluence at the tumor boundary is measured with a miniature isotropic probe (F). Tissue temperature is measured with a thermocouple system that is installed at the edge of the tumor (T).

fluence (J/cm^2) at the tumor boundary was measured with a miniature isotropic detector (Marijnissen *et al.*, 1985, 1987). Tumor temperature was determined with a needle thermocouple (Type C-N5, Exacon) connected to a read out instrument (Model MC-9200, Exacon) that was positioned at the edge of the tumor (Figure 8.1). The tumor periphery was chosen for these measurements, as this would be the most critical region for complete tumor cell destruction due to the central diffuser position.

Determination of Photodynamic Effects

On histological slides taken from animals sacrificed on the second day after PDT treatment, the areas of hepatic necrosis and vital or necrotic tumor were calculated by computer-assisted integration of the circumference (IBAS 2000, Kontron Bildanalyse GmbH, München, Germany). The maximal width of the rim of hepatic necrosis was determined by IBAS assisted measurements.

On specimens taken from animals sacrificed 36 days after PDT treatment, the tumor area was measured by IBAS to give an indication of tumor growth retardation.

Statistical Analysis

The values are expressed as means \pm standard error of the mean (SEM). Spearman's rank-order correlation was used to analyze the relation between percentage of liver or tumor necrosis, the ASAT, ALAT levels, the antipyrine elimination half-life ($T_{1/2}$) values and long-term tumor area on the energy applied. The relation between liver necrosis and energy in the control group treated with light energy only was tested after dichotomization, by the Mann-Whitney U test. The influence of energy on tumor remission was determined by an Exact-trend test. Other comparisons were made using the Student's t-test. A difference was considered to be significant at P values of <0.05 .

RESULTS

In one animal the tumor implant did not take; another animal died during anesthesia. All remaining animals survived and none of the animals showed signs of discomfort after PDT treatment.

On the day of laser illumination the mean \pm SEM visible tumor diameter of all animals ($n=106$) was 5.7 ± 0.1 mm, varying from 4.0-8.0 mm.

Temperature and Fluence

With 400 J/cm from the diffuser a fluence of 170 ± 30 J/cm^2 was measured at the boundary of 5.5 ± 0.5 mm diameter tumor ($n=5$). Slight changes in light penetration through the tumor could be observed during PDT treatment.

Baseline rectal temperature was $31.9 \pm 0.4^\circ\text{C}$ ($n=18$), remaining constant during PDT treatment. The tumor core temperature was $29.7 \pm 0.6^\circ\text{C}$, varying from 27.5 to 34.3°C . Generally, the temperature at the tumor boundary increased during illumination with a mean value of $3.3 \pm 0.3^\circ\text{C}$, ranging from 0.2 to 6°C . The actual tissue temperature was always less

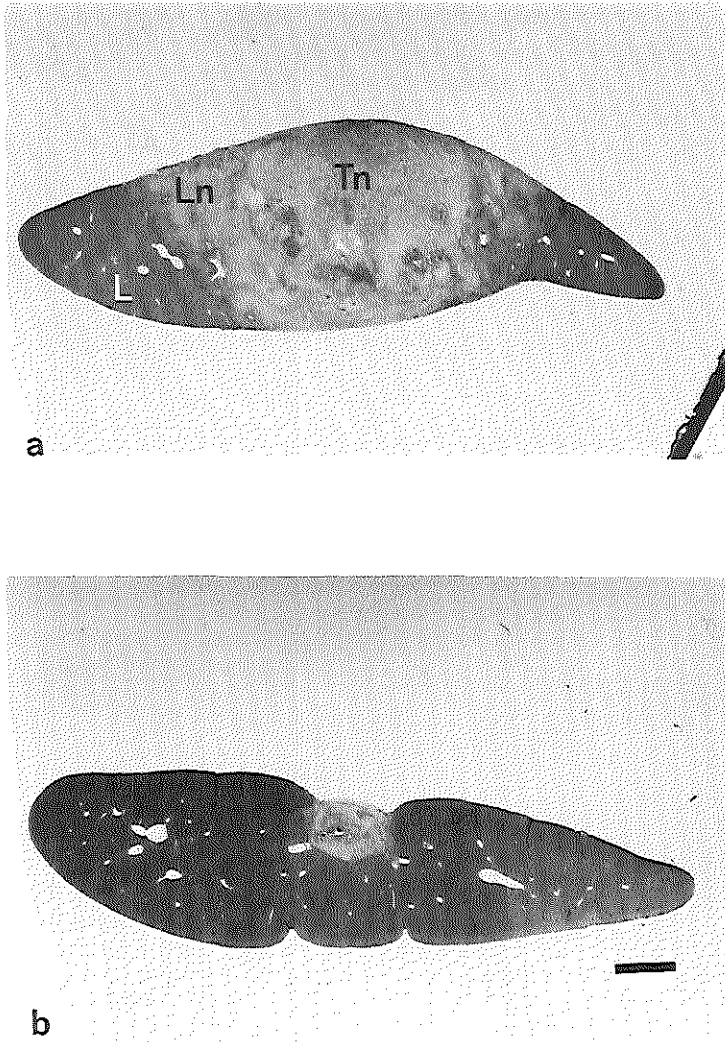


Figure 8.2. Histological overview of the tumor in the liver at different stages after PDT. (a) On the second day after PDT the tumor is largely necrotic, surrounded by a zone of necrotic liver tissue. (b) On day 36 the necrotic area has been replaced by connective scar tissue. This tumor shows complete remission. Tn, tumor necrosis; Ln, Liver necrosis; L, Normal liver tissue. Bar: 1.7 mm (hematoxylin, azophloxin & saffron stain).

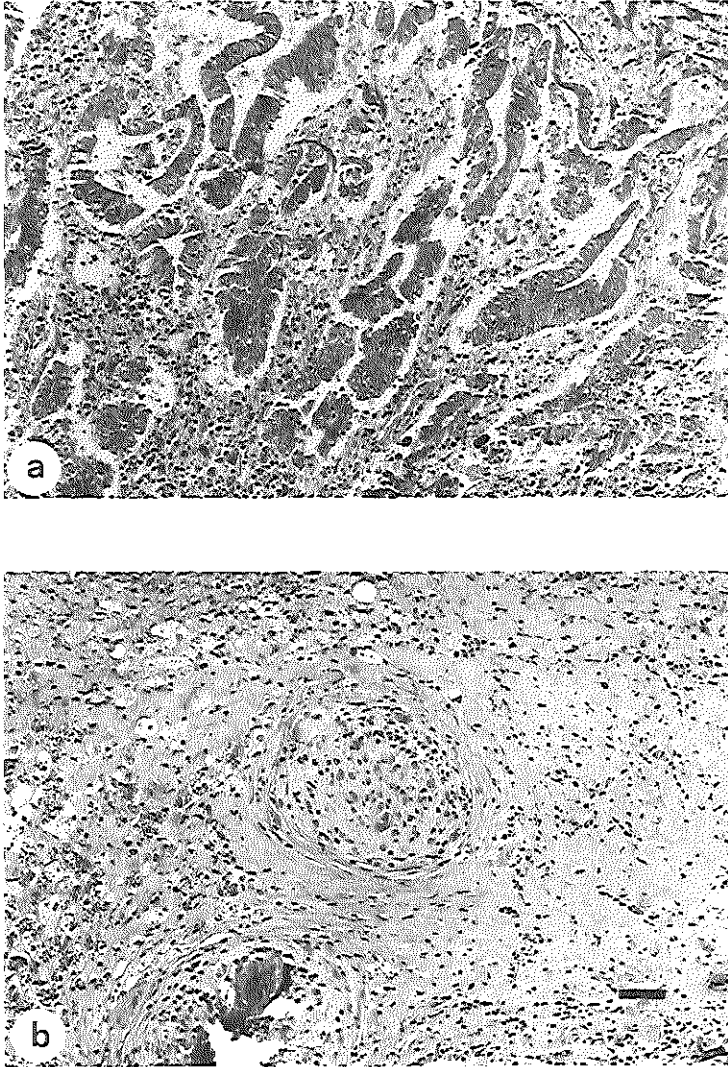


Figure 8.3. Histological sections of tumor tissue in the liver. (a) Tumor necrosis on the second day after PDT is characterized by disintegrated cells with acidophilic cytoplasm and pyknotic or fragmented nuclei. (b) Thirty-six days post-treatment a granulomatous reaction with multinucleated giant cells is present. Bar: 50 μm , (hematoxylin, azophloxin & saffron stain).

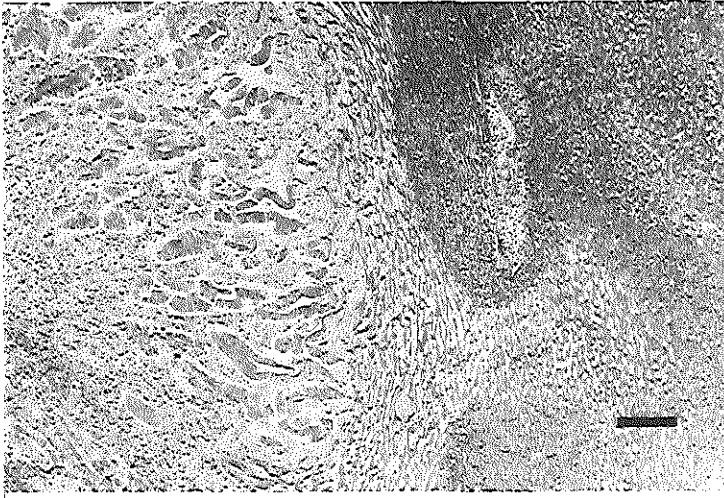


Figure 8.4. Histological section on the second day after PDT. The necrotic tumor is surrounded by a zone of hepatic necrosis, consisting of dilated sinusoids and deliquesced hepatocytes. The border between tumor and liver necrosis is infiltrated by inflammatory cells. Bar: 150 μ m (hematoxylin, azophloxin & saffron stain).

than 40°C. Tissue changes as previously observed after thermal laser therapy, such as charring, cavitation or elongation of cellular nuclei (Chapters 4-6) could not be identified in illuminated areas.

Histopathology

The general pattern of PDT induced tissue damage and subsequent healing was unaffected by the variations in light energy applied (Figure 8.2; for pre-treatment histology see Figure 2.4a). Sections on the second day after laser treatment showed massive tumor necrosis, characterized by cellular debris and disintegrated cells with acidophilic cytoplasm and pyknotic or fragmented nuclei (Figure 8.3a; for pre-treatment histology see Figure 2.1), surrounded by a polymorphonuclear inflammatory infiltrate (Figure 8.4). Depending on the amount of light energy applied, islands of vital tumor cells could be identified in the necrotic tumor area (Figure 8.5). Around this area a zone of necrotic liver tissue was visible, consisting of dilated sinusoids and deliquesced hepatocytes with vacuolated acidophilic cytoplasm without nuclei (Figures 8.2a, 8.4). Remarkably, the hepatic tissue had remained intact around the portal areas (Figure 8.6). A second zone of inflammatory infiltrate surrounded the hepatic necrosis.

Thirty-six days after PDT treatment two different situations could be observed:

1. Complete tumor remission (Figure 8.2b); the necrotic area was replaced by regenerated

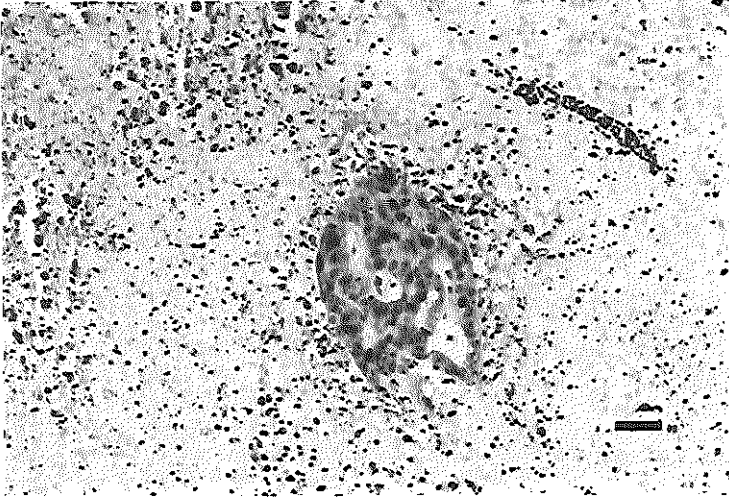


Figure 8.5. Histological section on day 2 after PDT. An island of vital tumor cells in the necrotic tumor area. Bar: 50 μm (hematoxylin, azophloxin & saffron stain).



Figure 8.6. Histological section on day 2 after PDT. Liver tissue around the portal areas has remained intact. Bar: 150 μm (hematoxylin, azophloxin & saffron stain).

liver tissue and connective scar tissue in which a granulomatous reaction with multi-nucleated giant cells was present (Figure 8.3b).

2. Tumor outgrowth, most certainly from the remaining islands of vital tumor tissue.

Short-term Photodynamic Effects

Tissue damage. The mean \pm SEM tumor diameter, derived from measurements on the tumor area ($n=71$), was 5.8 ± 0.1 mm. Maximal width of the surrounding rim of liver necrosis varied from 2.6 ± 0.2 mm, after 100 J/cm illumination to 3.7 ± 0.4 after 400 J/cm.

The results of the measurements on the areas of hepatic necrosis and vital or necrotic tumor are shown in Table 8.1. The total (i.e., vital plus necrotic) tumor area ranged from 10.2 to 36.9 mm², with a mean \pm SEM of 26.7 ± 0.7 mm² ($n=71$). The mean tumor necrosis varied from 3.4 ± 0.6 mm² after Photofrin administration only, to 23.6 ± 0.8 mm² in the experimental group treated with 1600 J/cm. The mean \pm SEM vital tumor area was 26.9 ± 1.7 mm² in controls after Photofrin only, and 0.2 ± 0.1 mm² after PDT with 1600 J/cm. Hepatic necrosis occurred in all experimental groups, with a mean maximal value of 30.5 ± 1.4 mm² after 1600 J/cm.

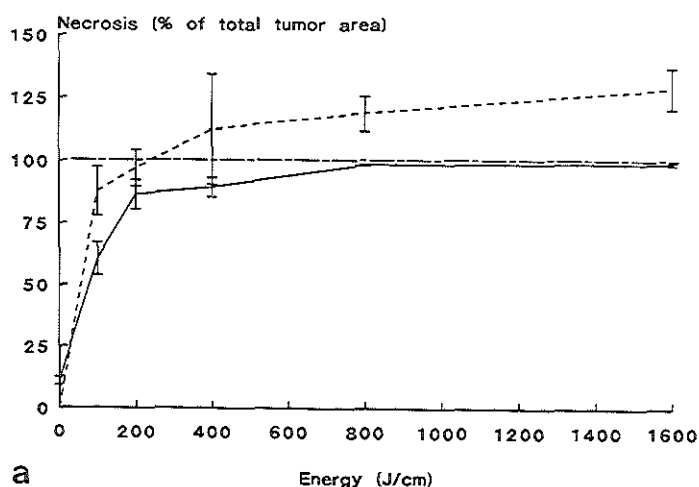
As the amount of tumor necrosis is related to tumor size, each measurement was expressed as percentage of the individual total tumor area. For comparison, the same was done for liver necrosis (Figure 8.7). Tumor necrosis was found to increase with light energy delivered, with mean values of $60.6\pm6.6\%$ at 100 J/cm compared with $99.0\pm0.6\%$ at 1600 J/cm ($P<0.001$).

Table 8.1. Mean \pm SEM area of hepatic necrosis, tumor necrosis and vital tumor tissue on the second day after PDT (in mm²).*

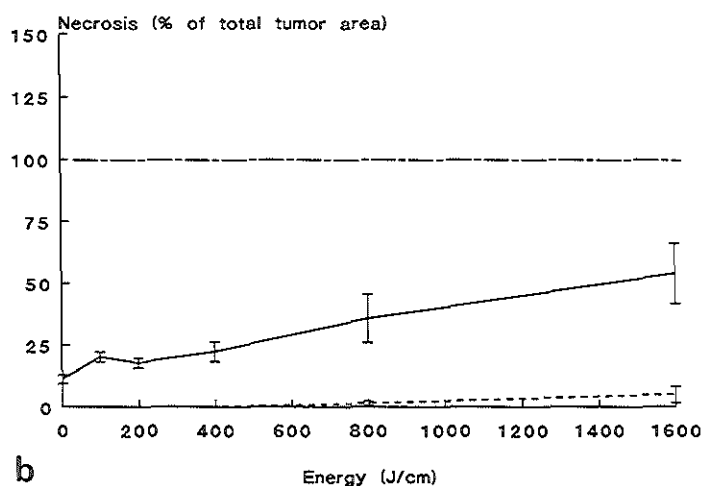
Energy (J/cm)	No. of animals	Tumor vital	Tumor necrosis	Liver necrosis
<i>Control groups†</i>				
Photofrin	6	26.9 ± 1.7	3.4 ± 0.6	
Diffuser	6	27.3 ± 1.5	4.8 ± 0.5	-
100	6	22.9 ± 0.8	5.8 ± 0.7	-
200	6	22.6 ± 1.6	4.9 ± 0.7	-
400	6	18.7 ± 2.7	5.1 ± 1.2	-
800	6	18.1 ± 3.7	8.7 ± 1.8	0.4 ± 0.3
1600	6	12.3 ± 2.9	15.8 ± 3.9	1.3 ± 1.0
<i>Experimental groups</i>				
100	6	10.2 ± 1.7	16.2 ± 2.5	22.2 ± 1.8
200	6	3.6 ± 1.5	23.1 ± 2.2	25.3 ± 1.1
400	6	2.5 ± 1.0	20.0 ± 1.4	25.8 ± 6.0
800	5	0.3 ± 0.1	23.2 ± 2.0	28.0 ± 2.9
1600	6	0.2 ± 0.1	23.6 ± 0.8	30.5 ± 1.4

*Laser illumination with 200 mW/cm was performed 2 days after Photofrin 5 mg/kg i.v..

†Control animals received either Photofrin only, diffuser insertion only, or laser illumination only.



a



b

Figure 8.7. Tumor (—) and liver (· · ·) necrosis as percentage of the individual total tumor area vs. energy delivered on the second day after laser treatment in (a) the experimental and (b) control group treated with laser light only. Each point represents the mean \pm SEM of 6 experimental results, except for the experimental group treated with 800 J/cm ($n=5$). Control animals treated with Photofrin only, served as starting point at energy level 0. The dashed line describes the total tumor area.

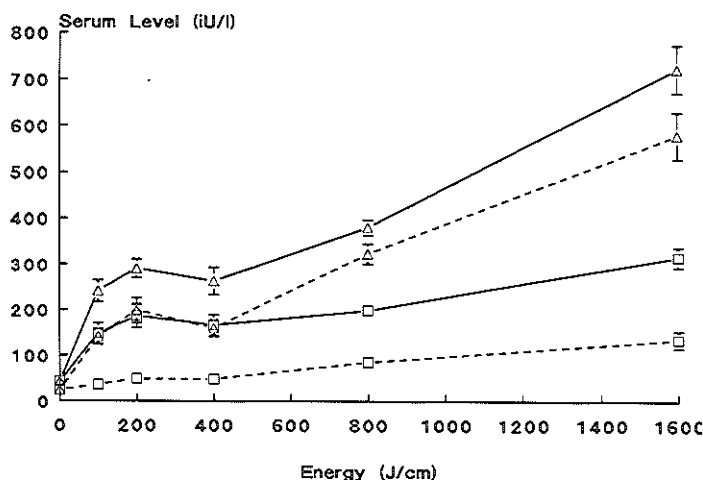


Figure 8.8. Serum ASAT (—) and ALAT (---) levels vs. energy delivered in the experimental group (Δ) and control group treated with laser light only (\square) on the first day after laser treatment. Animals treated with Photofrin only served as controls. Each point represents the mean \pm SEM of 6 experimental results.

Liver necrosis was also related to light energy, ranging from $87.7 \pm 9.8\%$ at 100 J/cm to $128.8 \pm 8.3\%$ at 1600 J/cm ($P=0.001$) (Figure 8.7a).

Control animals treated with Photofrin only, showed the usual preexistent central tumor necrosis, measuring $11.1 \pm 1.7\%$. Diffuser insertion did not cause significant additional damage ($P=0.09$). However, after laser illumination only, a significant relationship was found between tumor ($P=0.003$) or liver ($P=0.03$) necrosis and energy delivered, with tumor necrosis of $35.7 \pm 9.8\%$ at 800 J/cm and $54.0 \pm 12.3\%$ at 1600 J/cm, accompanied by liver necrosis of $1.4 \pm 0.9\%$ and $5.0 \pm 3.5\%$ respectively (Figure 8.7b). Tumor necrosis in this group was limited to the central area around the diffuser and had a similar appearance as the earlier described photodynamic damage. Liver necrosis occurred only at the dorsal tumor border, where the diffuser probably had penetrated hepatic tissue.

Serum ASAT/ALAT. Serum ASAT and ALAT levels on the first day post-treatment were increased in the experimental group and the control group treated with light only (Figure 8.8). The values were significantly related to the amount of light energy applied ($P<0.001$). After a plateau at 100 J/cm, however, a strong increase was found at energies over 400 J/cm. No difference was found between ALAT levels of control animals treated with Photofrin only compared to diffuser insertion only ($P=0.9$). ASAT levels, however, showed a significant difference, with values of 42.4 ± 3.1 iU/l after Photofrin only compared to 62.4 ± 7.7 iU/l after diffuser insertion ($P=0.01$).

On the second day post-treatment enzyme levels were still slightly increased with maximum values in the experimental group of 71.7 ± 3.9 iU/l for ALAT and 119.7 ± 7.5 iU/l for ASAT at 1600 J/cm.

Antipyrine clearance test. The antipyrine plasma elimination half-life levels on the second day after laser application were not related to energy applied ($P=0.29$) (Table 8.2).

Long-term effect on tumor remission

All tumors in control animals showed massive outgrowth with infiltration to adjacent tissue. In the experimental group, several animals showed complete tumor remission. Best results were obtained at 800 J/cm with complete remission in 4 out of 6 animals (Table 8.3). Owing to the unfavorable results at 1600 J/cm - merely 1 out of 6 tumors in complete remission - no significant relation was found between number of tumors in remission and light energy delivered ($P=0.08$). The size of the tumor area on day 36 after PDT (Table 8.3) was related to the amount of light energy delivered ($P<0.001$) as would be expected from the results on the second day post-treatment (Figure 8.7a).

DISCUSSION

In this study the ability of interstitial photodynamic therapy to cause major destruction of solid tumors within the liver was demonstrated. Histological examination showed tumor cell necrosis on day 2 post-treatment and connective scar tissue on day 36. Interstitial treatment enabled effective illumination of the tumor, resulting in complete tumor remission in 4 out of 6 cases at 800 J/cm from a 0.5 cm cylindrical diffuser. Despite local illumination, surrounding liver damage occurred at all energies applied. However, liver necrosis was limited to a distinct zone of 2-4 mm width and did not deteriorate liver function as measured by antipyrine clearance.

In previous studies, several attempts have been made to solve the problem of efficient photosensitizer accumulation in the liver. Kita *et al.* (1987) found that indocyanine green after intravenous injection, protects photosensitized hepatocytes against illumination with green light. Nishiwaki *et al.* (1989) used intraarterial administration of the photosensitizer Pheophorbide to cause selective accumulation in liver tumors. Interstitial therapy, however, can be applied in combination with Photofrin, the only clinically used photosensitizer, and additionally provides the possibility of treating deep seated solid tumors.

There are no data available on Photofrin distribution of intrahepatic tumor and surrounding liver at different time intervals after administration. We therefore based the interval between Photofrin administration and illumination on previous studies in experimental animals carrying extrahepatic tumors. These studies showed an optimal porphyrin concentration ratio between tumor and liver after a period of 2 days (Gomer & Dougherty, 1979; Cozzani *et al.*, 1984; Jori *et al.*, 1986).

An increase in light dose delivered, resulted in a higher percentage of tumor necrosis in the experimental group, with maximal values of $99.0 \pm 0.6\%$ at 1600 J/cm (Figure 8.7a). Tumor necrosis also appeared in control animals treated with laser light only (Figure 8.7b). Bown *et al.* (1986) have studied the effects of different power outputs on PDT in normal rat liver. They found that 400 mW red light from an interstitial bare tipped fiber significantly heated the tissue, resulting in charring at the fiber tip within 1 min.

Table 8.2. Mean \pm SEM antipyrine plasma elimination half-life ($T_{1/2}$) on the first day after laser treatment*.

Energy (J/cm)	No. of animals	$T_{1/2}$ (h)
Control†	5	2.0 \pm 0.1
100	4	2.0 \pm 0.1
200	6	1.9 \pm 0.0
400	6	1.9 \pm 0.1
800	6	2.1 \pm 0.1
1600	6	2.0 \pm 0.1

*Laser illumination with 200 mW/cm, 2 days after Photofrin (5 mg/kg i.v.).

†Control animals received Photofrin only.

Table 8.3. Tumor remission and vital tumor area on the 36th day after laser illumination.*

Energy (J/cm)	No. of tumors in remission†	Vital Tumor area (mm ²)‡						
		Individual value						Mean \pm SEM
Control§	0/6	160	162	185	203	260	281	209 \pm 21
100	0/5	106	119	135	145	-	396	180 \pm 54
200	2/6	0	0	8	124	162	170	77 \pm 34
400	2/6	0	0	2	16	29	30	13 \pm 6
800	4/6	0	0	0	0	14	31	8 \pm 5
1600	1/6	0	13	65	79	112	116	64 \pm 20

*Laser illumination with 200 mW/cm, 2 days after Photofrin (5 mg/kg i.v.).

†No. of tumors in complete remission / no. of animals.

‡Measured by computer assisted integration of the circumference.

§Control animals received Photofrin without any laser illumination.

The light transmission in the tissue dropped accordingly to under 10%. At 100 mW power output, however, light transmission remained constant and no thermal tissue changes were found. In the present study we used the same power output of 100 mW, from a 0.5 cm cylindrical diffuser (i.e., 200 mW/cm). With a diffuser, the light is emitted from a larger surface area resulting in a more uniform light delivery. Thus, the heat generated in this manner is much less localized and intense than with a bare fiber tip. Indeed, charring could not be observed on histological specimen and temperature at the tumor boundary was always less than 40°C. However, higher temperatures might have occurred at the diffuser, resulting in hyperthermic effects at longer exposure times (Field *et al.*, 1987). Indeed, tumor necrosis

in the control group treated with light only was limited to the area around the diffuser. Another explanation, however, might be the activation of preexistent endogenous porphyrins (Chapter 9).

Although PDT has been shown to be synergistic with hyperthermia (Waldow & Dougherty, 1984; Waldow *et al.*, 1987; Matsumoto *et al.*, 1990), thermal influences are normally avoided in fundamental studies to investigate exclusively the PDT effect. A power output of 200 mW/cm was therefore applied in this study. However, as PDT damage largely depends on the total energy delivered (Joules = Watts x seconds), the exposure time has to be correspondingly longer at lower dose rates. We used a maximal exposure time of 2 h and 13 min (1600 J/cm) in this study. In clinical PDT, however, higher power outputs may be applied (as long as charring is avoided) to keep exposure time within boundaries. For example, 400 mW/cm delivered interstitially during 8-12 min (200-300 J/cm) is a standard treatment for patients with endobronchial tumors (Balchum & Doiron, 1985).

Tumor growth retardation, as measured by the tumor area on the 36th day after PDT, was related to the amount of light energy delivered, as would be expected from the amount of tumor necrosis on the second day after treatment. Up to 800 J/cm, a similar relation was found for the number of tumors in complete remission. The unfavorable results at 1600 J/cm, however, led to an overall nonsignificant relation between tumor remission and energy applied, suggesting an optimum relation between light dose and tumor response (Table 8.3). From the current knowledge of the photodynamic reaction, however, these results can hardly be explained. Singlet oxygen, the most important cytotoxic agent in PDT, is generated via the so called Type II mechanism of photosensitized oxidation (Chapter 7). Upon absorption of a photon, the porphyrin molecule is brought to an excited singlet state that undergoes intersystem crossover to the excited triplet state. Transfer of energy from the triplet photosensitizer to available oxygen creates the reactive singlet oxygen. The electrophilic nature of singlet oxygen makes it very efficient at producing oxidized forms of biomolecules (Gomer, 1989a). Thus, the photocytotoxic reaction occurs exclusively during illumination, which makes it unlikely that doubling the light dose (i.e., from 800 J/cm to 1600 J/cm) would reduce the photodynamic effect.

The appearance of nests of apparently therapy resistant tumor cells in the necrotic area after PDT has previously been described by Pimstone *et al.* (1982) and Holt *et al.* (1985) in rat hepatoma. There could be several mechanisms underlying this phenomenon, assuming the heterogeneity of tumor tissue:

1. The incorporation of Photofrin in these cells is disturbed as a result of poor vascular supply or altered transmembrane passage which may cause low levels of photosensitizer.
2. The cells are in a dormant state with very low O₂ metabolism and no singlet oxygen production.
3. Vessels with a diameter larger than 1.3 mm produce a cytoprotective shadowing effect, thus preventing appropriate illumination of the cells (Pimstone *et al.*, 1982).
4. The total light dose is too low to achieve photodynamic destruction in all tumor cells. Kato *et al.* found an uneven distribution of Photofrin fluorescence in early stage bronchus carcinoma, which could be evidence for state 1) (H. Kato, Tokyo Medical College, Tokyo, Japan. *Personal communication*, 1991). The nests of vital tumor cells were randomly spread

over the necrotic tumor area and a clear relation to vascular structures could only be identified twice (statement 3). Liver damage, however, was strongly related to the liver anatomy, as hepatic cells survived around the portal areas (Figure 8.6). This phenomenon is probably due to a different hepatocyte environment (perfusion, and hence supply of nutrients) and enzyme content in the periportal compared to pericentral domains (Lamers *et al.*, 1989). Thus, substances such as unsaturated fatty acids, that act as oxygen scavengers, and higher levels of enzymes such as superoxide dismutases would prevent oxidative damage in the periportal areas (Jungermann & Katz, 1989; Byczkowski & Gessner, 1988; Gutteridge & Halliwell, 1990). Knowledge about the mechanism responsible for the survival of specific tumor cells could lead to treatment strategies causing complete tumor destruction. When for instance a low concentration of Photofrin is caused by efficient transmembrane transport of porphyrins out of the cells, Ca^{2+} blocking agents could be a solution. Photofrin delivery to intrahepatic tumors might be improved by increasing tumor capillary flow with appropriate vasoactive agents (Ackerman *et al.*, 1988). The mechanism responsible for porphyrin accumulation in tumors is still unclear. In a recent study, however, we showed that a decreased conversion to heme, owing to decreased ferrochelatase activity may be an important factor (Chapter 9). Dailey & Smith (1984) have shown that several representative porphyrins in Photofrin are substrates for ferrochelatase. Therefore, modulation of this enzyme could be another approach (Smith, 1987).

As the diffuser was inserted into the center of the tumor, higher light doses were applied to the tumor than to the surrounding liver tissue. However, on the second day post-treatment at all energies a rim of liver necrosis was visible around the tumor, whereas at lower energies tumor tissue had remained largely intact. This could be the result of the unfavorable porphyrin concentration ratio between liver and tumor, which was found 3:1 (liver to tumor) after intravenous Photofrin in this model (Chapter 9).

In this study, liver necrosis increased with energy delivered, but a plateau occurred beyond 400 J/cm, indicating that higher laser energies could be applied without much more liver damage. An important factor in this matter is the difference in optical properties between the dark red colored liver and the whitish tumor (Chapter 10). The hepatic tissue effectively absorbs 625 nm light, which limits the light penetration in liver, and by that limits liver damage. This difference in absorption coefficient might be beneficial in the clinical application, where the peripheral interstitial diffuser would produce a comparable amount of liver damage.

Serum ASAT and ALAT levels on the first and second day post-treatment were used as biochemical parameters for liver damage. Indeed, a significant relation between enzyme level and delivered light energy was found, confirming our measurements on the area of hepatic necrosis in the experimental group. However, the rise in ASAT level after diffuser insertion only, did not correspond to the normal histological appearance of surrounding liver tissue. Recently, we measured ASAT and ALAT levels in rat liver and tumor CC531 (Chapter 2). The ALAT activity in liver and tumor showed a ration of 40:1 (liver to tumor), whereas ASAT ratio was 2:1, indicating that the serum ALAT level may be the most appropriate parameter for liver damage in this model. Thus, the increase in serum ASAT after diffuser insertion is probably due to tumor, rather than liver damage. A similar explanation could be

applied to the rise in ASAT level post-treatment with light only, especially at energies ≤ 400 J/cm. In this group liver necrosis appeared at 800 and 1600 J/cm, resulting in a higher ALAT level (Figures 8.7, 8.8).

In this study, we used a single PDT treatment with a fixed diffuser position to determine the photodynamic effects as standardized as possible. We therefore chose a tumor model in the rat, where the mean diameter of the tumor at time of treatment was approximately 6 mm so that the effects on the tumor and on the adjacent liver tissue could be determined. Larger tumors, however, could be treated by multiple diffuser implantation (Marijnissen *et al.*, 1992). As the diffuser can be passed down a needle under ultrasound guiding, percutaneous treatment of several tumors at different liver lobes would be possible (Gatenby *et al.*, 1987). This local treatment of tumor can substantially reduce the surgical trauma and may as such diminish complications like bleeding and liver failure.

9. 5-Aminolevulinic acid-induced Endogenous Photosensitization

Adapted from: R. VAN HILLEGGERSBERG, J.W.O. VAN DEN BERG, W.J. KORT, O.T. TERPSTRA & J.H.P. WILSON. Selective Accumulation of Endogenously Produced Porphyrins in a Liver Metastasis Model in Rats. *Gastroenterology* 1992; 103: 647-651

INTRODUCTION

Photodynamic therapy (PDT) has received much attention in the past two decades as a means of treating certain malignant tumors (Dougherty, 1987; Pimstone, 1985; Kreimer-Birnbaum, 1989). This form of treatment is based on the accumulation of a photosensitizer in malignant tissue after systemic administration. Subsequent illumination with light of an appropriate wavelength creates a photochemical reaction that results on tissue destruction (Chapter 7). The photosensitizers mainly used are Hematoporphyrin derivative (HpD) a mixture of different porphyrins, and dihematoporphyrin ester/ether, an enriched form of HpD marketed as Photofrin® (Lederle Laboratories, Pearl River, NY, U.S.A.).

For selective tumor therapy more photosensitizer should accumulate in the tumor than in the surrounding tissue. Unfortunately, normal liver accumulates Photofrin efficiently, and higher levels have been found in the liver than in the malignant tissue (Holt *et al.*, 1985; Gomer & Dougherty, 1979; Bugelski *et al.*, 1981; Bellnier *et al.*, 1989). This means that Photofrin is not a suitable photosensitizer for PDT of liver cancer. As an alternative approach, we considered the possibility of using the varying capacity of tissues to metabolize porphyrins, as a means of photosensitization. It has been shown that porphobilinogen deaminase (PBGD) has higher activity in various malignant and regenerating tissues than in normal tissues; the opposite was found for ferrochelatase (Figure 9.1) (Rubino & Rasetti, 1966; Schoenfeld *et al.*, 1988; Dailey & Smith, 1984; Smith, 1987; Leibovici *et al.*, 1988). If the amount of porphobilinogen (PBG) available in the cell could be increased, the increased PBGD activity and the decreased activity of ferrochelatase would result in accumulation of porphyrins in the tumor to a greater extent than in surrounding tissue.

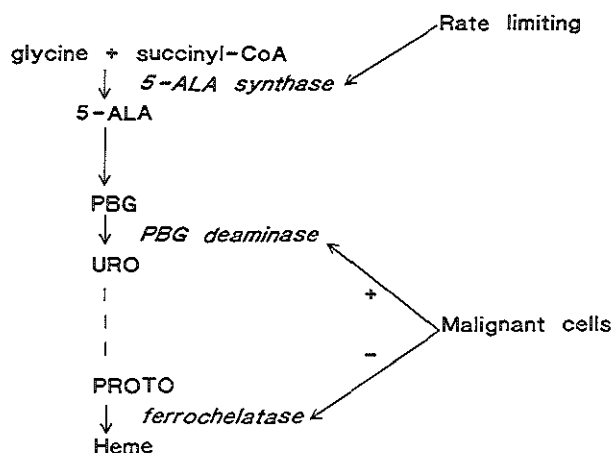


Figure 9.1. Schematic representation of the heme biosynthetic pathway. The first intermediate is 5-Aminolevulinic acid (ALA), a aminoketone, which is formed by the condensation of glycine and succinyl-CoA. Two molecules of ALA are combined to form porphobilinogen (PBG), a monopyrrole, and 4 molecules of PBG are combined to form uroporphyrinogen (URO), a tetrapyrrole. URO is converted to coproporphyrinogen (COPRO) and subsequently to protoporphyrin IX (PROTO). Malignant cells may have altered activities of PBG deaminase (PBGD) and ferrochelatase, which converts PROTO to heme.

In the present study, we used the rat liver metastases model to investigate this proposition. Shedlofsky *et al.* (1987) showed that cell membranes are much less permeable for PBG than for its precursor 5-aminolevulinic acid (ALA), a 5-carbon aminoketone (Figure 9.2). We therefore administered ALA as a substrate for porphyrin synthesis and measured porphyrin concentrations in tumor and liver tissue. For comparison we examined the porphyrin accumulation following a usual dose of Photofrin. In addition, ferrochelatase and PBGD activities were measured in tumor and liver tissue.

MATERIALS AND METHODS

Experimental Design

Thirty-seven rats were used for the experiments. They had free access to either tap water or a solution of ALA-HCL (Sigma Chemica Company, St. Louis, MO, U.S.A.) in tap water (2 mg/ml) that was freshly prepared every day. The animals were randomly allocated to two experiments: I, to assess the porphyrin concentration ratio between tumor and liver after oral ALA or intravenous Photofrin (n=26) and II, to determine the activity of PBGD and

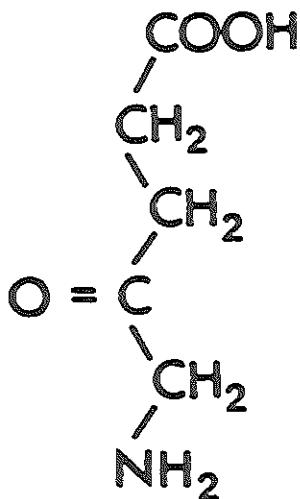


Figure 9.2. Molecular structure of 5-aminolevulinic acid (ALA), a 5-carbon aminoketone with a molecular weight of 167.

ferrochelatase in tumor and liver tissue (n=11).

In experiment I, the tumor was implanted in the liver (Chapter 2). The animals were randomly assigned to 6 groups of 3 or 6 animals each. Three groups received the ALA solution from either the 8th (n=6), 14th (n=3) or 17th (n=3) day after tumor implantation. In 2 other groups Photofrin® (Lederle Laboratories, Pearl River, NY, U.S.A.) was administered in a dose of either 2.5 mg/kg body weight (n=3) or 5 mg/kg body weight (n=6), by penile vein injection on the 17th day after implantation. The animals in the sixth group served as controls (n=6) and did not receive any medication. During treatment the animals were placed in metabolic cages to determine consumption of water or ALA solution, volume of urine excreted, and to collect urine samples for the measurement of porphyrin concentrations. The animals were kept in subdued light, with preservation of night-day rhythm, to avoid possible skin injuries as a result of porphyrin accumulation. On the 19th day after tumor implantation the animals were sacrificed. The median lobe of the liver was removed and the tumor, having a diameter of approximately 5 mm, was dissected. Liver tissue of at least 1 cm distance from the tumor and the entire dissected tumor were used for the porphyrin analysis.

In experiment II, a piece of tumor was inserted subcutaneously in the flank. Two months after inoculation the periphery of the tumor without central necrosis and the liver were isolated for ferrochelatase and PBGD determination.

Materials

The following reagents were purchased from Porphyrin Products (Logan, UT, U.S.A.): protoporphyrin IX (PROTO), disodium salt and zinc PROTO. Tris-HCl was purchased from Boehringer Mannheim (Mannheim, Germany), and other chemicals were purchased from Merck (Darmstadt, Germany).

Porphyrin Analysis

The analysis was carried out according to the method of Bayley & Needham (1986) with the following modifications. The tissue was suspended in saline (1:10 wt/vol) and homogenized in a tissue grinder. To 50 μ l of this homogenate were added 100 μ l of formic acid (0.8 mol/l), 800 μ l of acetone and 50 μ l of HCL (1.5 mol/l). The material was mixed and subsequently centrifuged for 4 minutes at 10,000 \times g. Aliquots of this supernatant were analyzed by reverse phase high-performance liquid chromatography (HPLC) on a 10-cm column (Lichrosorb RP.18, hypersil SAS; Chrompack, Middelburg, The Netherlands). Porphyrins were detected using their natural fluorescence with excitation and emission wavelengths of 405 and 625 nm, respectively. The elution solvent was a mixture consisting of 560 volumes of acetone, 240 volumes of methanol, 200 volumes of water, and 2 volumes of formic acid, 88% (wt/vol). The eluent flow was 1 ml/min. Calibration chromatograms were run with known concentrations of PROTO in 1.5 mol/l HCl. Before application, porphyrin standards were analyzed separately for their actual concentration using ultraviolet (UV) spectroscopy and the molar extinction coefficient ($E=207$ for 1 μ mol/ml at 407 nm). Recovery of porphyrins was checked by adding standard PROTO to the samples. A recovery of 80%-100% was regularly found during the assays.

Determination of Ferrochelatase and PBGD Activity

Ferrochelatase was measured by a modification of the method of Li *et al.* (1987), using zinc and PROTO as substrates. The samples were homogenized in water (1:10 wt/wt) using a Potter Elvehjem homogenizer (Kontess Glass Co., Vineland, NJ, U.S.A.). Fifty microliters of the homogenate was then added to 100 μ l 0.25 mol/l Tris-HCl buffer, pH 8.2, containing 10 g/l Triton X-100 (Sigma, St. Louis, MO, U.S.A.) and 1.75 mmol/l palmitic acid. Fifty μ l of a 250 μ mol/l solution of PROTO in 0.01 N KOH was added and the reaction started by the addition of 50 μ l of a 200 μ mol/l solution of zinc acetate in water. The mixture was incubated at 37°C for 60 min, and the reaction stopped by the addition of 1 ml of dimethylsulfoxide-methanol (30:70) solution. After centrifugation in an Eppendorf centrifuge (Eppendorf Gerätebau, Hamburg, Germany) for 5 minutes at maximum speed, 100 μ l of supernatant was injected on a Perkin Elmer HPLC (Gouda, The Netherlands) with a reversed phase Chrompack RP18 column, with acetone/methanol/water/formic acid (560:240:200:2) 1 ml/min as mobile phase. Zinc PROTO was detected by a Perkin Elmer LS40 fluorimeter, excitation wavelength 415 nm, emission wavelength 580 nm. Results were expressed as nanomoles per milligram of protein.

After an initial incubation at 55°C for 60 min and cooling to room temperature to destroy the activity of uroporphyrinogen decarboxylase and to prevent further metabolism of uroporphyrinogen, PBGD was measured as previously described by Wilson JHP *et al.* (1986).

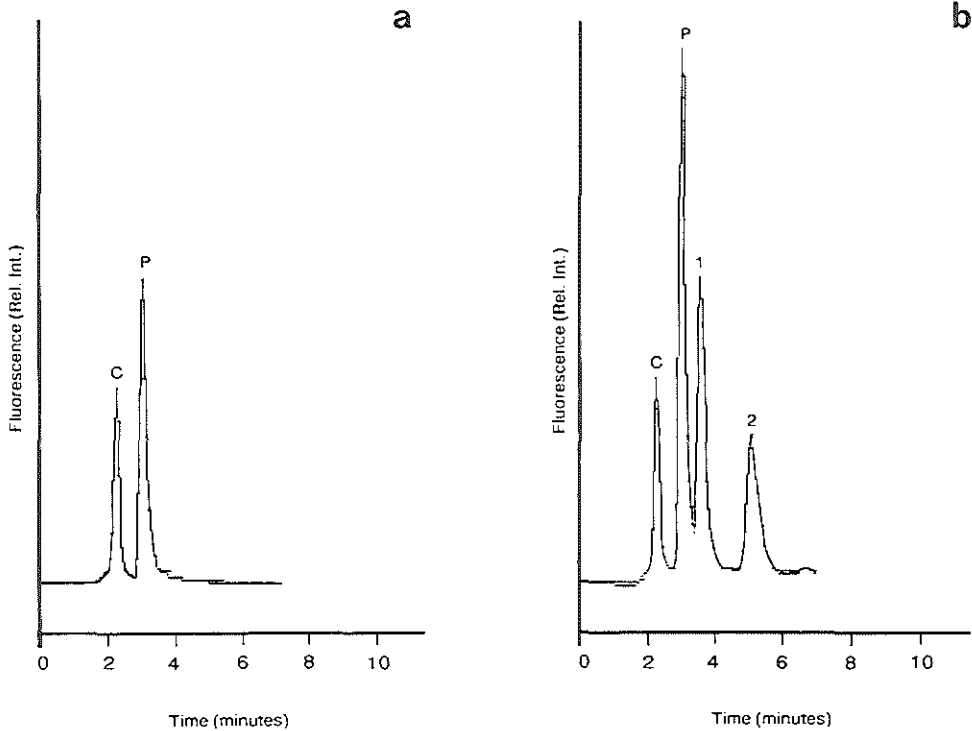


Figure 9.3. HPLC chromatogram of porphyrins in liver tissue (a) after 11 days of oral ALA 28 mg/day or (b) 2 days after a single dose of Photofrin 5 mg/kg i.v. (b). The various peaks were identified as follows: P, Protoporphyrin IX; C, Coproporphyrinogen III+I and Uroporphyrinogen III+I; 1 and 2, Photofrin compounds.

Protein was measured using the method of Lowry *et al.* (1951).

Statistical Analysis

The values are expressed as mean \pm standard error of the mean (SEM). The Kruskal-Wallis test and Spearman rank-order correlation for paired difference against time course were used to analyze the relation between the duration of ALA administration and the porphyrin concentration in liver and tumor, respectively. Other comparisons were made using Student's *t*-test. A significant difference was considered at *P* values of <0.05 .

RESULTS

All animals survived and none showed signs of discomfort. Skin lesions could not be seen macroscopically.

The mean \pm SEM daily water consumption in control and Photofrin-injected animals was 17.7 ± 0.2 ml. In ALA treated animals, this value was significantly lower, 14.3 ± 0.2 ml, possibly as a result of an unpleasant taste of the ALA solution. Because the ALA solution had a concentration of 2 mg/ml, the mean \pm SEM daily ALA intake was 28.6 ± 0.4 mg. The mean daily urine production in the group of ALA treated animals was 6.1 ± 0.1 ml, significantly lower than the value of 7.9 ± 0.1 ml found in control and Photofrin-injected animals.

The main porphyrin found in urine was coproporphyrinogen III+I (COPRO), the concentration of which increased from the first day of ALA treatment to a mean \pm SEM level of 12.2 ± 0.6 μ mol/l. In controls and Photofrin injected animals the mean COPRO concentration was 1.6 ± 0.1 μ mol/l.

Porphyrin Distribution

Two typical HPLC profiles of liver tissue after oral ALA and intravenous Photofrin administration are shown in Figure 9.3. In tumor and liver tissue of Photofrin-treated animals we found PROTO and COPRO+uroporphyrinogen (URO) as well as the Photofrin components. In ALA-treated animals, PROTO and COPRO+URO were identified.

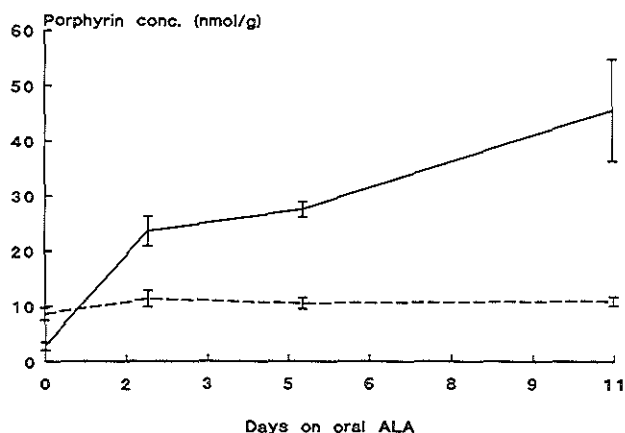


Figure 9.4. Total porphyrin concentration in tumor (—) and liver (---) vs. number of days on oral ALA. All measurements were made 19 days after tumor implantation. Each point represents the mean \pm SEM.

No difference was found in the amount of COPRO+URO in liver and tumor tissue after treatment with Photofrin or ALA compared with controls. However, PROTO accumulated progressively in the tumor with increasing duration of ALA administration ($P<0.001$), whereas no increase was found in normal liver ($P=0.7$) (Figure 9.4).

The total amount of porphyrins in liver or tumor tissue after treatment with ALA or

Table 9.1. Mean \pm SEM total tissue porphyrin concentration (nmol/g tissue) on day 19 after inoculation, after oral ALA or intravenous Photofrin*.

	Individual value			Mean		
	Tumor	Liver	Ratio	Tumor	Liver	Ratio
ALA 2 days	27.6	12.8	2:1	23.6 \pm 2.7	11.3 \pm 1.5	2:1
	24.7	8.4	3:1			
	18.4	12.6	2:1			
ALA 5 days	29.0	12.5	2:1	27.6 \pm 1.4	10.5 \pm 1.0	3:1
	28.9	9.5	3:1			
	24.8	9.4	3:1			
ALA 11 days	82.0	9.4	9:1	45.8 \pm 9.3	10.9 \pm 0.8	4:1
	65.1	11.1	6:1			
	40.6	10.8	4:1			
	31.0	11.8	3:1			
	30.6	14.1	2:1			
	25.2	8.1	3:1			
Ph II 2.5 mg/kg	2.5	7.8	1:3	3.0 \pm 0.3	8.4 \pm 0.8	1:3
	2.9	7.6	1:3			
	3.5	10.0	1:3			
Ph II 5.0 mg/kg	11.4	22.6	1:2	5.2 \pm 1.3	17.7 \pm 2.2	1:3
	4.7	20.3	1:4			
	4.6	24.4	1:5			
	4.3	12.7	1:3			
	3.5	12.5	1:4			
	2.8	13.9	1:5			
Controls	5.3	12.9	1:3	2.8 \pm 0.7	8.6 \pm 1.1	1:3
	3.2	10.8	1:3			
	2.2	6.6	1:3			
	1.9	6.2	1:3			
	1.7	6.3	1:4			

*Photofrin was administered i.v., on day 17.

Photofrin is listed in Table 9.1. The highest values were found in animals treated with ALA for 11 days (mean 45.8 ± 9.3 nmol/g tissue). In the liver this value was significantly lower, (mean 10.9 ± 0.8 nmol/g, $P < 0.01$) resulting in an average porphyrin concentration ratio between tumor and normal liver tissue of about 4:1. In contrast with this finding, the mean porphyrin concentration in the livers of animals treated with Photofrin was significantly higher ($P < 0.001$) than in the tumor resulting in a tumor to liver ratio of 1:3. This ratio was also found in control animals, with mean \pm SEM values in tumor and liver tissue of 2.8 ± 0.7 nmol/g and 8.6 ± 1.1 nmol/g, respectively.

Ferrochelatase and PBGD Activity

The ferrochelatase activity in tumor was found to be 0.84 ± 0.10 nmol/h of zinc PROTO per mg protein, a 3 fold decrease from that of normal liver tissue ($P < 0.001$). A 2 fold decrease in PBGD activity was found, with a mean \pm SEM activity in tumor of 49.3 ± 4.7 pmol/h of URO per mg protein ($P < 0.001$) (Table 9.2).

Table 9.2. Mean \pm SEM ferrochelatase and PBGD activity in tumor and normal liver tissue.*

Enzyme	Tumor	Liver
Ferrochelatase, nmol/h of zinc PROTO per mg protein	0.84 ± 0.10	2.47 ± 0.26
PBG deaminase, pmol/h of URO per mg protein	49.3 ± 4.7	78.8 ± 2.1

*n=11 for all groups.

DISCUSSION

In this study, oral administration of 5-aminolevulinic acid resulted in the progressive accumulation of porphyrin in a transplantable colon carcinoma, without accumulation in the surrounding liver tissue. After 11 days of ALA, the porphyrin concentration ratio between tumor and liver was 4:1 (after Photofrin this ratio was 1:3).

The choice of the ALA dosage was based on the normal activity of PBGD, which is the rate limiting enzyme in the synthesis of porphyrins during ALA administration (Kappas *et al.*, 1989). This activity is determined mainly by the activity in the liver and erythroid cells, 2.75 and 37.7 nmol/h of URO per gram of human tissue, respectively (Kappas *et al.*, 1989). Rat tissue weights (7.5 g liver and 5 g erythroid cells) were used to calculate the total PBGD activity (199 nmol/h of URO). Because the formation of PBG requires 2 molecules of ALA and the formation of URO requires 4 molecules of PBG, the PBGD activity per hour was multiplied by 8 to find the maximal turnover of ALA ($1.6 \mu\text{mol/h}$) (Figure 9.1). The mean daily water consumption of the animals (17 ml/day, previous observation) was used to choose the concentration of ALA (MW=167) in drinking water (0.4 mg/ml). To assure that a sufficient amount of ALA was applied, 5 times the calculated value was administered (2

mg/ml). In this study, the actual mean daily water consumption of ALA treated animals was lower (14 ml/day) than the value used for calculation (17 ml/day). The ALA intake, however, was sufficient (28 mg/day) to provide the estimated need for substrate.

The main product found after ALA treatment was PROTO. This substance has photosensitizing properties as evidenced by the severe cutaneous phototoxicity in erythropoietic protoporphyria (Kappas *et al.*, 1989). Moreover, destruction of malignant cells *in vitro* or skin tumors after local administration of ALA or PROTO and subsequent exposure to photoactivating light has been demonstrated (Menon *et al.*, 1989; Malik & Lugaci, 1987; Kennedy *et al.*, 1990). Because porphyrin accumulation is restricted to the tumor, PDT would act specifically on the tumor causing minimal damage to the adjacent tissue. Another application of ALA administration could be the early detection of malignant tissue, utilizing the fluorescence properties of PROTO during illumination with UV light. A recent study reports good correlation between the location of the red fluorescence and the phototoxic damage to specific structures in mouse skin after intraperitoneal administration of ALA and subsequent illumination (Divaris *et al.*, 1990).

This study is based on previous investigations in which the activity of ferrochelatase was found to be decreased while the opposite was found for PBGD in malignant and regenerating tissues (Rubino & Rasetti, 1966; Schoenfeld *et al.*, 1988; Dailey & Smith, 1984; Leibovici *et al.*, 1988). Measurements on the activity of these two enzymes in the tissues we examined showed a 3 fold decrease of ferrochelatase activity in coloncarcinoma CC531 (0.8 nmol/h of zinc PROTO per mg protein) compared to normal liver (2.47 nmol/h of zinc PROTO per mg protein), confirming our proposition about the mechanism of porphyrin accumulation after oral ALA. In contrast to other studies, however, PBGD was decreased 2 fold. The reason for low ferrochelatase activity in tumors might be the use of glycolysis rather than oxidative phosphorylation for their metabolism. Especially rapidly growing tumors contain lower activities of mitochondrial cytochrome oxidase (Friedkin, 1973; Weinhouse, 1960). Therefore, mitochondrial ferrochelatase would be deficient as well. The lipophilic protoporphyrin has been found to accumulate in mitochondria of rodent hepatic cells after feeding the animals with toxic compounds (griseofulvin and hexachlorobenzene), disturbing the endogenous heme synthesis (Sandberg & Romslo, 1981). Information about tissue ferrochelatase activity could be useful in predicting the effect of ALA administration on porphyrin accumulation in different tissues. Preliminary results show ferrochelatase activities in rat BN472 mamma carcinoma and rat BN175 fibrosarcoma comparable to those found in colon carcinoma CC531 used in this study. Further experiments should show to what extent the selective accumulation of porphyrins after ALA is related to the type of tumor and tissue.

Photofrin is a mixture of many different porphyrins some of which may be responsible for the photosensitizing activity, probably porphyrins linked via ester and/or ether bonds, and others for the tumor localizing properties (Dougherty, 1989; Manyak *et al.*, 1988; Gomer, 1989). Thus, the amount of tissue fluorescence after photosensitizer administration is not directly related to the possible effect of PDT. An advantage of endogenous photosensitization with ALA is that the main product is PROTO, a defined molecular structure with the potential of controlled PDT and quantitative detection of fluorescence (MacRobert *et al.*, 1989).

PART IV

PREDICTING LASER-TISSUE INTERACTION

10. Tissue Optical Properties at 633 nm and 1,064 nm

Adapted from: R.VAN HILLEGERSBERG, J.W. PICKERING, M. AALDERS & J.F. BEEK. Optical Properties of Rat Liver and Tumor at 633 nm and 1,064 nm: Photofrin enhances scattering. Lasers Surg Med 1993; 13: 31-39

INTRODUCTION

Two promising laser applications in oncology are photodynamic therapy (PDT) and thermal Nd:YAG laser coagulation. We investigated the use of these techniques in the previous chapters. Interstitial PDT could produce complete long-term destruction of experimental liver metastases combined with minimal liver damage (Chapter 8). In thermal laser therapy, we used the Nd:YAG laser for localized superficial or interstitial destruction of malignant tissue within the liver (Part II). To avoid carbonization, which prevents light penetration, a cylindrical diffusing fiber-tip was used in the interstitial application and superficial water-jet cooling in the noncontact laser mode. In this manner the intrahepatic tumor was selectively coagulated (Chapters 5, 6).

In the clinical situation, one would like to know which laser parameters (i.e., output power, exposure time, position and number of optical fibers) are required to treat a certain tumor, combined with minimal adjacent normal tissue damage. One approach is to model the light transport in the tissue, to determine the probability of a photon reaching a certain point in the tissue and therefore, to determine the local temperature rise (thermal laser therapy) or rate of photosensitizer activation (PDT). This requires knowledge of the intrinsic bulk optical parameters of the tissues for a particular wavelength: the absorption coefficient, μ_a , the scattering coefficient, μ_s , and the anisotropy factor, g . The reciprocal of the sum of the absorption and scattering coefficients gives the average path length of a photon through the tissue between scattering events, whilst the anisotropy factor is the average cosine of the scattering angle for all scattering events. Given these properties, one of several light transport models may be applied to predict the light distribution in tissue, e.g., 2-flux models, diffusion

theory, and Monte Carlo simulations (Patterson *et al.*, 1991a, 1991b; Flock *et al.*, 1987; Jacques & Prahl, 1987; Wilson & Adam, 1983). The temperature distribution and heat conduction may then be calculated (Dowden *et al.*, 1988).

This chapter presents optical properties of the rat liver and colon carcinoma at the relevant wavelengths for PDT (around 630 nm) and thermal therapy (1,064 nm) in normal and Photofrin sensitized tissue.

MATERIALS AND METHODS

Experimental Design

The measurements were performed, 2 months after subcutaneous implantation of a piece of tumor in the flank of 14 animals.

The animals were randomly assigned to 2 groups of 7 animals each. In the first group, Photofrin® (Lederle Laboratories, Pearl River, NY, U.S.A.) was administered in a dose of 5 mg/kg body weight by penile vein injection 48 h before determination of optical properties. After administration, the animals were kept in subdued light, with preservation of night-day rhythm, to avoid possible skin injuries as a result of Photofrin accumulation. The animals in the second group did not receive any medication. The animals were sacrificed, the tumor dissected and the left lateral lobe of the liver removed. The largest and smallest diameter of the tumor and the length and width of the left lateral liver lobe were measured with calipers. The periphery of the tumor without central necrosis was used for the optical measurements.

Determination of Tissue Optical Properties

Sample Preparation. Immediately after excision the tissues were sectioned 250–650 μm thick using a microtome knife and a custom-built stand in which the tissue was clamped. These margins were set to minimize a possible influence of large variations in tissue thickness on the measurements of optical properties. In pilot studies, a range of 250–650 μm was found to be most practicable in this particular experimental set-up. Normally two samples were taken from each liver or tumor. A sample was placed on a glass slide and a small quantity of phosphate-buffered saline was added to prevent air bubbles between tissue and slide. A second slide was then placed on top of the sample, and the two slides were clamped together. Aluminum spacers of approximately the same thickness of the sample were used between the slides to prevent compression of the sample. The sample thickness was determined by measuring the thickness of the slide-sample-slide arrangement and subtracting the thickness of the slides.

Measurement and Equipment. The sample was placed between two identical integrating spheres of 70 mm diameter with a circular sample port of 25 mm diameter (Figure 10.1), and illuminated with collimated light from either a 1 mW, 1 mm beam diameter, 632.8 nm HeNe laser (Polytec, Waldbronn, Germany) or an approximately 2 mm beam diameter, 1,064 nm Nd:YAG laser (SLT CL60, Malvern, U.S.A.). Measurements of the light fluence within each sphere and the collimated transmittance signal at a distance of 70 cm beyond the second sphere were made by Telefunken BPW 34 photodiodes (Germany) with a solid collection

angle of 5.5×10^{-4} sr (stereo radial).

The input light beams were chopped and the signals measured using standard lock-in-amplifier techniques (Model 5209, EG&G Princeton Applied Research, Princeton, NJ, U.S.A.). All measurements within the spheres were made relative to the signal when a 99% reflecting plate (Labsphere SRS-99-010, North Sutton, NH, U.S.A.) was placed at the sample aperture. All measurements on Photofrin sensitized tissue were carried out in subdued light.

With the sample in place, three measurements are necessary to obtain the optical properties:

1. The signal in the first sphere, mainly remitted light.
2. The signal in the second sphere, mainly diffuse transmitted light.
3. The signal that exits the second sphere, the collimated transmitted light.

In addition, there are background measurements made in each sphere without a sample present and reference signals made with a standard reflector in each sphere and of the collimated light with no sample present.

The collimated transmission measurement has in the past proved to be the most difficult to make because of the high attenuation by the sample. In order not to saturate the photodiode with the collimated signal without the sample present (the baseline 100% collimated transmission), we always used band pass filters with an attenuation of $(5.6 \pm 0.1) \times 10^{-3}$ at 632.8 nm and $(1.30 \pm 0.03) \times 10^{-2}$ at 1,064 nm. As a means of assessing the accuracy of the optical properties, the collimated signal with the sample present was

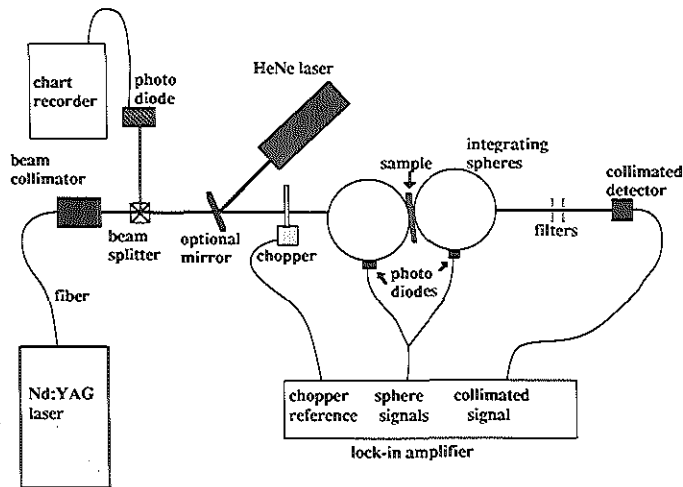


Figure 10.1. Two integrating spheres with an intervening sample. The sample may be illuminated by either a HeNe laser or a collimated beam from a Nd:YAG laser. The beams are chopped before entering the spheres and measurements are made with a lock-in-amplifier. The collimated signal may be attenuated by filters after it has passed through the spheres.

measured both with and without the filters present. Thus, when the collimated signal is low, the presence of the filters attenuating this signal may mean the photodiode is measuring signals only a little above its noise level. When the filters are removed, the signal on the photodiode is considerably stronger; however, there is an additional uncertainty introduced into the calculations due to the uncertainty in the filter attenuation coefficients.

Furthermore, for each sample, a full set of measurements was made at two different positions of the sample (i.e., after one set of measurements, the sample was displaced a few millimeters to allow the incident beam to fall on a different part of the tissue). This allowed some quantitative analysis of the variability in the optical properties within the samples.

Calculations. The method of determination of the optical properties from the three optical measurements and the sample thickness has been described in other articles (Pickering *et al.*, 1992a, 1992b; Prahl, 1988; Prahl *et al.*, 1993; Pickering, 1992). Briefly, the optical signals can be expressed in terms of the remittance, and diffuse and collimated transmittance of the sample through equations that account for the multiple exchange of light between the spheres through the sample (Prahl, 1988; Prahl *et al.*, 1993). With an initial guess of the optical properties, the remittance and transmittances for a sample are calculated using the adding-doubling solution to the equation of radiative transfer (Prahl, 1988; Prahl *et al.*, 1993). This also takes into account the refractive index mismatch between the air ($n=1.0$), glass ($n=1.54$), and sample ($n=1.37$) boundaries. The calculated and measured signals are compared, and a new set of optical properties are estimated. This inverse procedure continues until the calculated remittance and transmittances give identical signals to those measured (Pickering *et al.*, 1992b). The system has been extensively tested with tissue phantoms (Pickering *et al.*, 1992b) and used on other tissue types (Pickering, 1992).

Statistical Analysis

The optical properties are expressed as mean \pm standard error of the mean (SEM). The mean for each group of samples (e.g., liver at 632.8 nm) was calculated from the average of the two measurements made on each sample. The variability in the optical properties within a sample could be compared for different tissue types by expressing the difference between the two measurements made on each sample (by displacing the sample a few millimeters) as a percentage of the average of these two measurements. Thus, the mean of this percentage for each tissue group expresses the variability within a sample (i.e., intra-individual variation) independently of the variability between different samples (i.e., inter-individual variation). The student's *t*-test was employed for the difference between two means. A difference was considered to be significant at *P* values of <0.05 .

RESULTS

One tumor implant did not grow, so only the liver parameters could be determined in that animal. Another animal was sacrificed before optical measurements were possible, because the tumor size had become too large. Two months after tumor inoculation, the mean \pm SEM tumor diameter was $34\pm2 \times 29\pm2$ mm and the mean length and width of the left lateral lobe

of the liver was $43 \pm 3 \times 23 \pm 3$ mm. The sample size was generally large enough to cover the entire sample port, however, four times (2 tumors, 2 livers) a sample had to be composed of two tissue slabs. The optical parameters of these composed samples did not differ significantly from the normal samples. The mean \pm SEM thickness of the samples was 440 ± 10 μ m for liver and 430 ± 20 μ m for tumor.

Optical Properties

The mean \pm SEM optical properties are presented in Tables 10.1 and 10.2 for 632.8 nm and 1,064 nm respectively, with and without the addition of Photofrin. The reduced scattering coefficient,

$$\mu_s' = \mu_s (1 - g)$$

and the effective attenuation coefficient,

$$\mu_{\text{eff}} = \sqrt{3\mu_a (\mu_a + \mu_s (1 - g))}$$

are calculated from the measured optical properties. Additionally, Figures 10.2-10.4 show the average optical properties for every sample (i.e., the average of the two measurements made on each sample) illustrating the variation between samples.

Liver vs. Tumor. At 632.8 nm, the absorption coefficient was always greater in liver than in tumor (Table 10.1). Mean \pm SEM values were 3.8 ± 0.2 cm^{-1} for liver, compared with 1.4 ± 0.2 cm^{-1} for tumor ($P < 0.001$). For tissues with Photofrin, the anisotropy factor was smaller in tumor, 0.92 ± 0.01 , compared with liver, 0.946 ± 0.01 ($P < 0.05$). This smaller anisotropy contributed to a greater reduced scattering coefficient for tumor, 29 ± 6 cm^{-1} , compared to liver, 16.8 ± 0.5 cm^{-1} ($P < 0.025$). Overall, there was a greater effective attenuation coefficient for liver than tumor ($P < 0.005$ without Photofrin; $P < 0.05$ with Photofrin).

At 1,064 nm there was no significant difference in absorption between liver and tumor (Table 10.2); however, the mean \pm SEM scattering coefficient was higher in tumor, 180 ± 10 cm^{-1} , than in liver 151 ± 6 cm^{-1} ($P < 0.05$). With Photofrin the reduced scattering coefficient and effective attenuation coefficient were both higher for tumor than for liver ($P < 0.05$).

Tissue with Photofrin vs. Tissue without. At 632.8 nm, the addition of Photofrin did not alter the absorption coefficient in either of the tissue types (Table 10.1). However, there was an increase in scattering coefficient for both tissues. For liver, the mean \pm SEM scattering coefficient increased from 280 ± 10 cm^{-1} to 310 ± 10 cm^{-1} , while for tumor the mean value increased from 280 ± 20 cm^{-1} to 340 ± 20 cm^{-1} ($P < 0.025$). Furthermore, Photofrin administration decreased the mean anisotropy in tumor tissue from 0.946 ± 0.004 to 0.92 ± 0.01 ($P < 0.025$). Overall, these changes resulted in an increase in reduced scattering and effective attenuation for both tissues. The reduced scattering coefficient increased from 13 ± 1 cm^{-1} to 16.8 ± 0.5 cm^{-1} for liver ($P < 0.01$) and from 15 ± 2 cm^{-1} to 29 ± 6 cm^{-1} for tumor ($P < 0.025$). The effective attenuation coefficient increased from 13.8 ± 0.9 cm^{-1} to 16.0 ± 0.4 cm^{-1} for liver ($P < 0.05$) and 8.3 ± 0.9 cm^{-1} to 12 ± 2 cm^{-1} for tumor ($P < 0.05$).

Table 10.1. Mean \pm SEM optical properties measured with the HeNe (632.8 nm) laser.

Tissue Type	Number of samples, n	μ_a (cm ⁻¹)	μ_s (cm ⁻¹)	g	μ_s' (cm ⁻¹)	μ_{eff} (cm ⁻¹)
Liver	14	3.8 \pm 0.2	280 \pm 10	0.952 \pm 0.004	13 \pm 1	13.8 \pm 0.9
Liver+Photofrin	12	4.1 \pm 0.1	310 \pm 10	0.946 \pm 0.002	16.8 \pm 0.5	16.0 \pm 0.4
Tumor	14	1.4 \pm 0.2	280 \pm 20	0.946 \pm 0.004	15 \pm 2	8.3 \pm 0.9
Tumor+Photofrin	10	1.6 \pm 0.2	340 \pm 20	0.92 \pm 0.01	29 \pm 6	12 \pm 2

Table 10.2. Mean \pm SEM optical properties measured with the Nd:YAG (1,064 nm) laser.

Tissue Type	Number of samples, n	μ_a (cm ⁻¹)	μ_s (cm ⁻¹)	g	μ_s' (cm ⁻¹)	μ_{eff} (cm ⁻¹)
Liver	14	2.0 \pm 0.3	151 \pm 6	0.948 \pm 0.005	7.9 \pm 0.7	7.5 \pm 0.8
Liver+Photofrin	12	2.4 \pm 0.2	196 \pm 5	0.942 \pm 0.003	11.2 \pm 0.7	9.8 \pm 0.4
Tumor	14	2.5 \pm 0.5	180 \pm 10	0.952 \pm 0.005	9 \pm 1	9 \pm 1
Tumor+Photofrin	10	2.5 \pm 0.2	220 \pm 20	0.92 \pm 0.01	18 \pm 3	12 \pm 2

Similar results were found at 1,064 nm (Table 10.2). With Photofrin, an increase in scattering coefficient was found for both tissues; from 151 \pm 6 cm⁻¹ to 196 \pm 5 for liver ($P<0.001$) and from 180 \pm 10 cm⁻¹ to 220 \pm 20 cm⁻¹ for tumor ($P<0.05$). The anisotropy decreased for tumor from 0.952 \pm 0.005 to 0.92 \pm 0.01 ($P<0.025$). These events resulted in an increase in a reduced scattering for both tissue types: for liver from 7.9 \pm 0.7 cm⁻¹ to 11.2 \pm 0.7 cm⁻¹ and for tumor from 9 \pm 1 cm⁻¹ to 18 \pm 3 cm⁻¹ ($P<0.005$). The mean effective attenuation increased for liver from 7.5 \pm 0.8 cm⁻¹ to 9.8 \pm 0.4 cm⁻¹, $P<0.005$.

Variability within a Sample. There was less intra-individual variation in the anisotropy factor of the liver samples compared with the tumor samples at both 632.8 nm and 1,064 nm. At 632.8 nm, the mean variation was 0.39% for liver compared with 1.88% for tumor ($P<0.005$). With Photofrin these values were 0.57% for liver compared with 1.99% for tumor ($P<0.025$). At 1,064 nm, values were 0.42% compared with 1.37% without Photofrin ($P<0.01$), and 0.26% compared with 1.18% with Photofrin ($P<0.01$).

At 1,064 nm, there was also a lower variability in the absorption coefficient for liver than for tumor for samples without Photofrin, 9.32% for liver compared with 22.7% for tumor ($P<0.05$). These results reflect the less homogeneous appearance of tumor compared with liver.

Accuracy of the Technique. For only one optical property, the scattering coefficient at 632.8 nm for liver with the addition of Photofrin, was there a significant difference between measurements made with and without the filters present (310 cm⁻¹ compared with 290 cm⁻¹, $P<0.05$). The absorption coefficient exhibited a relatively larger standard error of the mean

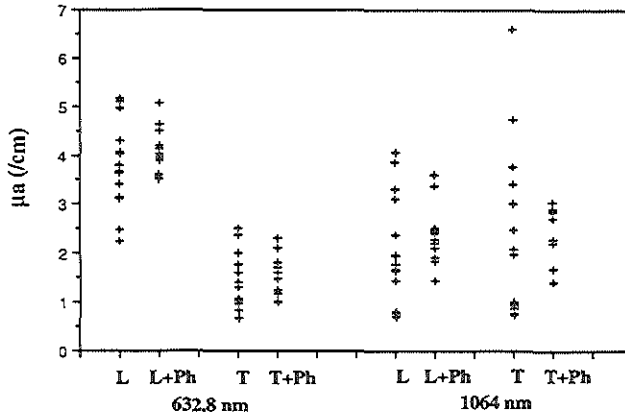


Figure 10.2. The absorption coefficient (μ_a) for all the samples of each tissue type at 632.8 nm and 1,064 nm. Each point represents the average of two measurements. L, Liver; T, tumor; Ph, Photofrin.

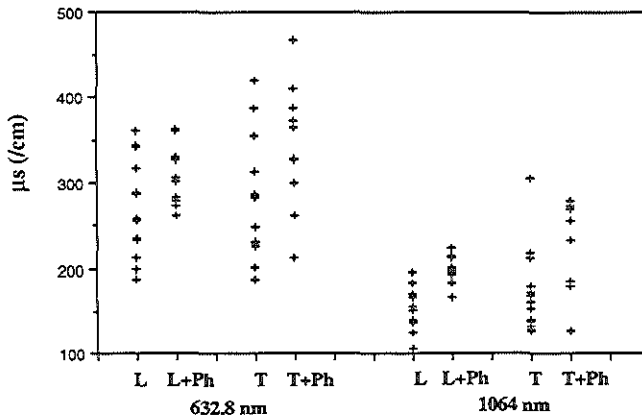


Figure 10.3. The scattering coefficient (μ_s) for all the samples of each tissue type at 632.8 nm and 1,064 nm. Each point represents the average of two measurements. L, liver; T, tumor; Ph, Photofrin.

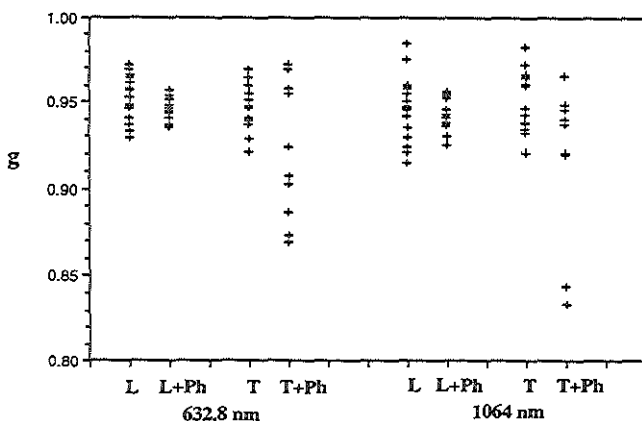


Figure 10.4. The anisotropy factor (g) for all the samples of each tissue type at 632.8 nm and 1,064 nm. Each point represents the average of two measurements. L, liver; T, tumor; Ph, Photofrin.

compared with the scattering coefficient, which in turn was relatively larger compared with that of the anisotropy factor (Figures 10.2-10.4).

DISCUSSION

In this study, the optical properties of normal and Photofrin sensitized rat colon carcinoma and liver were determined at 632.8 and 1,064 nm, using indirect methods with two integrating spheres. At 632.8 nm, the absorption coefficient in liver was significantly higher than in tumor (a factor of 2.7), whereas no difference was found for scattering. At 1,064 nm, however, the scattering coefficient was higher in tumor compared to liver (a factor of 1.2). Remarkably, scattering increased in both tissues and both wavelengths, 48 h after a usual 5 mg/kg intravenous Photofrin dose (factors of 1.1, liver 632.8 nm; 1.2, tumor 632.8 nm; 1.3, liver 1,064 nm; 1.2, tumor 1,064 nm).

The experimental method allowed an additional check on the accuracy of the measurements and statistics by calculating two sets of optical properties based on the measurement of the collimated signal (generally the most difficult to make) with and without a set of attenuating filters that are necessary for the collimated reference signal. Only one of the measured optical properties showed a significant difference due to the removal of the filter, suggesting that the collimated transmission measurements were made above the background noise level and in the linear response region of the photodiodes. Also, as the optical properties were determined twice for each sample (by moving the sample slightly), we were able to compare the variability of the optical properties within a sample (intra-individual variation).

Table 10.3. Optical properties of liver and tumor measured by various authors.

Species	μ_a (cm^{-1})	μ_s (cm^{-1})	g	μ_s' (cm^{-1})	μ_{eff} (cm^{-1})	Reference
<i>Liver at 630-635 nm</i>						
Rat	3.8	280	0.952	13	13.8	This Chapter
Rat	6.5	143.7	0.95	7.2	16.3	Parsa <i>et al.</i> (1989)
Bovine					10.6	Preus <i>et al.</i> (1982)
Bovine	3.21			5.23	6.8	Karagiannes <i>et al.</i> (1989)
Bovine	2.7			17.0	12.6	Wilson BC <i>et al.</i> (1986)
Rabbit					12.5	Wilson <i>et al.</i> (1985)
Human	3.2	414	0.95	20.7	15.1	Andreola <i>et al.</i> (1988)
Human	2.3	313	0.68	100	26.6	Marchessini <i>et al.</i> (1989)
<i>Liver at 1,064 nm</i>						
Rat	2.0	151	0.948	7.9	7.5	This Chapter
Rat	5.9	60.9	0.92	4.9	13.8	Parsa <i>et al.</i> (1989)
Bovine	0.53			1.76	1.9	Karagiannes <i>et al.</i> (1989)
Porcine	10.0					Macleod <i>et al.</i> (1988)
<i>Tumor at 630-635 nm</i>						
Rat adenocarcinoma	1.4	280	0.946	15	8.3	This Chapter
Rat rhabdomyosarcoma	1.1			7.0	5.2	Van Gemert <i>et al.</i> (1985)
Rat prostate	0.49	270	0.97	5.4-8.1	2.9-3.6	Arnfield <i>et al.</i> (1988)
Rat fibrosarcoma					4.4-9.8	Driver <i>et al.</i> (1988)
Rabbit VX2		$\mu_t=628$	0.639			Flock <i>et al.</i> (1987)
Human intracranial					3.9-5.9	Svaasand & Ellingsen (1985)
Human <i>in vivo</i>	31			941	214-340	Driver <i>et al.</i> (1991)
<i>Tumor at 1,064 nm</i>						
Rat adenocarcinoma	2.5	180	0.952	9	9	This Chapter
Human intracranial					1.9-3.3	Svaasand & Ellingsen (1985)

The absorption coefficient varies more within tumor than within liver. Additionally, there is a greater intra-individual variability in the anisotropy of tumor than liver. The difference in the standard errors of the different optical properties indicates that our measurement and calculation method yields the anisotropy more reproducible than the scattering coefficient, which in turn is more reproducible than the absorption coefficient. The relatively high standard error of the absorption coefficient is in part the result of measuring an absorption coefficient that is very small compared with the scattering coefficient.

There have been only a few studies of the optical properties of liver and even less of tumors despite their importance in laser medicine and surgery (Van Gemert *et al.*, 1985; Wilson *et al.*, 1985). Table 10.3 compares our results for tissue without Photofrin with those

of other studies. The most closely related of these is that of Parsa *et al.* (1989) in which the optical properties of rat liver were measured. Here, the technique was to use integrating spheres for the diffuse reflectance and diffuse transmittance measurements and a second sample, which had been cut very thinly after freezing for the collimated transmission measurements. The optical transmission measurements were then calculated using an iterative inverse diffusion approximation. The diffusion approximation is generally thought to be less accurate than the adding-doubling method used in our study (Prahl, 1988; Prahl *et al.*, 1993). Nevertheless, the absorption and scattering coefficients agree within a factor of two and the anisotropy is very similar.

Van Gemert *et al.* (1985) measured the optical properties of rat rhabdomyosarcoma at 630 nm. When converted from Kubelka-Munk properties to transport equation properties these are: $\mu_a = 1.1 \text{ cm}^{-1}$ and $\mu_s' = 7.0 \text{ cm}^{-1}$ (Cheong *et al.*, 1990), which compare with our $\mu_a = 1.4 \pm 0.6 \text{ cm}^{-1}$ and $\mu_s' = 15 \pm 8 \text{ cm}^{-1}$. Recently, Driver *et al.* (1991) gave a table of measured optical properties of different human tumors at 630 nm in which the variation was nearly two orders of magnitude in the absorption coefficient and over one order of magnitude in scattering. Thus, comparisons should actually be made between similar tumor types.

Photofrin has an absorption maximum near 632.8 nm (Manyak *et al.*, 1988), and it may be expected that the addition of Photofrin to tissue would increase the bulk absorption of that tissue at that wavelength. To the contrary, this study showed no such increase but rather an increase in overall scattering (reduction in the anisotropy factor and an increase in the scattering coefficient). As no attempt was made to filter fluorescence due to light absorption by Photofrin, it may be suggested that the fluorescent signal compensates for the light absorbed by the Photofrin and the resulting signal gives an anomalous measurement resulting in an apparent increase in scattering. However, this is unlikely because the fluorescence efficiency (fraction of absorbed energy that emitted as fluorescence) at 632.8 nm is low. From the data of Profio (1984), we estimate this to be less than 1.2×10^{-3} , which would not result in a significant quantity of light compared with the scattered light. Also, the Nd:YAG 1,064 nm light is not well absorbed by Photofrin, yet there was a similar increase in scattering properties as a result of the addition of Photofrin. One possible explanation is, that the Photofrin induces a reaction in the tissue that changes the tissue structure or composition slightly. In a previous study we examined this tumor implanted in rat liver before and 48 h after a 5 mg/kg intravenous dose of Photofrin (Chapter 8). However, light microscopical changes could not be identified in either the liver or the tumor on histological samples. Additionally, measurement of serum liver enzyme levels (ASAT and ALAT) did not indicate any liver damage due to the Photofrin.

In oncology it is important to predict how deep light will penetrate into the tissue, since complete destruction of the tumor must be achieved without major damage to the surrounding normal tissues. The optical properties given here are of particular relevance to experimental studies directed towards predicting regions of tissue necrosis using dosimetry calculations, or for optically detecting tumors. Also illustrated is the possible influence of Photofrin on the scattering properties of liver and tumor, suggesting that for modelling the dosimetry of photodynamic therapy the optical properties of photosensitized tissue should be used.

11. Ultrasonography of Nd:YAG Laser Coagulation

Adapted from: R. VAN HILLEGERSBERG, M.T. DE WITTE, W.J. KORT & O.T. TERPSTRA. Water-jet-cooled Nd:YAG Laser Coagulation of Experimental Liver Metastases: Correlation Between Ultrasonography and Histology. *Lasers Surg Med* 1993; 13: 332-343

INTRODUCTION

Thermal laser therapy is based on the transformation of light energy into heat, upon absorption in the tissue (Chapter 3). At temperatures of 60-140°C the tissue is coagulated, which can be observed macroscopically by blanching; at temperatures of 300-1000°C tissue ablation, vaporization and carbonization occur. For tumor coagulation the Neodymium: Yttrium-Aluminum-Garnet (Nd:YAG) laser is mostly used, as its wavelength of 1,064 nm penetrates up to 10 mm into tissue (Jacques, 1992). The light may be delivered noncontactly by aiming the laser beam on the tissue surface, or interstitially by implanting the light delivery fibers directly into the tissue.

In the studies described in Part II, we investigated the noncontact technique in experimental liver metastases. As others had reported extensive bleeding of the hepatic tissue during noncontact laser vaporization of intrahepatic tumors (Nims & McCaughan, 1983), we aimed at coagulating the tumor. It proved to be that without surface cooling, vaporization and carbonization occurred, precluding light penetration into deeper tissue regions (Chapter 4). Water-jet cooling during treatment prevented carbonization, resulting in perfect tissue coagulation with selective tumor destruction (Chapter 5).

Although Nd:YAG laser coagulation extends deeply into the tissue, the only visible effect is superficial. Optimal clinical application, however, would require knowledge of the quantitative and spatial extent of the lesion, to achieve complete tumor destruction, combined with minimal adjacent normal tissue damage. Several experimental studies report a good correspondence between ultrasonography and histology of laser induced coagulation

(Godlewski *et al.*, 1988; Dachman *et al.*, 1990; Bosman *et al.*, 1991). Until now, most research has been concentrated on the effects in normal liver, which is an excellent model as it comprises solid, homogeneous, and well-vascularized tissue that efficiently absorbs laser light. However, conditions in other tissues are often less ideal and very little is known about the effects on tumor and surrounding normal liver (Dachman *et al.*, 1990).

In the present study we therefore investigated the use of ultrasonography in assessing the extent of laser induced coagulation in the rat liver metastasis model.

MATERIALS AND METHODS

Experimental Design

Twenty-one rats were used for the experiments. Twenty days after intrahepatic tumor implantation a relaparotomy was made under anesthesia with Hypnorm[®] (Janssen Pharmaceutica B.V., Tilburg, The Netherlands), 1 mg/kg body weight i.m., and the visible diameter of the tumor was measured with sliding calipers. The animals were randomly assigned to 6 experimental groups and 1 control group of 3 animals each. In each experimental group laser therapy was performed with a water-jet-cooled Nd:YAG laser (for methods see Chapter 5), at previously fixed energy and power setting. One dose of laser energy (Joule = Watts x seconds of exposure) was applied in each respective treatment group, either 150, 300, 600, 1,200, 1,700 or 2,400 J, at a power setting of 10 W. The control group did not receive any laser treatment. Just pre-laser and immediately post-laser treatment, an ultrasound image of the tumor and surrounding liver was made. We were primarily interested in immediate laser effects, as in the clinical setting this information would allow direct assessment of the treatment effects, with eventually continuation of laser therapy in case of incomplete tumor destruction. Although Dachman *et al.* (1990) reported changes in the size of the lesion during 5-10 minutes after laser application, in our pilot studies, no differences were found in ultrasound images taken either immediately or at 5, 10, or 15 minutes post-treatment. Following ultrasonography, the animals were sacrificed and the livers removed for histological determination of the laser effects.

Ultrasonography

A high definition ultrasound device (A3200, Dornier, Deutsche Aerospace, Germany) was used. The 7.5 MHz small parts linear array transducer was placed transversely on the liver surface using a 2 x 9 cm ultrasound gel pad (Aquaflex, Parker Laboratories Inc., Orange, U.S.A.). The dimensions of a structure were determined by moving the ultrasound transducer at various angles to the tissue surface. When the optimal transducer position was found, the image was frozen. Following that, the maximal width and depth of the various structures were indicated directly on the ultrasound image, using the measurement facilities of the ultrasound device (Figure 11.1). The tumor (i.e., tumor core and total tumor) was measured immediately pre and post-laser. The coagulation zone (i.e., total tumor plus surrounding affected liver) was measured immediately post-laser (Figure 11.1).

The echogenicity of the various structures was always defined in comparison to the normal

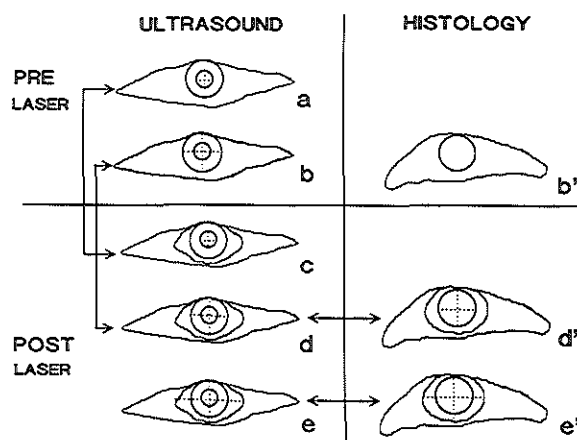


Figure 11.1. Schematic drawing of the various measurements made on ultrasound and histology pre and post-laser treatment. Pre-laser, (a) the hyperechoic focus and (b) total tumor were measured on ultrasound. (b') Pre-laser, histology was only used for morphological comparison to pre-laser ultrasonography. Post-laser, (c) the hyperechoic focus, (d) total tumor and (e) coagulation zone (i.e., total tumor plus surrounding liver damage) were measured on ultrasound. Post-laser histological measurements included (d') total tumor and (e') coagulation zone. The comparisons between pre-laser ultrasonography and post-laser ultrasonography, and between post-laser ultrasonography and post-laser histology are indicated by arrows.

hepatic parenchyma. Thus, a lesion was termed either hyperechoic (brighter than the surrounding hepatic parenchyma), isoechoic (the same brightness as the hepatic parenchyma) or hypoechoic (darker than the hepatic parenchyma).

Histology

Sections from the control group (pre-laser; $n=3$) were used to compare the morphology of untreated tumor and liver with ultrasonography (Figure 11.1). In the experimental groups (post-laser, $n=18$), the maximal width and depth of the total tumor and the coagulation zone (i.e., total tumor plus the surrounding rim of liver damage) were measured by computer-assisted image analysis (IBAS 2000, Kontron Bildanalyse GmbH, München, Germany) (Chapter 2). All measurements were performed without knowledge of the applied laser treatment parameters.

Statistical Analysis

The values are expressed as mean \pm standard error of the mean (SEM). A multiple regression model was used to analyze the relation of depth and width measurements between

histology and ultrasonography, and to determine the influence of energy on coagulation size measured on histology. Spearman's rank order correlation for paired difference (pre-laser minus post-laser) against energy applied was used to analyze the relation between total tumor size or hyperechoic focus on ultrasound pre versus post laser treatment. A difference was considered to be significant at P values of <0.05 .

RESULTS

All animals survived the procedure without complications. On the day of laser treatment the mean \pm SEM visible tumor diameter was 5.3 ± 0.1 mm ($n=21$).

Correspondence Between Ultrasonography and Histology

Pre-laser, the tumor could be identified in the normal hepatic parenchyma as a sphere, build up of a hyperechoic focus, surrounded by a concentric isoechoic layer. This isoechoic tumor periphery was separated from the normal hepatic parenchyma by a thin hypoechoic rim (Figure 11.2a), corresponding to a small zone of compressed hepatic tissue on histology. It proved to be, that the hyperechoic focus on ultrasound corresponded to the central tumor area (Figure 11.2a,b). On histology, this region had an irregular aspect, containing garland shaped areas of cellular fragmentation and fibrosis (the lighter central areas in Figure 11.2b), as well as clusters of vital tumor cells without acinus formation. The surrounding isoechoic zone on ultrasound represented viable tumor tissue (Figure 11.2a,b), which showed a regular acinus arrangement on histology.

Generally, laser treatment did not change the aspect of the tumor on ultrasound (Figure 11.3a,b). Indeed, histology did not show signs of tissue damage after laser energies of 150 J and 300 J. However, after energies of 600-2,400 J, characteristic changes of tumor coagulation were found (Chapters 4, 5): histological and cytological structures had remained intact and tumor cells had dark and spindled nuclei. In contrast to previous observations on day 1 post-laser (Chapter 5), tumor cells did not appear with acidophilic cytoplasm. Ultrasonography showed a clear hypoechoic area in the surrounding hepatic tissue at energies of 600-2,400 J (Figure 11.3b). On histology, this area corresponded to a rim of liver tissue with degenerative changes (Figure 11.3c), which could be divided into two zones:

1. An inner zone of hepatocytes with vacuolated acidophilic cytoplasm and normal nuclei (Figure 11.4a); the sinusoids in this layer were dilated containing interstitial edema.
2. A transition zone to normal hepatic tissue (Figure 11.4b,c); the sinusoids in this zone were hyperemic and the cellular cytoplasm was less vacuolated.

Measurements on Ultrasound

In the experimental groups, no difference was found between the pre-laser and post-laser size of the total tumor on ultrasonography ($n=18$) (Table 11.1). The overall pre and post-laser mean \pm SEM depth \times width of the hyperechoic focus was $2.7\pm0.1 \times 3.3\pm0.3$ mm and $2.9\pm0.1 \times 3.8\pm0.2$, respectively ($P=0.082$, $r_s=-0.342$ for depth; $P=0.080$, $r_s=-0.345$ for width).

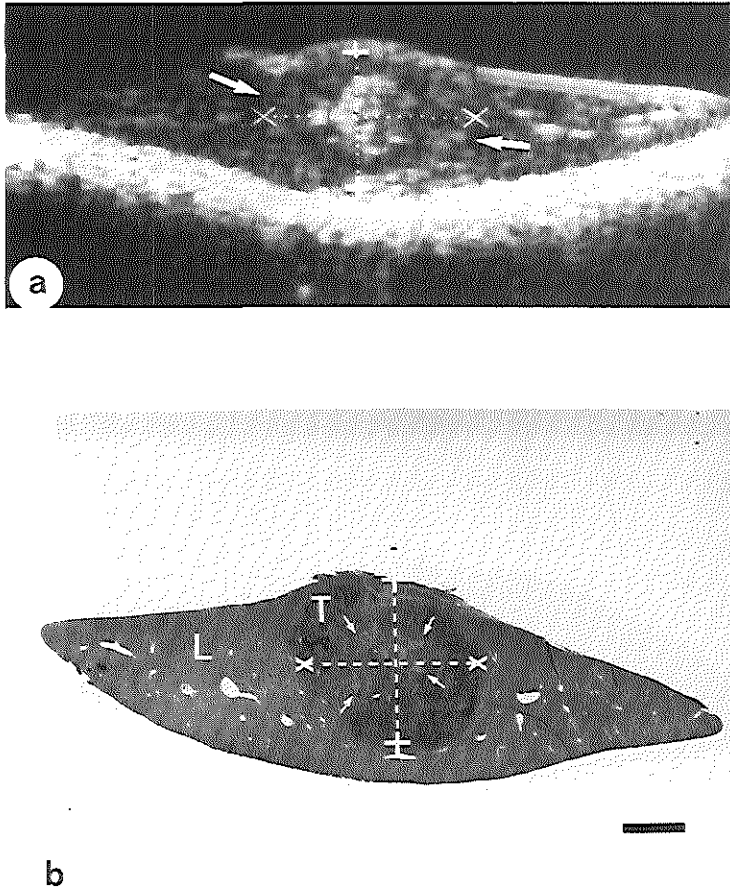


Figure 11.2. (a) Ultrasonography and (b) histology of an untreated tumor in the liver. The hyperechoic focus on ultrasound corresponds to the central tumor area on histology (between arrows), containing garland shaped areas of cellular fragmentation (the lighter central areas) and fibrosis, beside clusters of vital tumor cells without acinus formation. The surrounding isoechoic zone on ultrasound represents viable tumor tissue, which shows a regular acinus arrangement on histology. The isoechoic zone on ultrasound is separated from the hepatic parenchyma by a thin hypoechoic rim (arrows), corresponding to a small zone of compressed hepatic tissue. T, Tumor; L, Liver; + - +, Total tumor depth; X - X, Total tumor width. Bar: 1.7 mm (hematoxylin, azophloxin & saffron stain).

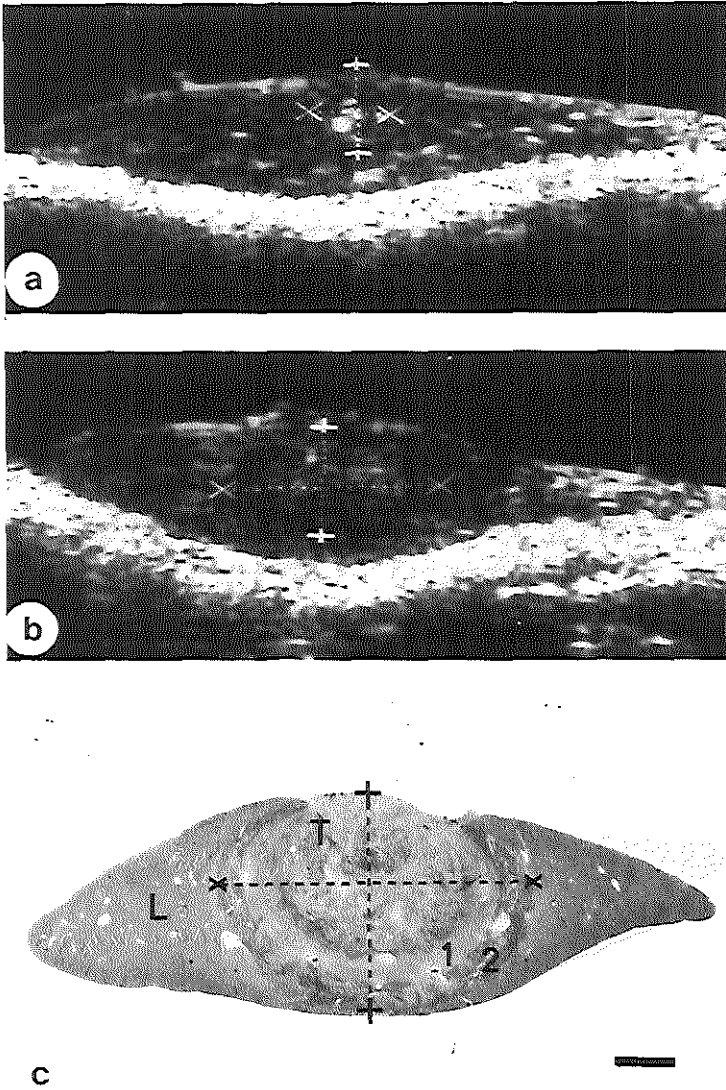


Figure 11.3. Ultrasonography (a) pre-laser and (b) post-laser, and (c) corresponding histology post-laser of a tumor in the liver treated with 1,200 J at 10 W. On ultrasound, laser treatment does not change the aspect of the tumor, whereas the surrounding hepatic damage appears hypoechoic compared to normal parenchyma. On histology the affected tumor is surrounded by a zone of liver damage, which can be separated into two zones, representing a decline in temperature towards the periphery of the lesion. T, Tumor; L, Liver; + - +, Coagulation depth; X - X, Coagulation width; 1, Inner zone of liver damage; 2, Outer transition zone to normal hepatic tissue. Bar: 1.7 mm, (hematoxylin, azophloxin & saffron stain).

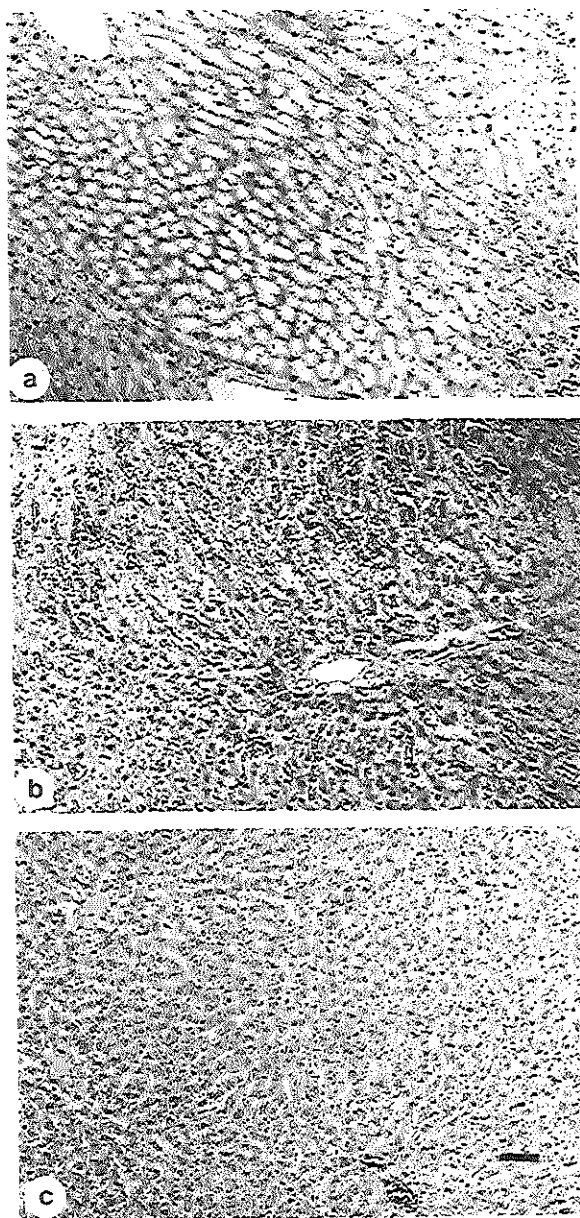


Figure 11.4. Histological sections of the rim of hepatic damage, surrounding the tumor immediately post-laser with 1,200 J (magnification of Figure 11.3c). Numbering corresponds to the text. (a) The inner zone (1) contains dilated edematous sinusoids and hepatocytes with vacuolated cytoplasm. (b) The outer transition zone (2) consists of cells with less vacuolated cytoplasm and hyperemic sinusoids. (c) Normal hepatic tissue. Bar: 50µm (hematoxylin, azophloxin & saffron stain).

Table 11.1. Mean \pm SEM depth and width of the total tumor and hyperechoic focus on ultrasound.*

Energy (J)	Hyperechoic focus				Total tumor			
	Pre-laser Depth	Width	Post-laser Depth	Width	Pre-laser Depth	Width	Post-laser Depth	Width
150	3.3 \pm 0.3	4.3 \pm 0.1	3.2 \pm 0.2	4.2 \pm 0.1	4.8 \pm 0.2	7.3 \pm 0.3	5.1 \pm 0.4	7.3 \pm 0.2
300	3.0 \pm 0.3	4.0 \pm 0.5	2.7 \pm 0.3	3.5 \pm 0.0	4.5 \pm 0.7	7.1 \pm 0.7	4.9 \pm 0.4	7.4 \pm 0.3
600	2.0 \pm 0.1	2.6 \pm 0.4	2.4 \pm 0.2	2.8 \pm 0.1	4.5 \pm 0.1	6.9 \pm 0.1	5.2 \pm 0.1	7.4 \pm 0.4
1200	2.2 \pm 0.4	2.8 \pm 0.8	3.1 \pm 0.2	4.9 \pm 0.6	4.2 \pm 0.3	5.8 \pm 1.6	4.0 \pm 0.6	6.3 \pm 0.7
1700	3.0 \pm 0.3	3.5 \pm 0.4	2.8 \pm 0.2	3.5 \pm 0.1	5.0 \pm 0.1	8.0 \pm 0.5	5.0 \pm 0.5	7.5 \pm 0.4
2400	2.7 \pm 0.2	3.6 \pm 0.2	3.2 \pm 0.0	3.8 \pm 0.2	3.6 \pm 0.7	5.6 \pm 0.9	4.5 \pm 0.7	6.6 \pm 1.7

*n=3 for all groups.

The mean depth \times width of the entire tumor was 4.4 \pm 0.2 \times 6.8 \pm 0.4 mm pre-laser and 4.8 \pm 0.2 \times 7.1 \pm 0.3 mm post-laser ($P=0.288$, $r_s=-0.141$ for depth; $P=0.306$, $r_s=-0.129$ for width).

Measurements on Histology

The measurements on histology were all made post-treatment (n=18) (Figure 11.1). Mean \pm SEM total tumor depth \times width was 5.3 \pm 0.2 \times 5.9 \pm 0.2 mm. Coagulation width was directly related to the amount of energy applied and was fitted by a logarithmic curve ($P<0.0001$, $R^2=0.983$) (Figure 11.5a). Width values ranged from 5.9 \pm 0.4 mm at 150 J to 9.3 \pm 0.3 mm at 1,200 J. Coagulation depth was also fitted logarithmically to the amount of laser energy delivered ($P=0.048$, $R^2=0.174$) (Figure 11.5b). Mean depth values varied from 5.2 \pm 0.5 mm at 300 J to 6.6 \pm 0.2 mm at 1,700 J. As the central tumor area displayed an irregular pattern, exact depth and width of this area could not be defined properly on histological specimen.

Correlation Between Measurements on Ultrasound and Histology

Figures 11.6 and 11.7 compare the results of the post-laser measurements on ultrasound and histology. Coagulation size on ultrasound versus histology showed a significant correlation ($P=0.015$, $r=0.57$ for depth; $P=0.012$, $r=0.58$ for width) (Figure 11.6a,b). The total tumor size correlated well too ($P=0.004$, $r=0.64$ for depth; $P=0.002$, $r=0.68$ for width) (Figure 11.7a,b). Width measurements were generally larger on ultrasound than on histology, whereas the opposite was found for depth.

DISCUSSION

In this study, laser coagulation of the transplantable rat colon carcinoma and surrounding liver tissue was determined by ultrasonography and histology. On ultrasound, tumors of 5-6 mm in diameter presented as isoechoic entities with a hyperechoic center.

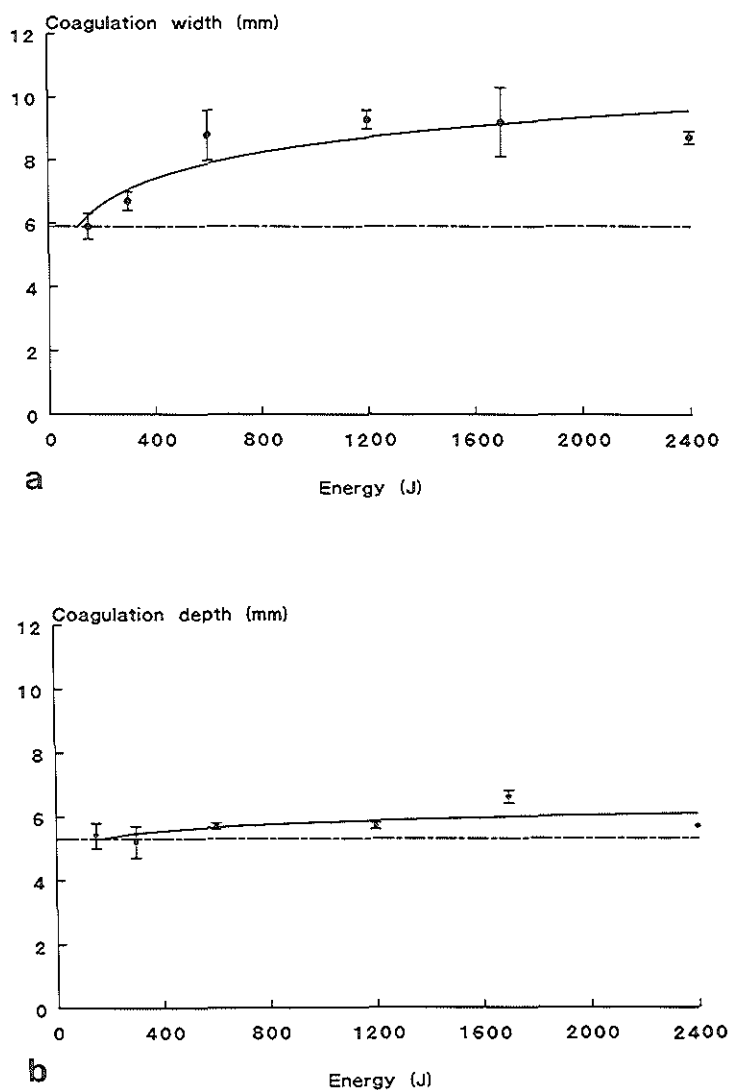


Figure 11.5. (a) Coagulation width and (b) depth on histology immediately post-laser vs. energy delivered. Each point represents the mean \pm SEM of 3 experimental results. The dashed line describes the mean tumor size (depth: 5.3 ± 0.2 mm, width: 5.9 ± 0.2 mm).

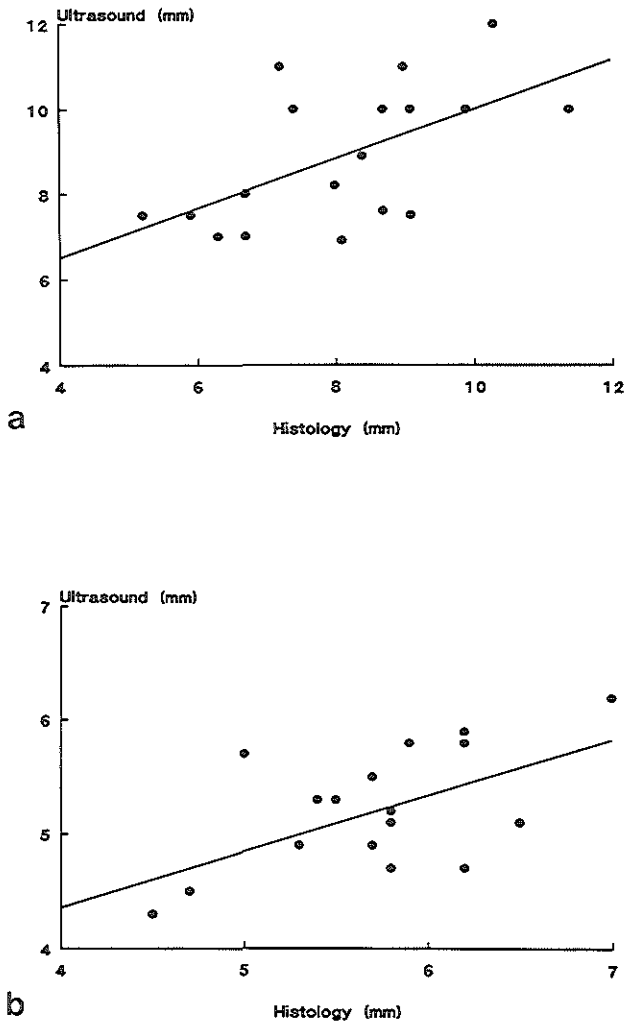


Figure 11.6. (a) Total coagulation width and (b) depth on histology vs. ultrasonography, immediately post laser treatment with energies of either 150, 300, 600, 1,200, 1,700 or 2,400 J at 10 W.

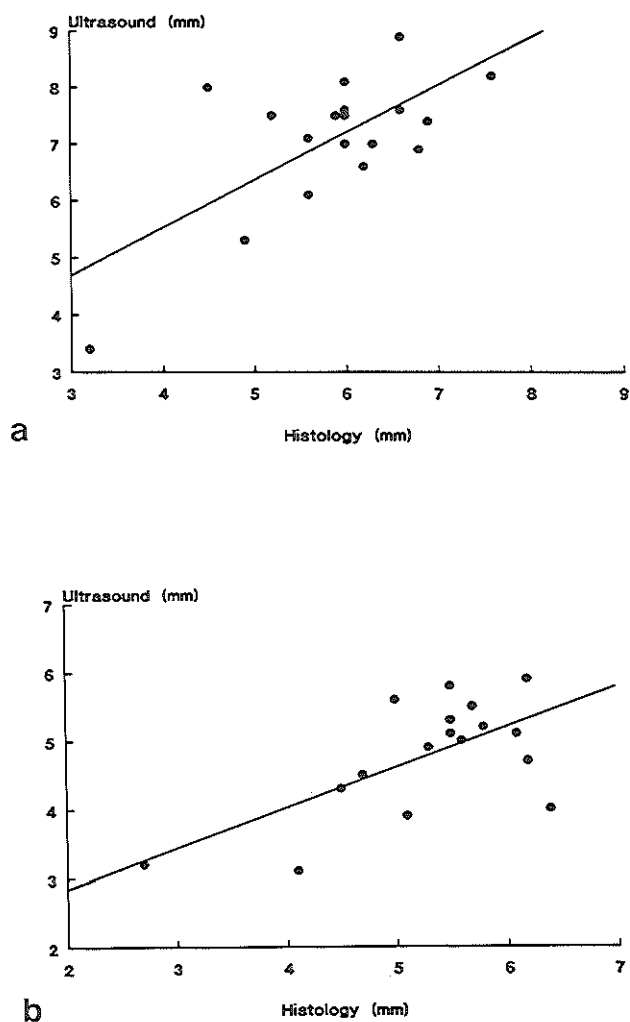


Figure 11.7. (a) Total tumor width and (b) depth on histology vs. ultrasonography, immediately post laser treatment with energies of either 150, 300, 600, 1,200, 1,700 or 2,400 J at 10 W.

In general, the tumor aspect and size on ultrasound did not change as a result of laser coagulation. On histology, the tumor showed characteristic changes of laser coagulation after 600-2,400 J. At these laser energies, surrounding affected liver tissue appeared hypoechoic on ultrasound, corresponding to the zone of hepatic damage on histological samples. A good correlation was found between the size of the entire coagulation zone (i.e., total tumor plus surrounding hepatic damage) on ultrasound and histology.

Imaging laser induced tissue coagulation is one of the major challenges in the field of laser medicine. Methods such as thermocouple or light detector insertion, can provide information about the light distribution or heat development at different points in the tissue (Daikuzono *et al.*, 1988; Jacques & Prahl, 1987; Davis *et al.*, 1988; Marijnissen & Star, 1987). These parameters may be used as feedback tools for laser adjustment during therapy, to achieve optimal localized tumor destruction. However, the probes have to be placed directly into the tissue, their position is rather critical and they provide only information about the possible changes in the tissue (e.g., at a certain temperature level). Radiodiagnostic techniques, such as ultrasonography or magnetic resonance imaging (MRI), would enable:

1. The direct visualization of the laser induced coagulation.
2. Non-invasive application with the possibility of lesion follow-up.

Other investigators have studied the use of MRI as a means of visualizing laser coagulation. Jolezs *et al.* (1988), Anzai *et al.* (1991) and recently Tracz *et al.* (1992) reported good correspondence of the MR-image to reversible and irreversible thermal tissue changes using *in vitro* and *in vivo* models. Unfortunately, the currently available conventional MRI needs several minutes to collect data for an image, which causes disturbance owing to respiratory movements of the liver (A.R. Bleier, Harvard Medical School, Department of Radiology, Boston, MA, USA. *Personal communication*, 1991). When faster devices become available, MRI may be useful in determining the amount of intrahepatic laser coagulation.

An important advantage of ultrasonography compared to MRI is the possibility of intraoperative utilization, allowing direct assessment of the treatment effects, with eventually continuation of laser therapy at a single procedure in case of incomplete tumor destruction. In percutaneous interstitial laser therapy, ultrasonography has been performed during treatment to monitor the development of a lesion, allowing instantaneous adjustment of laser parameters (Bosman *et al.*, 1991). It has to be established whether the water-jet technique can be applied in a laparoscopic procedure, which would have important advantages in palliative therapy. However, for intended curation an operative approach is desirable, as under such circumstances tumor staging and optimal identification of the metastases is of utmost importance (Foster, 1990; Steele & Ravikumar, 1989). In clinical studies, intraoperative ultrasonography was found to be the most accurate method of detecting colorectal liver metastases (De Jong *et al.*, 1989; Schreve *et al.*, 1984; Charnley *et al.*, 1991). Human hepatic metastases may be either hyperechoic, hypoechoic or mixed echogenic (Delorme & Kaick, 1992). Characteristically, metastases from colorectal cancer display hyperechoic compared to the hepatic tissue, possibly with a surrounding hypoechoic halo ("bull's eye") (Olsen, 1990; Bruneton *et al.*, 1982; Beyer, 1981). More or less the same pattern was found for the rat colon carcinoma used in this study. The hyperechoic focus corresponded to the central tumor area found on histology. The preexistent central necrosis in these relatively small tumors

consists of solid material, and displays a garland like pattern (Figure 11.2b). In larger tumors the necrosis often becomes liquid, which may appear anechoic or hypoechoic on ultrasound. The exact mechanism underlying hyperechogenicity of the central necrosis is unclear. Marchal *et al.* (1985) demonstrated correspondence between strongly reflective hepatic metastases on ultrasound and irregular histologic configuration due to either hypervascularity or an irregular pattern of fibrosis. Indeed, in our model the central tumor necrosis displayed irregular with increased fibrosis, which may be responsible for the hyperechogenicity. The adjacent isoechoic area represented viable tumor tissue. This isoechoic tumor periphery was separated from the hepatic parenchyma by a thin hypoechoic rim, corresponding to a small zone of compressed hepatic tissue, which probably represents actively growing tumor (Beyer, 1981) (Figure 11.2a).

Previous experimental studies on normal tissue demonstrated coagulation as an increase in echodensity on the ultrasound image (Godlewski *et al.*, 1988; Dachman *et al.*, 1990; Bosman *et al.*, 1991; Littrup *et al.*, 1988). Such an increase was not found post-laser coagulation of the mixed echogenic colon carcinoma used in this study. This observation may very well represent the situation in clinical practice, as 84% of the hepatic metastases from colorectal cancer appear echogenic at intraoperative ultrasonography (Olsen, 1990). In this study, the liver tissue around the tumor presented hypoechoic post treatment with higher laser energies. Dachman *et al.* (1990) and recently Steger *et al.* (1992) found a similar hypoechoic area around an echogenic focus produced by laser in normal pig and canine liver. In a clinical study, Steger *et al.* (1989a) demonstrated hypoechogenicity around a hepatic metastasis treated with interstitial Nd:YAG laser. This hypoechoic zone may correspond to a lesser degree of thermal tissue damage (compared to the echogenic coagulation) combined with the development of edema.

In general, width measurements on ultrasound were larger than on histology, whereas the opposite was found for depth. These differences may be explained by flattening of the liver as a result of pressure of the gel pad and ultrasound transducer. We have used open surgery in this model to determine laser and ultrasound parameters as standardized as possible and the use of a gel pad window was necessary to obtain an image of the superficial tumor.

Previous histological studies on laser tissue-interactions have shown 2 different types of thermal tissue damage:

1. Coagulation necrosis, which appears immediately post treatment resulting in heat fixation of the tissue as a result of protein denaturation.
2. Indirect thermal damage which appears about 1 day post laser therapy.

This delay of necrosis is attributed to a different mechanism of destruction, namely the inactivation of vital enzymes which comes to expression during metabolism (Thomsen, 1991; Van Hillegersberg *et al.*, 1992; Brackett *et al.*, 1986).

In this study, the tumor showed coagulation necrosis after energies of 600-2,400 J. The rim of liver damage that surrounded the tumor immediately post laser treatment could be divided into 2 different zones (Figure 11.4a,b). These zones represent a decline in temperature towards the periphery of the lesion. The inner zone contained hepatocytes with vacuolated acidophilic cytoplasm and normal nuclei, corresponding to type 1 thermal damage as referred to above. The outer transition zone consisted of cells with less vacuolated cytoplasm and

hyperemic sinusoids, probably corresponding to type 2. In Chapter 5, we investigated water-jet-cooled Nd:YAG laser effects on day 1 and 36 post-therapy. Indeed, on day 1 the transition zone had become largely necrotic, containing deliquesced cells without nuclei. The histological aspect of the inner zone had not changed during the subsequent period of 36 days, probably as result of heat-fixation. In this study, the size of coagulation measured on histology included both zones of hepatic damage. As a good correlation was found between coagulation size on histology and ultrasonography, the hypoechoic area on ultrasound would probably represent the entire rim (both zones) of liver damage.

The shape of the laser-induced lesion was ellipsoid, with coagulation depth as the short axis ($\{\text{total tumor size}\} + \{\text{rim of hepatic damage}\}$) and coagulation width as the long axis ($\{\text{total tumor size}\} + 2\{\text{rim of hepatic damage}\}$) (Figure 11.3c). At lower energies, coagulation depth did not reach the hepatic tissue, whereas lateral liver damage was always found from 300 J-2,400 J (Figure 11.5). The shape of coagulation is the complex result of many parameters, such as laser wavelength, surface cooling, and optical properties, heat capacity, thermal conductance and vascularization of the tissue. The whitish colon carcinoma appears to be a slightly better scattering medium for Nd:YAG laser light than the surrounding liver tissue (Chapter 10). Water-jet-cooling shifts the maximal tissue temperature to a zone located within the tissue, normally occurring at the tissue surface (Svaasand *et al.*, 1985). Thus, most probably light and temperature distribution were divided equally around the margins of the total tumor sphere, resulting in a homogeneous rim of hepatic necrosis (Figure 11.3c).

The aim of this study was to assess whether laser coagulation of tumor and surrounding liver could be identified by ultrasonography. As laser coagulation did not effect the appearance of the tumor on ultrasound, the amount of tumor destruction could not be judged by the image of the tumor itself. However, the coagulation size (i.e., total tumor plus surrounding rim of hepatic damage) on ultrasound correlated well to the coagulation size on histology. This last parameter showed a significant relation with laser energy applied (Figure 11.5a,b). In Chapter 5, long-term observations showed a significant relation between the percentage of tumors in complete remission and the amount of laser energy applied. Thus, final tumor necrosis may be judged immediately post laser treatment by the total lesion size on ultrasound, i.e., the size of the surrounding hypoechoic rim of hepatic damage. Further studies should confirm this proposition.

PART V

GENERAL DISCUSSION

12. General Discussion: Considerations for Clinical Application

The rationale of treating hepatic metastases of colon cancer is based on the substantial improvement of survival rates after surgical resection in selected patients (Sugarbaker, 1993). However, accompanied destruction of normal hepatic tissue limits the application of this procedure. In this study we investigated the use of laser treatment as a means of selective destruction of tumor tissue within the liver, using a rat tumor model for hepatic metastasis of colon cancer.

THERMAL THERAPY

The noncontact Neodymium:Yttrium Aluminum Garnet (Nd:YAG) laser was used in combination with a focussing handpiece. A power output of 20 W was applied in pulsed mode, at energies of either 60, 120 or 180 J. As we aimed at coagulating the tumor, a pulsed temporal mode was used with 0.3 s pause between laser pulses of 0.5 s, to allow cooling of the tissue between laser exposure. The laser beam was focussed at the center of the tumor sphere to achieve maximal heat conduction from this point to the tumor margins. Histology of the lesions at various intervals post-treatment (0-8 days) showed a superficial coagulation necrosis at the lowest laser energy (60 J), whereas at higher energies (120 J, 180 J) ablation and carbonization occurred. The charred tissue effectively absorbed the laser light, which hindered light transfer to the underlying tumor regions and therefore total in depth tumor destruction was not accomplished. Probably, tissue temperatures at the higher energy range, were much above the coagulation range (60-140°C), owing to the relative high power setting, focussing of the laser light upon the tissue, and short period of cooling between the laser pulses (Meijering *et al.*, 1993).

In the succeeding study, we therefore investigated the possibility of cooling the tissue surface during Nd:YAG laser treatment in order to avoid charring and to attain absolute tumor coagulation. For that purpose, laser fiber was enclosed within a teflon hose, through which a saline solution was pumped, resulting in a water-jet which transmitted the laser beam

beyond the fiber tip (Sander *et al.*, 1988). Tissue cooling allowed irradiation with energies of 2,400 J, at either 10 or 20 W, without tissue carbonization or ablation. The water-jet enabled precise targeting on the tissue surface, resulting in tumor coagulation, combined with minimal liver damage. The maximal depth of tissue damage was 10 mm, measured after 1,700 J and 20 W. The short-term diameter of the induced lesion was 22% larger at a power setting of 20 W than at a power setting of 10 W. It has to be established to what extent higher power settings can enlarge the diameter of the induced lesion. The maximal power setting at which water-cooling can still avoid carbonization will be related to the laser energy applied and the temperature of the cooling-water. Complete tumor remission was found in this study, related to the laser energy delivered, but irrespective of the power setting applied. This may imply that within the power and energy range delivered, the degree of tumor coagulation is primarily determined by the delivered laser energy, i.e., exposure time to a temperature within the coagulation range.

In the two studies described above, the laser light was delivered noncontactly by aiming the laser beam on the tissue surface. This may be a proper treatment modality for superficial tumors, avoiding spread of tumor cells and bleeding as a result of tissue manipulation. However, deep seated tumors may not be accessible in the noncontact mode owing to limited light penetration. For that purpose, we investigated interstitial light delivery, implanting the laser fiber directly into the malignant tissue. The heat generated by a bare tipped fiber is very localized, inducing a blackish clot at the insertion site, which suppresses the light transmission into the tissue (Mathewson *et al.*, 1987). The charring transforms the bare fiber tip from a distributed heat source into a point heat source (Wyman *et al.*, 1992). We therefore developed a cylindrical diffusing fiber-tip, to provide for homogeneous heat distribution by uniform light delivery. Indeed, the use of this tip allowed gentle tissue heating within the coagulation range, resulting in sharply defined tumor coagulation without any charring with 4 W/cm and up to 4,800 J/cm. The light transmission did not decrease during treatment; on the contrary, an increase in fluence rate was found during laser treatment (up to 170%), probably as a result of the changing optical properties of the coagulating tissue. The total lesion size increased with energy applied to a maximum of 11 mm after 4 W/cm and 4,800 J/cm, leading to complete tumor remission 3 out of 4 animals. The lesion size found with the cylindrical diffuser is comparable to the that found in previous studies using the bare fiber, suggesting that preservation of light transmission would not significantly increase the treatment range. However, higher output powers can probably be applied to the cylindrical diffuser before tissue ablation occurs. The tissue ablation creates a cavity around the fiber, which strongly suppresses heat transfer into the tissue. It is therefore proposed that with a cylindrical diffuser higher coagulation volumes can be reached. Definite conclusions can only be drawn after comparing the various methods in the same experimental set-up under standardized conditions.

Post-Nd:YAG Laser Histology

With the noncontact technique, 5 different zones of tumor destruction were found, representing the decreasing levels of energy absorbed by the tissue at an increasing radius from the point of maximal laser energy. In the center of the tumor elevation of tissue temperature to 300-1000°C probably occurred, leading to tissue carbonization and ablation (zone 1 and 2). In the adjacent zone (zone 3) temperatures >100°C resulted in vaporization of tissue water content, creating tissue cavities filled with steam. Towards the tumor periphery protein denaturation occurred (temperatures of >60°C), resulting in tissue coagulation (zone 4). At the tumor margins (zone 5) temperatures between 45 and 60°C probably resulted in reversible and irreversible cellular damage. It was found that histological laser effects could be determined most properly on the first or second day post-treatment.

Tumor coagulation showed characteristic cellular changes: spindle formed cells with pyknotic elongated nuclei. These changes are thought to be secondary to the collapse of the cytoskeleton (Thomsen, 1991). With the water-jet, cavities of boiled tissue water were often observed at the border between tumor and liver. These cavities were not found after the interstitial application; probably tissue temperatures were lower than with the water-jet. The only marked difference between the coagulated cells immediately post-laser and on the first day post-laser, was the appearance of acidophilic cytoplasm in the latter, indicating cellular necrosis.

The histological structures of the coagulated tissue had remained intact up to even 36 days post-treatment. Most probably, only the tissue frame had remained, consisting of denatured tissue proteins. The heat-fixed tissue is hardly infiltrated by inflammatory cells and is therefore cleared up very slowly. Enzymatically induced lysis and subsequent phagocytosis may be hampered owing to protein denaturation and the relative absence of tissue water, which evaporated during laser heating. Especially at higher laser energies applied, tumor outgrowth could not be observed in these coagulated areas. We demonstrated that these coagulated areas do not incorporate bromodeoxyuridine (a thymidine analogue), which evidences absence of proliferative activity.

The rim of liver damage, that surrounded the tumor immediately post-laser treatment could be divided into 2 different zones. The inner zone contained hepatocytes with vacuolated acidophilic cytoplasm and normal nuclei, while the outer transition zone consisted of cells with less vacuolated cytoplasm and hyperemic sinusoids. On day 1 post-laser, the transition zone had become largely necrotic, containing deliquesced cells without nuclei. This delay of necrosis is attributed to a different mechanism of destruction, namely the inactivation of vital enzymes, which comes to expression during metabolism. The histological aspect of the inner zone had not changed during the subsequent period of 36 days, probably as result of the heat-fixation as mentioned above.

In conclusion, 2 different types of thermal tissue damage can be distinguished in Nd:YAG laser coagulation:

1. Coagulation necrosis, which appears immediately post treatment, resulting in heat-fixation of the tissue as a result of protein denaturation.
2. Indirect thermal damage which appears about 1 day post laser therapy.

PHOTODYNAMIC THERAPY

As mentioned previously, to be of potential value as alternative to partial hepatic resection, a treatment modality should cause complete tumor destruction combined with minimal hepatic damage. However, especially in an organ as liver, selectivity in photosensitizer accumulation had not been achieved, and superficial tumor illumination had caused substantial liver necrosis (Pimstone *et al.*, 1982). Our research was therefore directed towards either selective light delivery after photosensitization with Photofrin, or selective photosensitizer accumulation.

In our first approach, we investigated the effects of photodynamic therapy (PDT) on tissue photosensitized with Photofrin (5 mg/kg i.v.), using interstitial tumor illumination to achieve selectively. An argon-pumped dye laser was used to generate light of 625 nm. To provide for homogeneous light delivery a custom-built 0.5 cm cylindrical diffusing fiber-end was used (Marijnissen *et al.*, 1985).

Interstitial light delivery enabled effective illumination of the tumor, resulting in major tumor destruction. Surrounding liver damage was limited to a distinct zone of 2-4 mm width and did not deteriorate liver function as measured by antipyrine clearance. Liver damage was strongly related to the liver anatomy as hepatic cells survived around the portal areas. This phenomenon is probably due to a different hepatocyte environment (perfusion, and hence supply of nutrients) and enzyme content in the periportal compared to pericentral domains (Lamers *et al.*, 1989). Short-term liver necrosis increased with energy delivered, but a plateau occurred beyond 400 J/cm, indicating that higher laser energies could be applied without much more liver damage. Probably, the hepatic tissue effectively absorbed 625 nm light, which limited the light penetration in liver, and by that limited hepatic damage. Tumor necrosis also increased with light dose delivered, to 99% of the original tumor area after 1,600 J/cm at 200 mW/cm. Depending on the amount of light energy applied, islands of vital tumor cells could be identified in the necrotic tumor area. The appearance these apparently therapy resistant tumor cells has previously been described in rat hepatoma (Pimstone *et al.*, 1982; Holt *et al.*, 1985). There could be several mechanisms underlying this phenomenon, assuming the heterogeneity of tumor tissue. For example, these tumor cells may not incorporate sufficient Photofrin or may have low metabolism and correspondingly low singlet oxygen production.

Tumor growth retardation was significantly related to the amount of light energy delivered as would be expected from the short-term observations. Up to 800 J/cm, a similar relation was found for the number of tumors in complete remission. Unfavorable results at 1,600 J/cm, however, led to an overall nonsignificant relation between tumor remission and energy applied, suggesting an optimum relation between light dose and tumor response. In the present stage of knowledge of the photodynamic reaction these results can hardly be explained. Better understanding of photodynamic toxicity and the mechanism responsible for survival of specific tumor cells may lead to treatment strategies causing complete tumor destruction.

In our second approach, we considered the possibility of using the varying capacity of tissues to metabolize porphyrins, as a means of selective photosensitization. In every cell

porphyrins are produced as precursors of heme. Previous studies had demonstrated altered activities of the enzymes of the heme biosynthetic pathway in malignant and regenerating tissues; the activity of ferrochelatase, which converts protoporphyrin IX (PROTO) to heme, would be decreased while the opposite was found for porphobilinogen deaminase (PBGD) (Dailey & Smith, 1984). Thus, if the amount of 5-aminolevulinic acid (ALA) available in the cell could be increased, the higher activity of PBGD and lower activity of ferrochelatase would result in accumulation of porphyrins in the tumor, whereas in the normal surrounding hepatic tissue porphyrins would be metabolized to heme. We therefore administered ALA in drinking water during 2-11 days and subsequently tissue porphyrin concentrations were measured in tumor and liver. For comparison porphyrin accumulation was also determined following a usual dose of Photofrin. Furthermore, ferrochelatase and PBGD activities were measured in the tumor and liver.

Oral administration of ALA (28 mg/day) resulted in the progressive accumulation of porphyrins in the tumor, without accumulation in the surrounding liver tissue. After 11 days of ALA the porphyrin concentration ratio between tumor and liver was 4:1 (after Photofrin this ratio was 1:3). The main product found in the tissues after ALA treatment was PROTO. This substance has photosensitizing properties as evidenced by the severe cutaneous phototoxicity in erythropoietic protoporphyria (Kappas *et al.*, 1989) and the good results of studies on PDT after the topical application of ALA to skin lesions (Kennedy & Pottier, 1992). A recent clinical pilot study reports the selective accumulation of PROTO in colorectal carcinoma (compared to adjacent mucosa), measured by fluorescence 4-6 h after oral administration of ALA 60 mg/kg (n=1) or 30 mg/kg (selectivity in 1 out of 2 patients) (Loh *et al.*, 1993). It has to be established whether the oral administration of ALA can indeed cause effective and more selective photodynamic destruction of intrahepatic tumors. Another application of ALA administration could be the early detection of malignant tissue, utilizing the fluorescence properties of PROTO during illumination with ultraviolet light (Bedwell *et al.*, 1992).

Analysis of the activity of PBGD and ferrochelatase in the tissues, showed a 3 fold decrease of ferrochelatase activity in tumor compared to normal liver, confirming our proposition about the mechanism of porphyrin accumulation after oral ALA. In contrast to other studies, however, PBGD was decreased 2 fold. Information about tissue ferrochelatase activity could be useful in predicting the effect of ALA administration on porphyrin accumulation in different tissues. Our preliminary results show a similar decrease of ferrochelatase activities in rat mamma carcinoma and fibrosarcoma. Further experiments should show to what extent the selective accumulation of porphyrins after ALA is related to the type of tumor and tissue.

Post-PDT Histology

Sections on the second day after PDT showed massive tumor necrosis, characterized by cellular debris and disintegrated cells with acidophilic cytoplasm and pyknotic or fragmented nuclei, surrounded by a polymorphonuclear inflammatory infiltrate. PDT induced damage could clearly be distinguished from the vital tumor tissue.

The surrounding necrotic liver tissue consisted of deliquesced hepatocytes with vacuolated

acidophilic cytoplasm without nuclei, containing dilated sinusoids. A second zone of inflammatory infiltrate surrounded the hepatic necrosis.

Thirty-six days after PDT treatment the necrotic area was replaced by regenerated liver tissue and connective scar tissue in which a granulomatous reaction with multinucleated giant cells was present.

PREDICTING LASER-TISSUE INTERACTION

As described in the previous sections, interstitial PDT or thermal Nd:YAG laser coagulation can produce complete destruction of experimental liver metastases combined with minimal liver damage. In both treatment modalities, the induced tissue damage extends deeply into the tissue, whereas the only visible effect is superficial. In the clinical situation, however, one would like to predict the quantitative and spatial extent of a lesion, in order to preset laser parameters, i.e., output power, exposure time, position and number of optical fibers. We used two different approaches that may contribute to better knowledge of laser-tissue interaction.

Our first approach was to determine the optical properties of the tissues, for modelling the light transport; estimating temperature rise or photosensitizer activation. Modelling the light transport in the tissue requires knowledge of the intrinsic bulk optical properties of the tissues for a particular wavelength (Patterson *et al.*, 1991b): the absorption coefficient, μ_a , the scattering coefficient, μ_s , and the average cosine of the scattering angle (the anisotropy factor, g). We therefore determined the optical properties of normal and Photofrin sensitized rat colon carcinoma and liver at the relevant wavelengths for PDT (around 630 nm) and thermal therapy (1,064 nm), using indirect methods with two identical integrating spheres.

At 632.8 nm the absorption coefficient in the dark red colored liver was significantly higher than in tumor (a factor of 2.7), whereas no difference was found for scattering. At 1,064 nm, however, the whitish colon carcinoma appeared to be a better scattering medium than the surrounding liver tissue. Remarkably, scattering increased in both tissues and both wavelengths, 48 h after a usual 5 mg/kg intravenous Photofrin dose. As Photofrin has an absorption maximum near 632.8 nm (Star *et al.*, 1990), it was expected that the addition of Photofrin would increase the bulk absorption of tissue at that wavelength. To the contrary this study showed no such increase but rather an increase in overall scattering. It is unlikely that the fluorescence of Photofrin during illumination compensated for the light absorbed by the Photofrin, because the fluorescence efficiency (fraction of absorbed energy that emitted as fluorescence) at 632.8 nm is too low compared with the scattered light (Profio, 1984). Also, the Nd:YAG 1,064 nm light is not well absorbed by Photofrin, yet there was a similar increase in scattering properties as a result of the addition of Photofrin. A possible explanation is that Photofrin induces a reaction in the tissue that changes the tissue structure or composition slightly, suggesting that for modelling the dosimetry of PDT, the optical properties of photosensitized tissue should be used.

In our second approach, we investigated the use of ultrasonography as a means of imaging Nd:YAG laser coagulation. Several experimental studies had reported a good correspondence

between ultrasonography and histology of laser induced coagulation in normal liver (Dachman *et al.*, 1990; Bosman *et al.*, 1991). However, very little was known about the effects on tumor and surrounding normal tissue. In our liver metastasis model, we therefore compared ultrasonography with histology of water-jet cooled Nd:YAG laser-induced lesions at 10 W and 150-2,400 J.

Untreated tumors presented as isoechoic entities with a hyperechoic center. The hyperechoic focus corresponded to the central tumor area found on histology. The irregular histologic configuration of this central area may be responsible for the hyperechogenicity (Marchal *et al.*, 1985). The surrounding isoechoic zone on ultrasound represented vital tumor tissue. A similar pattern is found in most human hepatic metastases from colorectal cancer (Olsen, 1990; Delorme & Kaick, 1992). In contrast to previous experimental studies on liver, the tumor aspect and size on ultrasound did not change as a result of laser coagulation. On histology, however, after 600-2,400 J the tumor showed characteristic changes of laser coagulation as described previously. At these laser energies, surrounding affected liver tissue appeared hypoechoic on ultrasound, corresponding a zone of hepatic damage on histological samples. Dachman *et al.* (1990) and recently Steger *et al.* (1992) found a similar hypoechoic area around an echogenic focus produced by laser in normal pig and canine liver. This hypoechoic zone may correspond to a lesser degree of thermal tissue damage (compared to the echogenic coagulation) combined with the development of edema.

A significant correlation was found between the size of the entire coagulation zone (i.e., total tumor plus surrounding hepatic damage) on ultrasound and histology. This coagulation size on histology showed a significant relation with laser energy applied. As in previous studies, tumor remission was directly related to laser energy applied, final tumor necrosis may be judged immediately post laser treatment by the total lesion size on ultrasound (i.e., the size of the hypoechoic rim of hepatic damage). Further studies should confirm this proposition.

GENERAL CONSIDERATIONS FOR CLINICAL APPLICATION

In this study, laser therapy has been found to produce discrete areas of tissue necrosis combined with minimal liver damage. In thermal laser therapy we used the Nd:YAG laser, with a wavelength of 1,064 nm for localized superficial or interstitial tumor destruction. To avoid carbonization, which prevents light penetration, a cylindrical diffusing fiber-tip was used in the interstitial application and superficial water-jet cooling in the noncontact laser mode. In PDT of Photofrin sensitized tissue, we used interstitial light delivery for selective illumination of the malignant tissue. Photodynamically induced damage was found to heal faster and with less scar than the coagulation induced by heat. Thirty-six days after treatment the damaged area had been completely cleared up and replaced by connective scar tissue. However, the presence of apparently therapy resistant cells after PDT may have consequences its clinical application.

In our experimental set-up we used a fixed fiber position and single exposure time for standardized determination of the tissue effects. In the clinical setting, however, repeated exposure and/or step-like movements of the fiber along the tissue surface may be needed to

treat larger tumors. Similarly, a diffusing length of 0.5 cm was chosen to treat tumors with a mean diameter of 5.5 mm. Larger lesions may be produced with a longer diffuser length, higher laser power (thermal therapy), or multiple diffuser implantation. The diffusers can be applied simultaneously from one laser source using a beam splitting device (Steger *et al.*, 1992; Marijnissen *et al.*, 1992). Mathematical models have been developed to predict the insertion place and number of fibers required to treat a certain tissue volume by thermal or photodynamic therapy (Davis *et al.*, 1988; Bolin *et al.*, 1987). Measurements of the fluence rate at the tumor boundary could give an indication of the actual light dose delivered, which allows comparison between different clinical or experimental treatments.

The interstitial techniques may be performed percutaneously on an ambulatory basis. Ultrasound scanning can be used to position the fiber correctly within the tumor and monitor the development of thermal necrosis in real time and through the subsequent period of healing (Steger *et al.*, 1989, 1992; Dachman *et al.*, 1990). Metastases previously inaccessible for surgery may be treated intraoperatively under ultrasound guidance. It has to be noted, that the introduction of interstitial laser probes may predispose to infection in the induced necrosis. Thus, antibiotic prophylaxis and monitoring for infection are probably required (Schneider, 1992). A recent article reports on a case where a subcutaneous metastasis developed at the site of a percutaneous needle puncture for biopsy of suspicious liver metastasis of colon cancer (Goletti *et al.*, 1992). There are no data available on the chance of tumor spread owing to tissue manipulation by laser fiber insertion. However, cellular spread as a result of fiber removal will probably not occur, as those tumor cells attached to the diffuser will have received the highest light dose and will therefore be completely destructed.

With the water-jet technique, a zone of steam vacuoles was found at the periphery of the coagulated tumor. The generation of these vacuoles is usually a slow process, however explosive vaporization ("popcorn" effect) may occur). The popcorn effect should always be avoided as the explosion may cause damage to larger vessels or gas emboli. It has to be established whether the water-jet technique can be applied in a laparoscopic procedure, which would have important advantages in palliative therapy. However, a disadvantage of a laparoscopic technique may be the limited accessibility of certain parts of the liver. For intended curation an operative approach may be desirable anyway, as under such circumstances tumor staging and optimal identification of the metastases is of utmost importance (Foster, 1990; Lind *et al.*, 1992). Preoperative radiologic studies can demonstrate the number of metastases and their relation to vascular and ductal structures in the liver. However, tumor spread to the hepatic lymph nodes, or small tumor nodules (<5 mm) within the liver or on the peritoneal surface are below the detection threshold (Sugarbaker, 1990).

PDT has been shown synergistic with hyperthermia (generally 45.5°C for 30 min) delivered either simultaneously or within 30 min of PDT illumination (Matsumoto *et al.*, 1990; Glassberg *et al.*, 1991). Potentiation decreased with increasing time between PDT and heat delivery (Waldow, 1985, 1987). For heat generation, a Neodymium:Yttrium-Aluminum-Garnet (Nd:YAG) laser is very useful, as the light used to activate the photosensitizer (630 nm) and the light used to produce hyperthermia (1,064 nm) can be guided through the same quartz fiber (Mang, 1990). Tumors localized contiguous to major hepatic veins or vena cava

may also be treated by a combination of interstitial Nd:YAG laser coagulation and PDT. Under these circumstances blood flow might hinder adequate heating of the tumor deposit. In combination therapy, however, rapid blood flow may rather confer some protection to the vessel wall.

There will always remain a relatively large group of patients in which curation can not be achieved owing to extrahepatic disease. Curation will also be limited in patients with widespread hepatic metastases. Although it may be theoretically possible to selectively destroy all tumor deposits, therapy is limited by the biological status of the disease (Hughes *et al.*, 1988; Steele & Ravikumar, 1989). In these patients there may be a place for palliation. Palliative treatment should have minimal or no side effects and should preferably be performed on an ambulatory basis (Bengmark, 1989). As laser therapy can be applied percutaneously, it could very well fulfil the demands of such treatment and hospital stay could be substantially reduced (in liver resection post-operative stay averages 10-16 days) (Lind *et al.*, 1992).

Thus, laser therapy could be:

1. An alternative to surgical resection, aiming at curation with less complications.
2. An extension of the therapeutic possibilities for the group of patients not amenable to surgery (i.e., high-risk patients or patients with irresectable metastases).

Several studies have reported the need of a 1 cm resection margin to achieve complete intrahepatic tumor removal (Scheele *et al.* 1990; Cady *et al.*, 1992). It has to be established whether this policy must be adapted to laser therapy. The situation after hepatic resection may differ significantly from local laser destruction. Surgical manipulation may represent an important cause of recurrence following hepatic resection, as was demonstrated in animal experiments (Nishizaki *et al.*, 1990; Mitzutani, 1992). Furthermore, hepatic wedge resection has been found to stimulate experimental tumor formation on the site of trauma (Murthy *et al.*, 1989). A disadvantage of incorporating a rim of normal hepatic tissue could be an increased growth stimulus to possible occult micrometastases (Panis *et al.* 1992; Loizidu *et al.*, 1991; Mitzutani *et al.* 1992). There has been increasing evidence of release of hepatic growth factors following partial hepatectomy that may stimulate liver as well as tumor regeneration (Namieno *et al.*, 1991; Asaga *et al.*, 1991; Loizidu *et al.*, 1991).

There are very few clinical studies on thermal interstitial laser therapy in hepatic tumors (Steger *et al.*, 1989) and none of clinical PDT. We believe that our studies have justified Phase I clinical studies to investigate the feasibility of the laser techniques described in this study.

Summary

PART I GENERAL INTRODUCTION

1. Hepatic Metastases: Aims of the Study

In The Netherlands annually about 7400 new cases of colon and rectum carcinoma are diagnosed; ultimately liver metastases develop in over 50% of patients. Mean survival time in untreated patients with hepatic metastases from colorectal carcinoma is approximately 6 months. Surgical resection is the only curative treatment currently available, leading to 5-year survival rates of 20-40% in selected patients. However, only 10-20% of patients are amenable for surgery and the operative morbidity and mortality rates are relatively high, owing to associated normal tissue damage. These limitations may be overcome by laser therapy, producing localized thermal or photochemical tumor destruction. The studies described in this thesis were all aimed at investigating this proposition.

2. Tumor Model and Parameters for Tissue Damage

A rat tumor model for hepatic metastasis of colon cancer was chosen to investigate the effects of the various treatments under standardized *in vivo* conditions. A piece of syngeneic colon adenocarcinoma CC531 was implanted in the liver of Wag/Rij rats. Laser treatment was performed on day 20 after implantation; at that time the tumor was approximately 6 mm in diameter. The tissue at various periods post-treatment was evaluated by light microscopy. On day 1 and 2 post-treatment liver damage was determined by serum aspartate aminotransferase (ASAT) and alanine aminotransferase (ALAT); liver function was measured by serum antipyrine clearance on day 1 or 2. Complete tumor remission was considered when no vital tumor tissue could be observed by light microscopy on day 36 post-treatment.

PART II THERMAL THERAPY

3. Fundamentals of Laser Medicine

Laser light is generated by a process of light amplification by stimulated emission of radiation. This light has unique properties that enable transmission of high amounts of energy to a narrowly defined location. The first working laser was built in 1960. Shortly thereafter medical applications were explored and currently lasers are used in almost any medical specialty. Biological effects may be thermal, chemical or mechanical. The majority of

medical procedures involve thermal destruction by coagulation ($>60^{\circ}\text{C}$) or tissue ablation ($>300^{\circ}\text{C}$). For a certain tissue type the scattering coefficient (μ_s), absorption coefficient (μ_a) and the average cosine of the scattering angle (anisotropy factor, g) determine light distribution, while thermal diffusion depends on the rate of heat conduction, heat storage and blood perfusion. The laser medium determines the emitted laser wavelength. The most commonly used medical lasers are CO_2 (10,600 nm), Nd:YAG (1,064 nm) and Argon (488/515 nm). The CO_2 laser requires transmission through articulating arms with mirrors, whereas Nd:YAG and Argon can be transmitted through flexible quartz fibers. Important laser parameters are: the contact/noncontact mode, focus mode, output power (W), exposure time (s), temporal mode and delivered energy ($J=W \times s$). The CO_2 lasers are mainly used for high precision tissue ablation; Nd:YAG lasers can coagulate or vaporize larger tissue areas and Argon laser applications involve vascular destruction, based on selective absorption by hemoglobin.

4. Noncontact Nd:YAG Laser Treatment

The noncontact Nd:YAG laser was investigated using a focussing handpiece with either 60, 120, or 180 J at 20 W in pulsed temporal mode (0.5 s exposure, 0.3 s pause). The pulsed temporal mode was used to allow tissue cooling down during the time pauses. To assess the effects upon the tissues three animals were sacrificed immediately after treatment, and 1, 2, 4, and 8 days later. Five different zones could be distinguished of which the maximal depth and width were measured by light microscopy: (1) a superficial crater of ablated tissue covered with (2) a small zone of carbonized tissue, (3) underlain by a thin layer of cavities, (4) a zone of heat coagulation necrosis consisting of elongated, distorted cells with pyknotic nuclei and (5) from days 1 to 8 after treatment a broad surrounding zone of thermally damaged cells. Laser effects could be determined most accurately on days 1 and 2 after treatment. Multiple linear regression analysis indicated a linear relationship between laser energy and depth of tumor damage ($P < 0.01$). However, total in depth tumor destruction was not accomplished. At lower laser energies tissue coagulation was only superficial, whereas at higher energies vaporization and carbonization occurred which precluded light penetration. Tumor destruction was limited to a zone just underneath the dark coloring carbonized tissue. In the succeeding study we therefore investigated the use of superficial water cooling to prevent charring and vaporization.

5. Water-jet-cooled Nd:YAG Laser Coagulation

The water-jet-cooled Nd:YAG laser system consisted of a flexible quartz fiber enclosed within a teflon hose which was clenched to the fiber by an apical metal tip. Through the aperture between the fiber and hose a saline solution was pumped using a roller pump, resulting in a water-jet which transmitted the laser beam beyond the fiber tip with a spot size of 1 mm. The water jet was pointed to the middle of the tumor and laser therapy was performed with 600, 850, 1,200, 1,700 or 2,400 J at a power setting of either 10 or 20 W. Light microscopic examination on day 1 post-treatment showed a lesion of up to 10 mm in diameter without carbonization. The tumor showed characteristic changes of heat coagulation, surrounded by a rim of necrotic liver tissue. At 20 W liver damage was 22% larger than at

10 W ($P=0.0001$). A significant relationship was found between laser energy and liver damage ($P=0.01$), with complete tumor destruction in all animals at 2,400 J. These results suggest that laser energy mainly determines the degree of tissue necrosis, whereas power output mainly determines the size of the lesion. No deterioration in liver function was found. In conclusion, the water-jet-cooled Nd:YAG laser can produce coagulation necrosis of a superficial solid coloncarcinoma combined with minor liver damage.

6. Interstitial Nd:YAG Laser Coagulation

Owing to limited light penetration into the tissue, larger or deep seated hepatic metastases may only be treated by implanting the light delivery fibers directly into the tumor. In previous studies this interstitial Nd:YAG laser therapy had resulted in charring of the bare-tipped laser fiber which reduced the light transmission into the tissue. We therefore developed a cylindrical diffusing fiber-tip with Helioseal[®] as the diffusing coating, to provide for homogeneous light distribution. Interstitial application was investigated at 4 W/cm from the 0.5 cm cylindrical diffuser and either 600, 1,200, 2,400, 3,400, or 4,800 J/cm. Temperature and fluence rate were measured at the tumor boundary. Tumor proliferative activity was assessed by bromodeoxyuridine (BrdU) incorporation. Fluence rate increased during laser treatment up to 170%; mean temperature increased logarithmically to 69.7°C. Light microscopy on day 2 post-treatment showed coagulation necrosis of 7-11 mm without charring. The tumor showed a mixed pattern of coagulated and deliquesced areas surrounded by hepatic necrosis. Lesion size and liver enzymes increased logarithmically with laser energy applied ($P<0.0001$). No deterioration in liver function was found. The histological structures of the coagulated tumor could often still be identified on day 36 post-treatment owing to heat fixation. This coagulated tissue did not label with BrdU, indicating lack of proliferative activity. Best long-term results were obtained at 4,800 J/cm with complete tumor remission in 3 out of 4 animals. The results of this study show the ability of interstitial laser coagulation to cause selective destruction of colonic tumor deposits within the liver.

PART III PHOTODYNAMIC THERAPY

7. Fundamentals of Photodynamic Therapy

Photodynamic therapy (PDT) is a cancer treatment modality based on the accumulation of a photosensitizer with low systemic toxicity in malignant tissue. Subsequent illumination induces a photochemical reaction with singlet oxygen production, resulting in destruction of biomolecules and subcellular organelles. The first full clinical report of PDT dates from 1976. Hematoporphyrin derivative, a complex mixture of porphyrins, was initially used as photosensitizer. An enriched fraction (Photofrin[®]) is now the most commonly used clinical agent. After systemic administration porphyrins bind to albumin and lipoproteins. Accumulation occurs mainly in tumor and organs of the reticuloendothelial system. The light of an argon-dye laser can be tuned to the appropriate wavelength and delivered either superficially, interstitially or intraluminally. Light distribution can be assessed by using a

radiation transport model and tissue optical properties, or direct measurement with light detectors. The effects of PDT depend in a complex way on: (1) characteristics, tissue concentration and localization of the photosensitizer, (2) the target tissue optical properties and oxygenation and (3) activation wavelength, power density and treatment regimen. PDT of hepatic tumors has been restricted by the preferential retention of photosensitizers in liver tissue, causing considerable normal tissue damage at superficial illumination. Our studies were therefore aimed at (1) selective light delivery and (2) selective photosensitizer accumulation.

8. Interstitial Photodynamic Therapy

Interstitial PDT as a means of selective tumor illumination was investigated after photosensitization with Photofrin (5 mg/kg i.v.) 2 days pre-illumination. Tumors were illuminated with 625 nm light, at 200 mW/cm from a 0.5 cm cylindrical diffuser and either 100, 200, 400, 800, or 1,600 J/cm. Control groups received either laser illumination only, Photofrin only or diffuser insertion only. Tissue effects were studied by light microscopy and computer assisted integration of the circumference of damaged areas. Sections on the second day after illumination showed massive tumor necrosis, however, islands of vital tumor cells could often be identified in the damaged areas. The necrotic tumor area was surrounded by a zone of deliquesced liver cells. Tumor and liver necrosis increased with light dose delivered ($P < 0.001$). The entire lesion healed with little scar. Best long-term results were obtained at 800 J/cm with complete tumor remission in 4 out of 6 animals. Despite local illumination, surrounding liver damage occurred at all energies applied. However, liver necrosis was limited to a distinct zone of 2-4 mm width and did not deteriorate liver function as measured by antipyrine clearance. The results of this study show the ability of interstitial PDT to cause major destruction of tumor tissue in the liver combined with minimal liver damage.

9. 5-Aminolevulinic acid-induced Endogenous Photosensitization

Endogenous porphyrins are produced in every cell as precursors of heme in the heme biosynthetic pathway. Previous studies had shown a lower ferrochelatase and higher porphobilinogen deaminase (PBGD) activity in malignant tissues. We therefore considered the possibility of using this varying capacity of tumor to metabolize porphyrins as a means of selective photosensitization. Groups of 3-6 animals each were given 5-aminolevulinic acid (ALA) 2 mg/ml in drinking water from the 8th, 14th or 17th day after intrahepatic tumor implantation. For comparison, 2 other groups received Photofrin either 2.5 or 5 mg/kg i.v. on day 17. On day 19 the livers were removed and porphyrin concentrations measured in normal liver and tumor by solvent extraction and high-performance liquid chromatography. Protoporphyrin accumulated progressively in the tumor with increasing duration of ALA administration, whereas no increase was found in normal liver. After 11 days of ALA the porphyrin concentration ratio between tumor and liver was 4:1. In contrast, after Photofrin, the concentration was higher in normal liver than in the tumor (1:3, tumor:liver). Enzyme measurements showed a 3 fold lower ferrochelatase in tumor compared to liver. In conclusion, oral administration of ALA results in the progressive accumulation of

protoporphyrin (PROTO) in a transplantable colon carcinoma, without accumulation in the surrounding liver tissue. This selective accumulation of porphyrins appears to be due to a relative ferrochelatase deficiency in malignant tissue. ALA administration may be a suitable approach to photosensitizing liver tumors for photodynamic therapy or to early detection of tumors by fluorescence in ultraviolet light.

PART IV PREDICTING LASER-TISSUE INTERACTION

10. Tissue Optical Properties at 633 nm and 1,064 nm

The optical properties of tissue may be used to predict the light distribution in tissue and thereby the effects of PDT or Nd:YAG laser coagulation. Therefore, absorption and scattering coefficients and the anisotropy factor were measured in rat liver and tumor at 632.8 and 1,064 nm. The tumor was implanted subcutaneously in 2 groups of 7 animals. In one group Photofrin was administered (5 mg/kg i.v.) 2 days before determination of optical properties. Two months after implantation, samples were taken from tumor and liver and optical properties determined using indirect methods with two integrating spheres at 632.8 nm (HeNe laser) or 1,064 nm (Nd:YAG laser). The absorption coefficient was larger in liver than in tumor at 632.8 nm ($P < 0.0005$), whereas the scattering coefficient was larger in tumor than in liver at 1064 nm ($P < 0.05$). Addition of Photofrin increased the scattering coefficient in liver and in tumor at both wavelengths and decreased the anisotropy in tumor ($P < 0.025$), suggesting that for modelling the dosimetry of PDT the optical properties of photosensitized tissue should be used.

11. Ultrasonography of Nd:YAG Laser Coagulation

To establish the value of ultrasonography in imaging laser coagulation of tumor and surrounding tissue, we determined the relation between measurements on ultrasound and histology post-laser therapy. Tumors were treated with the water-jet-cooled Nd:YAG laser at 10 W and either 150, 300, 600, 1,200, 1,700, or 2,400 J. Ultrasonography was done just pre- and immediately post-laser treatment. The animals were sacrificed and livers removed for light microscopical evaluation. Depth and width of coagulation were measured directly on ultrasound, and on histological samples by computer-assisted image analysis. Laser treatment did not change the echogenic aspect of the tumor on ultrasound. However, liver damage appeared hypoechoic compared to normal liver. A significant correlation was found between the total size of the lesion on ultrasound and histology ($P = 0.015$, $r = 0.57$ for depth; $P = 0.012$, $r = 0.58$ for width), suggesting that laser induced tumor destruction may be derived from the amount of surrounding hepatic damage on ultrasound.

PART V GENERAL DISCUSSION

12. General Discussion

In our studies, laser therapy has been found to produce discrete tumor necrosis combined with minimal liver damage. In thermal laser therapy we used the Nd:YAG laser for localized superficial or interstitial tumor destruction. To avoid carbonization, which prevents light penetration, a cylindrical diffusing fiber-tip was used in the interstitial application and superficial water-jet cooling in the noncontact laser mode. In PDT of Photofrin sensitized tissue, we used interstitial light delivery for selective illumination of the malignant tissue. Photodynamically induced damage was found to heal faster and with less scar than the coagulation induced by heat. However, the presence of apparently therapy resistant cells after PDT may have consequences its clinical application. ALA induced endogenous photosensitization led to selective accumulation of porphyrins in the malignant tissue. It has to be established whether this strategy can indeed cause effective and more selective photodynamic destruction of intrahepatic tumors. In our experimental set-up we used a fixed fiber position and single exposure time for standardized determination of the tissue effects. In the clinical setting treatment of larger tumors may require repeated exposure and/or step-like movements of the fiber along the tissue surface, higher laser power, longer diffuser length, or multiple diffuser implantation. Techniques to predict laser-tissue interaction, such as modeling the light transport using the optical properties of tissue or determining the extent of the lesion using ultrasonography, may further refine laser therapy. As laser light can be guided through flexible delivery systems, treatment may be performed percutaneously on an ambulatory basis. At the same time, tumors previously inaccessible for surgery may be treated intraoperatively under ultrasound guidance. Thus, laser therapy could be (1) an alternative to current surgical resection, aiming at curation with less complications, or (2) an extension of therapeutic possibilities for the group of patients not amenable to surgery. Moreover, as laser therapy may have limited side effects, it may have a place in palliation of patients in which curation can not be achieved owing to extrahepatic disease. There are very few clinical studies on thermal interstitial laser therapy in hepatic tumors and none of clinical PDT. We believe that our studies have justified Phase I clinical studies to investigate the feasibility of the laser techniques described here.

Samenvatting

DEEL I ALGEMENE INLEIDING

1. Levermetastasen: Doel van de studie

Jaarlijks worden in Nederland ongeveer 7400 nieuwe gevallen van colon- en rectumcarcinoom gediagnostiseerd. Bij 50% van deze patiënten ontstaat in het beloop van de ziekte levermetastasen. De gemiddelde overleving bij onbehandelde patiënten met levermetastasen van colorectale tumoren is ongeveer 6 maanden. Chirurgische resectie is op dit moment de enige curatieve behandeling, met verbetering van de 5 jaars overleving tot 20-40% in een geselecteerde patiëntengroep. Helaas komt slechts 10-20% van de patiënten in aanmerking voor deze therapie en zijn de operatieve morbiditeit en mortaliteit relatief hoog, doordat aanzienlijke schade aan het normale leverweefsel optreedt. Betere resultaten worden daarom verwacht van een behandelingsmodaliteit die de metastase selectief zou kunnen destrueren. Met de laser kan zeer nauwkeurig lichtenergie over gebracht worden op weefsel, waardoor het mogelijk zou kunnen zijn het tumorweefsel selectief thermisch of fotochemisch te vernietigen. De beschreven studies hadden tot doel deze hypothese te toetsen.

2. Tumor Model and Parameters voor Weefselschade

Er werd gebruik gemaakt van een levermetastasemodel in de rat, zodat het effect van de verschillende behandelingen onder gestandaardiseerde *in vivo* condities kon worden onderzocht. Een stukje syngene colon adenocarcinoom CC531 werd geïmplanterd in de lever van Wag/Rij ratten. Laserbehandeling vond plaats op dag 20 na implantatie; de tumor was dan ongeveer 6 mm in diameter. Het effect op het weefsel werd lichtmicroscopisch bestudeerd op verschillende tijdstippen na behandeling. Op dag 1 en 2 na behandeling werd de mate van leverschade bepaald met behulp van serum waarden van de enzymen aspartaat aminotransferase (ASAT) en alanine aminotransferase (ALAT); de leverfunctie werd gemeten door serum antipyrine klaring op dag 1 of 2 na behandeling. Wanneer op dag 36 na behandeling lichtmicroscopisch geen vitaal tumorweefsel werd gevonden, werd gesproken van volledige remissie.

DEEL II THERMISCHE THERAPIE

3. Grondbeginselen van Medische Lasertoepassingen

Laserlicht wordt geproduceerd door gestimuleerde emissie en versterking van licht: "*light amplification by stimulated emission of radiation*". Dit licht heeft unieke eigenschappen, waardoor een nauw omschreven hoeveelheid energie kan worden overgebracht op het weefsel. De eerste operationele laser werd gebouwd in 1960. Kort daarna werden medische toepassingen onderzocht en op dit moment wordt de laser in bijna alle medische specialismen gebruikt. De effecten op het weefsel kunnen thermisch, chemisch, of mechanisch zijn. De meeste medische lasertoepassingen maken gebruik van thermische destructie door weefselcoagulatie ($>60^{\circ}\text{C}$) of ablatie ($>300^{\circ}\text{C}$). Voor een bepaald soort weefsel bepalen de verstrooiingscoëfficiënt (μ_s), absorptiecoëfficiënt (μ_a) en gemiddelde cosinus van de hoek van verstrooiing (anisotropiefactor, g) de verdeling van het licht in het weefsel; de warmte diffusie is afhankelijk van warmtegeleiding, warmteopslag capaciteit en bloedperfusie. Het lasermedium bepaalt de golflengte van het uitgezonden licht. De meest gebruikte medische lasers zijn de CO_2 (10.600 nm), Nd:YAG (1.064 nm) en Argon (488/515 nm). Het CO_2 laserlicht kan alleen door starre buizen met spiegels worden voortgeleid, terwijl Nd:YAG- en Argonlicht door flexibele quartzfibers kan worden gestuurd. Belangrijke laserparameters zijn: de contact/noncontactmodus, focusmodus, uitgangsvermogen (W), belichtingstijd (s), tijdsmodus en totaal geleverde energie ($J=W \times s$). De Argonlaser wordt voornamelijk gebruikt voor destructie van vasculaire structuren, aangezien Argonlicht sterk wordt geabsorbeerd door hemoglobine. De CO_2 lasers worden voornamelijk gebruikt voor nauwkeurige weefselablatie, terwijl Nd:YAG lasers meer geschikt zijn voor coagulatie of evaporisatie van grotere weefseldelen. Aangezien oppervlakkige ablatie van levertumoren had geleid tot sterke bloeding van het leverweefsel, was ons doel het tumorweefsel met de Nd:YAG laser selectief te coaguleren.

4. Noncontact Nd:YAG Laser Behandeling

De noncontact Nd:YAG laser werd onderzocht in combinatie met een focuserend handstuk. Energieën van 60, 120, of 180 J werden toegediend bij een uitgangsvermogen van 20 W in de gepulste tijdsmodus (0,5 s belichting / 0,3 s pauze). De gepulste modus werd gebruikt met als doel het weefsel de gelegenheid te geven af te koelen in de pauzes tussen de laserpulsen. Om het effect op het weefsel te bepalen, werden de lesies bestudeerd onmiddellijk na behandeling, en 1, 2, 4, en 8 dagen later. De weefselschade kon worden onderverdeeld in vijf verschillende zones, waarvan de maximale diepte en breedte lichtmicroscopisch werd gemeten: (1) een oppervlakkige krater van geableerd weefsel bedekt met (2) een dunne laag gecarboniseerd weefsel, (3) daaronder een laag met kleine holtes, (4) een zone van coagulatieneecrose bestaande uit lange, vervormde cellen met pyknotische kernen, en (5) vanaf dag 1-8 na behandeling een brede aangrenzende zone met thermisch beschadigde cellen. De lasereffecten konden het nauwkeurigst worden bepaald op dag 1 en 2 na behandeling. Multiple lineaire regressie-analyse liet een lineaire relatie zien tussen toegediende laserenergie en diepte van tumorschade ($P < 0,01$). Totale tumordestructie werd echter niet bereikt. Bij lagere laserenergieën ontstond alleen oppervlakkige coagulatie, terwijl

bij hogere energieën evaporisatie en carbonisatie ontstond, met als gevolg een verminderde transmissie van licht door het weefsel. De tumorschade was daardoor beperkt tot een smalle laag onder het gecarboniseerde weefsel. In de volgende studie werd daarom onderzocht of oppervlakkige waterkoeling deze carbonisatie en evaporisatie zou kunnen voorkomen.

5. Water-straal-gekoelde Nd:YAG Laser Coagulatie

Het water-straal-gekoelde Nd:YAG lasersysteem bestond uit een flexibele quartzfiber in een teflonslang die aan de fiber was bevestigd met een apicale metalen tip. Door de ruimte tussen slang en fiber werd een zoutoplossing gepompt met een rollerpomp. Hierdoor ontstond een waterstraal met een diameter van ongeveer 1 mm, die het laserlicht verder voortgeleidde vanaf de fibertip. De waterstraal werd gericht op het midden van de tumor en laserbehandeling werd uitgevoerd met energieën van 600, 850, 1.200, 1.700 of 2.400 J bij een uitgangsvermogen van 10 of 20 W. Lichtmicroscopisch werd op dag 1 na behandeling een lesie van maximaal 10 mm gevonden zonder enige carbonisatie. Het tumorweefsel was gecoaguleerd met karakteristieke histologische veranderingen, omgeven door een rand van necrotisch leverweefsel. Bij 20 W werd 22% meer leverschade gevonden dan bij 10 W ($P=0,0001$). Een significante relatie werd gevonden tussen toegediende laserenergie en leverschade ($P=0,01$), met complete remissie in alle dieren behandeld met 2.400 J. Deze resultaten geven aan dat de laserenergie voornamelijk de mate van necrose bepaalt, terwijl het uitgangsvermogen van de laser voornamelijk de grootte van de lesie bepaalt. Veranderingen in leverfunctie werden niet gevonden. Concluderend kan worden gesteld dat de water-straal-gekoelde Nd:YAG laser in staat is oppervlakkig solide tumorweefsel selectief te coaguleren, zonder veel schade aan het omliggende leverweefsel.

6. Interstitiële Nd:YAG Laser Coagulatie

Door de beperkte penetratie van laserlicht in het weefsel, zijn grotere of diep gelegen tumoren waarschijnlijk alleen te behandelen door de laser fiber(s) direct in het tumor weefsel te implanteren (interstitiële therapie). Andere auteurs vonden met deze techniek een sterke carbonisatie aan het kale fiberruiteinde, waardoor de transmissie van licht naar het weefsel aanzienlijk werd beperkt. Daarom ontwikkelden wij een cilindrisch verstrooiend fiberruiteinde, met Helioseal® als verstrooiende bekleding, om zo een homogene lichtverdeling in het weefsel te verkrijgen. De interstitiële therapie werd onderzocht bij 4 W/cm uit de 0,5 cm lange cilindrische verstrooier en 600, 1.200, 2.400, 3.400, of 4.800 J/cm. Temperatuur en lichtintensiteit werden gemeten aan de tumorrand. Informatie over de mate van tumorproliferatie werd verkregen door bromodeoxyuridine (BrdU) incorporatie. De lichtintensiteit nam toe gedurende behandeling tot een maximum van 170%; de gemiddelde temperatuur nam logaritmisches toe tot 69,7°C. Lichtmicroscopie op dag 2 na behandeling liet coagulatieneecrose zien van 7-11 mm in diameter zonder enige carbonisatie. De tumorneecrose bestond uit gebieden met coagulatie- en colliquatieneecrose, omgeven door een zone van leverschade. De grootte van de lesie nam logaritmisches toe met de toegediende energie, wat werd bevestigd door de serumwaarden van de leverenzymen ($P<0,0001$). Veranderingen in leverfunctie werden niet gevonden. Het gecoaguleerde tumorweefsel kon vaak 36 dagen na behandeling nog worden gevonden als gevolg van hittefixatie. Dit gecoaguleerde materiaal

kleurde immunocytochemisch niet aan na incubatie met BrdU, wat wijst op afwezigheid van enige tumorcelproliferatie. De beste lange-termijn-resultaten werden gevonden na 4.800 J/cm, met complete tumorremissie in 3 van de 4 behandelde dieren. Deze studie laat zien dat interstitiële Nd:YAG laserbehandeling selectieve tumordestructie kan veroorzaken.

DEEL III PHOTODYNAMISCHE THERAPIE

7. Grondbeginselen van Photodynamische Therapie

Photodynamische therapie (PDT) is een behandelingsmodaliteit die is gebaseerd op de ophoping van een fotogevoelige stof met lage systemische toxiciteit in maligne weefsel. Daaropvolgende belichting induceert een fotochemische reactie waarbij enkelvoudige zuurstof ontstaat, die zorgt voor schade aan biomoleculen en celorganellen. De eerste klinische studie is uit 1976. Hematoporfyrinederivaat, een complex mengsel van porfyrynes, werd in eerste instantie gebruikt als fotogevoelige stof. Op dit moment is Photofrin[®], een verrijkte actieve vorm, de meest gebruikte klinische stof. Na systemische toediening binden de porfyrynes aan albumine en lipoproteïnen. Accumulatie vindt voornamelijk plaats in maligne weefsel en organen van het reticuloendotheliale systeem. Het licht van de Argon-dye laser kan worden afgesteld op de geschikte golflengte, waarna oppervlakkig, interstitieel of intraluminaal kan worden belicht. De lichtverdeling in het weefsel kan worden voorspeld met een stralingstransportmodel indien de optische eigenschappen van het weefsel bekend zijn, of door directe metingen met lichtdetectoren. De effecten van PDT zijn de complexe resultante van: (1) de eigenschappen, weefselconcentratie en lokalisatie van de fotogevoelige stof, (2) de optische eigenschappen en oxygenatie van het behandelde weefsel, en (3) golflengte van het activerende licht, uitgangsvermogen en behandelingsschema. De toepassing van PDT in levertumoren werd altijd beperkt door de sterke ophoping van fotogevoelige stoffen in het leverweefsel waardoor aanzienlijke leverschade ontstaat bij oppervlakkige tumorbelichting. Ons onderzoek was daarom gericht op: (1) selectieve tumorbelichting, en (2) selectieve ophoping van de fotogevoelige stof in de tumor.

8. Interstitiële Photodynamische Therapie

Interstitiële belichting werd gebruikt als een manier van selectieve belichting van het tumorweefsel na fotosensibilisatie met Photofrin (5 mg/kg i.v.), 2 dagen vóór behandeling. De tumoren werden belicht met licht van 625 nm, bij 200 mW/cm uit een 0,5 cm lang cilindrisch verstrooiend fiberuiteinde en 100, 200, 400, 800, of 1.600 J/cm. Controlegroepen werden behandeld met of alleen laserbelichting, of alleen Photofrin, of alleen fiberinsertie. De weefseffecten werden bestudeerd met behulp van lichtmicroscopie en computerintegratie van de omtrek van de aangedane gebieden. Op dag 2 na belichting werd forse tumornecrose gevonden, echter eilandjes van vitale tumorcellen waren vaak nog aanwezig in het beschadigde weefsel. Dit necrotische gebied werd omringd door een zone van levercolliquatienecrose. Tumor- en levernecrose namen toe met de toegediende lichtdosis ($P < 0,001$). De totale lesie genas zonder veel littekenvorming. De beste lange-termijn-resultaten werden gevonden na 800 J/cm met complete tumorremissie in 4 van de 6

behandelde dieren. Ondanks de lokale belichting, werd omringende levernecrose gevonden bij alle toegediende energieën. Deze leverschade was echter beperkt tot een nauwomschreven zone van 2-4 mm breed en had geen effect op de leverfunctie gemeten met antipyrineklaring. De resultaten van deze studie geven aan dat interstitiële PDT in staat is belangrijke tumorschade te induceren zonder grote schade aan het omliggende leverweefsel.

9. 5-Aminolevulinezuur-geïnduceerde Endogene Fotosensibilisatie

Endogene porfyrynes worden in iedere cel geproduceerd als voorlopers van heem. Andere auteurs hadden aangetoond dat er mogelijk een lagere ferrochelatase en hogere porfobilinogeen deaminase (PBGD) activiteit zou kunnen bestaan in maligne weefsel. Dit verschil in vermogen om porfyrynes te metaboliseren zou kunnen worden gebruikt om weefsel endogeen te fotosensibiliseren. Om dit te onderzoeken werd aan groepen van 3-6 dieren 5-aminolevulinezuur (ALA) in een concentratie van 2 mg/ml in drinkwater toegediend van de 8e, 14e, of 17e dag na tumorimplantatie. Ter vergelijking werd aan 2 andere groepen Photofrin toegediend in een dosis van 2.5 of 5 mg/kg i.v. op dag 17. Op dag 19 werd de porfyryneconcentratie gemeten in lever en tumor door extractie en high pressure liquid chromatography (HPLC). Protoporfyryne bleek in toenemende mate op te hopen in de tumor gedurende ALA toediening, terwijl geen toename werd gevonden in de lever. Na 11 dagen ALA per os was de porfyryneconcentratieverhouding tussen tumor en lever 4:1. Daarentegen werd na Photofrin een hogere porfyryne concentratie in de lever gevonden dan in de tumor (1:3, tumor:lever). Enzymmetingen lieten een 3 voudige lagere ferrochelataseactiviteit zien in tumor ten opzichte van lever. Concluderend, resulteert de orale toediening van ALA in een toenemende protoporfyryne (PROTO) concentratie in het transplanteerbare coloncarcinoom, zonder ophoping in het omliggende leverweefsel. Deze selectieve porfyryne-ophoping ontstaat waarschijnlijk door een relatieve ferrochelatasedeficiëntie in maligne weefsel. Toediening van ALA zou een selectieve manier van fotosensibilisatie van levertumoren kunnen zijn voor PDT. Bovendien zou de ophoping van porfyrynes vroege detectie van tumoren mogelijk kunnen maken door fluorescentie onder belichting met ultraviolet licht.

DEEL IV VOORSPELLEN VAN LASER-WEFSEL INTERACTIE

10. Optische Eigenschappen van Weefsel bij 633 nm en 1.064 nm

De optische eigenschappen van weefsel kunnen worden gebruikt om de lichtverdeling in het weefsel te voorspellen en daarmee de effecten van PDT of thermische Nd:YAG lasercoagulatie. Om die reden werd de absorptie- en verstrooiingscoëfficiënt en de anisotropiefactor gemeten in het lever- en tumorweefsel bij 632,8 and 1.064 nm. De tumor werd subcutaan geïmplantieerd in 2 groepen van ieder 7 dieren. In één van beide groepen werd Photofrin toegediend (5 mg/kg i.v.) 2 dagen vóór bepaling van de optische eigenschappen. Twee maanden na implantatie werden coupes gesneden van tumor en lever en werden de optische eigenschappen bepaald met een indirecte methode tussen twee integrerende bollen bij 632,8 nm (HeNe laser) of 1.064 nm (Nd:YAG laser). De absorptiecoëfficiënt was groter in lever dan in tumor bij 632,8 nm ($P < 0,0005$), terwijl de

verstrooiingscoëfficiënt groter was in tumor dan in lever bij 1.064 nm ($P < 0,05$). Voorafgaande toediening van Photofrin zorgde bij beide golflengten voor een toename in verstrooiing in zowel tumor als lever en een afname in anisotropie in tumor ($P < 0,025$). Hieruit blijkt dat voor de bepaling van lichtdistributie bij PDT, de optische eigenschappen van gefotosensibiliseerd weefsel moeten worden gebruikt.

11. Echografie van Nd:YAG Laser Coagulatie

Om te bepalen of lasercoagulatie van tumor en omgeven leverweefsel zichtbaar gemaakt kan worden met echografie, werd de relatie bepaald tussen metingen van de lesies op echo en histologie na laserbehandeling. De tumoren werden behandeld met de water-straal-gekoelde Nd:YAG laser bij 10 W en 150, 300, 600, 1.200, 1.700, of 2.400 J. Echografie werd net vóór- en meteen na laserbehandeling verricht. Hierna werden de dieren opgeofferd en werden de levers verwijderd voor lichtmicroscopische evaluatie. De diepte en breedte van de coagulatie werden meteen op de echo gemeten en op histologie met behulp van computerbeeldanalyse. Het echogene aspect van de tumor op de echografie veranderde niet na laserbehandeling. Leverschade, daarentegen was echoarm in vergelijking tot normaal leverweefsel. De grootte van de totale lesie op echo was significant gerelateerd aan die op histologie ($P = 0,015$, $r = 0,57$ voor diepte; $P = 0,012$, $r = 0,58$ voor breedte), suggererend dat de laser-geïnduceerde tumorschade zou kunnen worden afgeleid aan de hoeveelheid omringende leverschade op echografie.

DEEL V ALGEMENE DISCUSSIE

12. Algemene Discussie

De beschreven studies laten zien dat de laser nauw omschreven tumorschade kan induceren met minimale omliggende leverschade. Bij thermische therapie werd gebruik gemaakt van de Nd:YAG laser om de tumor lokaal superficiaal of intersitiëel te destrueren. Om carbonisatie te voorkomen, wat lichtpenetratie verhindert, werd een cilindrisch verstrooiend fiberuiteinde gebruikt voor de interstitiële toepassing en oppervlakkige waterstraalkoeling in de noncontact modus. Bij PDT van Photofrin gesensitiseerd weefsel werd de interstitiële toediening gebruikt voor selectieve tumorbelichting. Photodynamisch geïnduceerde schade heelde sneller met minder littekenweefsel dan de hittecoagulatie, maar de aanwezigheid van mogelijk therapiebestendige cellen na PDT kan consequenties hebben voor de klinische toepassingsmogelijkheden. ALA- geïnduceerde endogene photosensibilisatie leidde tot selectieve accumulatie van porfyrynes in het maligne weefsel. Verder onderzoek zal moeten aantonen of met deze methode inderdaad effectieve en selectievere photodynamische schade kan worden veroorzaakt. Bij de experimenten hebben wij gebruik gemaakt van een gefixeerde fiberpositie en eenmalige belichting om de weefseffecten gestandaardiseerd te kunnen bepalen. Behandeling van grotere tumoren in de klinische situatie vereist echter aanpassingen zoals meerdere belichtingen en/of stapsgewijs bewegen van de fiber over het weefseloppervlak, hogere uitgangsvermogens (thermische therapie), langere lengte van het verstrooiende fiberuiteinde, of multiple fiber implantatie. Technieken die laser-weefsel-

interactie kunnen voorspellen, zoals stralingstransportmodellen (m.b.v. de optische eigenschappen van weefsel) of echografie, zouden laserbehandeling verder kunnen verfijnen. Aangezien laserlicht door flexibele fibers kan worden gestuurd, behoort percutane behandeling, eventueel op poliklinische basis, tot de mogelijkheden. Bovendien zouden chirurgisch moeilijk bereikbare of onbehandelbare tumoren peroperatief kunnen worden behandeld onder echografische controle. Laserbehandeling zou dus: (1) een alternatief kunnen zijn voor huidige chirurgische resectie, daarbij strevend naar curatie met minder operatieve complicaties, of (2) een uitbreiding van de therapeutische mogelijkheden in de groep patiënten die niet in aanmerking komt voor chirurgische therapie. Aangezien lasertherapie waarschijnlijk een minimale belasting betekent voor de patiënt, is palliatieve behandeling bij patiënten met extrahepatische metastasen wellicht ook mogelijk. Op dit moment is er nog zeer weinig ervaring met klinische toepassing van interstitiële thermische therapie in intrahepatische tumoren en nog totaal geen ervaring met PDT in de lever. Wij menen dat ons onderzoek Fase I klinische studies heeft gerechtvaardigd, om de toepasbaarheid van de hier beschreven lasertechnieken te bepalen.

References

- ABSTEN GT. The Neodymium: Yttrium Aluminum Garnet (Nd:YAG) laser. *Biomed Instrumen Technol* 1990; 24: 10-18.
- ABSTEN GT. Physics and lasers. *Obstet Gynecol Clin N Am* 1991; 18: 407-427.
- ACKERMAN NB, JACOBS R, BLOOM ND, POON TT. Increased capillary flow in intrahepatic tumors due to α -adrenergic effects of catecholamines. *Cancer* 1988; 61: 1550-1554.
- ALLISON DJ, BOOTH A. Arterial embolization in the management of liver metastases. *Cardiovasc Intervent Radiol* 1990; 13: 161-168.
- ANDERSON JH, GOLDBERG JA, BESSANT RG, KERR DJ, MCKILLOP JH, STEWART I, COOKE TG, MCARDLE CS. Glas Yttrium-90 microspheres for patients with colorectal liver metastases. *Radiother Oncol* 1992; 25: 137-139.
- ANDERSON RL & KAPP DS. Hyperthermia in cancer therapy: Current status. *Med J Aus* 1990; 152: 310-315.
- ANDREASEN PB, RANEK L, STATLAND BE, TYGSTRUP N. Clearance of antipyrine: Dependence of quantitative liver function. *Eur J Clin Invest* 1974; 4: 129-134.
- ANDREOLA S, BERTONI A, MARCHESINI R, MELLONI E. Evaluation of optical characteristics of different human tissues in vitro (abstr.). *Lasers Surg Med* 1988; 8: 142.
- ANZAI Y, LUFKIN RB, SAXTON RE, FETTERMAN H, FARAHANI K, LAYFIELD LJ, JOLESZ FC, HANAFEE WH. Nd:YAG interstitial laser phototherapy guided by magnetic resonance imaging in an ex vivo model: Dosimetry of laser-MR-tissue interaction. *Laryngoscope* 1991; 101: 755-760.
- ARNFIELD M, GONZALEZ S, LEA P, TULIP J, MCPHEE M. Cylindrical irradiation fibre tip for photodynamic therapy. *Lasers Surg Med* 1986; 6: 150-154.
- ARNFIELD MR, TULIP J, MCPHEE MS. Optical propagation in tissue with anisotropic scattering. *IEEE Trans Biomed Eng* 1988; 35: 372-381.
- ARNFIELD MR, TULIP T, CHETNER M, MCPHEE MS. Optical dosimetry for interstitial photodynamic therapy. *Med Phys* 1989; 16: 602-608.
- ATHAR MCA, ELMETS CA, BICKERS DR, MUKHTAR H. A novel mechanism for the generation of superoxide anions in hematoporphyrin derivative-mediated cutaneous photosensitization: Activation of the xanthine oxidase pathway. *J Clin Invest* 1989; 83: 1137-1143.
- AULER HL & BANZER G. Untersuchungen über die Rolle der Porphyrine bei geschwulstkranken Menschen und Tieren. *Z Krebsforsch* 1942; 53: 65-68.
- BAGGISH MS. High-power-density carbon dioxide laser therapy for early cervical neoplasia. *Am J Obstet Gynecol* 1980a; 136: 117-125.
- BAGGISH MS. Carbon dioxide laser treatment for condylomata acuminata venereal infections. *Obstet Gynecol* 1980b; 55: 711-715.

- BALCHUM OJ & DOIRON DR. Photoradiation therapy of endobronchial lung cancer: Large obstructing tumours, nonobstructing tumours and early stage bronchial cancer lesions. *Clin Chest Med* 1985; 6: 255-275.
- BALLANTYNE GH & QUIN J. Surgical treatment of liver metastases in patients with colorectal cancer. *Cancer* 1993; 71 (Suppl): 4252-4266.
- BASFORD JR. Low-energy laser therapy: Controversies and new research findings. *Lasers Surg Med* 1989; 9: 1-5.
- BASOV NG & PROKHOROV AM. Possible methods for obtaining active molecules for a molecular generator. *J Exp Theoret Phys USSR* 1955; 28: 249.
- BAYLEY GG & NEEDHAM LL. Simultaneous quantification of erythrocyte zinc protoporphyrin and protoporphyrin IX by liquid chromatography. *Clin Chem* 1986; 32: 2137-2142.
- BEDWELL J, MACROBERT AJ, PHILLIPS D, BOWN SG. Fluorescence distribution and photodynamic effect of ALA-induced PP IX in the DMH rat colonic tumour model. *Br J Cancer* 1992; 65: 818-824.
- BEEMS EM, DUBBELMAN TMAR, LUGTENBURG J, VAN BEST JA, SMEETS MFMA, BOEGHEIM JPJ. Photosensitizing properties of bacteriochlorophyllin-a and bacteriochlorin-a, two derivatives of bacteriochlorophyll-a. *Photochem Photobiol* 1987; 46: 639-643.
- BEISLAND HO & KVERNEBO K. The microcirculation in Neodymium-YAG laser irradiated and in electrocoagulated urinary bladder tumors evaluated with laser Doppler flowmetry. *Urol Res* 1986; 14: 149-152.
- BÉLANGER PM, DORÉ F, LABRECQUE G. Monthly variations in the clearance of antipyrine in the rat. *Res Commun Chem Path Pharmacol* 1984; 46: 53-65.
- BELLINA JH. Gynecology applications of the laser. *Contemp Gynecol Obstet* 1974; 4: 24-34.
- BELLNIER DA, HO YK, PANDEY RK, MISSERT JR, DOUGHERTY TJ. Distribution and elimination of Photofrin II in mice. *Photochem Photobiol* 1989; 50: 221-228.
- BEN-HUR E & ROSENTHAL I. The phthalocyanines: A new class of mammalian cells photosensitizers with a potential for cancer phototherapy. *Int J Radiat Biol* 1985; 47: 145-147.
- BENDEREV TV, CHMIEL JS, CARONE FA, SCHAEFFER AJ. Dosimetry study of Nd:YAG laser damage to canine renal cortex. *Lasers Surg Med* 1987; 7: 363-369.
- BENGMARK S, JEPPSSON B, LUNDERQUIST A, TRANBERG KG, PERSSON B. Tumour calcification following repeated hepatic dearterialization in patients: A preliminary communication. *Br J Surg* 1988; 75: 525-526.
- BENGMARK S. Palliative treatment of hepatic tumours. *Br J Surg* 1989; 76: 771-773.
- BENGMARK S & HALFSTROM L. The natural history of primary and secondary malignant tumors of the liver I: The prognosis for patients with hepatic metastases from colonic and rectal carcinoma by laparotomy. *Cancer* 1969; 23: 198-202.
- BETTAG M, ULRICH F, SCHOBEL R, FÜRST G, LANGEN KJ, SABEL M, KIWI JCW. Stereotactic laser therapy in cerebral gliomas. *Acta Neurochir* 1991; 52 (Suppl): 81-83.
- BLASCHKE TF. Protein binding and kinetics of drugs in liver diseases. *Clin Pharmacokinet* 1977; 2: 32-44.
- BLUMGART LH & ALLISON DJ. Resection and embolization in the management of secondary hepatic tumors. *World J Surg* 1982; 6: 32-45.
- BOLIN FP, PREUSS LE, TAYLOR RC. Optimization of photodynamic therapy light dose distribution and treatment volume by multi-fiber insertions. *Photochem Photobiol* 1987; 46: 609-617.

- BONNET R & BERENBAUM M. Porphyrins as photosensitizers. *Ciba Found Symp* 1989; 146: 40-59.
- BORNER M, CASTIGLIONE M, TRILLER J, BAER HU, SOUCEK M, BLUMGART L, BRUNNER K. Considerable side effects of chemoembolization for colorectal carcinoma metastatic to the liver. *Ann Oncol* 1992; 3: 113-115.
- BOSMAN S, PHOA SSK, BOSMA A, VAN GEMERT MJC. Effect of percutaneous interstitial thermal laser on normal liver of pigs: Sonographic and histopathological correlations. *Br J Surg* 1991; 78: 572-575.
- BOULNOIS JL. Photophysical processes in recent medical laser developments: A review. *Lasers Med Sci* 1986; 1: 47-66.
- BOWN SG. Phototherapy of tumors. *World J Surg* 1983; 7: 700-709.
- BOWN SG, TRALAU CJ, COLERIDGE-SMITH PD, AKDEMIR D, WIEMAN TJ. Photodynamic therapy with porphyrin and phthalocyanine sensitisation: Quantitative studies in normal rat liver. *Br J Cancer* 1986; 54: 43-52.
- BOYLE DG & POTTER WR. Photobleaching of Photofrin II as a means of eliminating skin photosensitivity. *Photochem Photobiol* 1987; 46: 997-1001.
- BRACKETT KA, SANKAR MY, JOFFE SN. Effects of Nd: YAG laser photoradiation on intra-abdominal tissues: A histological study of tissue damage versus power density applied. *Lasers Surg Med* 1986; 6: 123-130.
- BRASSEUR N, HASRAT A, LANGLOIS, WAGNER JR, ROUSSEAU J, VAN LIER JE. Biological activities of phthalocyanines: Photodynamic therapy of EMT-6 mammary tumors in mice with sulfonated phthalocyanines. *Photochem Photobiol* 1987; 45: 581-586.
- BREEDIS C & YOUNG G. The blood supply of neoplasma in the liver. *Am J Pathol* 1954; 30: 369-377.
- BUETTNER GR & NEED MJ. Hydrogen peroxide and hydroxyl free radical production by hematoporphyrin derivative, ascorbate and light. *Cancer Lett* 1985; 25: 297-304.
- BUGELSKI PJ, PORTER CW, DOUGHERTY TJ. Autoradiographic distribution of hematoporphyrin derivative in normal and tumor tissue of the mouse. *Cancer Res* 1981; 41: 4606-4612.
- BYCZKOWSKI JZ & GESSNER T. Biological role of superoxide ion-radical. *Int J Biochem* 1988; 20: 569-580.
- CADY B. Natural history of primary and secondary tumors of the liver. *Semin Oncol* 1983; 10: 127-133.
- CADY B, STONE MD, McDERMOTT WV, JENKINS RL, BOTHE A, LAVIN PT, LOVETT EJ, STEELE GD. Technical and biological factors in disease-free survival after hepatic resection for colorectal cancer metastases. *Arch Surg* 1992; 127: 561-569.
- CASTRÉN-PERSONS M, LIPASTI J, PUOLAKKAINEN P, SCHRÖDER T. Laser-induced hyperthermia: Comparison of two different methods. *Lasers Surg Med* 1992; 12: 665-668.
- CASTRO DJ, ABERGEL RP, MEEKER C, DWYER RM, LESAVOY MA, UITTO J. Effects of the Nd:YAG laser on DNA synthesis and collagen production in human skin fibroblast cultures. *Ann Plast Surg* 1983; 11: 214-222.
- CHAPMAN JD, STOBBE CC, ARNFIELD MR, SANTUS JL, MCPHEE MS. Oxygen dependency of tumor cell killing in vitro by light-activated Photofrin II. *Radiat Res* 1991; 126: 73-79.
- CHARNLEY RM, MORRIS DL, DENNISON AR, AMAR SS, HARDCASTLE JD. Detection of colorectal liver metastases using intraoperative ultrasonography. *Br J Surg* 1991; 78: 45-48.

- CHARNLEY RM, DORAN J, MORRIS DL. Cryotherapy for liver metastases: A new approach. *Br J Surg* 1989; 76: 1040-1041.
- CHEMALY P jr. Phase III trials of photodynamic therapy now under way. *J Natl Cancer Inst* 1989; 81: 975-976.
- CHEONG WF, PRAHL SA, WELCH AJ. A review of optical properties of biological tissues. *IEEE J Quant Elect* 1990; 26: 2166-2185.
- CHEVINSKI AH & MINTON JP. Ablation of recurrent and metastatic intraabdominal tumor with the CO₂ laser. *Lasers Surg Med* 1990; 10: 5-11.
- COLE DJ, FERGUSON CM. Complications of hepatic resection for colorectal carcinoma metastases. *Am Surgeon* 1992; 58: 88-91.
- CORSON SL, UNGER M, KWA D, BATZER FR, GOCIAL B. Laparoscopic laser treatment of endometriosis with the Nd:YAG sapphire probe. *Am J Obstet Gynecol* 1989; 160: 718-723.
- COTLIAR AM, SCHUBERT HD, MANDEL ER, TROKEL SL. Excimer laser radial keratotomy. *Ophthalmology* 1985; 92: 206-208.
- COWLED PA & FORBES IJ. Modification by vasoactive drugs of tumor destruction by photodynamic therapy with hematoporphyrin derivative. *Br J Cancer* 1989; 59: 904-909.
- COZZANI I, JORI G, REDDI E, TOMIO L, ZORAT PL, SICURO T, MALVALDI G. Interaction of free and liposome-bound porphyrins with normal and malignant cells: Biochemical and photosensitization studies in vitro and in vivo. In: *Porphyrins in tumour therapy*, Andreoni A & Cubbedu R (eds). Plenum Press, New York & London. 1984: 157-165.
- DACHMAN AH, MCGEEHEE JA, BEAM TE, BURRIS JA, POWELL DA. US-guided percutaneous laser ablation of liver tissue in a chronic pig model. *Radiology* 1990; 176: 129-133.
- DAIKUZONO N, SUZUKI S, TAJIRI H, TSUNEKAWA H, OHYAMA M, JOFFE SN. Laser thermia: A new computer-controlled contact Nd:YAG system for interstitial local hyperthermia. *Lasers Surg Med* 1988; 8: 254-258.
- DAILEY HA & SMITH A. Differential interaction of porphyrins used in photoradiation therapy with ferrochelatase. *Biochem J* 1984; 223: 441-445.
- DAVIS M, DOWDEN J, STEGER A, KAPADIA P, WHITING P. A mathematical model for interstitial laser treatment of tumours using four fibres. *Lasers Med Sci* 1988; 4: 41-53.
- DE JONG KP, TERPSTRA OT, BLANKENSTEIJN JD, LAMÉRIS JS. Intraoperative ultrasonography and ultrasonic dissection in liver surgery. *Am J Gastroenterol* 1989; 84: 933-936.
- DELORME S, VAN KAICK G. Sonographie fokaler Leberveränderungen: Praktische Hinweise Für die Differential diagnostik. *Radiologe* 1992; 32: 198-206.
- DERBYSHIRE GJ, BOGEN DK, UNGER M. Thermally induced optical property changes in myocardium at 1.06 μm . *Lasers Surg Med* 1990; 10: 28-34.
- D'HALLEWIN MA, BAERT L, MARIJNISSEN JP, STAR WM. Whole bladder wall photodynamic therapy with in situ light dosimetry for carcinoma in situ of the bladder. *J Urol* 1992; 148: 1152-1155.
- DIAMOND I, GRANELLI SG, McDONAGH AF, NIELSEN S, WILSON CB, JAENICKE R. Photodynamic therapy of malignant tumors. *Lancet* 1972; 2: 1175-1177.
- DIVARIS DXG, KENNEDY JC, POTTIER RH. Phototoxic damage to sebaceous glands and hair follicles of mice after systemic administration of 5-aminolevulinic acid correlates with localized protoporphyrin IX fluorescence. *Am J Pathol* 1990; 136: 891-897.
- DIXON JA. Current laser applications in general surgery. *Ann Surg* 1988; 207: 355-372.
- DODD NJ, MOORE JV, POPPITT DG, WOOD B. In vivo magnetic resonance imaging of the effects of photodynamic therapy. *Br J Cancer* 1989; 60: 164-167.

- DOIRON DR, SVAASAND LO, PROFIO AE. Light dosimetry in tissue: Application to photoradiation therapy. *Adv Exp Med Biol* 1983; 160: 63-76.
- DOUGHERTY TJ, GRINDEY GB, FIEL R, WEISHAUP KR BOYLE DG. Photoradiation therapy II: Cure of animal tumors with hematoporphyrin and light. *J Natl Cancer Inst* 1975; 55: 115-121.
- DOUGHERTY TJ, THOMA RE, BOYLE DG, WEISHAUP KR. Interstitial photoradiation therapy for primary solid tumours in pet cats and dogs. *Cancer Res* 1981; 41: 401-404.
- DOUGHERTY TJ. Photodynamic therapy (PDT) of malignant tumors. *Crit Rev Oncol Hematol* 1984; 2: 83-116.
- DOUGHERTY TJ, POTTER WR, WEISHAUP KR. The structure of the active component of hematoporphyrin derivative. *Prog Clin Biol Res* 1984; 170: 301-314.
- DOUGHERTY TJ. Photosensitization of malignant tumors. *Semin Surg Oncol* 1986; 2: 24-37.
- DOUGHERTY TJ. Photosensitizers: Therapy and detection of malignant tumours. *Photochem Photobiol* 1987a; 45: 879-889.
- DOUGHERTY TJ. Studies on the structure of porphyrins contained in Photofrin II. *Photochem Photobiol* 1987b; 46: 569-573.
- DOUGHERTY TJ. Photodynamic therapy: New approaches. *Semin Surg Oncol* 1989; 5: 6-16.
- DOUGHERTY TJ, COOPER MT, MANG TS. Cutaneous phototoxic occurrences in patients receiving Photofrin. *Lasers Surg Med* 1990; 10: 485-488.
- DOUGHERTY TJ & MARCUS SL. Photodynamic therapy. *Eur J Cancer* 1992; 28A: 1734-1742.
- DOWDEN J, JORDAN T, KAPADIA P. Temperature distribution produced by a cylindrical etched fibre tip in laser treatment of tumours by local hyperthermia. *Lasers Med Sci* 1988; 3: 47-54.
- DOWLATSHAHI K, BANGERT JD, HAKLIN MF, RHODES CK, WEINSTEIN RS, ECONOMOU SG. Protection of fibre function by para-axial fluid flow in interstitial laser therapy of malignant tumors. *Lasers Surg Med* 1990; 10: 322-327.
- DRITSCHILO A, HARTEK KW, THOMAS D, NAUTA R, HOLT R, LEE TC, RUSTGI S, RODGERS J. Intraoperative radiation therapy of hepatic metastases: Technical aspects and report of a pilot study. *Int J Radiat Oncol Biol Phys* 1988; 14: 1007-1011.
- DRIVER I, FEATHER JW, KING PR, GIBSON D. In vivo light dosimetry in interstitial photoradiation therapy (PRT). *Proc SPIE Int Soc Opt Eng OE Laser '88* 1988; 98-102.
- DRIVER I, LOWDELL CP, ASH DV. in vivo measurement of the optical interaction coefficients of human tumours at 630 nm. *Phys Med Biol* 1991; 36: 805-813.
- DUNLOP PRC & HOWARD GCW. Has hyperthermia a place in cancer treatment? *Clin Radiol* 1989; 40: 76-82.
- EINSTEIN A. Zur quantentheorie der Strahlung. *Physikal Z* 1917; 18: 121-128.
- ELIAS Z, POWERS SK, ATSTUPENAS E, BROWN JT. Hyperthermia from interstitial laser irradiation in normal rat brain. *Lasers Surg Med* 1987; 7: 370-375.
- ENSMINGER W. Hepatic arterial chemotherapy for primary and metastatic liver cancers. *Cancer Chemother Pharmacol* 1989; 23 (Suppl): S68-S73.
- EVENSEN JF, MALIK Z, MOAN J. Ultrastructural changes in the nuclei of human carcinoma cells after photodynamic treatment with hematoporphyrin derivative and with tetrasodium-meso-tetra-(4-sulphonatophenyl) porphine. *Lasers Med Sci* 1988; 3: 195-206.
- FERRARIO A, RUCKER N, RYTER SW, DOIRON DR, GOMER CJ. Direct comparison of in-vitro and in-vivo Photofrin-II mediated photosensitization using a pulsed KTP pumped dye laser and continuous wave argon ion pumped dye laser. *Lasers Surg Med* 1991; 11: 404-410.
- FIELD SB. Hyperthermia in the treatment of cancer. *Phys Med Biol* 1987; 32: 789-811.

- FIGGE FHJ, WEILAND GS, MANGANIELLO LOJ. Cancer detection and therapy: Affinity of neoplastic, embryonic and traumatized tissues for porphyrins and metalloporphyrins. *Roy Soc Exp Biol Med* 1948; 68: 640-641.
- FINGAR VH, WIEMAN TJ, DOAK KW. Role of thromboxane and prostacyclin release on photodynamic therapy-induced tumour destruction. *Cancer Res* 1990; 50: 2599-2603.
- FINLAY IG & MCARDLE CS. Occult hepatic metastases in colorectal carcinoma. *Br J Surg* 1986; 73: 732-735.
- FISHER JC. Principles of safety in laser surgery and therapy. In: *Basic and advanced laser surgery in gynecology*, Baggish MS (ed). East Norwalk, Conn, Appleton-Century Crofts. 1985: 85-130.
- FLEISCHER D. Endoscopic laser therapy for esophageal cancer: Present status with emphasis on past and future. *Lasers Surg Med* 1989; 9: 6-16.
- FLOCK ST, WILSON BC, PATTERSON MS. Total attenuation coefficients and scattering phase functions of tissues and phantom materials at 633 nm. *Med Phys* 1987; 14: 835-841.
- FOOTE CS. Definition of type I and type II photosensitized oxidation. *Photochem Photobiol* 1991; 54: 659.
- FOSTER JH. Surgical treatment of metastatic liver tumors. *Hepato-gastroenterol* 1990; 37: 182-187.
- FRANCO D. The management of liver metastases. *Br J Hosp Med* 1991; 45: 284-290.
- FRANK RN. Visual fields and electro-retinography following extensive photocoagulation. *Arch Ophthalmol* 1975; 93: 591-598.
- FRAZIER OH, DIETRICH EB, JOHANSSON B, CONGER JL, BURNETT CM, BYLOCK A, KADIPASAOGLU KA. Preliminary results of intraoperative excimer laser angioplasty: Phase 1: An adjunct to coronary artery bypass surgery. *Lasers Surg Med* 1992; 12: 7-12.
- FRIEDKIN M. The biochemist's outlook on cancer research. *Fed Proc Fed Am Soc Exp Biol* 1973; 32: 2148-2153.
- GATENBY RA, HAMMOND ND, BROWN DQ. Tumour therapy with hematoporphyrin derivative and laser via a percutaneous fiberoptic technique: Preclinical experiments. *Radiology* 1987; 163: 167-171.
- GIBSON SL, CECKLER TL, BRYANT TG, HILF R. Effects of laser photodynamic therapy on tumor phosphate levels and pH assessed by ³¹P-NMR spectroscopy. *Cancer Biochem Biophys* 1989; 10: 319-328.
- GIBSON SL, VANDERMEID KR, MURANT RS, RAUBERTAS RF, HILF R. Effects of various photoradiation regimens on the antitumor efficacy of photodynamic therapy for R3230 AC mammary carcinomas. *Cancer Res* 1990; 50: 7236-7241.
- GIJBSERS GHM, BREEDERVELD D, VAN GEMERT MJC, BOON TA, LANGELAAR J, RETTSCHNICK RPH. In vivo fluorescence excitation spectra of hematoporphyrin-derivative. *Lasers Life Sci* 1986: 29-48.
- GIJBSERS GHM, SPRANGERS LH, VAN DEN BROECKE DG, VAN WIERINGEN N, BRUGMANS MJP, VAN GEMERT MJC. Temperature increase during in vitro 308 nm excimer laser ablation of porcine aortic tissue. *Proc SPIE* 1991; 1425: 94-101.
- GIROTTI AW. Photodynamic lipid peroxidation in biological systems. *Photochem Photobiol* 1990; 51: 497-509.
- GLASSBERG E, LEWANDOWSKI L, HALCIN C, LASK G, UITTO J. Hyperthermia potentiates the effects of aluminum phthalocyanine tetrasulfonate-mediated photodynamic toxicity in human malignant and normal cell lines. *Lasers Surg Med* 1991; 11: 432-439.

- GODLEWSKI G, ROUY S, PIGNODEL C, OULD-SAID H, ELEDJAM JJ, BOURGEOIS JM, SAMBUC P. Deep localized Neodymium (Nd)-YAG laser photocoagulation in liver using a new water cooled and echoguided handpiece. *Lasers Surg Med* 1988; 8: 501-509.
- GOLDMAN L, INGELMAN JM, RICHFIELD DF. Impact of the laser on nevi and melanomas. *Arch Dermatol* 1964; 90: 71-75.
- GOLETTI O, CHIARUGI M, BUCCIANI P, MACCHIARINI P. Subcutaneous implantation of liver metastases after fine needle biopsy. *Eur J Surg Oncol* 1992; 18: 636-737.
- GOMER CJ & DOUGHERTY TJ. Determination of (^3H)- and (^{14}C) hematoporphyrin derivative distribution in malignant and normal tissue. *Cancer Res* 1979; 39: 146-151.
- GOMER CJ, DOIRON DR, RUCKER N, RAZUM NJ, FOUNTAIN SW. Action spectrum (620-640 nm) for hematoporphyrin derivative induced cell killing. *Photochem Photobiol* 1984a; 39: 365-368.
- GOMER CJ & RAZUN NJ. Acute skin response in albino mice following porphyrin photosensitization under oxic and anoxic conditions. *Photochem Photobiol* 1984b; 40: 435-439.
- GOMER CJ, FERRARIO A, HAYASHI N, RUCKER N, SZIRTH BC, MURPHREE AL. Molecular, cellular, and tissue responses following photodynamic therapy. *Lasers Surg Med* 1988a; 8: 450-463.
- GOMER CJ, RUCKER N, MURPHREE AL. Differential cell photosensitivity following porphyrin photodynamic therapy. *Cancer Res* 1988b; 48: 4539-4542.
- GOMER CJ. Photodynamic therapy in the treatment of malignancies. *Semin Hematol* 1989; 26: 27-34.
- GOMER CJ, RUCKER N, FERRARIO A, WONG S. Properties and applications of photodynamic therapy. *Radiat Res* 1989; 120: 1-18.
- GONZALEZ S, ARNFIELD MR, MEEKER BE, TULIP J, LAKEY WH, CHAPMAN JD, MCPHEE MS. Treatment of Dunning R3327-AT rat prostate tumors with photodynamic therapy in combination with misonidazole. *Cancer Res* 1986; 46: 2858-2862.
- GORDON JP, ZEIGER HJ, TOWNES CH. Molecular microwave oscillator and new hyperfine structure in the micro wave spectrum NH_3 . *Phys Rev* 1954; 95: 282.
- GORDON JP, ZEIGER HJ, TOWNES CH. Maser: New type of micro wave amplifier, frequency standard, and spectrometer. *Phys Rev* 1955; 99: 1264-1274.
- GRAY BN, ANDERSON JE, BURTON MA, VAN HAZEL G, CODDE J, MORGAN C, KLEMP P. Regression of liver metastases following treatment with Yttrium-90 microspheres. *Aus N Z J Surg* 1992; 62: 105-110.
- GRIECO A, BARONE C, COLETTA P, CASTELLANO R, RAGAZZONI E, CASSANO A, ASTONE A, GAMBASSI G. Antipyrine metabolism in patients with liver metastases from colorectal cancer. *Cancer* 1992; 70: 1477-1482.
- GUTTERIDGE JMC & HALLIWELL B. The measurement and mechanism of lipid peroxidation in biological systems. *TIBS* 1990; 15: 129-135.
- HAHL J, HAAPIAINEN R, OVASKA J, PUOLAKKAINEN P, SCHRÖDER T. Laser-induced hyperthermia in the treatment of liver tumors. *Lasers Surg Med* 1990; 10: 319-321.
- HAINA D, LANDTHALER M. Fundamentals of laser light interaction with human tissue, especially in the cardiovascular system. *Thorac Cardiovasc Surg* 1988; 36: 118-125.
- HALLDORSSON T., LANGERHOLC J., SENATORI L., FUNK H. Thermal action of laser irradiation in biological material monitored by egg-white coagulation. *Appl Opt* 1981; 20: 822-825.
- HASHIMOTO D, TAKAMI M, IDEZUKI Y. In depth radiation therapy by YAG laser for malignant tumors of the liver under ultrasonic imaging (abstr.). *Gastroenterology* 1985; 88: 1663.

- HAYDEN RE, MCLEAR PW, MORGAN AR, BISCHOFF JK. Verdicts in photodynamic therapy of squamous cell carcinoma. *Am J Otolaryngol* 1990; 11: 125-130.
- HENDERSON B. An isotropic dosimetry probe for monitoring light in tissue, theoretical and experimental assessment. *PhD thesis*, Heriot-Watt University, Edinburgh, Great-Britain. 1990.
- HENDERSON BW, WALDOW SM, MANG TS, POTTER WR, MALONE PB, DOUGHERTY TM. Tumor destruction and kinetics of tumor cell death in two experimental mouse tumors following photodynamic therapy. *Cancer Res* 1985; 45: 572-576.
- HENDERSON BW & BELLNIER DA. Tissue localization of photosensitizers and the mechanism of photodynamic tissue destruction. *Ciba Found Symp* 1989; 146: 113-130.
- HENDERSON BW & FINGAR VH. Oxygen limitation of direct tumour cell kill during photodynamic treatment of a murine tumour model. *Photochem Photobiol* 1989; 49: 299-304.
- HENNIGAN TW, EARLAM S, ALLEN-MERSH TG. Is liver to lung shunting in colorectal liver metastasis the cause of toxicity following treatment with cytotoxic microsphere aggregates? *Br J Cancer* 1992; 66: 1169-1170.
- HEPPNER F & ASCHER PW. Erste Versuche mit dem Laserstrahl in der Behandlung neurochirurgischer Erkrankungen. *Zentralbl Neurochir* 1977; 38: 77-86.
- HIGGINS GM & ANDERSON RM. Experimental pathology of the liver I: Restoration of the liver of the white rat following partial surgical removal. *Arch Pathol* 1931; 12: 186-202.
- HIGUCHI N, BLEIER AR, JOLESZ FA, COLUCCI VM, MORRIS JH. Magnetic resonance imaging of the acute effects of interstitial neodymium:YAG laser irradiation on tissues. *Invest Radiol* 1992; 27: 814-821.
- HODGSON WJB, MORGAN J, BYRNE D, DELGUERCIO LR. Hepatic resections for primary and metastatic tumors using the ultrasonic surgical dissector. *Am J Surg* 1992; 163: 246-250.
- HOFSTETTER AG, KEIDITSCH E, SCHMIEDT E, FRANK F. Der Neodymium YAG laser in der Urologie: Der zeitiger Stand der klinischen Erfahrungen. *Fortschr Med* 1984; 102: 885-890.
- HOLT S, TULIP J, HAMILTON D, CUMMINS J, FIELDS A, DICK C. Experimental laser phototherapy of the morris 7777 hepatoma in the rat. *Hepatology* 1985; 5: 175-180.
- HOMEIDA M, ROBERTS CJ, HALLIWELL M, READ AE, BRANCH RA. Antipyrine clearance per unit volume liver: An assessment of hepatic function in chronic liver disease. *Gut* 1979; 20: 596-601.
- HUANG GT, WANG TH, SHEU JC, DAIKUZONO N, SUNG JL, WU MZ, CHEN DS. Low-power laserthermia for the treatment of small hepatocellular carcinoma. *Eur J Cancer* 1991; 27: 1622-1627.
- HUGHES KS, SIMON R, SONGHORABODI S & 45 others. Resection of the liver for colorectal carcinoma metastases: A multi-institutional study of indications for resection. *Surgery* 1988; 103: 278-288.
- HUNTER JG & DIXON JA. Lasers in cardiovascular surgery: Current Status. *Western J Med* 1985; 142: 506-510.
- JAKO GJ. Laser surgery of the vocal cords: An experimental study with carbon dioxide lasers on dogs. *Laryngoscope* 1972; 82: 2204-2216.
- JACQUES SL & PRAHL SA. Modeling optical and thermal distributions in tissue during laser irradiation. *Lasers Surg Med* 1987; 6: 494-503.
- JACQUES SL, ALTER CA, PRAHL SA. Angular dependence of He-Ne laser light scattering by human dermis. *Lasers Life Sci* 1988; 1: 309-333.
- JACQUES SL. Laser-Tissue interactions: Photochemical, photothermal, and photomechanical. *Surg Clin N Am* 1992; 72: 531-558.

- JAFFE BM, DONEGAN WL, WATSON F, SPRATT JS jr. Factors influencing survival in patients with untreated hepatic metastases. *Surg Gynecol Obstet* 1968; 127: 1-11.
- JOFFE SN & SCHRÖDER T. Lasers in general surgery. *Adv Surg* 1987; 20: 125-154.
- JOLESZ FA, BLEIER AR, JAKAB P, RUENZEL PW, HUTTL K, JAKO GJ. MR imaging of laser-tissue interactions. *Radiology* 1988; 168: 249-253.
- JORI G & SPIKES JD. Photochemistry of porphyrins. In: *Topics in Photomedicine*. Smith KC (ed). Plenum Press, New York & London. 1984: 183-318.
- JORI G, BELTRAMINI M, REDDI E, SALVATO B, PAGVAN A, ZIRON L, TOMIO L, TSANOV T. Evidence for a major role of plasma lipoproteins as hematoporphyrin carriers in vivo. *Cancer Lett* 1984; 24: 291-297.
- JORI G, REDDI E, COZZANI I, TOMIO L. Controlled targeting of different subcellular sites by porphyrins in tumour-bearing mice. *Br J Cancer* 1986; 53: 615-621.
- JORI G. Photodynamic therapy of solid tumors. *Radiat Phys Chem* 1987; 30: 375-380.
- JORI G. In vivo transport and pharmacokinetic behavior of tumour photosensitizers. *Ciba Found Symp* 1989; 146: 78-94.
- JORI G. Photosensitized processes in-vivo: Proposed phototherapeutic applications. *Photochem Photobiol* 1990; 52: 439-443.
- JUNGERMANN K & KATZ N. Functional specialization of different hepatocyte populations. *Physiol Rev* 1989; 69: 709-764.
- KAPPAS A, SASSA S, GALBRAITH RA, NORDMANN Y. The porphyrias. In: *The metabolic basis of inherited disease I*, Scriver CR, Beaudet AL, Sly WS, Valle D (eds). McGraw-Hill Information Services Company, New York: 6ths ed. 1989: 1305-1365.
- KARAGIANNES JL, ZHANG Z, GROSSWEINER B, GROSSWEINER LI. Applications of 1-D diffusion approximation to the optics of tissues and tissue phantoms. *Appl Opt* 1989; 28: 2316-2317.
- KASTLER AJ. Birth of the maser and laser. *Nature* 1985; 316: 307-309.
- KEENE JP, KESSEL D, LAND EJ, REDMOND RW, TRUSCOTT TG. Direct detection of singlet oxygen sensitized by hematoporphyrin and related compounds. *Photochem Photobiol* 1986; 43: 117-120.
- KEIDITSCH E, HOFSTETTER A, ROTHENBERGER K, MAIWALD H, STERN J, PENSEL J, FRANK F. Comparative morphological investigations of the effects of the neodymium-YAG laser and electrocoagulation in experimental animal research. In: *Gynaecologic laser surgery*, Bellina JH (ed). Plenum Publishing, New York. 1981: 327-336.
- KEIDITSCH E. Morphological fundamentals in the treatment of tumors with the Neodymium-YAG laser. *Eur Urol* 1986; 12 (Suppl) 1: 12-16.
- KELLY JF & SNELL ME. Hematoporphyrin derivative: A possible aid in the diagnosis and therapy of carcinoma of the bladder. *J Urol* 1976; 155: 150-151.
- KEMENY N. Review of regional therapy of liver metastases in colorectal cancer. *Semin Oncol* 1992; 19 (Suppl): 155-162.
- KENNEDY JC, POTTIER RH, PROSS DC. Photodynamic therapy with endogenous protoporphyrin IX: Basic principles and present clinical experience. *J Photochem Photobiol B* 1990; 6: 143-148.
- KENNEDY JC & POTTIER RH. Endogenous protoporphyrin IX, a clinically useful photosensitizer for photodynamic therapy. *J Photochem Photobiol B* 1992; 14: 275-292.
- KESSEL D. Porphyrin-lipoprotein association as a factor in porphyrin localization. *Cancer Lett* 1986a; 33: 183-188.

- KESSEL D. Sites of photosensitization by derivatives of hematoporphyrin. *Photochem Photobiol* 1986b; 44: 489-493.
- KESSEL D, THOMPSON P, MUSSELMAN B, CHANG CK. Probing the structure and stability of the tumor localizing derivative of hematoporphyrin by reductive cleavage with LiAlH_4 . *Cancer Res* 1987; 47: 4642-4645.
- KIEFHABER P, NATH G, MORITZ K. Endoscopic control of massive gastrointestinal hemorrhage by irradiation with a high power neodymium-YAG laser. *Prog Surg* 1977; 15: 140-155.
- KITA K, ITAOSHIMA T, ITO T, OGAWA H, UKIDA M, KITADAI M, HATTORI S, MIZUTANI S, TANAKA R, ANDOH M, KOIDE N, TANABE T, KONDOH H, JITOKU M, NAGASHIMA H. Photodynamic therapy of rat liver cancer: Protection of the normal liver by indocyanine green. *Gastroenterol Jpn* 1987; 22: 465-473.
- KONGSHAUG M, MOAN J, BROWN SB. The distribution of porphyrins with different tumour localizing ability among human plasma proteins. *Br J Cancer* 1989; 59: 184-188.
- KORBELIK M & HUNG J. Cellular delivery and retention of Photofrin II: The effects of interaction with human plasma proteins. *Photochem Photobiol* 1991; 53: 501-510.
- KRASNER N. Palliative laser therapy for tumors of the gastrointestinal tract. *Billiere Clin Gastroenterol* 1991; 5: 37-57.
- KREIMER-BIRNBAUM M. Modified porphyrins, chlorins, phthalocyanines and purpurins: Second-generation photosensitizers for photodynamic therapy. *Semin Hematol* 1989; 26: 157-173.
- LAMERS WH, MOORMAN AFM, CHARLES R. The metabolic lobulus, a key to the architecture of the liver *RBC* 1989; 19: 5-26.
- LEIBOVICI L, SCHOENFELD N, YEHOSHUA HA, MAMET R, RAKOWSKI E, SHINDEL A, ATSMON A. Activity of porphobilinogen deaminase in peripheral blood mononuclear cells of patients with metastatic cancer. *Cancer* 1988; 62: 2297-2300.
- LEKKA MP, PAPAGIANNOULIS L, ELIADES GC, CAPUTO AA. A comparative in vitro study on visible light-cured sealants. *J Oral Rehabil* 1989; 16: 287-299.
- LI F, LIM CK, PETERS TJ. An HPLC assay for rat liver ferrochelatase activity. *Biomed Chromatogr* 1987; 2: 164-168.
- LIND DS, PARKER GA, HORSLEY JS, KORNSTEIN MJ, NEIFELD JP, BEAR HD, LAWRENCE W. Formal hepatic resection of colorectal liver metastases: Ploidy and prognosis. *Ann Surg* 1992; 215: 677-684.
- LIPOW M. Laser physics made simple. *Curr Prob Obstet Gynecol Fertil* 1986; 9: 445-493.
- LIPSON RL, BALDES EJ, OLSEN AM. The use of a derivative of hematoporphyrin in tumour detection. *J Natl Cancer Inst* 1961; 26: 1-11.
- LITTRUP PJ, LEE F, BORLAZA GS, SACKNOFF EJ, TORP-PEDERSEN S, GRAY JM. Percutaneous ablation of canine prostate using transrectal ultrasound guidance absolute ethanol and Nd:YAG laser. *Invest Radiol* 1988; 23: 734-739.
- LIVRAGHI TG, VETTORI C, LAZZARONI S. Liver metastases: Results of percutaneous alcohol injection in 14 patients. *Radiology* 1991; 179: 709-712.
- LOH CS, MACROBERT AJ, BEDWELL J, REGULA J, KRASNER N, BOWN SG. Oral versus intravenous administration of 5-aminolevulinic acid for photodynamic therapy. *Br J Cancer* 1993; 68: 41-51.
- LOIZIDOU MC, LAWRENCE RJ, HOLT S, CARTY NJ, COOPER AJ, ALEXANDER P, TAYLOR I. Facilitation by partial hepatectomy of tumor growth within the rat liver following intraportal injection of syngeneic tumor cells. *Clin Exp Metastasis* 1991; 9: 335-349.

- LOK, NETHERLANDS CANCER REGISTRY. Cancer incidence in the Netherlands, 1989. Utrecht. 1992.
- LOWRY OH, ROSEBROUGH NJ, FARR AL, RANDALL RJ. Protein measurement with the folinphenol reagent. *J Biol Chem* 1951; 193: 265-275.
- LUOMA PV & SOTANIEMI EA. Saliva and plasma clearance of antipyrine as reflectors of liver function. *Eur J Drug Metabol Pharmacokinet* 1981; 6: 261-264.
- MACLEOD JS, BLANC D, COLLES MJ. Measurement of the optical absorption coefficient at 1.06 micrometers of various tissues using the photoacoustic effect (abstr.). *Laser Surg Med* 1988; 8: 143.
- MACROBERT AJ, BOWN SG, PHILLIPS D. What are the ideal properties for a sensitizer ? *Ciba Found Symp* 1989; 146: 4-16.
- MAIMAN TH. Stimulated optical radiation in ruby. *Nature* 1960; 187: 493-494.
- MALIK Z & LUGACI H. Destruction of erythroleukemic cells by photoactivation of endogenous porphyrins. *Br J Cancer* 1987; 56: 589-595.
- MANG TS, DOUGHERTY TJ, POTTER WR, BOYLE DG, SOMER S, MOAN J. Photobleaching of porphyrins used in photodynamic therapy and implications for therapy. *Photochem Photobiol* 1987; 45: 501-506.
- MANG TS. Combination studies of hyperthermia induced by neodymium:yttrium-aluminum-garnet (Nd:YAG) laser as an adjuvant to photodynamic therapy. *Lasers Surg Med* 1990; 10: 173-178.
- MANYAK MJ, RUSSO A, SMITH PD, GLATSTEIN E. Photodynamic therapy. *J Clin Oncol* 1988; 6: 380-391.
- MARCHAL G, TSHIBWABWA-TUMBA E, OYEN R, PYLYSER K, GODDEERIS R. Correlation of sonographic patterns in liver metastases with histology and microangiography. *Invest Radiol* 1985; 20: 79-84.
- MARCHESSINI R, BERTONI A, ANDREOLA S, MELLONI E, SICHIRIOLLA AE. Extinction and absorption coefficients and scattering phase functions of human tissues in vitro. *Appl Opt* 1989; 28: 2318-2324.
- MARIJNISSEN JPA, STAR WM, VERSTEEG AAC, FRANKEN NAP. Pilot study on the interstitial HPD-PDT in rats bearing solid mammary carcinoma or rhabdomyosarcoma. In: *Photodynamic therapy of tumours and other diseases*, Jori G, Perria C (eds). Libera Progetto, Padova. 1985: 387-390.
- MARIJNISSEN JPA & STAR WM. Quantitative light dosimetry in vitro and in vivo. *Lasers Med Sci* 1987; 2: 235-241.
- MARIJNISSEN JPA, JANSEN H, STAR WM. Treatment system from whole bladder wall photodynamic therapy with in vivo monitoring and control of light dose rate and dose. *J Urol* 1989; 142: 1351-1355.
- MARIJNISSEN JPA, VERSTEEG JAC, STAR WM, VAN PUTTEN WLJ. Tumour and normal tissue response to interstitial photodynamic therapy of the rat R-1 rhabdomyosarcoma. *Int J Radiat Oncol Biol Phys* 1992; 22: 963-972.
- MARQUET RL, WESTBROEK DL, JEEKEL J. Interferon treatment of a transplantable rat colon adenocarcinoma: Importance of tumor site. *Int J Cancer* 1984; 33: 689-692.
- MARSHALL J, TROKEL S, ROTHERY S, SCHUBERT H. An ultrastructural study of corneal incisions induced by an excimer laser at 193 nm. *Ophthalmology* 1985; 92: 749-758.
- MASTERS A & BOWN SG. Interstitial laser hyperthermia in the treatment of tumours. *Lasers Med Sci* 1990; 5: 129-136.

- MASTERS A, STEGER AC, BOWN SG. Role of interstitial therapy in the treatment of liver cancer. *Br J Surg* 1991; 78: 518-523.
- MASTERS & BOWN. Interstitial laser hyperthermia. *Semin Surg Oncol* 1992; 8: 242-249.
- MATHUS-VLIEGEN EMH. The role of laser in gastroenterology. *PhD thesis*, University of Amsterdam, Amsterdam, The Netherlands. 1988.
- MATSUMOTO N, SAITO H, MIYOSHI N, NAKANISHI K, FUKUDA M. Combination effect of hyperthermia and photodynamic therapy on colon carcinoma. *Arch Otolaryngol Head Neck Surg* 1990; 116: 824-829.
- MATSUMOTO R, SELIG AM, COLUCCI VM, JOLESZ FA. Interstitial laser ablation in normal rabbit liver: Trial to maximize the size of laser induced lesions. *Lasers Surg Med* 1992; 12: 650-658.
- MATTHEWSON K, COLERIDGE-SMITH P, O'SULLIVAN JP, NORTHFIELD TC, BOWN SG. Biological effects of intrahepatic Neodymium:Yttrium-Aluminum-Garnet laser photocoagulation in rats. *Gastroenterology* 1987; 93: 550-557.
- MATTHEWSON K, BARTON T, LEWIN MR, O'SULLIVAN JP, NORTHFIELD TC, BOWN SG. Low power interstitial Nd:YAG laser photocoagulation in normal and neoplastic rat colon. *Gut* 1988; 29: 27-34.
- MATTHEWSON K, BARR H, TRALAU C, BOWN SG. Low power interstitial Nd YAG laser photocoagulation: Studies in a transplantable fibrosarcoma. *Br J Surg* 1989; 76: 378-381.
- MATTIELLO J, EVELHOCH JL, BROWN E, SCHAAP AP, HETZEL FW. Effect of photodynamic therapy on RIF-1 tumor metabolism and blood flow examined by ^{31}P and ^2H NMR spectroscopy. *NMR Biomed* 1990; 3: 64-70.
- MCKENZIE AL. Physics of thermal processes in laser-tissue interaction. *Phys Med Biol* 1990; 35: 1175-1209.
- MENON IA, PERSAD SD, HABERMAN HF. A comparison of the phototoxicity of protoporphyrin, coproporphyrin and uroporphyrin using a cellular system in vitro. *Clin Biochem* 1989; 22: 197-200.
- MESTER E, MESTER AF, MESTER A. The biomedical effects of laser application. *Lasers Surg Med* 1985; 5: 31-39.
- MEYER-BETZ F. Untersuchungen über die biologische (photodynamische) Wirkung des Hematoporphyrins und andere Derivate des Bluts und Gallenfarbstoffs. *Arch Dtsch Klin Med* 1913; 112: 476-503.
- MEIJERING LJT, VAN GEMERT MJC, GIJSBERS GHM, WELCH AJ. Radial time constants to approximate bio-heat equation. *Lasers Surg Med* 1993 (in press).
- MITCHELL JB, MCPHEARSON S, DEGRAFF W, GAMSON J, ZABELL A, RUSSO A. Oxygen dependence of hematoporphyrin derivative induced photoinactivation of Chinese Hamster cells. *Cancer Res* 1985; 45: 2008-2011.
- MIZUTANI J, HIRAOKA T, YAMASHITA R, MIYAUCHI Y. Promotion of hepatic metastases by liver resection in the rat. *Br J Cancer* 1992; 65: 794-797.
- MOAN J & SOMMER S. Oxygen dependence of the photosensitizing effect of hematoporphyrin derivative in NHIK-3025 cells. *Cancer Res* 1985; 45: 1608-1610.
- MOAN J, BERG K, KVAM E, WESTERN A, MALIK Z, RÜCK A, SCHNECKENBURGER H. Intracellular localization of photosensitizers. *Ciba Found Symp* 1989; 146: 95-111.
- MOORE RB, CHAPMAN JD, MORKRZANOWSKI AD, ARNFIELD MR, MCPHEE MS, MCEWAN AJ. Non-invasive monitoring of photodynamic therapy with $^{99\text{m}}$ Technetium HMPAO scintigraphy. *Br J Cancer* 1992; 65: 491-497.

- MOORE JV, DODD NJ, WOOD B. Proton nuclear magnetic resonance imaging as a predictor of the outcome of photodynamic therapy of tumours. *Br J Radiol* 1989; 62: 869-870.
- MORDON SR, CORNIL AH, BRUNETAUD JM, GOSSELIN B, MOSCHETTO Y. Nd-YAG laser thermal effect: Comparative study of coagulation in rat liver in vivo by continuous wave and high power pulsed lasers. *Lasers Med Sci* 1987; 2: 285-294.
- MORGAN AR, GARBO GM, KREIMER-BIRNBAUM, KECK RW, CHAUDHURI K, SELMAN SH. Morphological study of the combined effect of purpurin derivatives and light on transplantable rat bladder tumors. *Cancer Res* 1987a; 47: 496-498.
- MORGAN AR, RAMPERSAUD A, KECK RW, SELMAN SH. Verdins: New photosensitizers for photodynamic therapy. *Photochem Photobiol* 1987b; 46: 441-444.
- MULLER PJ & WILSON BC. Photodynamic therapy of malignant primary brain tumors: Clinical effects, post-operative ICP, and light penetration of the brain. *Photochem Photobiol* 1987; 46: 929-935.
- MURRAY A, MITCHELL DC, WOOD RFM. Lasers in surgery. *Br J Surg* 1992; 79: 21-26.
- MURTHY SM, GOLDSCHMIDT RA, RAO LN, AMMIRATI M, BUCHMANN T, SCANLON EF. The influence of surgical trauma on experimental metastasis. *Cancer* 1989; 64: 2035-2044.
- NAMIENO T, TAKEICHI N, HATA Y, UCHINO J, KOBAYASHI H. Kinetic changes of liver regeneration and hepatocellular carcinoma cells after partial hepatectomy in rats. *Gastroenterol Jpn* 1991; 26: 29-36.
- NATH G. Endlich das ideale Laser-Skalpel für die Medizin. *Laser Elektropt* 1972; 1: 49-50.
- NAUTA RJ, HERES EK, THOMAS DS *et al.* Intraoperative single dose radiotherapy. *Arch Surg* 1987; 122: 1392-1395.
- NELSON JS, LIAW LH, BERNS MW. Tumor destruction in photodynamic therapy. *Photochem Photobiol* 1987a; 46: 829-835.
- NELSON JS, ROBERTS WG, BERNS MW. in vivo studies on the utilization of mono-L-aspartyl chlorin (NPe6) for photodynamic therapy. *Cancer Res* 1987b; 47: 4681-4685.
- NELSON JS, KIMEL S, BROWN L, BERNS MW. Glucose administration combined with photodynamic therapy of cancer improves therapeutic efficacy. *Lasers Surg Med* 1992; 12: 153-158.
- NIMS TA & MCCAUGHAN JS. Clinical experience with CO₂ Laser vaporization of neoplasm. *Lasers Surg Med* 1983; 3: 265-268.
- NISHIWAKI Y, NAKAMURA S, SAKAGUCHI S. New method of photosensitizer accumulation for photodynamic therapy in an experimental liver tumour. *Lasers Surg Med* 1989; 9: 254-263.
- NISHIZAKI T, MATSUMATA T, KANEMATSU T, YASUNAGA C, SUGIMACHI K. Surgical manipulation of VX2 carcinoma in the rabbit liver evokes enhancement of metastasis. *J Surg Res* 1990; 49: 92-97.
- NODA S, KAWATA S, MIYOSHI S, MINAMI Y, TARUI S. Antipyrine clearance per unit liver volume in cirrhotics with and without hepatocellular carcinoma indicating a correlation with histological change of the liver. *Gastroenterol Jpn* 1989; 24: 159-163.
- NOE JM, BARSKY SH, GEER DE, ROSEN S. Port-wine stains and the response to Argon laser therapy: Successful treatment and predictive role of color, age and biopsy. *Plast Reconstr Surg* 1980; 65: 130-136.
- NOLSØE C, TORP-PEDERSEN S, OLLDAG E, HOLM HH. Bare fibre low power Nd-YAG laser interstitial hyperthermia: Comparison between diffuser tip and non-modified tip, an in vitro study. *Lasers Med Sci* 1992; 7: 1-7.

- NUOMA PV & SOTANIEMI EA. Saliva and plasma clearance of antipyrine as reflection of liver function. *Eur J Drug Metab Pharmacokinet* 1981; 6: 261-264.
- NUUTINEN P, ESKELINEN M, SURAKKA M, MARIN S, ALHAVA E. Low power interstitial hyperthermia in the treatment of ductal carcinoma of the pancreas: An experimental study with Syrian golden hamsters. *Lasers Med Sci* 1992; 7: 45-48.
- OKUNAKA T, ECKHAUSER ML, KATO H, BOMAMINIO A, YAMAMOTO H, AIZAWA K, SARASUA MM, KOEHLER KA. Correlation between photodynamic efficacy of differing porphyrins and membrane partitioning behavior. *Lasers Surg Med* 1992; 12: 98-103.
- OLSEN AK. Intraoperative ultrasonography and the detection of liver metastases in patients with colorectal cancer. *Br J Surg* 1990; 77: 998-999.
- OSEROFF AR, ARA G, OHUOHA D, APRILLE J, BOMMER JC, YARMUSH ML, FOLEY J, CINCOTTA L. Strategies for selective cancer photochemotherapy: Antibody-targeted and selective carcinoma cell photolysis. *Photochem Photobiol* 1987; 46: 83-96.
- PANDEY RK, BELLNIER DA, SMITH KM, DOUGHERTY TJ. Chlorin and porphyrin derivatives as potential photosensitizers in photodynamic therapy. *Photochem Photobiol* 1991; 53: 65-72.
- PANGKA VS, MORGAN AR, DOPHIN D. Diels-Alder reactions of protoporphyrin IX dimethyl ester with electron-deficient alkynes. *J Org Chem* 1986; 51: 1094-1100.
- PANIS Y, RIBEIRO J, CHRÉTIEN Y, NORDLINGER B. Dormant liver metastases: An experimental study. *Br J Surg* 1992; 79: 221-223.
- PANJEHPUR M, OVERHOLT BF, MILLIGAN AJ, SWAGGERTY MW, WILKINSON JE, KLEBANOW ER. Nd:YAG laser-induced interstitial hyperthermia using a long frosted contact probe. *Lasers Surg Med* 1990; 10: 16-24.
- PANTEGHINI M. Aspartate aminotransferase isoenzymes. *Clin Biochem* 1990; 23: 311-319.
- PARSA P, JACQUES SL, NISHIOKA NS. Optical properties of rat liver between 350 and 2200 nm. *Appl Opt* 1989; 28: 2325-2330.
- PATTERSON MS, WILSON BC, WYMAN DR. The propagation of optical radiation in tissue I: Models of radiation transport and their application. *Lasers Med Sci* 1991a; 6: 155-168.
- PATTERSON MS, WILSON BC, WYMAN DR. The propagation of optical radiation in tissue II: Optical properties of tissues and resulting fluence distributions. *Lasers Med Sci* 1991b; 6: 379-390.
- PERSSON BOG, JEPPSSON B, TRANBERG KG, BENGMARK S. Repeated intermittent dearterialization in the treatment of liver tumors (abstr.). *HPB Surg* 1992; 5 (Suppl): 26.
- PETRELLI N, BHUPENDRA G, PIEDMONTE M, HERRERA L. Morbidity and survival of liver resection for colorectal adenocarcinoma. *Dis Colon Rectum* 1991; 34: 899-904.
- PETTROVICH ZB, LANGHOLZ M, ASTRAHAN M, AMAMI B. Deep microwave hyperthermia of metastatic tumors of the liver. *Rec Res Cancer Res* 1988; 107: 243-248.
- PHILLIP MJ, MCMAHON JD, O'HARA MD, HETZEL FW, AMSTERDAMSKY C, SCHAAP AP. Effects of hematoporphyrin (HpD) and a chemiluminescence system on the growth of transplanted tumors in C3H/HeJ mice. *Prog Clin Biol Res* 1984; 170: 563-569.
- PICKERING JW. Optical property changes as a result of protein denature in albumen and yolk. *J Photochem Photobiol B* 1992; 16: 101-111.
- PICKERING JW, MOES CJM, STERENBORG HJCM, PRAHL SA, VAN GEMERT MJC. Two integrating spheres with an intervening scattering sample. *J Opt Soc Am A* 1992a; 9: 621-631.
- PICKERING JW, PRAHL SA, VAN WIERINGEN N, BEEK JF, STERENBORG HJCM, VAN GEMERT MJC. A double integrating sphere system to measure optical properties of tissue. *Appl Opt* 1992b; 32: 399-410.

- PIGLIUCCI GM, IORIO B, VENDITTI D, FIORITO R, VITTORINI V, CERVELLI V, CASCIANI CU. Perspectives and hopes for the 1990s. *Adv Exp Med Biol* 1990; 267: 293-296.
- PIMSTONE NR, HORNER IJ, SHAYLOR-BILLINGS J, GANDHI SN. Hematoporphyrin-augmented phototherapy in experimental liver cancer in the rat. *SPIE Lasers Med Surg* 1982; 357: 60-67.
- PIMSTONE NR. Utility of porphyrins and light in the diagnosis and treatment of malignancy. *Hepatology* 1985; 5: 338-340.
- POLANYI TG, BREDEMEIER HC, DAVIS TW jr. A CO₂ laser for surgical research. *Med Biol Eng Comput* 1970; 8: 541-528.
- POLANYI TG. Physics of surgery with lasers. *Clin Chest Med* 1985; 6: 179-202.
- POTTER WR, MANG TS, DOUGHERTY TJ. The theory of photodynamic dosimetry: Consequences of photodestruction of sensitizer. *Photochem Photobiol* 1987; 46: 97-101.
- POTTIER R, CHOW YFA, LAPLATE JP, TRUSCOTT TG, KENNEDY JC, BEINER LA. Non-invasive technique for obtaining fluorescence excitation and emission spectra in vivo. *Photochem Photobiol* 1986; 44: 679-687.
- POULSEN HE. One sample antipyrine clearance after 90% partial hepatectomy in the rat. *Liver* 1985; 5: 200-204.
- PRAHL SA. Light transport in tissue. *PhD thesis*, University of Texas, Austin, Texas, USA. 1988.
- PRAHL SA, VAN GEMERT MJC, WELCH AJ. Determining the optical properties of turbid media by using the adding-doubling method. *Appl Opt* 1993; 32: 559-568.
- PREUSS LE, BOLIN FP, CAIN BW. Tissue as a medium for laser light transport-implications for photoradiation therapy. *Proc Soc Phot Opt Instru Eng* 1982; 357: 77-84.
- PROFIO AE. Laser excited fluorescence of hematoporphyrin derivative for diagnosis of cancer. *IEEE J Quant Electron* 1984; 12: 1502-1507.
- QUEBBEMAN EJ, SKIBBA JL, PETROFF RJ jr. A technique for isolated hyperthermic liver perfusion. *J Surg Oncol* 1984; 27: 141-145.
- RAAB O. Über die Wirkung fluoreszierender Stoffe auf Infusoria. *Z Biol* 1900; 39: 524-526.
- RAKESTRAW SL, TOMPKINS RG, YARMUSH ML. Antibody-targeted photolysis: In vitro studies with Sn(IV) chlorin e6 covalently bound to monoclonal antibodies using a modified dextran carrier. *Proc Natl Acad Sci USA* 1990; 87: 4217-4221.
- RAVIKUMAR TS, KANE R, CADY B, JENKINS RL, McDERMOTT W, ONIK G, CLOUSE M, STEELE G jr. Hepatic cryosurgery with intraoperative ultrasound monitoring for metastatic colon carcinoma. *Arch Surg* 1987; 122: 403-409.
- RAZUM N, BALCHUM OJ, PROFIO AE, CARSTENS F. Skin photosensitivity: Duration and intensity following intravenous hematoporphyrin derivatives, HpD, and DHE. *Photochem Photobiol* 1987; 46: 925-928.
- REINHOLD HS & OVERGAARD J. Hyperthermia in clinical oncology. *Eur J Cancer* 1990; 26: 915-916.
- RICHTER AM, KELLY B, CHOW J, LIU DJ, DOLPHIN D, LEVY JG. Preliminary studies on a more effective phototoxic agent than hematoporphyrin. *J Natl Cancer Inst* 1987; 79: 1327-1332.
- RIS HB, ALTERMATT HJ, INDERBITZI R, HESS R, NACHBUR B, STEWART JCM, WANG Q, LIM CK, BONNETT R, BERENBAUM MC, ALTHAUS U. Photodynamic therapy with chlorins for diffuse malignant mesothelioma: Initial clinical results. *Br J Cancer* 1991; 64: 1116-1120.
- ROBERTS WG, SHIAU FY, NELSON JS, SMITH KM, BERNIS MW. In vitro characterization of monoaspartyl chlorin e6 and diaspartyl chlorin e6 for photodynamic therapy. *J Natl Cancer Inst* 1988; 80: 330-336.

- ROBERTS WG, SMITH KM, MCCULLOUGH, BERNIS MW. Skin photosensitivity and photodestruction of several potential photodynamic sensitizers. *Photochem Photobiol* 1989; 49: 431-438.
- ROBERTS WG, KLEIN MK, LOOMIS M, WELDY S, BERNIS MW. Photodynamic therapy of spontaneous cancers in felines, canines, and snakes with chloro-aluminum sulfonated phthalocyanine. *J Natl Cancer Inst* 1991; 83:18-23.
- ROBERTZ-VAUPEL GM, LINDECKEN KD, EDEKI T, FUNKE C, BELWON S, DENGLER HJ. Disposition of antipyrine in patients with extensive metastatic liver disease. *Eur J Clin Pharmacol* 1992; 42: 465-469.
- ROBINS HI, HUGANDER A, COHEN JD. Whole body hyperthermia in the treatment of neoplastic disease. *Radiol Clin N Am* 1989; 9: 183-185.
- ROSENBERG C, TADIR Y, BRASLAVSKY D, FISCH B, KARNI Z, OVADIA J. Endometrial laser ablation in rabbits: A comparative study of three laser types. *Lasers Surg Med* 1990; 10: 66-73.
- ROSENTHAL I. Phthalocyanines as photodynamic sensitizers. *Photochem Photobiol* 1991; 53: 859-870.
- RUBINO GF & RASETTI L. Porphyrin metabolism in human neoplastic tissues. *Panminerva Med* 1966; 8: 290-292.
- SALET C & MORENO G. Photosensitization of mitochondria: Molecular and cellular aspects. *J Photochem Photobiol B* 1990; 5: 133-150.
- SANDBERG S & ROMSLO I. Phototoxicity of protoporphyrin as related to its subcellular localization in mice livers after short-term feeding with griseofulvin. *Biochem J* 1981; 198: 67-74.
- SANDER R, POESL H, FRANK F, MEISTER P, STROBEL M, SPUHLER A. A Nd:YAG laser with a water-guided laser beam: A new transmission system. *Gastrointest Endosc* 1988; 34: 336-338.
- SANDER R, POESL H, ZUERN W, SPUHLER A, BRAIDA M. The water jet- guided Nd:YAG laser in the treatment of gastroduodenal ulcer with a visible vessel: A randomized controlled and prospective study. *Endoscopy* 1989; 21: 217-220.
- SAPOZINK MD, GIBBS FA jr, THOMSON JW, ELTRINGHAM JR, STEWART JR. A comparison of deep regional hyperthermia from an annular array and a concentric coil in the same patients. *Int J Radiat Oncol Biol Phys* 1985; 11: 179-190.
- SCHAWLOW AL & TOWNES CH. Infrared and optical masers. *Phys Rev* 1958; 112: 1940-1949.
- SCHEELE J, STANGL R, ALTENDORF-HOFMAN A. Hepatic metastases from colorectal carcinoma: Impact on the natural history. *Br J Surg* 1990; 77: 1241-1246.
- SCHMELLER NT & HOFSTETTER AG. Laser treatment of ureteral tumors. *J Urology* 1989; 141: 840-843.
- SCHNEIDER PD. Liver resection and laser hyperthermia. *Surg Clin N Am* 1992; 72: 623-639.
- SCHOBER R, BETTAG M, SABEL M, ULRICH F, HESSEL S. Fine structure of zonal changes in experimental Nd:YAG laser-induced interstitial hyperthermia. *Lasers Surg Med* 1993; 13: 234-241.
- SCHOENFELD N, EPSTEIN O, LAHAV M, MAMET R, SHAKLAI M, ATSMON A. The heme biosynthetic pathway in lymphocytes of patients with malignant lymphoproliferative disorders. *Cancer Lett* 1988; 43: 43-48.
- SCHREVE RH, TERPSTRA OT, AUSEMA L, LAMERIS JS, VAN SEIJEN AJ, JEEKEL J. Detection of liver metastases: A prospective study comparing liver enzymes, scintigraphy, ultrasonography and computed tomography. *Br J Surg* 1984; 71: 947-949.
- SCHRÖDER T, BRACKETT K, JOFFE SN. An experimental study of the effects of electrocautery and various lasers on gastrointestinal tissue. *Surgery* 1987; 101: 691-697.

- SCHRÖDER T, PUOLAKKAINEN PA, HAHN J, RÄMÖ OJ. Case report: Fatal air embolism as a complication of laser-induced hyperthermia. *Lasers Surg Med* 1989; 9: 183-185.
- SCHUITMAKER JJ, VAN BEST JA, VAN DELFT JL, DUBBELMAN TA, OOSTERHUIS JA, DE WOLF-ROUENDAAL D. Bacteriochlorin-a, a new photosensitizer in photodynamic therapy: in vivo results. *Invest Ophthalmol Vis Sci* 1990; 31: 1444-1450.
- SCHUTTE B, REYDERS MMJ, BOSMAN FT, BLIJHAM GH. Effect of tissue fixation on anti-bromodeoxyuridine immunohistochemistry. *J Histochem Cytochem* 1987; 35: 1343-1345.
- SCHWARTZ S, ABSOLON K, VERMUND H. Some relationships of porphyrins, x-rays, and tumors. *Univ Minnesota Med Bull* 1955; 7: 7-13.
- SELMAN SH, KREIMER-BIRNBAUM M, KLAUNIG JE, GOLDBLATT PJ, KECK RW, BRITTON SL. Blood flow in transplantable bladder tumors treated with hematoporphyrin derivative and light. *Cancer Res* 1984; 44: 1924-1927.
- SELMAN SH, GARBO GM, KECK RW, KREIMER-BIRNBAUM M, MORGAN AR. A dose response analysis of purpurin derivatives used as photosensitizers for the photodynamic treatment of transplantable FANFT-induced urothelial tumors. *J Urol* 1987; 137: 1255-1257.
- SHARGEL L, CHEUNG WM, YU ABC. High-pressure liquid chromatographic analysis of antipyrine in small plasma samples. *J Pharm Sci* 1979; 68: 1052-1054.
- SHEDLOFSKY SI, SINCLAIR PR, BONKOVSKY HL, HEALEY JF, SWIM AT, ROBINSON JM. Haem synthesis from exogenous 5-aminolaevulinate in cultured chick-embryo hepatocytes: Effects of inducers of cytochromes P-450. *Biochem J* 1987; 248: 229-236.
- SHERMAN DM, WEICHELBAUM RE, ORDER SE, CLOUD L, TREY C, PIRO AJ. Palliation of hepatic metastases. *Cancer* 1978; 41: 2013-2017.
- SHERMAN KE. Alanine aminotransferase in clinical practice: A review. *Arch intern Med* 1991; 151: 260-265.
- SHIINA S, YASUDA H, MUTO H, TAGAWA K, UNUMA T, IBUKURO K, INOUE Y, TAKA NASHI R. Percutaneous ethanol injection in the treatment of liver neoplasms. *ARJ Am J Roentgenol* 1987; 149: 949-952.
- SMITH A. Mechanisms of toxicity of photoactivated artificial porphyrins: Role of porphyrin-protein interactions. *Ann N Y Acad Sci* 1987; 514: 309-322.
- SPIKES JD & JORI G. Photodynamic therapy of tumours and other diseases. *Lasers Med Sci* 1987; 2: 3-15.
- SPLINTER R, SVENSON RH, LITTMANN L, TUNTELDER JR, CHUANG CH, TATSIS GP, THOMPSON M. Optical properties of normal, diseased, and laser photocoagulated myocardium at the Nd:YAG wavelength. *Lasers Surg Med* 1991; 11: 117-124.
- SRINIVASAN R. Ablation of polymers and biological tissue by ultraviolet lasers. *Science* 1986; 234: 559-565.
- STAR WM, MARIJNISSEN HPA, VAN DEN BERG-BLOK AE, VERSTEEG JAC, FRANKEN KAP, REINHOLD HS. Destruction of rat mammary tumour and normal tissue microcirculation by hematoporphyrin derivative photoradiation observed in vivo in sandwich observation chambers. *Cancer Res* 1986; 46: 2532-2540.
- STAR W, VERSTEEG JC, VAN PUTTEN W, MARIJNISSEN HA. Wavelength dependence of hematoporphyrin derivative photodynamic treatment effects on rat ears. *Photochem Photobiol* 1990; 52: 547-554.
- STAR WM, WILSON BC, PATTERSON MS. Light delivery and optical dosimetry in photodynamic therapy of solid tumors. In: *Photodynamic therapy: Basic principles and clinical applications*, Henderson BW & Dougherty TJ (eds). Marcel Dekker Inc, New York. 1992: 335-367.

- STEELE G & RAVIKUMAR TS. Resection of hepatic metastases from colorectal cancer: Biologic perspectives. *Ann Surg* 1989; 210: 127-138.
- STEGER AC, LEES WR, WALMSLEY K, BOWN SG. Interstitial laser hyperthermia: A new approach to local destruction of tumours. *Br Med J* 1989a; 299: 362-365.
- STEGER AC, MASTERS A, LEES WR, WALMSLEY K, BOWN SG. Interstitial laser hyperthermia (lett). *Br Med J* 1989b; 299: 1219-1220.
- STEGER AC. Interstitial laser hyperthermia for the treatment of hepatic and pancreatic tumours. *Photochem Photobiol* 1991; 53: 837-844.
- STEGER AC, LEES WR, SHORVON P, WALMSLEY K, BOWN SG. Multiple-fibre low-power interstitial laser hyperthermia: Studies in the normal liver. *Br J Surg* 1992; 79: 139-145.
- STEIN BS. Laser physics and tissue interaction. *Urol Clin N Am* 1986; 13: 365-380.
- STERN J, ENDERS S, FRANK F. Biologische Wirkung des thermischen Lasers. *Der Chirurg* 1988; 59: 61-67.
- ST PETER JV, AWNI WM. Quantifying hepatic function in the presence of liver disease with phenazone (antipyrine) and its metabolites. *Clin Pharmacokinet* 1991; 20: 50-65.
- STRONG MS, JAKO GJ, POLANYI T, WALLACE RA. Laser surgery in the aerodigestive tract. *Am J Surg* 1973; 126: 529-533.
- SUC B, PANIS Y, BELGHITI J, FÉKÉTÉ F. "Natural history" of hepatectomy. *Br J Surg* 1992; 79: 39-42.
- SUGARBAKER PH & KEMENY N. Management of metastatic cancer to the liver. *Adv Surg* 1989; 22: 1-56.
- SUGARBAKER PH. Surgical decision making for large bowel cancer metastatic to the liver. *Radiology* 1990; 174: 621-626.
- SUGARBAKER PH. Metastatic inefficiency: The scientific basis for resection of liver metastases from colorectal cancer. *J Surg Oncol* 1993; 3 (Suppl): 158-160.
- SUGIYAMA K, SAKAI T, FUJISHIMA I, RYU H, UEMURA K, YOKOYAMA T. Stereotactic interstitial laser-hyperthermia using Nd:YAG laser. *Stereotact Funct Neurosurg* 1990; 54+55: 501-505.
- SVAASAND LO, BOERSLID T, OEVERAASEN M. Thermal and optical properties of living tissue: Application to laser-induced hyperthermia. *Lasers Surg Med* 1985; 5: 589-602.
- SVAASAND LO & ELLINGSON R. Optical penetration in human intracranial tumors. *Photochem Photobiol* 1985; 41: 73-76.
- SWEETLAND HM, WYMAN A, ROGERS K. Interstitial laser hyperthermia (lett). *Br Med J* 1989; 299: 918.
- THOMAS JP & GIROTTI AW. Glucose administration augments in vivo uptake and phototoxicity of the tumor-localizing fraction of hematoporphyrin derivative. *Photochem Photobiol* 1989; 49: 241-247.
- THOMAS S, PENSEL J, ENGELHARDT R, MEYER W, HOFSTETTER AG. The pulsed dye laser versus the Q-switched Nd:YAG laser in laser-induced shock-wave lithotripsy. *Lasers Surg Med* 1988; 8: 363-370.
- THOMSEN S. Pathologic analysis of photothermal and photomechanical effects of laser-tissue interaction. *Photochem Photobiol* 1991; 53: 825-835.
- TRACZ RA, WYMAN DR, LITTLE PB, TOWNER RA, STEWART WA, SCHATZ SW, PENNOCK PW, WILSON BC. Magnetic resonance imaging of interstitial laser photocoagulation in brain. *Lasers Surg Med* 1992; 12: 165-173.

- TRACZ RA, WYMAN DR, LITTLE PB, TOWNER RA, STEWART WA, SCHATZ SW, WILSON BC, PENNOCK PW, JANZEN EG. Comparison of magnetic resonance images and the histopathological findings of lesions induced by interstitial laser photocoagulation in the brain. *Lasers Surg Med* 1993; 13: 45-54.
- TRALAU CJ, YOUNG AR, WALKER NP, VERNON DI, MACROBERT AJ, BROWN SB, BOWN SG. Mouse skin photosensitivity with dihematoporphyrin ether (DHE) and aluminum sulphonated phthalocyanine (AISPc): A comparative study. *Photochem Photobiol* 1989; 49: 305-312.
- TROMBERG BJ, ORENSTEIN A, KIMEL S, BARKER SJ, HYATT J, NELSON JS, BERNIS MW. in vivo tumor oxygen tension measurements for the evaluation of the efficiency of photodynamic therapy. *Photochem Photobiol* 1990; 52: 375-385.
- VALENZO DP. Photomodification of biological membranes with emphasis on singlet oxygen mechanisms. *Photochem Photobiol* 1987; 46: 147-160.
- VAN EDEN PJ, STEGER AC, BOWN SG. Fibre tip considerations for low power laser interstitial hyperthermia (abstr.). *Lasers Med Sci* 1988; 3: 336.
- VAN EYKEN P, HIELE M, FEVERY J, GEBOES K, VANTRAPPEN G, PENNINGCKX F, DESMET VJ, RUTGEERTS P. Comparative study of low power neodymium-YAG laser interstitial hyperthermia versus ethanol injection for controlled hepatic tissue destruction. *Lasers Med Sci* 1991; 6: 35-41.
- VAN HERCK H, BAUMANS V, DE BOER SF, VAN DER GUGTEN J, VAN WOERKOM AB, BEYNEN AC. Endocrine stress response in rats subjected to singular orbital puncture while under diethyl-ether anaesthesia. *Lab Anim* 1991; 25: 325-329.
- VAN HERCK H, BAUMANS V, VAN DER CRAATS NR, HESP APM, MEIJER GW, VAN TINTELEN G, WALVOORT HC, BEYNEN AC. Histological changes in the orbital region of rats after orbital puncture. *Lab Anim* 1992; 26: 53-58.
- VAN GEMERT MJC, DE KLEIJN WJA, HULSBERGEN HENNING JP. Temperature behavior of a model portwine stain during Argon laser coagulation. *Phys Med Biol* 1982; 27: 1089-1104.
- VAN GEMERT JC, BERENBAUM MC, GIJSBERTS GHM. Wavelength and light-dose dependence in tumour phototherapy with hematoporphyrin derivative. *Br J Cancer* 1985; 52: 43-49.
- VAN HILLEGERSBERG R, KORT WJ, TEN KATE FJW, TERPSTRA OT. Water-jet-cooled Nd:YAG laser coagulation: Selective destruction of rat liver metastases. *Lasers Surg Med* 1991; 11: 445-454.
- VAN HILLEGERSBERG R, KORT WJ, VERMEIJ M, TERPSTRA OT. Treatment of experimental liver metastases with a noncontact neodymium:YAG laser. *J Surg Res* 1992a; 53: 128-135.
- VAN HILLEGERSBERG R, MARIJNISSEN JPA, KORT WJ, ZONDERVAN PE, TERPSTRA OT, STAR WM. Interstitial photodynamic therapy in a rat liver metastasis model. *Br J Cancer* 1992b; 66: 1005-1014.
- VAN HILLEGERSBERG R, VAN DEN BERG JWO, KORT WJ, TERPSTRA OT, WILSON JHP. Selective accumulation of endogenously produced porphyrins in a liver metastasis model in rats. *Gastroenterology* 1992c; 103: 647-651.
- VAN HILLEGERSBERG R, PICKERING JW, AALDERS M, BEEK JF. Optical properties of rat liver and tumor at 633 nm and 1064 nm: Photofrin enhances scattering. *Lasers Surg Med* 1993; 13: 31-39.

- VAN OOLIJEN B, WIGGERS T, MEIJER S, VAN DER HEIJDE MN, SLOOFF MJH, VAN DER VELDE CJH, OBERTOP H, GOUMA DJ, BRUGGINK EDM, LANGE JF, MUNTING JDK, RUTTEN APM, RUTTEN HJT, DE VRIES JE, GROOT G, ZOETMULDER FAN, VAN PUTTEN WLJ. Hepatic resections for colorectal metastases in The Netherlands: A multiinstitutional 10-year study. *Cancer* 1992; 70: 28-34.
- VAN STEVENINCK J, TIJSSEN K, BOEGHEIM JP, VAN DER ZEE J, DUBBELMAN TM. Photodynamic generation of hydroxyl radicals by hematoporphyrin derivative and light. *Photochem Photobiol* 1986; 44: 711-716.
- VERDAASDONK RM, JANSEN ED, HOLSTEGE FC, BORST C. Mechanism of CW Nd:YAG laser recanalization with modified fiber tips: Influence of temperature and axial force on tissue penetration in vitro. *Lasers Surg Med* 1991; 11: 204-212.
- VESELL ES, PASSANANTI GT, GLENWRIGHT PA, DVORCHIK BH. Studies on the disposition of antipyrine, aminopyrine, and phenacetin using plasma, saliva, and urine. *Clin Pharmacol Ther* 1975; 18: 259-272.
- VON TAPPEINER H & JESIONEK A. Therapeutische Versuche mit fluoreszierenden Stoffen. *München Med Wochenschr* 1903; 47: 2042-2044.
- WAGNER JS, ADSON MA, VAN HEERDEN JA, ADSON MH, ILSTRUP DW. The natural history of hepatic metastases from colorectal cancer: A comparison with resective treatment. *Ann Surg* 1984; 199: 502-508.
- WALDOW SM & DOUGHERTY TJ. Interaction of hyperthermia and photoradiation therapy. *Radiat Res* 1984; 97: 380-385.
- WALDOW SM, HENDERSON BW, DOUGHERTY TJ. Potentiation of photodynamic therapy by heat: Effect of sequence and time interval between treatments in vivo. *Lasers Surg Med* 1985; 5: 83-94.
- WALDOW SM, HENDERSON BW, DOUGHERTY TJ. Hyperthermic potentiation of photodynamic therapy employing Photofrin I and II: Comparison of results using three animal tumour models. *Lasers Surg Med* 1987; 7: 12-22.
- WEINHOUSE S. In: *Aminoacids, proteins and cancer biochemistry*, JT Edsall (ed). Academic Press, New York. 1960: 109-119.
- WEISHAUP T, GOMER CJ, DOUGHERTY TJ. Identification of singlet oxygen as the cytotoxic agent in photoactivation of a murine tumour. *Cancer Res* 1976; 36: 2326-2329.
- WELCH JP & DONALDSON GA. The clinical correlation of an autopsy study of recurrent colorectal cancer. *Ann Surg* 1979; 189: 496-502.
- WELCH AJ. The thermal response of laser irradiated tissue. *IEEE J Quantum Electron* 1984; 20: 1471-1480.
- WELCH AJ, PEARCE JA, DILLER KR, YOON G, CHEONG WF. Heat generation in laser irradiated tissue. *J Biom Eng* 1989; 111: 62-68.
- WELCH AJ, MOTAMED I, RASTEGAR S, LECARPENTIER GL, JANSEN D. Laser thermal ablation. *Photochem Photobiol* 1991; 53: 815-823.
- WILLS EJ, FINDLAY JM, MCMANUS JP. Effects of hyperthermia therapy on the liver II: Morphological observations. *J Clin Pathol* 1976; 29: 1-10.
- WILSON BC & ADAM G. A Monte Carlo model for the absorption and flux distributions of light in tissue. *Med Phys* 1983; 10: 824-830.
- WILSON BC, JEEVES WP, LOWE DM. In vivo and post mortem measurements of the attenuation spectra of light in mammalian tissues. *Photochem Photobiol* 1985; 42: 153-162.

- WILSON BC, PATTERSON MS, BURNS DM. Effect of photosensitizer concentration in tissue on the penetration depth of photoactivating light. *Lasers Med Sci* 1986; 1: 235-244.
- WILSON BC & PATTERSON MS. The physics of photodynamic therapy. *Phys Med Biol* 1986; 31: 327-360.
- WILSON BC. Photodynamic therapy: Light delivery and dosage for second-generation photosensitizers. *Ciba Found Symp* 1989; 146: 60-77.
- WILSON BC & VAN LIER JE. Radiolabelled photosensitizers for tumor imaging and photodynamic therapy. *J Photochem Photobiol B* 1989; 3: 459-463.
- WILSON JHP, DE ROOY FWM, TE VELDE K. Acute intermittent porphyria in the Netherlands: Heterogeneity of the enzyme porphobilinogen deaminase. *Neth J Med* 1986; 29: 393-399.
- WILSON JHP, VAN HILLEGGERSBERG R, VAN DEN BERG JWO, KORT WJ, TERPSTRA OT. Photodynamic therapy for gastrointestinal tumours. *Scand J Gastroenterol* 1991; 26 (Suppl) 188: 20-25.
- WIRTH FP, DOWNING EF, CANNON CL, BAKER RP. Experience with the Neodymium:Yttrium-Aluminum-Garnet laser in forty-two cases. *Neurosurgery* 1987; 21: 867-871.
- WOOD CB, GILLIS CR, BLUMGART LH. A retrospective study of the natural history of patients with liver metastases from colorectal cancer. *Clin Oncol* 1976; 2: 285-288.
- WYMAN DR, WHELAN WM, WILSON BC. Interstitial laser photocoagulation: Nd:YAG 1064 nm optical fiber source compared to point heat source. *Lasers Surg Med* 1992; 12: 659-664.
- YAHN WZ & STRULLY KJ. Blood vessel anastomosis by laser and other biomedical applications. *J Assoc Adv Med Instr* 1966; 1: 28-31.
- YANG R, RESCORLA FJ, REILLY CR, FAUGHT PR, SANGHVI NT, LUMENG L, FRANKLIN TD, GROSFELD JL. A reproducible rat liver cancer model for experimental therapy: Introducing a technique of intrahepatic tumor implantation. *J Surg Res* 1992; 52: 193-198.
- YANG Y, WELCH AJ, RYLANDER HG. Rate process parameters of albumen. *Lasers Surg Med* 1991; 11: 188-190.
- ZHOU C. Mechanisms of tumor necrosis induced by photodynamic therapy. *J Photochem Photobiol* 1989; 3: 299-318.
- ZIMMERMANN HJ. Experimental hepatotoxicity. In: *Hepatotoxicity*, Zimmerman HJ (ed). Appleton-Century Croft, New York. 1978: 172-178.
- ZIMMERMANN I, STERN J, FRANK F, KEIDITSCH E, HOFSTETTER A. Interception of lymphatic drainage by Nd:YAG laser irradiation in rat urinary bladder. *Lasers Surg Med* 1984; 4: 167-172.
- ZWENG HC & FLOCKS M. Retinal laser photocoagulation. *Trans Am Acad Ophthalmol Otolaryngol* 1967; 71: 39-45.

Subject Index

- 5-aminolevulinic acid 83
 - membrane permeability 104
 - molecular structure 105
 - oral dosage 110
 - porphyrin distribution 108
 - predicting administration-effect 111
 - in drinking water 104
- Ablation 25
- Absorption coefficient 21, 115
- Absorption spectrum
 - Argon laser 23
 - CO₂ laser 23
 - hemoglobin 23
 - Nd:YAG laser 23
 - porphyrins 77
 - soret band 76
 - water 23
- Acronym laser 17
- Adding-doubling solution 118
- Aims of the study 4
- Alcohol injection 2
- Aminotransferases 10
- Anisotropy factor 22, 115
- Antipyrine clearance
 - partial hepatic resection 12
 - interstitial Nd:YAG 64
 - interstitial PDT 98
 - measure of liver function 12, 13
 - method of determination 12
 - water-jet Nd:YAG 46
- Argon laser 23, 28
- Argon-dye laser 80, 84
- ASAT/ALAT serum level
 - cellular localization 10
 - liver:tumor ratio 12
 - interstitial Nd:YAG 60
 - interstitial PDT 97
 - measure for liver damage 10
 - method of determination 10
 - water-jet Nd:YAG 46
- Attenuation coefficient 21
- Bacteriochlorin-a 83, 84
- Band pass filters 117
- Beam splitter 69, 81, 148
- Beer's law 21
- Benzo-porphyrin derivative 83
- Bladder cancer PDT 74, 81
- Bromodeoxyuridine
 - methods 58
 - tumor incorporation 60
- Carbonization 27, 33
- Charring 67
- Chemotherapy 1
- Chlorin e6 82
- Clinical laser application
 - aiming at curation 149
 - aiming at palliation 149
 - fluence rate measurement 148
 - infection 148
 - interstitial techniques 148
 - laparoscopy 148
 - multiple fiber implantation 148
 - ultrasonography 148
- CO₂ laser 23
 - light delivery 23
 - tissue damage 27
- Coagulation 33
 - BrdU incorporation 60
 - ultrasonography 137
- Coherent light 17
- Collimated light 17
- Collimated transmission 117
- Colon carcinoma CC531 7
 - central necrosis histology 8, 128
 - central necrosis ultrasound 136
 - day 36 histology 9

SUBJECT INDEX

- Colorectal carcinoma
 - incidence 1
- Combination therapy 85
 - glucose injection and PDT 85
 - hyperthermia and PDT 85, 148
 - hypoxic toxins and PDT 85
 - vasoactive drugs and PDT 85
- Coproporphyrinogen 108
- Crater of ablation 33
- Cryotherapy 2
- Cylindrical diffuser
 - ceramic 69
 - Helioseal 57, 69
 - in photodynamic therapy 81
 - interstitial PDT 79, 99
 - interstitial Nd:YAG 56
- Defocus 24
- Diffusion approximation 124
- Diode laser 84
- Dye laser 20
 - dye fluid 23, 80
- Effective attenuation coefficient 119
- Electromagnetic spectrum 18
- Endogenous photosensitization 103
 - 5-aminolevulinic acid 83
 - coproporphyrinogen 108
 - porphyrin analysis 106
 - porphyrins tumor:liver 110
 - protoporphyrin 83, 108
 - skin photosensitivity 83
 - uroporphyrinogen 108
- Energy
 - definition 24
 - effect on tissue damage 49
- Energy fluence
 - definition 81
- Excimer laser 26
- Ferrochelatase
 - activity 103
 - analysis 106
 - cytochrome oxydase 111
 - colon carcinoma CC531 110
 - decreased tumor activity 83
 - fibrosarcoma BN175 111
 - liver 110
 - mamma carcinoma BN472 111
 - porphyrin accumulation 111
- Fiber transmission 24
- Floxuridine 2
- Fluence rate measurement
 - clinical application 148
 - interstitial Nd:YAG 57
 - interstitial PDT 90, 99
 - isotropic detector 57
 - in optical properties 116
- Fluorescence efficiency 124
- Focus mode 24
- Focussing handpiece 32
- Gold vapor laser 80
- Heat distribution
 - blood perfusion 27
 - charring 67
 - conduction 27
 - light penetration 64
 - point heat source 67
 - point optical source 67
 - storage 27
 - tissue cooling 24
 - transfer 27
 - zones of tissue destruction 36
- Heat-fixation 48
- Helioseal 57
 - scattering properties 69
- Hematoporphyrin derivative
 - structure 74
- Heme synthetic pathway 104
- Hepatic artery embolization 3
- Hepatic artery ligation 2
- Histology
 - computer-assisted measurements 9
- Histology thermal laser
 - carbonization 33
 - coagulation 33, 43, 59
 - crater of ablation 33
 - day 0 33, 128
 - day 1 33
 - day 2 33, 37
 - day 4 33
 - day 8 34
 - heat-fixation 48

SUBJECT INDEX

- interstitial Nd:YAG 59
 - noncontact Nd:YAG 32
 - water-jet Nd:YAG 41, 138
 - zones of liver damage 128
- Histopathology
 - light microscopy 9
- History
 - hematoporphyrin 73
 - laser 17
 - maser 17
 - medical laser 17
 - photodynamic therapy 73
- Hydrofluoric acid 56
- Hyperthermia 3, 51, 85, 99, 148
- IBAS 2000 9
- Indocyanine green 98
- Integrating spheres 116
- Interstitial laser fibers
 - charring 57
 - gas cooling 66
 - liquid cooling 64
 - sapphire tip 66
- Interstitial Nd:YAG laser
 - charring 55
 - introduction 51
 - light transmission 64
 - maximum coagulation volume 67
 - review literature 52
 - tissue temperature 68
- Interstitial PDT 87
 - exposure time 100
 - histopathology 93
 - hyperthermia 99
 - light delivery 80, 89
 - light dosimetry 81
 - liver damage 98
 - liver necrosis 101
 - serum ASAT/ALAT 101
 - surviving hepatic cells 101
 - temperature measurements 90
 - therapy resistant cells 100
 - tumor remission 100
- Intersystem crossing 77
- Intracavitary light delivery 80
- Intraluminal light delivery 80
- Irradiance
 - definition 24
- Isotropic detector 57, 67
 - dosimetry in PDT 81
- Kiton-red 80
- KTP laser 84
- Kubelka-Munk properties 124
- Laser
 - energy 24
 - history 17
 - light delivery 23
 - medium 20
 - physics 19
 - resonator chamber 20
 - wavelength 22
- Laser light
 - coherent 17
 - collimated 17
 - molecular basis 19
 - monochromatic 17
 - population inversion 20
 - spontaneous emission 19
 - stimulated emission 20
- Laser medium
 - Argon 20
 - CO₂ 20
 - Nd:YAG 20
- Laser-tissue interaction 25, 26
 - back scattering 81
 - feedback tools 136
 - fluence in tissue 20
 - imaging techniques 136
 - light penetration 76
 - light transport model 115
 - MRI 136
 - photoablation 27
 - photomechanical effects 26
 - reflection 20
 - scattering 20
 - transmission 20
 - ultrasonography 136
- Light Delivery 23, 80, 84
 - contact probe 24
 - cylindrical diffuser 24
 - focussing handpiece 32

SUBJECT INDEX

- interstitial therapy 80
- intracavitary 80
- intraluminal 80
- Light distribution 81
- Light sources in PDT 79, 84
 - argon-dye laser 80, 84
 - chemiluminescent activator 84
 - conventional lamps 79
 - diode laser 84
 - gold vapor laser 80
 - Helium Neon laser 80
 - interstitial PDT 88
 - KTP dye laser 84
- Light transmission
 - carbonization 64
- Light transport model 115
- Lipoproteins
 - LDL mediated endocytosis 82
 - porphyrin binding 76
- Liver metastases
 - alcohol injection 2
 - chemotherapy 1
 - colorectal carcinoma 1
 - cryotherapy 2
 - hepatic artery embolization 3
 - hepatic artery ligation 2
 - hyperthermia 3
 - incidence 1
 - radiotherapy 2
 - surgical resection 3
 - survival untreated 1
 - treatment modalities 1
 - ultrasound appearance 136, 137
- Liver rat
 - liver lobes 12
 - portion of body weight 12
- Lock-in-amplifier 117
- Long-term laser effects
 - determination of 9
 - interstitial Nd:YAG 64, 68
 - interstitial PDT 98
 - water-jet 47
- Low power laser 25
- Maser 17
- Medical laser applications
 - bladder cancer PDT 74, 81
 - cutaneous procedures 17
 - gynecology 17
 - mesothelioma, PDT 83
 - neurosurgery 18
 - operating microscope 17
 - ophthalmology 17, 28
- Microspheres 3
- Monitoring PDT
 - singlet oxygen production 84
- Monochromatic light 17
- Nd:YAG laser 23
 - penetration depth 125
 - noncontact Nd:YAG 36
- Optical properties 20, 115, 119
 - absorption coefficient 21
 - anisotropy factor 22
 - attenuation coefficient 21
 - influence of Photofrin 124
 - liver vs. tumor 119
 - livers 123
 - method of determination 116
 - penetration depth 21
 - reduced scattering coefficient 22
 - scattering coefficient 21
 - tissue with Photofrin 119
 - tumors 123
- Optical properties determination
 - adding-doubling solution 118
 - band pass filters 117
 - calculations 118
 - collimated transmission 117
 - equipment 116
 - integrating spheres 116
 - inter-individual variation 120, 122
 - intra-individual variation 120
 - lock-in-amplifier 116
 - photodiodes 116
 - sample preparation 116
- Parameters for tissue damage
 - antipyrine clearance 12
 - histopathology 9
 - serum ASAT/ALAT 10
- Penetration depth 21
- Phase I clinical studies 149

SUBJECT INDEX

- Pheophorbide 98
- Photoablation 27
- Photobleaching 78
- Photodiodes 116
- Photodynamic destruction
 - cellular sites 79
 - liver damage 87
 - mitochondria 79
 - radicals 78
 - singlet oxygen 77
 - tumor vasculature 79, 85
 - tumoricidal depth 82
 - type I reaction 78
 - type II reaction 77
- Photodynamic therapy
 - basic principle 73
 - combination therapy 85
 - effect on normal liver 98
 - future directions 82
 - histopathology 93
 - history 73
 - irradiation regimen 81, 84
 - monitoring 84
 - skin photosensitivity 75
- Photofrin
 - cellular uptake 76
 - excitation wavelength 76
 - fluorescence efficiency 124
 - illumination interval 75
 - increased scattering 124
 - LD50 75
 - liver accumulation 108
 - pharmacokinetics 75
 - plasma clearance 75
 - structure 74
 - toxicology 75
 - treatment interval 98
 - tumor CC531 accumulation 108
- Photomechanical effect 26
- Photosensitizer
 - absorption coefficient 81
 - accumulation in liver 87
 - ideal properties 82
 - intersystem crossing 77
 - liposome bound 82
 - liver accumulation 98
 - pharmacokinetics 75
 - photobleaching 78
 - second-generation 82
 - selective accumulation 103
 - singlet state 77
 - toxicology 75
 - triplet state 77
 - triplet state yield 78
- Phthalocyanines 82
- Plank's constant 19
- Point heat source 67
- Point optical source 67
- Popcorn effect 27, 148
- Population inversion 20
- Porphobilinogen deaminase
 - CC531 activity 110
 - liver activity 110
 - tissue activity 103
 - tissue analysis 106
- Porphyrins
 - absorption spectrum 77
 - accumulation after ALA 83
 - metabolism 103
 - photochemistry 76
 - serum distribution 76
 - tissue accumulation 76
 - tissue analysis 106
 - tumor accumulation 101
- Power setting
 - effect on lesion extent 49
- Prefocus 24
- Prognosis metastasectomy
 - carcino-embryonic antigen 2, 4
 - Dukes' classification 4
 - number of metastases 4, 149
 - resected weight 4
 - satellite nodules 4
 - surgical margin 4
- Protoporphyrin IX 83, 108
 - fluorescence detection 111
 - photosensitizing properties 111
- Pulsed mode 24, 32
- Purpurins 83
- Radicals, PDT 78

SUBJECT INDEX

- Radiotherapy 2
- Rat tumor model 7
- Reduced scattering coefficient 22, 119
- Resection of liver metastases
 - complications 4
 - contraindications 3
 - factors influencing prognosis 3
 - morbidity rate 4
 - mortality rate 4
 - postoperative stay 4, 149
 - recurrence 4
 - resection margin 4, 149
 - 5-year survival rate 3
- Resonator chamber 20
- Rhodamine B 80, 78
- Scattering
 - effect on fluence 81
- Scattering coefficient 21, 115
- Second-generation sensitizers 82
- Short-term Laser Effects
 - interstitial Nd:YAG 60, 68
 - interstitial PDT 95
 - water-jet Nd:YAG 43, 132
- Singlet oxygen 77, 84
- Skin photosensitivity 75, 83
- Soret band 76
- Surgical resection 3
- Temperature measurement
 - interstitial Nd:YAG 57
 - interstitial PDT 90
- Thermal properties 27
- Thermal tissue damage 27
 - ablation 27
 - Argon laser 28
 - carbonization 27, 51
 - CO₂ laser 27
 - coagulation 27, 28, 51
 - delayed necrosis 137
 - irradiation time 27
 - laser energy 49
 - laser power 49
 - popcorn effect 27
 - temperature 27, 51
 - vaporization 27
 - zones of liver damage 137
 - zones of tissue damage 36
- Toxicology
 - Photofrin 75
 - phthalocyanine 82
- Triplet state yield 78
- Tumor model
 - antipyrine clearance 12
 - intrahepatic tumor cell injection 8
 - intraportal tumor cell injection 8
 - lyostypt 8
 - macroscopic appearance 10
 - spill of tumor cells 7, 9
 - three main liver lobes 12
 - tumor measurements 8
- Tumor remission
 - definition 9
- Type I reaction, PDT 78
- Type II reaction, PDT 77
- Ultrasonography
 - definition of echogenicity 126
 - clinical application 148
 - correspondence with histology 128
 - determining tumor coagulation 138
 - fiber positioning 69
 - hypoechoic liver damage 137
 - imaging liver metastasis 136
 - lesion size versus histology 132
 - liver coagulation 125
 - methods 126
 - post-laser tumor 128
 - pre-laser tumor 128
 - time interval post-laser 126
 - tumor size 128
 - transducer 126
- Uroporphyrinogen 108
- Verdins 83
- Wag/Rij rats 7
 - daily urine production 108
 - daily water consumption 108
 - liver lobes 12
- Water-jet fiber system 41

Dankwoord

Op deze plaats wil ik al diegenen bedanken die de afgelopen jaren hebben bijgedragen aan de totstandkoming van dit proefschrift. Zonder hen was dit werk niet mogelijk geweest.

Mijn ouders, lieve Maartje en Mark ik wil jullie bedanken voor de mogelijkheden die jullie mij hebben geboden, de Montessoriaanse opvoeding en de liefde en toewijding waarmee jullie ons altijd hebben begeleid, gesteund en gestimuleerd.

Mijn promotor Prof. Dr. O.T. Terpstra, beste Onno ik kan me nog goed herinneren hoe ik als student in het vijfde jaar van mijn studie voor het eerst op jouw kamer kwam en je mij vertelde over de verschillende onderzoekslijnen op het Laboratorium voor Chirurgie. Tijdens dat gesprek stelde je voor om een onderzoek op te starten naar de laserbehandeling van galstenen of levertumoren. Jouw geweldig enthousiasme en fascinatie voor wetenschappelijk onderzoek wist je meteen op mij over te brengen en dat is in de jaren daarna zo gebleven. Het vertrouwen dat je van het begin af aan in mij stelde, je bereikbaarheid voor wetenschappelijke of organisatorische problemen en de precisie en snelheid waarmee je de verschillende versies van een manuscript wist te corrigeren heb ik altijd enorm gewaardeerd.

Mijn co-promotor Dr. W.J. Kort, beste Wil jij hebt me van het begin af aan opgevangen op het lab en je was er letterlijk en figuurlijk altijd. Je wist het evenwicht te vinden tussen het geven van een grote mate van zelfstandigheid en tegelijkertijd het bijbrengen van de vele facetten van het wetenschappelijk onderzoek. Jouw enorme ervaring heeft ervoor gezorgd dat de talrijke hindernissen niet hoefden worden genomen, werden geanticipeerd, of werden opgelost. Je hebt me geleerd efficiënt te werken en altijd te streven naar een "(zo) goed (mogelijke) laboratory practice", daarbij in belangrijke mate rekening houdend met de dieren. Op de momenten dat ik er echt geen gat meer in zag, was je vaak in staat een complexe studie te reduceren tot een eenvoudig probleem. Ik wil je hartelijk danken voor je vriendschap en de goede tijd die ik op het lab heb gehad.

Prof. J.H.P. Wilson, beste Paul je was al in een heel vroeg stadium betrokken bij het onderzoek. Door je grote expertise op het gebied van het porfyriene-metabolisme bedacht je een op dat moment geheel nieuwe benadering van fotosensibilisatie. Dat die theorie in de praktijk ook bleek te werken, was voor iedereen een grote sensatie. Je hebt het mogelijk gemaakt dat ik de resultaten op verschillende plaatsen kon vertellen en was voor mij als een tweede promotor.

Prof. Dr. Ir. M.J.C. van Gemert, beste Martin we hebben elkaar eigenlijk leren kennen in Aken waar je op het idee kwam de optische eigenschappen van de weefsels te bepalen. Zoals jij zegt ontspruiten dit soort plannen het best tussen twee sessies in, op een terrasje in de zon. Hartelijk dank voor je gastvrijheid, je adviezen, en je bereidheid in de commissie zitting te

nemen.

Prof. Dr. J. Jeekel dank ik voor zijn bereidheid het manuscript te beoordelen en zitting te nemen in de commissie.

De Nederlandse Lever Darm Stichting heeft dit onderzoek gedurende twee en een half jaar financieel ondersteund en daarnaast bijgedragen aan de financiering van congresbezoeken. Zonder die steun was onderzoek doen op deze manier nooit mogelijk geweest.

De hele groep van het Laboratorium voor Chirurgie wil ik hartelijk danken voor de technische en organisatorische ondersteuning en vooral voor de goede sfeer die onontbeerlijk is geweest. De volgende mensen waren direct bij het onderzoek betrokken: Pim van Schalkwijk adviseerde over de te volgen biochemische analyse en deed alle bepalingen. Ineke Hekking en Thijs van Aken waren altijd bereid om waar nodig te helpen bij het verrichten van de experimenten. Olga Pelgrim verzorgde nauwkeurig en snel de histologie. Bij Ron Briegoos waren de dieren in goede handen. "Kas" Kasbergen en Marijke Lagerman waren altijd flexibel wanneer iets (meestal op het laatste moment) moest worden geregeld. Erik Ridderhof wist altijd en overal een oplossing, zijn overlijden begin 1992 was voor iedereen een groot verlies.

Mijn latere kamergenoten Olivier Busch, Harold Lont en Nico Durante dank ik voor hun collegialiteit en begrip. Geranne J.G.M. Kromwijk dank ik voor haar idee en inzet bij het verkrijgen van verlenging van het project.

M. Vermeij heeft geholpen bij het beoordelen van de histologie tijdens de opstartfase van het onderzoek. Beste Marcel, omdat op dat moment alle laser weefsel effecten nog volledig nieuw waren hebben we heel wat tijd achter de microscoop doorgebracht om het een en ander te doorgronden. Dank je voor het geduld en nauwkeurigheid waarmee je dat hebt gedaan. Prof. dr. F.J.W. ten Kate en Drs. P.E. Zondervan dank ik voor hun deskundige hulp bij de daaropvolgende studies. Lianne A. Sorber heeft de IBAS geprogrammeerd en was altijd bereikbaar voor vragen, Frank van der Panne heeft de macrofoto's gemaakt van de histologie bij de laatste studies.

Dr. Wim J. van den Berg en de groep van het Lab Interne II, met name Annie Edixhoven-Bosdijk, wil ik danken voor hun samenwerking en het verrichten van de porfyryne-chemie die vaak moest plaatsvinden naast de al drukke lopende projecten.

A. Caldenhove heeft zorg gedragen voor de laser-technische ondersteuning. Beste Anton, dankzij jou waren de laser en verschillende fibersystemen altijd paraat.

Ing. P.J. Sterrenburg, beste Pieter je hebt me vooral in het begin bijgestaan met je kennis op het gebied van de laser-fysica. Dank je voor de (lange) interessante discussies die onder meer hebben geleid tot de studie met de water-jet.

De PDT-groep van de Dr. Daniël den Hoed Kliniek is gedurende de gehele periode nauw bij het onderzoek betrokken geweest. Het belangrijkste deel van de studie naar interstitiële photodynamische therapie heeft op hun lab plaatsgevonden. Ik wil Dr. Willem M. Star en Ing. Hans P.A. Marijnissen hartelijk danken voor de gastvrijheid en de samenwerking; de dye laser heeft heel wat uurtjes extra moeten draaien. Jeanne Versteeg en later Nynke van der Veen dank ik voor hun hulp bij de dierverzorging en experimenten.

Drs. H.J. van Staveren, beste Hugo dankzij jou is uiteindelijk mijn wens om een studie naar interstitiële thermische laser behandeling te doen en ideeën daarover op te schrijven in

vervulling gegaan. Jij had de kennis in huis om de benodigde fiber te maken en je was bereid om binnen het beperkte tijdsbestek ook op minder aantrekkelijke tijden er voor te gaan.

Drs. M.T. de Witte, beste Marcel hetzelfde geldt voor het onderzoek met behulp van jouw ECHO. Het was goed samen te experimenteren en leuk om mee te maken hoe je initiële cynisme omsloeg in tomeloos enthousiasme. Dat je voor onze experimenten zelfs vrij kreeg uit de kliniek was vooral te danken aan Dr. J.S. Laméris. Beste Han, onze samenwerking is in het begin niet zo soepel verlopen maar de studie is er gelukkig toch gekomen. Na Hong Kong kan het niet meer stuk.

Drs. P.G.H. Mulder, beste Paul je hebt me bij de verwerking van de resultaten van de meeste studies met je statistische kennis bijgestaan. Hartelijk dank voor het feit dat ik met vragen altijd bij je terecht kon.

De groep van het Laser Centrum in het AMC dank ik voor de goede samenwerking tijdens de gemeenschappelijke studie maar ook daarnaast. Maurice Aalders heeft de integrerende-bollen-opstelling van een Nd:YAG laser voorzien en bij de experimenten bediend, en Dr. Johan F. Beek heeft zorg gedragen voor de goede organisatie en mij in korte tijd het "grote coupes snijden" bijgebracht. Dr. J.W. Pickering, dear John I was impressed by your accuracy and speed in preparing and writing an article. It was a pleasure working with you.

Jos, jij bent iemand van het eerste uur. Toen ik nog nooit een computer had aangeraakt (behalve voor pacman) wist jij van mijn eerste resultaten al fraaie grafieken uit te draaien. Je was mijn docent bij de cursus "Computers en programmeren" in Leiden, wat een onmisbare introductie is geweest. Dank, dat je mij ook als paranimf wilt bijstaan. Marcel, dank dat je als paranimf onze vriendenclub wilt vertegenwoordigen.

Tot slot Jacqueline, lieve Jacque je hebt alles vanaf het eerste telefoontje meegemaakt (zonder jou had ik misschien toch niet gebeld). De echte full-time start van het onderzoek betekende min of meer het einde van onze studententijd. Dat ik de afgelopen jaren vaak meer met het onderzoek was getrouwd dan met jou was niet altijd even gemakkelijk. Toch heb je me in al die tijd geweldig gesteund. Je hebt bij nacht en ontij geholpen met experimenten, ieder praatje aangehoord, en met alles volledig meegeleefd. Aanstaand weekend gaan we fietsen.

Curriculum Vitae

Richard van Hillegersberg werd geboren op 31 maart 1966 te Rotterdam. Hij volgde middelbaar onderwijs aan de Scholengemeenschap Montessori Lyceum Rotterdam, waar hij het eindexamen Atheneum B behaalde in juni 1984. In datzelfde jaar begon hij met de studie Geneeskunde aan de Erasmus Universiteit Rotterdam, waar het doctoraalexamen werd behaald in juli 1989.

Zijn interesse voor wetenschappelijk onderzoek ontstond in het tweede jaar van de studie Geneeskunde (1986), toen hij betrokken was bij onderzoek naar de interpretatie van CT-scans op de afdelingen Neurologie en Medische Psychologie van de Erasmus Universiteit Rotterdam.

Gedurende het vijfde jaar van zijn studie (1988-1989) werkte hij op het Laboratorium voor Chirurgie van de Erasmus Universiteit aan een onderzoek naar de behandeling van levermetastasen met de laser onder leiding van Prof. Dr. O.T. Terpstra en Dr. W.J. Kort. De resultaten van dit onderzoek vormden de basis voor het project "Experimentele Laser Behandeling van Levermetastasen", wat vanaf februari 1990 door De Nederlandse Lever Darm Stichting werd ondersteund voor twee jaar; in februari 1992 werd een half jaar verlenging verkregen. Gedurende deze periode was hij op dit project werkzaam als wetenschappelijk onderzoeker verbonden aan de afdeling Algemene Heelkunde van de Erasmus Universiteit Rotterdam (hoofd Prof. Dr. J. Jeekel), en verrichtte hij het in dit proefschrift beschreven onderzoek. De "ex-artikel 9" status voor het uitvoeren van dierexperimenteel onderzoek verkreeg hij in mei 1990. Het onderzoek beschreven in Hoofdstuk 5 ontving in mei 1991 de "Resident Research Award of the American Society for Laser Medicine and Surgery".

In september 1992 hervatte hij de studie Geneeskunde aan de Erasmus Universiteit Rotterdam en begon met de co-schappen.

